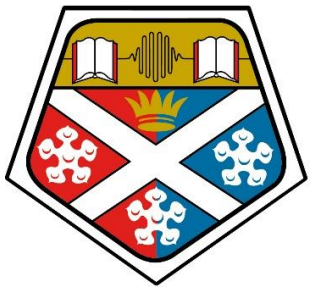

University of Strathclyde Glasgow

Strathclyde Institute of Pharmaceutical and Biomedical Sciences

Faculty of Science

Investigating the immunomodulatory effects of Non-Ionic Surfactant Vesicles to combat viral sepsis

Logan Mackie

Thesis presented in fulfilment of the requirement for the degree of Doctor of Philosophy

2024

Declaration

This thesis is the result of the author's original research. It has been composed by the author and has not been previously submitted for examination which has led to the award of a degree.

The copyright of this thesis belongs to the author under the terms of the United Kingdom Copyright Acts as qualified by University of Strathclyde Regulation 3.50. Due acknowledgement must always be made of the use of any material contained in, or derived from, this thesis.

Signed:

Date:

Acknowledgments

On many occasions I have invoked the myth of Sisyphus when referring to both the writing of this thesis and my PhD journey in general. Condemned by the gods to eternally roll a boulder up a hill, only to have it roll back down upon reaching the summit. I have often felt that this is an apt assessment of the scientific process.

I must thank my parents, Michele and Kenneth, partner Hannah, and family for being a constant source of encouragement and belief in my ability. Without your support this thesis would not exist and thus, this work belongs as much to them as it does to me.

To my mum, dad, and brother (Niven) in particular, thank you for making my upbringing a joyful experience. I am as weird as I am because of you. I think my need to explore very boring things stems from all those trips in the caravan to random small towns across this weird little island.

To Hannah, thank you for enduring endless rants about cytokines, transcription factors, and frustrating data. Our adventures over the course of this degree kept me going and eating food with you has motivated me as much as anything else. You deserve a nice holiday as much as me at this point, so let us go together.

To my science family:

Prof Craig Roberts – Thank you for trusting me and giving me this opportunity. Most of my life as a scientist has been determined by the guidance and help that you have provided me with, and it's been a fun time too. Darkening your office door has become a rewarding hobby.

Dr Stuart Woods and Dr Jonathan McGahon – Thank you for training me despite my absolute ineptitude when we first met. Stuart, you instilled in me the value of fear as a teaching tool despite being a big softie at heart. Jonny, I do most of my lab work the way I do from watching you, and it has worked out pretty well so far.

Holly Van Dessel – Thank you for being my constant companion in the lab and enduring so much. Co-parenting our one brain cell has been like owning a 19-year-old cat that occasionally catches a mouse instead of bringing a leaf home. Now you have to put me in your acknowledgments, gotcha!

Prof Riccardo D'Elia – Thank you for being my science step-dad and providing great insight (and anecdotes) into scary pathogens. Long days during *in vivo* experiments didn't feel so bad with you helping out.

Dr Ally Hughes, Dr David Mark, Jack Stone, John Morgan-Riordan, Dr Lily Morgan-Riordan - Thanks for being such good friends and (mostly) rolling your eyes at things I say and (occasionally) laughing at them. Our dinners and hangouts have been fun, even for an introvert. It has been great pretending to be an adult with you.

To floor six and the creatures that inhabit it: Thank you for making me feel part of a team, or a weird, dysfunctional tribe. This shared experience has provided me with many excuses to procrastinate, but I would say it was worth it. If I mention one name, I would have to mention them all, so I won't.

Declan Gallacher and Cara Burns – thanks for staying friends with me despite my best efforts. Our infrequent meetups feel like coming home to a houseful of clowns – chaotic but comforting.

Thank you to abrasive music, the colour black, terse language, crude humour, beans, lentils, chickpeas (and other legumes), abandoned hobbies, looking at little guys on my phone, cooking when I am bored, and rational thinking.

Sisyphus may have his boulder, but the people above are my rock.

Contents

Abstract

Current anti-inflammatory therapies often utilise a single mechanism of action and come with a range of side-effects that reduce the scope of therapeutic applications. One such therapy is the conventional corticosteroid, dexamethasone used to treat the hyperinflammatory response-induced sepsis associated with severe SARS-CoV-2 infection. This drug has displayed poor efficacy in early stages of SARS-CoV-2 infection, alongside side effects such as weight gain, mood changes, vision impairment, osteoporosis, and poor glycaemic control in diabetic patients - a cohort at greater risk of death from SARS-CoV-2 infection. Herein, I explore Non-Ionic Surfactant Vesicles (NISV) as an immunomodulatory therapy for the treatment of viral infection induced sepsis. I compare NISV and dexamethasone by examining modulation of cytokine production in TLR7 and TLR8 stimulated bone marrow derived macrophages (BMDM) using ELISA and Cytometric bead array, alongside transcriptomic and metabolomic analyses. I also investigate NISV size as a factor in their immunomodulatory effects. I demonstrate that whilst dexamethasone displays broad immunosuppression of cytokines regardless of TLR stimulation, NISV differentially modulate cytokine production dependent on specific TLR activation. This effect is generally retained as NISV size decreases, with a small increase in potency. Whilst NISV effects on energy metabolism are minor, I observe an increase in phospholipid synthesis and regulation of the anti-inflammatory TCA cycle metabolite itaconate in treated cells. Finally, I demonstrate that whilst both NISV and dexamethasone downregulate NF-kB activation, NISV also control inflammation through downregulation of the non-canonical NLRP3 inflammasome. Here, I broadly present NISV as an immunomodulatory therapy that can transcriptionally regulate inflammation-associated gene expression through multiple regulatory pathways in a way that dexamethasone cannot. These results support further investigation of NISV as an alternative anti-inflammatory to widely used corticosteroids during virally induced sepsis.

1 Introduction

1.1 Pandemics

Viral infections, and thusly pandemics, have been a constant challenge to humanity throughout history. Recorded accounts from 431 BCE by the Athenian historian and general Thucydides note his first-hand experience with a viral pandemic that has been postulated to be caused by Ebola virus, or a form of smallpox. The symptoms are described: "abrupt onset, persons in good health were seized first with strong fevers, redness and burning of the eyes, and the inside of the mouth, both the throat and tongue, immediately was bloody-looking and expelled an unusually foul breath. Following these came sneezing, hoarseness . . . A powerful cough . . . and every kind of bilious vomiting . . . and in most cases an empty heaving ensued that produced a strong spasm that ended quickly or lasted quite a while". The infected were subject to high fever, alongside redness, ulcers, and blisters wracking the skin. Eventually the disease spread to the bowels to cause extreme diarrhoea, proving fatal after only 1 week *(Thucydides, 431 BCE; Olson, 1996; Cunha, 2004)*. Whilst this is somewhat accepted to be the first recorded viral pandemic, outbreaks of various viral pathogens such as influenza *(Morens, et al., 2010; Kilbourne, 2006)* smallpox *(Thèves, Crubézy, and Biagini, 2016)* and yellow fever *(Gianchecchi, et al., 2022)* have been a constant companion to us.

The recent incursion of SARS-CoV-2 which has claimed the lives of nearly 7 million people (WHO 2023) is but one of many viral pandemics that we have faced in the last two centuries. The last 40 years alone have seen the rise of Human Immunodeficiency Virus (HIV), Influenza strains such as H1N1, Ebola and Zika virus, Middle Eastern Respiratory Syndrome Coronavirus (MERS-CoV), and of course the previously mentioned ongoing SARS-CoV-2 outbreak *(Roychoudhury, et al., 2020).*

Undeniably, the frequency of pandemics can be attributed in part to the actions of man, with studies suggesting that the coming decades will see a three-fold increase in the probability of occurrence of pandemics *(Marani, et al., 2021).* With the human population swelling to 8 billion, overpopulation contributes greatly to many of the factors underlying generation of viral pandemics. Whilst population growth rate has slowed since reaching its peak of 2.1% between 1955 and 1975 *(Roser, et al., 2013),* the problem of overpopulation persists, resulting in increased consumption which drives urbanization of wildlife areas for both raw materials, living space, and food. Destruction of animal ecosystems decreases biodiversity, creating an ideal environment for the rapid transmission of disease as demonstrated by the increase in West Nile Virus transmission correlating with low avian biodiversity *(Ezenwa, et*

al., 2006). Zoonotic reservoirs exist within the animal population and an estimated 1.67 million undiscovered zoonotic viruses exist in nature *(Carroll, et al., 2018).* Closer contact between humans, including consumption of non-domesticated species as food have increased the rate of zoonotic transmission into the human population *(Jones, et al., 2008).* A likely zoonotic source of SARS-CoV-2 is postulated to be the bats being sold in wet markets in Wuhan, China. Disregarding animal welfare concerns, reliance on factory farming for the production of meat creates great opportunity for emergent viral infections with closely packed, often wounded animals stored in unsanitary conditions *(Jones, et al., 2013).* Other than viruses, over-use of antibiotics in factory farming contributes to the generation of drug-resistant bacterial zoonoses *(Spernovasilis, et al., 2021).* Whilst viruses remain the main driver of pandemics, previous outbreaks of bacteria infections, notably *Yersinia pestis* (Plague), highlight the ability of prokaryotic pathogens to cause widespread disease *(Barbieri, et al., 2020).*

The factors described above also unequivocally contribute to climate change with overwhelming scientific consensus agreeing that human actions have significantly altered the planet's climate and ecosystems *(IPCC, 2022),* with some proposing the current era be designated as the Anthropocene epoch due to the lasting geological effects of massive increase in industrialisation *(Lewis and Maslin, 2015).*

Global temperature increase is likely to see the encroachment of viruses relegated to tropical climates spread to previously cooler locales by insects and animals, with migration patterns shifting, or geographical ranges shifting *(Chen, et al., 2011; Carlson, et al., 2022).* Alongside this, an increase in global temperature will increase the frequency of natural disasters such as flooding, which in developing nations may see an increase waterborne viral transmission. The opposite effect is also true, with droughts forcing humans to rely on unsafe drinking water to survive, creating an interface for pathogen exposure *(Leal, et al., 2022).*

Regardless of climate and ecological effects, socio-economic factors contribute greatly to the persistence of infectious and pandemic-capable pathogens, with developing nations lacking the infrastructure to combat emerging threats, which in turn creates a vicious cycle. Those that suffer infection often experience debilitating symptoms that remove them from work (many rely on agricultural work for their direct sustenance), which in turn contributes to poverty, worsening living conditions, and therefore exposure to infectious disease *(Lindahl, and Grace, 2015).*

WHO recently defined a list of pathogens with epidemic or pandemic potential that lack sufficient or have no current medical countermeasures in order to prioritise and direct global research. Of this list, only 2 pathogens are not viral in nature; the unknown "Disease X" that

accounts for an as-of-yet undiscovered pandemic capable pathogen that may arise and cause novel disease, and plague *(WHO, 2022).* A common factor amongst recent viral outbreaks (and dominating the WHO list of pandemic capable pathogens of priority) is the genomic structure of these viruses, each carrying single-stranded RNA genomes. Generally, viruses can be broadly categorised based on the Baltimore classification scheme devised by David Baltimore in 1971 (Baltimore, 1971; Koonin, Krupovic, Agol, 2021) with the recent viral pathogens mentioned above belonging entirely to class IV, V, and VI.

Particularly, for Ebola, Zika, MERS-CoV and SARS-CoV-2, these viruses belong to class IV as they possess positive-sense single-stranded RNA genomes (+ssRNA). As this RNA is the same polarity as the mRNA needed for translation in host cells, viral proteins are directly translated upon infection, and thus can be efficiently expressed by host cellular machinery. Alongside this, +ssRNA viruses generate a strand of -ssRNA from the original +ssRNA that serves as a template for the generation of more +ssRNA by an RNA-dependent RNA polymerase (RdRp) that acts solely upon this template, leaving host RNAs untouched. This copy of the viral genome is packed into new virions, allowing replication and dissemination of the virus throughout the host (Rampersad and Tennant, 2018; V'Kovski, et al., 2021). Despite the similarities in genomic structure, the pathogenesis of viruses can differ greatly.

1.2 Viral pathogenesis

Pathogenesis of a viral disease varies from pathogen to pathogen. The ability of viruses to manipulate the host cells allows for the manifestation of many conditions and disease states. Commonly, acute viral infection may cause the well-known symptoms of fever, fatigue and bodily aches, alongside localised symptoms such as rashes or cutaneous lesions *(Doshi, et al., 2020),* digestive issues such as diarrhoea or nausea *(Karst, and Tibbetts, 2016),* and respiratory tract problems such as cough, sore throat, and blocked nose *(Mifsud, et al., 2021).* The mechanisms behind these symptoms may vary depending on the virus but there is a general schema that is involved in the pathological progression of a viral infection, closely interwoven with the viral life cycle.

Initially, viral entry requires overcoming the innate barriers of the body such as mucous, cilia, and the tight junctions between epithelial cells, a process which can be enhanced by damage to mucosal surfaces, as well as infection damaging these sites itself. Once inside the host, viral entry to target cells is initiated, allowing for the processing of the viral genome by host cell machinery and subsequent production of viral proteins and copies of the genome. After assembly of new virions, the virus will spread to other cells by exiting the infected cell through direct lysis of the cell or viral budding. This process is then repeated, disseminating virus in the local area, and spreading the damage to cells *(Jones, et al.,*

2021). Typical resolution of a viral infection involves detection by the innate immune system and the generation of inflammation, alongside recruitment of the adaptive immune system to enhance cell-mediated effects. The virulence of a virus in concert with the effectiveness and speed of the immune response contributes greatly to the development of disease. Outside of acute illness from localised inflammation and viral shedding/lysis of cells, viruses have been implicated in a variety of conditions including immunosuppression and oncogenesis.

An example of a virus that is associated with immunosuppression is HIV. Infection with HIV may cause immunosuppression through preferential infection of CD4+ T cells and subsequent depletion of this lymphocyte population. This can progress to acquired immunodeficiency syndrome (AIDS) and death *(Moir, et al., 2011).* Viral immunosuppression is present in other viruses such as Epstein-Barr virus, Respiratory syncytial virus, and SARS, often utilised as a method of immune evasion to facilitate viral persistence. Immunosuppression also provides the increased opportunity for co-infection with other pathogens *(Alcami, and Koszinowski, 2000).* The mechanisms behind immunosuppression involve dysregulation of normal immune function, which some viruses actively utilise outside of infecting immune cells and subsequent lysis. For example, some viruses encode genes for immunoregulatory proteins that once transcribed by the host cell may dampen the immune response. This includes homologues of complement regulatory proteins, as well as virally expressed FC receptors that can bind to the FC region of antibodies and inhibit the activation of immune cells *(Sinha, et al., 2021; Jenks, et al., 2019).*

Some viruses employ mechanisms that have an oncogenic effect, explicitly encoding genes for the transcription of oncogenic proteins, or through the inactivation of tumour suppressor genes. Alongside this, the viral life cycle may promote increased rate of DNA damage whilst decreasing the ability of the host cell to conduct repairs *(Elkhalifa, et al., 2023).* The oncogenic effects of viruses have been implicated in around 15-20% of all cancers, with the culprits including hepatitis B and C virus, human papillomavirus, Epstein-Barr virus, and Kaposi sarcoma-associated herpesvirus *(zur Hausen, and de Villiers, 2014; Moore, and Chang, 2010).* Viruses can also alter the normal functioning of cells by skewing the metabolic processes of host cells to favour viral replication and subvert immune detection. This can manifest as altered glucose metabolism, with an increase in glycolysis even under aerobic conditions. This effect is also commonly observed in cancer cells and is termed the Warburg effect. Alongside this, pathways that favour the generation of fatty acids and nucleotides can be increased to create an optimal environment for the replication of viral genomes and packaging into new envelopes *(Girdhar, et al., 2021).*

Once inside the host cell, viral RNA is released into the cytoplasm where it may encounter mechanisms for the removal of intracellular pathogens such as detection by pattern recognition receptors (PRR) like Toll-like receptors (TLR) or Rig-I like receptors (RLR). When viral RNA manages to evade these PRR, then mechanisms such as the sequestosome 1-like receptors (SLRs) can initiate removal in an autophagic process known as xenophagy (Sharma, et al., 2018; Deretic, Saitoh, and Akira, 2013). During an infection, it is likely that some pathogen associated molecular patterns (PAMPs) like viral RNA will be detected by PRR (either by infecting a host cell expressing MDA5 or RIG-I or by phagocytosis of free viral PAMPs by innate immune cells such as macrophages (Mφ) or dendritic cells (DCs) and detection by TLR7/8) and thus initiate an immune response *(Thompson, et al., 2011).* PRR may also be activated by Damage associated molecular patterns (DAMPs), generation of pro-inflammatory factors like Tumour necrosis factor alpha (TNFα) or Interleukin-1 family members (IL-1), or damage-modified endogenous molecules like oxidation-specific epitopes and extracellular matrix compounds (ECM) *(Land, 2021).* Upon recognition of PAMPs or DAMPs by PRR, anti-viral and pro-inflammatory processes begin as part of the innate immune response to begin pathogen clearance.

Ideally, the immune system can control and effectively eliminate viral infections, however, in some cases the activity of immune cells can be detrimental to the host. Mφ and DCs can release soluble mediators that serve to recruit/activate other immune cells including effector cells of the adaptive immune system. Activation of cells by these mediators can generate a feedback loop whereby those cells produce cytokines themselves, increasing local immune activity. In the short-term this is accompanied by contained inflammation due to cell influx and the subsequent killing of infected cells by processes such as programmed cell death (apoptosis) or necrosis which can cause the release of cell contents into the extracellular space and perpetuate further immune activation through the previously mentioned DAMPs. Whilst in theory this should resolve infection, many viruses have developed mechanisms to evade the immune system and remain at large in the host. If the infection is not cleared quickly and persists despite the efforts of the immune system, pro-inflammatory signalling can spread throughout the body. This leads to the generation of a systemic hyperinflammatory response which can progress to a condition known as sepsis *(Nedeva, et al., 2019).*

1.3 The global burden of Sepsis

Sepsis can be described as “life-threatening organ dysfunction caused by a dysregulated host response to infection”, last defined in 2016 by The Third International Consensus Definitions for Sepsis and Sceptic Shock *(Singer, et al., 2016).* A recent study conducted in

2017 aimed to evaluate the global burden of sepsis, which revealed 48.8million cases and 11 million deaths each year. Areas with the highest incidence of sepsis included low- and middle-income countries, predominantly in the regions of sub-Saharan Africa, south, east, and southeast Asia, and Oceania. Furthermore, over half of the deaths associated with sepsis occurred in children *(Rudd, et al., 2020).* A major contributor to high sepsis incidence in sub-Saharan Africa is HIV, which facilitates co-infection with *M. tuberculosis*, and *S. Pneumoniae* primarily in young people *(Lewis et al., 2019).* In southeast Asia, the leading cause of Sepsis is also viral in nature, with ssRNA viruses such as influenza, Dengue virus, norovirus, and respiratory syncytial virus making a major contribution *(Mehta, et al., 2022)*. The risk factors for the development of sepsis are also prevalent in the developed world. Outside of both infection and those at the extremes of age (e.g., infants and the elderly), those with chronic illnesses including diabetes, chronic obstructive pulmonary disease (COPD), chronic kidney disease (CKD) are more likely to develop sepsis *(de Araújo, et al., 2023).* Other features such as low socioeconomic status and malnutrition increase the chances of sepsis, with both factors often coming hand in hand in developing or rural areas alongside higher prevalence of chronic infection *(Abugroun, et al., 2021).*

These findings support the urgent need for the development of a novel, low-cost, treatment for sepsis that can be provided to often rural communities that lack the infrastructure needed to secure vital healthcare and aftercare *(Rudd et al., 2018).* However, this does not take into account the burden of sepsis experienced during the SARS-CoV-2 pandemic, which highlights that viral sepsis is not a condition relegated to developing nations. Some studies indicate as many as 1 in 3 patients hospitalised due to SARS-CoV-2 infection experience sepsis, with 70.8% of these sepsis cases being caused by SARS-Cov-2 without co-infection *(Shappell, et al., 2022),* whereas others put the figure closer to 1 in 20 *(Abumayyaleh, et al., 2021)*. Of those infected with the virus, the mortality rate differs depdendent on the severity of infection, with mild disease (e.g., non-ventilated) patients at 22% mortality, and 53% in severe disease patients (e.g., invasively ventilated) *(Heubner, et al., 2022).*

The features of severe SARS-Cov-2 infection overlap considerably with that of sepsis and sceptic shock, including thrombotic tendency, inflammatory bursts, disseminated intravascular coagulation, and multi-organ failure *(Zafer et al., 2021*) Alongside this, the respiratory aspects of SARS-CoV-2 infection include reduced capacity for oxygen saturation due to acute respiratory distress syndrome (ARDS) which disrupts the integrity of alveoli *(Batah, and Fabro, 2021).* ARDS alone has been shown to hospitalise 61-81% of those presenting with the condition *(Gibson, Qin, and Puah, 2020).* Examining the cytokines implicated in severe SARS-Cov-2 disease, IL-1, IL-4, IL-6, IL-7, IL-10, IL-12, IL-13, IL-17, M-CSF, GM-CSF, IP-10, IFN-γ, MCP-1, and TNFα have been observed at atypical levels in

serum *(Declerq, et al., 2022; Vaz de Paula, et al., 2020; Coomes, and Haghbayan, 2020; Wang, et al., 2021; Lu, et al., 2021; Moll-Bernardes, et al., 2021; Hasan, et al., 2021; Eichhorn, et al., 2023; Quartuccio, et al., 2021; Lang, et al., 2020; Guo, et al., 2022; Todorović-Raković, et al., 2021),* with many of these cytokines playing a role in the progression of sepsis.

1.4 SARS-CoV-2, the novel coronavirus

Undeniably, the covid-19 pandemic has been one of the largest medical challenges in recent history, and the causative agent has cemented itself as a serious contributor to the development of sepsis and hyperinflammatory CSS conditions.

SARS-CoV-2 belongs to the family *Coronaviridae* alongside SARS-CoV-1 and MERS-CoV and causes severe respiratory disease. Despite intense global efforts to comprehensively characterise the SARS-CoV-2, the short time since its discovery has demanded that researchers use other viruses to inform their understanding of covid-19. In the context of respiratory virus infections, previous outbreaks such as H1N1and H5N1 influenza, and coronavirus outbreaks such as MERS, SARS have provided insight into the mechanisms of our current understanding of SARS-CoV-2 disease progression *(Irani, 2022; Havasi, et al., 2022).* The virus gains entry to the host typically through droplet transmission, with large droplets settling on surfaces, leading to contact with host hands and transfer to the eyes, mouth, or nose. Aerosolised forms of the virus in smaller droplets can also be inhaled by the host and travel to the airways where the virus can take hold, entering through Angiotensin-converting enzyme (ACE2) expressed highly on the surface of airway epithelial cells *(Rutter, et al., 2021; Ashraf, et al.,2021).* Initially infected cells are likely to be the epithelial cells of the nasopharynx.

The SARS-CoV-2 **(Fig. 1, Fig. 2)** virion contains the structural proteins of a nucleocapsid (N), membrane (M), envelope (E), and spike (S) proteins. The S protein is a glycoprotein that is formed as a homotrimer and presents in multiple copies on the surface of the virion (giving the virion the appearance of a crown for which it is named - corona) and mediates entry to host cells. The S protein must also be cleaved into two subunits (S1 and S2) by the protease furin after biosynthesis but before release from the host cell. The S2 subunit also contains a fusion peptide to facilitate membrane fusion *(Jackson, et al., 2022).* These subunits work in conjunction to bind to host ACE2 (S1) and the membrane of the host cell (S2), where the serine protease TMPRSS2 cleaves S2 at a location termed the S2' site to activate and free the fusion peptide, allowing membrane fusion and viral genome delivery. This process of

cleavage can also occur after ACE2 mediated endocytosis of the virion, with cathepsin L cleaving the S2'site, allowing access to the host cytoplasm *(Hoffaman, et al., 2020).*

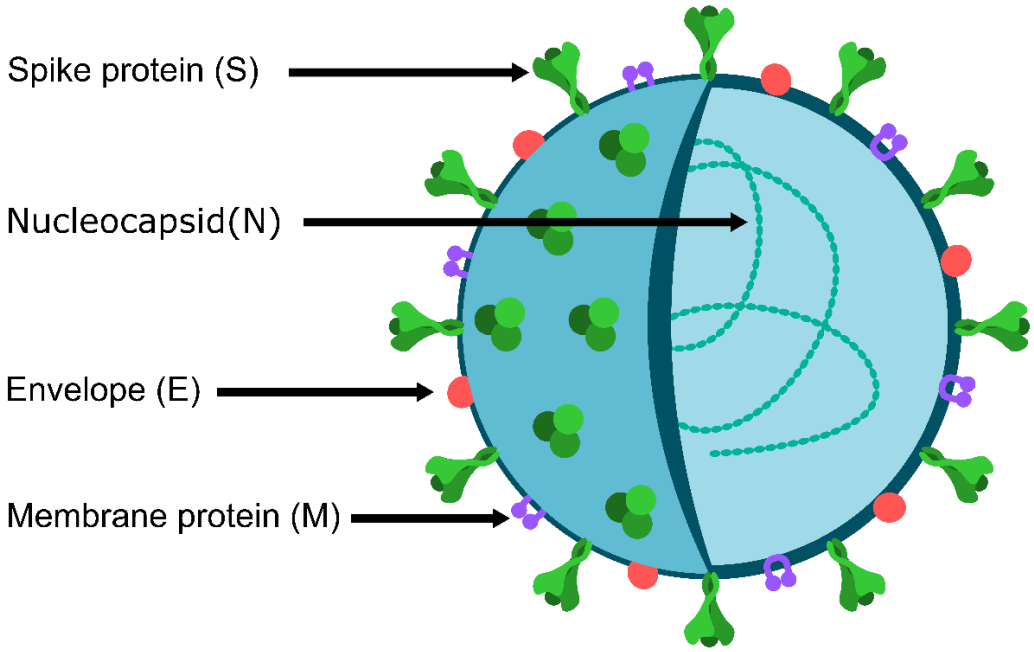

Figure 1: Structure and proteins of SARS-CoV-2. *The +ssRNA genome of SARS-CoV-2 is composed of around 30kb, located inside a nucleocapsid and further protected by a viral envelope. The genome encodes genes for four structural proteins; the spike protein (S), which is present as a trimeric structure on the surface of the virion and must be cleaved to initiate binding and fusion of the particle with the host cell; the Nucleocapsid (N) and Envelope (E) mentioned above; and the membrane protein, which is the most abundant glycoprotein encoded by the virus (Satarker, and Nampoothiri, 2020).*

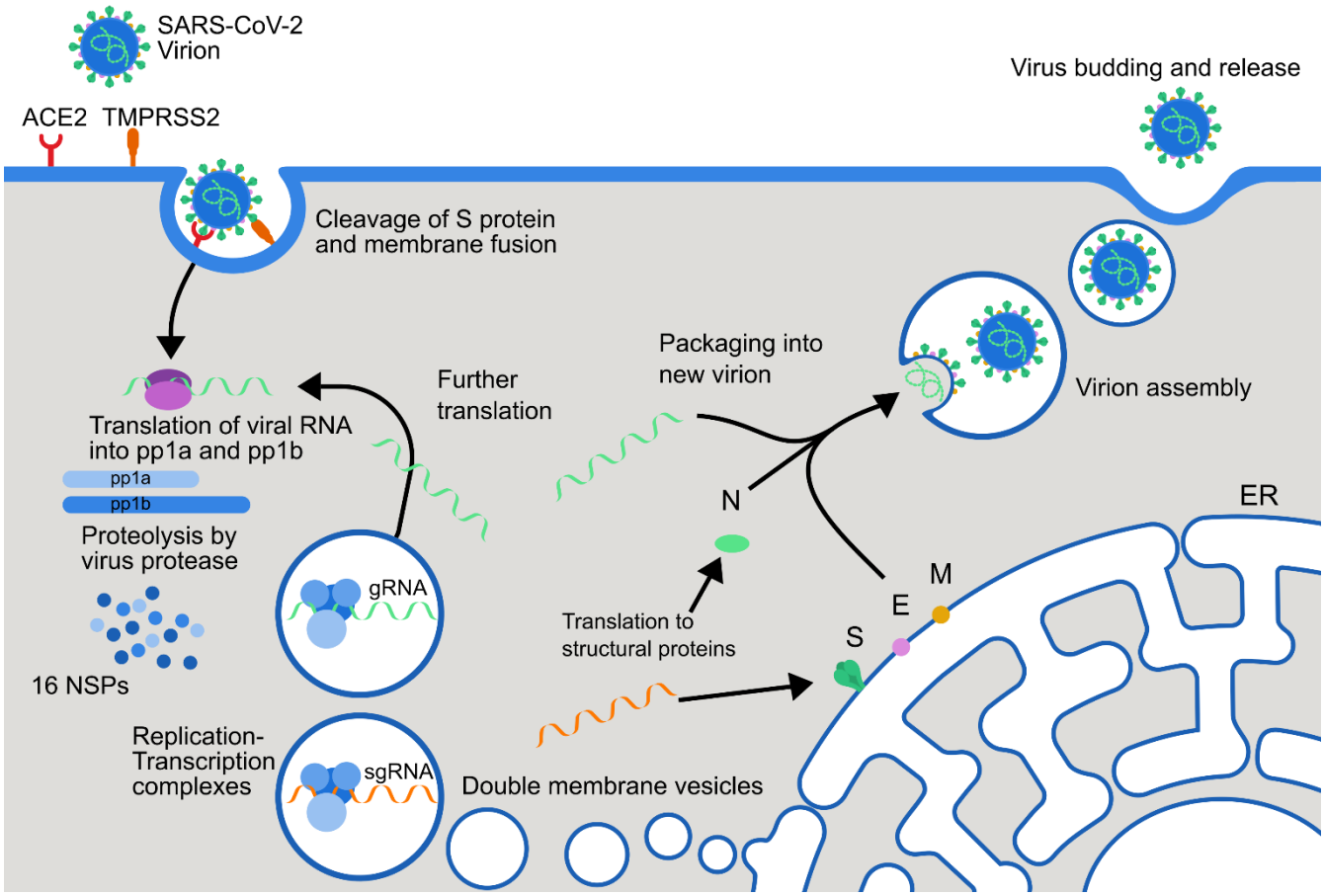

Figure 2: Viral replication cycle of SARS-CoV-2. *SARS-CoV-2 virion binds to the target cell through association of spike protein with ACE2. The spike protein is then cleaved by a membrane bound serine protease TMPRSS2 to reveal the fusion peptide and initiate membrane fusion. Viral genomic material enters the cytoplasm and is translated by host cell ribosomes into 2 large polyproteins, pp1a and pp1b. These polyproteins are subject to proteolytic cleavage by a virally encoded protease that yields 16 non-structural proteins (NSPs). These proteins form replication-transcription complexes housed within double membrane vesicles and synthesise genomic RNA (gRNA) or sub-genomic RNA (sgRNA). gRNA can be used for the translation of more NSPs, or packaged into new virion, whereas sgRNA is used for the translation of structural proteins. Of these structural proteins, spike (S), envelope (E) and membrane (M) are produced in the endoplasmic reticulum, whereas the nucleocapsid protein (N) is formed in the cytoplasm. These components are then assembled into new virion in the endoplasmic reticulum-golgi intermediate complex (ERGIC). The virus is then released into the extracellular space via budding or eventual lysis of the host cell.*

SARS-CoV-2 employs a range of strategies to evade destruction such as the creation of double membraned vesicle "replication factories" produced from ER membranes. These vesicles allow transcription to occur whilst shielding viral motifs from PRRs. Furthermore, some variants of SARS-CoV-2 such as Delta encode a polypeptide that can interact with Major histocompatibility complex I (MHC I) and selectively degrade these antigen presenting molecules in lysosomes as a form of autophagy. This reduces the effectiveness of T cell mediated cytotoxicity and allows virally infected host cells to persist until the virus has completed replication. Alongside reducing cell-mediated immunity, SARS-CoV-2 can also impair the interferon response that contributes to anti-viral defence *(Rubio-Casillas, Redwan, and Uversky, 2022).*

Despite these methods used to perturb the immune system, eventual detection of viruses leads to an immune response, which in some cases can result in hyperactive production of pro-inflammatory and anti-viral mediators in an uncontrolled manner. In mild cases of SARS-CoV-2 infection, resident lung Mφ are able to effectively contain and clear the virus using a measured inflammatory response. In severe infection, there is greater disruption of the air-blood interface due to destruction of epithelial, endothelial and lung capillary cells. This causes blood plasma components to be exuded into the airways, which prompts tissue-resident immune cells to release chemoattractants that traffic infiltrating monocytes and macrophages to the site, which in turn propagate a sustained and uncontrolled inflammatory response *(Li, et al., 2020; Ragab, et al., 2020).* Outside of the immune response to a virus upon detection, monocytes and macrophages may be targets of infection for specific viruses (such as SARS-CoV-2). Initially, the characteristics of monocytes may seem to make unattractive hosts for viruses due to their short half-life and non-dividing nature. However, a “Trojan Horse” effect has been observed that can be described in two main scenarios. Chiefly, upon infection with a virus, monocytes may differentiate into macrophages and enter tissues from the blood, carrying the virus with them. In another aspect, macrophages conduct a great degree of interaction with other cells (antigen presentation and costimulatory activation of T cells for example) and thus can facilitate transfer of a virus to another cell population *(Nikitina, et al., 2018).* Once inside these tissues, resident macrophages are often the first contact with the virus and serve to initiate and often sustain the inflammatory response. This may be through continual detection of

uncontrolled viral replication, or the trail of cellular damage left in its wake triggering PRR with DAMPs. For example, in SARS-CoV-2, alveolar macrophages have been implicated in sustaining inflammation through persistent IFN signalling and NLRP3 inflammasome activation at peak infection *(Sefik, et al., 2022)*.

Clearly, a large factor in this persistent inflammatory state is the previously mentioned “cytokine storm”, first named in 1993 by James L Ferrara during studies of graft-versus-host disease *(Ferrara, et al., 1993).* Currently there is no concrete definition of cytokine storm, but it is generally agreed upon that it encompasses a systemic inflammatory response to infection perpetuated by over-active cytokine signalling resulting in pervasive inflammation. Clinically, the term cytokine storm is used less frequently, with related conditions such as systemic inflammatory response syndrome (SIRS), and multiple organ dysfunction syndrome (MODS), and ARDS being discussed. As the range of conditions which cytokine storm contributes to becomes increasingly wide, the term cytokine storm syndromes (CSS) have been developed to simplify discussion and diagnosis *(Canna, and Behrens, 2012).* Study of viruses like H5N1 influenza reveal that high viral load and cytokine storm are associated with fatality. The use of antivirals can control viral replication and can achieve good results in the early stages of infection, but inability to control cytokine storm in late stages of the illness is detrimental to patient health. Consistent with other CSS, raised cytokine levels of IL-6, IL-10, and IFN-y were observed in the infected. Heightened levels of cytokine and chemokine production during infection has been correlated with poor disease outcomes in both animal models and clinical studies on humans *(de Jong, et al., 2006).* As mentioned previously, key players in the generation of cytokines, and thus cytokine storm are the cells of the innate immune system.

1.5 Innate immunity

The innate immune system comprises a range of cells and serum proteins that work in concert to survey, detect, and initiate a quick response to invading pathogens. As the adaptive immune system, including B and T cells, takes around 3-5 days to clonally expand and mount a defence, proper functioning of the innate immune system is critical for control of infection in the early stages *(Medzhitov, and Janeway, 2000).* Unlike the adaptive immune system, receptors present on the cell such as Mφ, neutrophils, DCs, natural killer (NK) cells, are germline encoded, and thus are genetically predetermined to detect classes of pathogen without the specificity

imparted by the somatic recombination of B and T cell receptors *(Janeway, and Medzhitov, 2002).* Regardless, recognition of PAMPs by these PRR are sufficient to mount a generalised reaction that will begin the transition to a more specific response. Infection of non-immune cells such as epithelial cells can contribute to the recognition of a pathogen through the detection of double stranded RNA transcription intermediates of the virus in the cytoplasm using MDA5. This leads to production of type I and type III interferons, which can act in both a paracrine or autocrine manner to generate an immediate anti-viral response. A key player in this response is the Mφ.

Mφ are 25-30μm phagocytic cells that are derived from monocytes after entering a tissue from the blood *(Lendeckel, et al. 2022).* They were first described by Metchnikoff in the late 19th century, with our understanding of their function and phenotypical diversity continuing to expand to this day *(Epelman, et al., 2014)*. Mφ play several roles **(Fig. 3)** including recognition of PAMPs and phagocytosis of pathogens *(Taylor, et al., 2005),* production of soluble mediators such as cytokine and chemokines to initiate a pro-inflammatory response *(Arango Duque, and Descoteaux, 2014),* tissue healing and maintenance of homeostasis *(Wynn, and Vanella, 2016)*, and release of antimicrobial compounds to help destroy invaders *(Nathan, and Hibbs, 1991; Herb, and Scramm, 2021).*

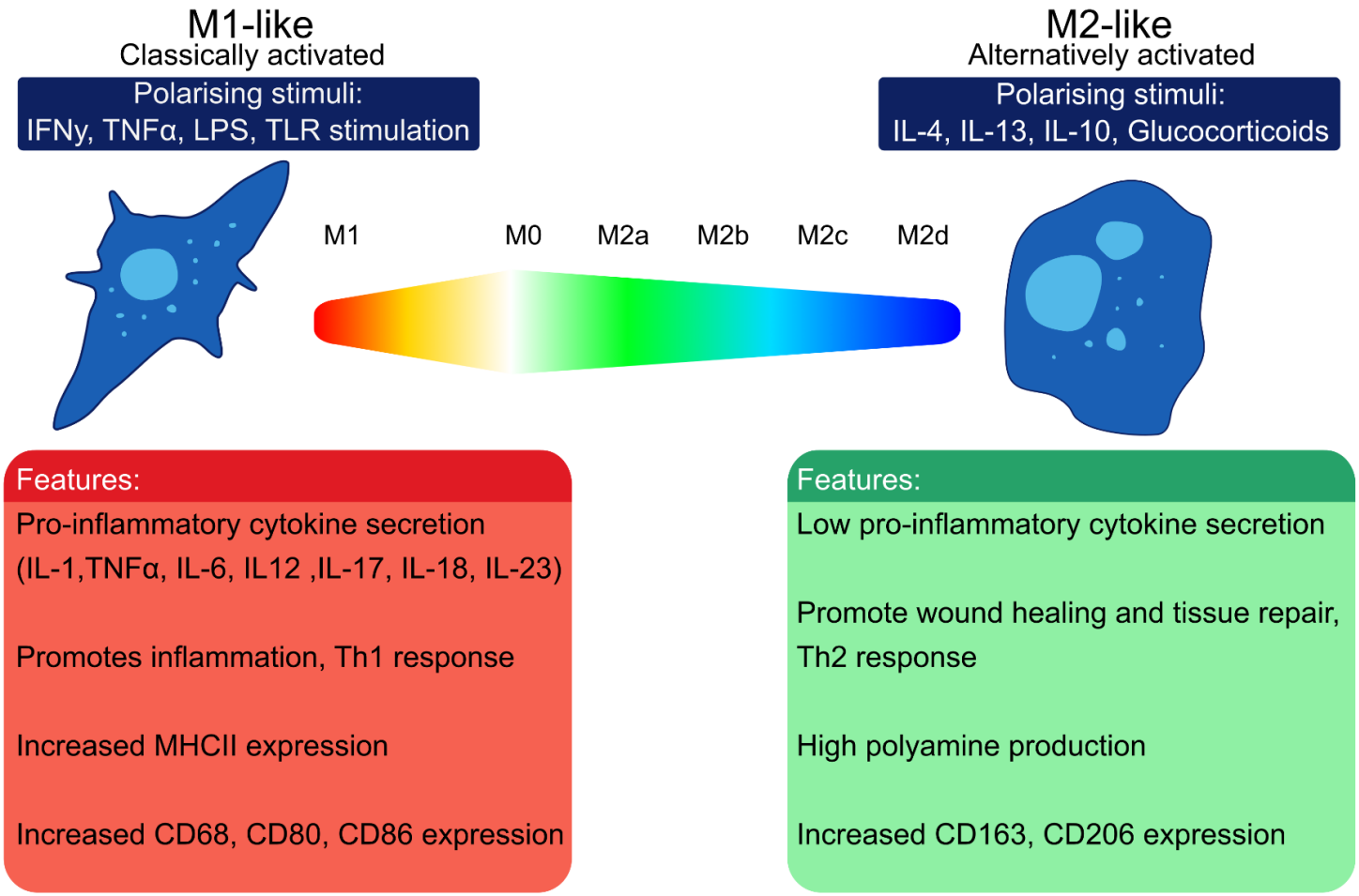

Figure 3: Spectrum of macrophage activation/phenotypes. *Macrophages have previously been characterised by their activation state, with M1 designating "classically activated" macrophages and M2 designated "alternatively activated" macrophages. Since this designation, a wide spectrum of macrophage phenotypes has been characterised, and thus dissolves the prior notion of a macrophage activation binary. For naming conventions, pro-inflammatory macrophages comprise the M1 status, whereas a plethora of macrophage phenotypes encompassing the M2 subset due to non-classical activation rather than a single alternative activation but show broad similarity in their general function. Whilst M2 display a greater anti-inflammatory capacity than M1 macrophages, the Th1 and Th2 response which contributes to their polarisation is not necessarily anti or pro inflammatory. Instead, this response deals with the resolution of intracellular pathogens (Th1) or large extracellular pathogens such as helminths, as well as activation of the allergic response(Th2).*

During patrol of tissues, Mφ may encounter PAMPs, which they can detect using a variety of PRRs such as the TLRs *(Akira, et al., 2006),* C-type lectin receptors (CLRs) *(Weis, et al., 1998)*, NOD-like receptors (NLRs) *(Franchi, et al., 2009),* and RIG-I-like receptors (RLRs) *(Kawai, and Akira, 2006),* among others *(Taylor, et al, 2005)*. Focusing on the TLR family **(Fig. 4)**, 10 receptors have been identified in humans (TLR1-10) *(Barreiro, et al., 2009),* and 12 in mice (TLR1-9,11,12). TLRs are glycoproteins embedded in the plasma membrane or sequestered in endosomal compartments of cells and have 3 domains: an ectodomain that interfaces with the PAMP; transmembrane domain that spans the plasma membrane; and the intracellular Toll/interleukin-1 receptor (TIR) domain required for recruitment of adaptor proteins and signal transduction *(O'Neill, et al., 2007; Jin, and Lee, 2008).* Binding of a PAMP requires the ectodomain of the receptor, which is comprised of 16-28 leucine-rich repeats, with TLR7, TLR8, and TLR9 containing 27 repeats and a z-loop separating two smaller regions of LRR, rather than the single long LRR found in other TLR. This creates a horse-shoe shaped binding pocket *(Matsushima, et al., 2007)*. TLR exist as both homodimers and heterodimers (TLR1/2, TLR2/6) *(Farhat, et al.,2008).* Binding of the TLR ligand causes dimerization of the receptors, which brings the TIR domains into close proximity. This initiates recruitment of adaptor proteins which initiate signal transduction for the transcription of genes, with products dependent on the TLR stimulated and the transcription factor involved *(Bovijn, et al., 2012).* For example, whilst some TLRs are present on the surface of cells, other TLRs involved in the detection intracellular pathogens are trafficked to endosomes, with their ectodomain residing within the endosomal compartment. This occurs with TLR3, TLR7, TLR8, and TLR9, which are concerned with detecting dsRNA (TLR3), ssRNA (TLR7 + 8) from viruses, and CpG motifs on DNA from either bacteria or viruses (TLR9*) (Lind, et al., 2022).* The location of these receptors also serves to place a barrier between their binding domains and self-RNA that may exist in the extracellular space, reducing the likelihood of self-reactivity and development of autoimmune disorders *(Barton, and Kagan, 2009)*.

To enable interaction of these endosomal TLR with their cognate ligand, Mφ must engulf pathogens, or particles that arise from the lysis of infected cells. This can be achieved through a few mechanisms, dependent on particle size *(Flanagan, et al., 2012).* For particles below 0.5μm, cells may utilise endocytosis, which is either mediated by endocytic proteins (such as clathrin, or caveolin) from the cytoplasm clustering on the intracellular side of the plasma membrane, and then bending the

membrane around that which it is trying to engulf. Bending the membrane to create an invagination may require some rearrangement of actin, but this is more prevalent with larger particles. The membrane invagination containing the cargo is then separated from the main plasma membrane by scission, with the protein coat disassembling to be used in other endocytic events *(Kaksonen, and Roux, 2018).* The cargo-loaded intracellular vesicle can then merge with the endosome, exposing the cargo to TLR for detection, binding to MHCII for presentation, or degradation by lysosome fusion. For larger particles (>0.5μm), cells utilise phagocytosis. Whilst this mechanism is not exclusive to Mφ, it is much more efficient in this class of professional antigen presenting cells (APCs) which also includes DCs and B cells *(Gaudino, and Kumar, 2019).* This process is distinct from the self-sampling and presentation of endogenous peptides that is performed by all nucleated human cells through MHC I and allows the identification of potentially pathogenic invaders by the immune system. Although, DCs have the ability to cross-present antigen they have engulfed using MHCI to direct CD8+ T cells towards infected *cells (Joffre, et al., 2012).*

Due to the large size of the particles being ingested, phagocytosis is reliant on actin rearrangement, with studies displaying that inhibition of actin polymerase disrupts the ability of cells to engulf large particles *(Baranov, et al., 2021; Jaumouillé, and Waterman, 2020).* It has also been demonstrated that phagocytes may engulf particles much larger than themselves using IgG opsonisation *(Cannon, and Swanson, 1992).* Mφ may also use micropinocytosis or macropinocytosis, which have been studied less thoroughly than endocytosis and phagocytosis. Macropinocytosis is used for the ingestion of particles larger than 250nm, involving “ruffles” in the plasma membrane surrounding particles, driven by actin rearrangement, whereas micropinocytosis is used for smaller particles and may be achieved through clathrin or caveolin dependent means *(Canton, 2018).*

Whether expressed on the surface of cells or requiring the engulfment of particles, TLR recognition of pathogenic motifs initiates an intracellular signalling cascade of phosphorylation and de-phosphorylation, resulting in the translocation of transcription factors such as Nuclear factor kappa-light-chain-enhancer of activated B cells (NF-kB) in the cytoplasm to the nucleus. Once inside the nuclear membrane, these elements bind to DNA and begin transcription of genes for the production of

cytokines, chemokines, and other excreted mediators. This serves to generate a focus of inflammation at the site of infection *(Kawai, and Akira, 2007).*

Alongside Mφ, and other APCs, serum proteins such as the complement system can aid in the detection and destruction of invading pathogens through opsonisation or lysis via the membrane attack complex. The complement system was first discovered in 1896 by Jules Bordet and Paul Ehrlich and is comprised of more than 30 heat-labile serum or cell associated proteins that “complement” the anti-pathogenic effects of the heat-stable antibodies *(Kolev, and Kemper 2017)*. Complement may be activated in multiple ways, with classical, alternative, and lectin activation pathways available.

During classical activation (also known as antibody mediated activation) of the complement cascade, the C1q complex comprised of the serine protease subunits C1s and C1r bind to the Fc region of antibodies such as IgM and IgG1. After binding, these subunits cleave the complement proteins C2 and C4 into two subunits each. At this point, the lectin pathway also meets the classical pathway. The class of PRRs known as mannose-binding lectins (MBLs) recognise conserved carbohydrate motifs on pathogens and upon activation can express MBL-associated serine proteases which can cleave C4 and C2 as during classical complement activation. The larger subunits (termed C4a and C2b) form the C3 convertase. This may then cleave inactive C3 into two subunits, C3a which acts as an anaphylatoxin, and C3b which can opsonise pathogens and increase their recognition by the immune system including a feedback loop mediated by the alternative complement activation pathway. A second molecule of C3b may bind to the C3 convertase complex to form C5 convertase, which can cleave C5 into C5a and C5b. C5b is involved in recruiting further proteins (C6, C7, C8, C9) to form the membrane attack complex, triggering pore formation and lysis of invading microbes *(Dunkelberger, and Song, 2010).*

The alternative pathway involves C3b (generated either through spontaneous hydrolysis of C3 or through cleavage by C3 convertase) opsonising the surface of pathogens. Note, that as C3b can directly bind to pathogens, this pathway of complement does not require the involvement of antibodies or PRRs. During opsonisation, a serum protein known as factor B binds to C3b and is then cleaved by factor D. Of the two subunits generated from this proteolytic cleavage, the larger fragment (Bb) interacts with the opsonised C3b and free C3b to form the alternate

complex C5 convertase. Both alternate convertases mediate the same cleavage as the classical/lectin pathway counterparts. Subunits resulting from these cleavage events such as C3a, C4a, C5a act as anaphylatoxins and promote inflammation by increasing chemotaxis and activation of macrophages, mast cells, and other inflammatory immune effectors *(Harboe, and Mollnes, 2008; Klos, et al., 2009).*

Figure 4: TLR location and adaptor protein. *TLR are comprised of 3 main domains. The binding domain is formed at the N-terminus and contains leucine-rich repeats (LRR). A transmembrane domain (TMD) comprised of a single helix spans the membrane and is linked to the Toll/interleukin-1 receptor (TIR) domain at the C-terminus. TLR may be expressed on the cell surface, such as TLR4, or localise to endosomes such as TLR3, TLR7, and TLR8. Upon binding of the PAMP to the TLR, dimerization of the receptors occurs bringing both TIR into close contact, allowing recruitment of the adaptor protein to initiate intracellular signalling. All TLR use MyD88 as an adaptor protein except TLR3 which uses TRIF. Notably, TLR4 found on the cell surface may be internalised after receptor binding and once inside endosomes may initiate signalling using TRIF, making TLR4 the only TLR that uses both TRIF and MyD88 pathways.*

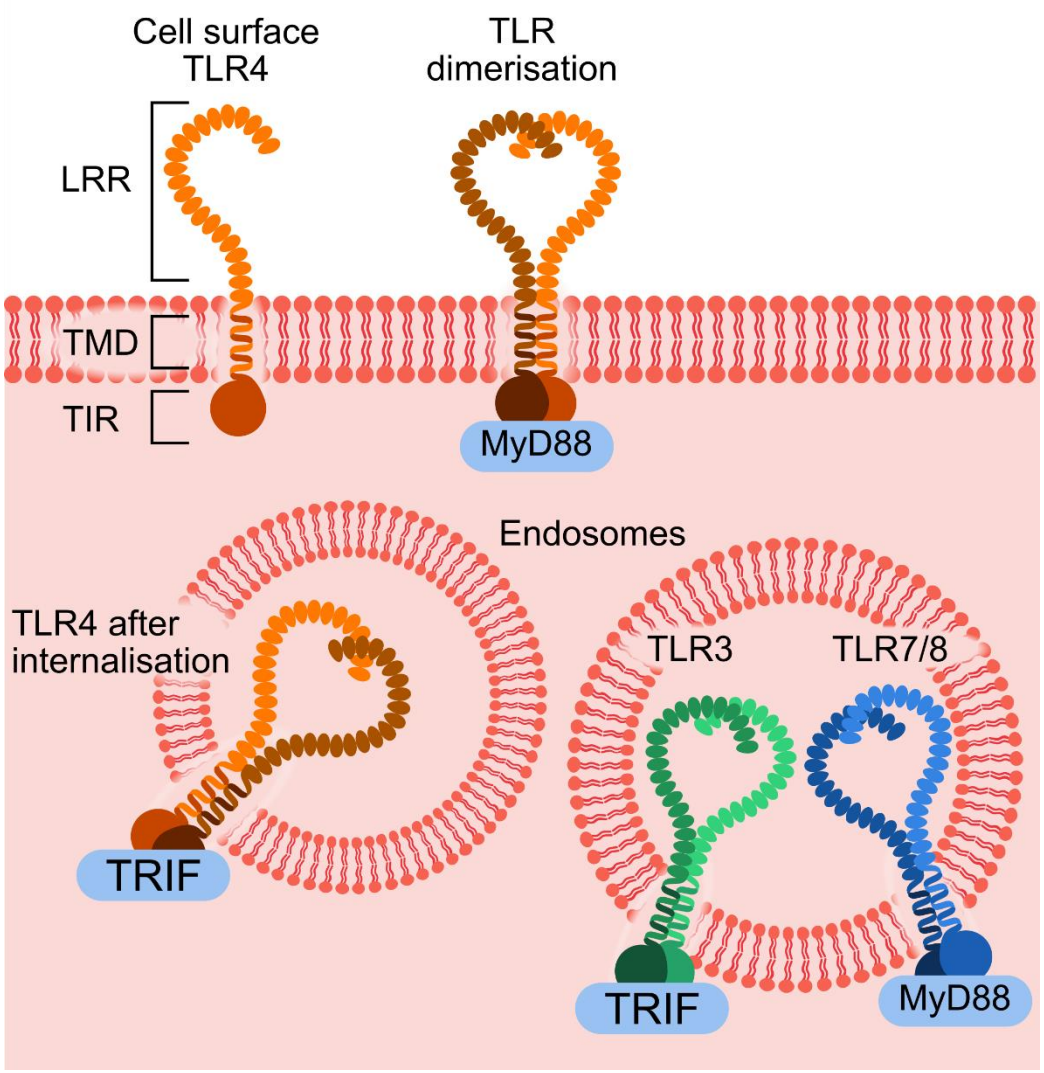

1.6 Cytokines, drivers of inflammation

As mentioned previously, cytokines play a key role in the generation of inflammation, and loss of cytokine regulation can lead to systemic inflammatory responses that range from damaging to fatal for the host. Cytokines can be defined as small, secreted proteins that regulate the proliferation and activation of immune cells but may also act on non-immune cells. Often, the actions of cytokines are pleiotropic, with one cytokine acting upon multiple cell types, and multiple cell types secreting a particular cytokine. Alongside this, there is a degree of redundancy in cytokines, with different cytokines eliciting similar effects. Other than helper T cells, Mφ and DCs are the main producers of cytokines *(Zhang, and An, 2007)*. When discussing the propagation of inflammation, IL-6 plays an important role as a pro-inflammatory cytokine, and is thus implicated in a variety of inflammatory conditions including rheumatoid arthritis *(Pandolfi, et al., 2020)*, cancer *(Chang, et al., 2013; Kumari, et al, 2016)*, inflammatory bowel disease *(Schreiber, et al.,2021),* asthma *(Jevnikar, et al., 2019)*, vascular disease *(Kang, et al., 2021),* and namely covid-19 *(Zizzo, et al., 2022; Zhao, 2022; Wang, et al., 2022).*

Cytokines may also be grouped into two categories on the basis of the secretory pathway used to facilitate their release into the extracellular space. Most cytokines utilise the canonical pathway of protein secretion involving the endoplasmic reticulum (ER), golgi body, and secretory vesicles to achieve exocytosis. These cytokines share a common feature with many secreted proteins of an N-terminal signal peptide, or “leader” peptide which traffics the translated protein to the ER to initiate this process. Contrasting with this are the so-called “leaderless” cytokines that lack this signal peptide and thus must achieve release from the cells via alternative, “non-canonical” pathways *(Sitia, and Rubartelli, 2020).* These cytokines include the IL-1 family members, IL-1α, IL-1β, and IL-18, and may utilise pores, shedding of microvesicles, or pyroptosis (programmed pro-inflammatory cell death) to escape the cytosol. IL-1 also presents another deviation from the general schema of cytokines, as it resides as pro-protein (Pro-IL-1α, Pro-IL-1β) in the cytoplasm after transcription, requiring proteolytic cleavage to form the mature IL-1 cytokines *(Lopez-Castejon, and Brough, 2011).*

Alongside IL-1α and IL-1β, key cytokines involved in the development of cytokine storm include IL-6, IL-12, TNF-α, IL-8 and MIP-1α. These cytokines have been implicated in a systemic inflammatory response after trauma or surgery *(Mokart, et al., 2002; Hildebrand, et al., 2005)*, with IL-6 and IL-12 particularly important in the development of sepsis *(Gouel-Chéron, et al., 2012; Pierrakos, and Vincent, 2010; Vivas, et al., 2021; Hensler, et al., 1998; Frimpong, et al., 2022)*. Whilst we discuss cytokines in broad terms here, greater detail is provided later in the relevant chapters.

The pro-inflammatory action of IL-6 includes induction of the acute phase proteins in the liver such as fibrinogen, C-reactive protein, haptoglobin, and serum amyloid A. These proteins can be considered part of the complement system and are raised for 24-48 hours after infection *(Schmidt-Arras, and Rose-John, 2016)*. IL-6 also contributes to the transition from acute inflammation to chronic inflammation through the recruitment of immune cells. Cells present at the site of inflammation during the acute phase include neutrophils and monocytes, whereas sustained IL-6 signalling attracts Mφ and lymphocytes by causing increased release of Monocyte chemoattractant protein-1 (MCP-1) and (in humans) IL-8 from the local cells. this perpetuates the immune activity and causes the inflammation to become chronic *(Ryan, and Majno, 1977; Gabay, 2006)*. Other effects of IL-6 on lymphocytes include promoting the expansion of plasma B cells, and induction of increased immunoglobulin production, as well as stimulating CD4+ T cell differentiation *(Dienz, and Rincon, 2008; Maeda, et al., 2010).* IL-6 also shifts the balance of TH17 to Treg cells by promoting TH17 differentiation from naïve T cells in the presence of TGF-β, whilst inhibiting Treg differentiation *(Kimura, and Kishimoto, 2010).*

During SARS-Cov-2 infection, high levels of IL-6 have been correlated with poor patient prognosis, and can predict the severity of disease *(Santa Cruz, et al., 2021; Chen, et al., 2020).* Furthermore, inhibition of IL-6, by blocking the IL-6 receptor using a monoclonal antibody such as tocilizumab or sarilumab, improved mortality and increased the number of organ support free-days of patients *(Rubin, et al., 2021).*

IL-12 is also an important cytokine in the response to a viral infection. Mainly produced by Mφ, DCs, and B cells, IL-12 functions as a promoter of the TH1 response through the differentiation of naïve T cells into T helper 1 cells (Trinchieri, 1998; Ma, et al., 2015). To further polarise the immune response towards the

resolution of intracellular pathogen infection, IL-12 can inhibit the differentiation of TH2 cells through downregulation of GATA3 *(Usui, et al., 2006).* The anti-viral effects of IL-12 are seen as an increase in IFNy and TNFα production from activated T cells and NK cells *(Zheng, et al., 2016).* IL-12 has been implicated in disease severity of SARS-CoV-2 infection with high serum levels of the cytokine found in those patients experiencing severe covid-19 *(Tjan, et al., 2021).* Through the promotion of T cells and thus an increase in Mφ-activating IFNy, IL-12 can create a feedback loop of persistent immune cell activation that is characteristic of cytokine storm *(Costela-Ruiz, et al., 2020).*

The mechanisms of IL-6 and IL-12 action are discussed in greater detail in chapter 3.

1.7 Treating inflammation (in viral sepsis)

Clearly, control of inflammatory processes (or lack thereof) is a determinant of outcomes in both viral infections, cytokine storm, and subsequent progression to sepsis. Interlinked with inflammation and sepsis is coagulopathy, which has been observed in both SARS-CoV-2 sepsis and non-viral sepsis *(Savla, et al., 2021).* Cytokine signalling has pleiotropic effects on many cell types including vascular endothelial cells that triggers the release of the integral membrane protein tissue factor (TF). TF can initiate the production of thrombin and fibrinogen, leading to platelet activation and thrombosis *(Butenas, et al., 2009).* As sepsis and cytokine storm are systemic, this leads to disseminated intervascular coagulation and subsequently tissue damage and death. Thus, it is clear that controlling inflammation lies at the heart of much sepsis pathology *(Simmons, and Pittet, 2015).* Currently, the treatment options used to quell inflammation include the commonly used non-steroidal anti-inflammatory drugs NSAIDs such as ibuprofen or naproxen. NSAIDs exert their effects through inhibition of cyclooxygenase enzymes COX-1 and COX-2 required for the synthesis of prostanoids from arachidonic acid, with some studies indicating that the level of prostanoids like prostaglandin E_2 and thromboxane A_2 are increased in the blood of SARS-CoV-2 infected patients vs healthy controls *(Perico, et al., 2023).* However, many of these NSAIDs are non-selective for COX-2, which is the enzyme involved in the mediation of pain and inflammation. In the process of inhibiting COX-2, COX-1 inhibition can have detrimental effects on the ability to maintain gastrointestinal homeostasis. Prolonged

NSAID use may lead to ulcers, dyspepsia, and damage to the lining of the gastrointestinal tract *(Choi, et al., 2009).*

Alternatively, biologic treatments such a monoclonal antibody (mAb) have been trialled for covid-19 treatment, notably tocilizumab and sarilumab which target the IL-6R and block the binding of IL-6 *(Abidi, et al., 2022).* Other mAbs, have been approved for use in mild severity covid-19 cases, such as casirivimab and imdevimab which target the spike protein of the SARS-CoV-2 virion, restricting binding to ACE2 and thus viral entry. Treatment with these mAbs have decreased the chances of hospitalisation in high-risk patients *(Mawazi, et al., 2022).*

Both of the above treatments are typically used in mild to moderate cases of SARS-CoV-2 infection but are not appropriate for the treatment of severe disease. As the over-active immune system perpetuates a systemic pro-inflammatory response, the focus of drug treatment shifts from controlling viral replication and mild inflammation to avoiding sceptic shock and organ failure by strong downregulation of the immune system *(D'Elia, et al., 2013).* To achieve this, corticosteroid drugs have been used, namely dexamethasone **(Fig. 5).** Around 25 more potent than hydrocortisone, and around 6 times more potent than prednisolone, dexamethasone is a strong immunosuppressant drug that has displayed effective reductions in patient mortality when administered to those in late-stage SARS-CoV-2 infection as demonstrated in the RECOVERY trial *(RECOVERY, 2021).* Dexamethasone exerts its actions through binding to the ubiquitously expressed glucocorticoid receptor (GR), inducing a conformational change and allowing dissociation of chaperone proteins that cement GR in the cytoplasm. After translocation of the complex to the nucleus GR can bind to glucocorticoid response elements (GRE) in DNA and elicit either transrepression, or transactivation, affecting gene transcription. Direct repression of genes that encode pro-inflammatory proteins such as cytokines can reduce the magnitude of the immune response effectively *(King, et al., 2013).* This process is independent of any action on the machinery involved in protein synthesis. To further balance the immune system, transactivation of genes that encode anti-inflammatory proteins may occur. GR-corticosteroid complexes have also been implicated in the inhibition of NF-kB and AP-1 through a process known as tethering. As transcription factors, both NF-kB and AP-1 can be induced by stimuli such as TLR signalling, IL-1R signalling and T and B cell signalling to translocate to the nucleus and initiate binding of genes. Particularly, NF-kB and AP-1 are involved in the transcriptional

regulation of many pro-inflammatory genes, and thus inhibition of these factors can reduce inflammation *(Liu, et al., 2017).* The ligand bound GR complex can exert transrepression by tethering to the DNA bound transcription factors and abrogating their transcriptional activity *(De Bosscher, et al., 2003).* Furthermore, the GR-Corticosteroid complex can promote the binding of IKKβ (the inhibitor of NF-kB) to the transcription factor and trap it within the cytoplasm *(Bekhbat, et al., 2017).*

Despite being recommended for many inflammatory conditions, corticosteroid drugs are not without their drawbacks. Chiefly, the broad immunosuppression that is imparted upon the patient. Whilst this does achieve the goals of reducing the inflammatory response, it acts as an immunosuppressive sledgehammer rather than a selective immunomodulator. Immediate side effects of reduced wound healing time, and susceptibility to infection with other pathogens are noted *(Youssef, et al., 2016)* (although this is debated in covid-19 context *(Ritter, et al., 2021)*), with long term use resulting in skin thinning, gastrointestinal issues, and changes in mood/mental health. One mechanistic effect of long-term dexamethasone use is the reduction in total T cells. This effect is achieved through a number of mechanisms including a repression of CD28 co-stimulation reducing differentiation of Naïve T cells, as well as depletion of peripheral blood lymphocytes (*Aston, et al., 2019; Giles, et al., 2018).* This side effect is concerning as in the severe cases of SARS-CoV-2 where dexamethasone would be administered, lymphopenia was also observed. Following the pro-inflammatory stage of SARS-CoV-2 infection there has been observed an immunosuppressive phase characterised by lymphopenia affecting CD4+ and CD8+ T cells. Lymphopenia has been shown to be present in greater than 80% of patients admitted to hospital and those suffering fatal complications of disease experience increased immune cell depletion over time *(Liu, et al., 2020).* Thus, the degree of immune cell depletion correlates with severity of disease *(Tavakolpour, et al., 2020; Huang, and Pranata, 2020; Xiang, et al., 2021).*

The effect of dexamethasone on pyroptosis and subsequent release of IL-1 cytokines is a matter of debate as there have been few studies directly investigating this interaction and these provide contrasting arguments. Some evidence provided during experiments examining dexamethasone induced skeletal muscle atrophy supports dexamethasone as an instigator of pyroptosis. Alone, the glucocorticoid induced pyroptosis and atrophy of mytotubes, whereas knockdown of the protein gasdermin D and NLRP3 inhibited this effect, indicating involvement of the

inflammasome in glucocorticoid pyroptosis *(Tan, et al., 2022; Fappi, et al., 2019).* Other studies, even those produced by the same lab, have claimed that dexamethasone can protect against this effect by decreasing expression of NLRP3/caspase-1 dependent pyroptosis during treatment of corneal alkali burns *(Tan, et al., 2022)*. Potentially, long term GC exposure can elicit induction of the inflammasome, whereas the short-term immediate effects of dexamethasone may control this effect. Therefore, it is clear that whilst an effective emergency treatment for hyperinflammatory diseases, the effect of dexamethasone may vary and is not without drawbacks. Ideally, the ability to selectively reduce some aspects of the inflammatory response, whilst retaining the ability of the immune system to respond to viral infections is the desired characteristics of a potential SARS-CoV-2 treatment. To this end, we introduce the non-ionic surfactant vesicle.

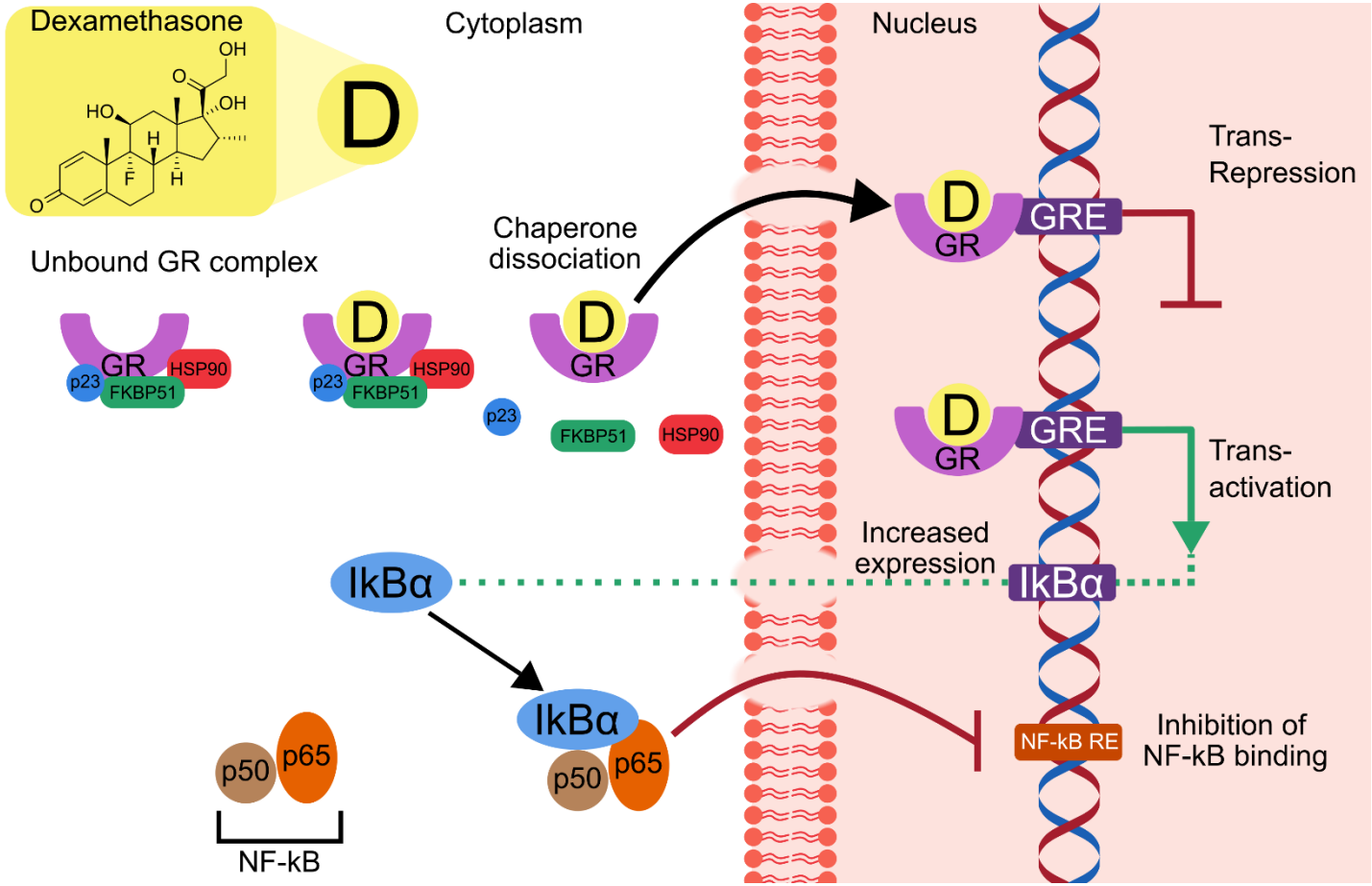

Figure 5. Mechanisms of dexamethasone action. *Dexamethasone binds to the glucocorticoid receptor (GR) in the cytoplasm. When unbound, GR is held in the cytoplasm in a high ligand-affinity state by a complex of chaperone proteins including HSP90, p23, and FKBP51. Once bound by a either an endogenous glucocorticoid such as cortisol, or a synthetic glucocorticoid such as dexamethasone, the chaperone proteins dissociate and the ligand-GR complex quickly translocates to the nucleus via a nuclear pore. Once inside, the complex will bind glucocorticoid receptor response elements (GRE) and cause either transactivation or transrepression to cause an immunosuppressive effect. Transactivation may include increasing expression of genes for anti-inflammatory cytokines such as IL-10 or TGF-β, whereas transrepression may inhibit expression of pro-inflammatory cytokines such as IL-6 and IL-1. Dexamethasone may directly interact with transcription factors such as NF-kB by tethering or through interaction with IkBα, trapping NF-kB in the cytoplasm.*

1.8 NISV and their applications

Non-ionic surfactant vesicles (NISV, alternatively termed niosomes) are nano to micro scale vesicles that are structurally similar to liposomes but utilise single-tailed synthetic surfactants to form bilayer vesicles rather than lipids **(Fig. 6)**. NISV were first developed in the cosmetic industry at the L'Oreal laboratories in the 70's and then patented as niosomes in the late 80's as a formulation of "lipid spherules" that can entrap cosmetic or pharmaceutical compounds and protect them from external conditions *(Handjani, et al., 1989).* Due to their basis in synthetic surfactants rather than phospholipids, NISV have a number of advantages over liposomes, chiefly being their ability to resist oxidation and high temperatures to a greater degree, increasing their stability and ease of storage. Furthermore, NISV are attractive to industry-scale manufacturing as surfactants are generally cheaper than phospholipids and production methods can avoid the use of pharmaceutically unacceptable solvents *(Vora and Jain, 1998).*

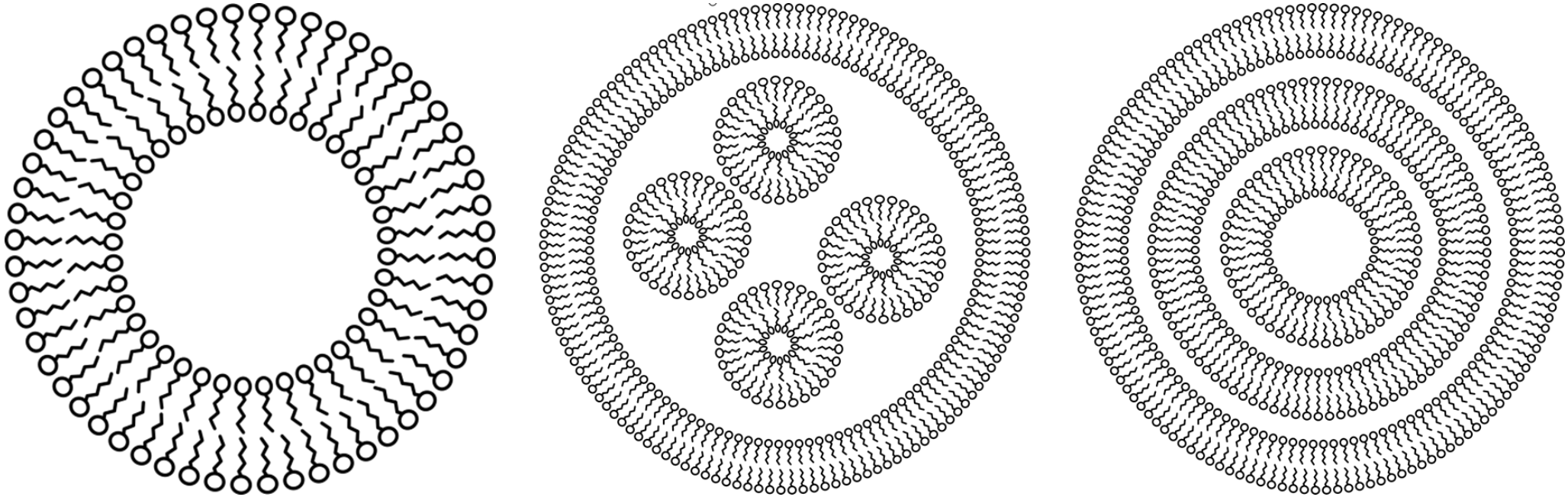

Figure 6: Possible physical structures of NISV: *NISV are comprised of a surfactant bilayer which self-assembles due to the polar nature of the surfactant monomer. Hydrophilic head groups remain on the surface of the membrane, whereas the hydrophobic tail groups partition themselves within the bilayer, generating an intermembrane region where hydrophobic drugs may be loaded. A large aqueous core may be present in unilamellar NISV (Left) which allows loading of water-soluble payloads. In multilamellar NISV, (centre, right) the aqueous core may contain multiple smaller NISV (centre, also known as multivesicular vesicles) or concentric layers of NISV (right). The variety in NISV configuration provides options for loading and delivery tailored to each payload.*

Typically, NISV are comprised of one or multiple surfactant bilayers separated by an aqueous partition creating a hydrophobic area inside the bilayer and containing a hollow aqueous hydrophillic core. The presence of a single bilayer (unilamellar) or multiple bilayers (multilamellar) is influenced mostly through production method and components used lending itself to alternative loading options *(Bailie, et al., 1985; Kazi, et al., 2010).* Vesicles may be produced using a range of components but conventional formulations utilise 3 key molecules: the main surfactant monomer (monopalmitoyl glycerol (MPG), 1-O-hexadecyl-sn-glycerol (HG), Span 60 etc.), a stabilising sterol such as cholesterol or its derivatives, and a charged amphiphilic surfactant such as dicetyl phosphate (DCP) for negatively charged vesicles or stearylamine (SA) for positively charged vesicles.

The focus of this thesis will be NISV comprised of MPG, Cholesterol, and DCP. These components are combined in a defined molar ratio of 5:4:1 of MPG:Cholesterol:DCP *(Brewer and Alexander, 1992).* NISV can be prepared using a variety of methods. The two main methods described in this thesis are the Melt method and microfluidic assembly. Both of these methods rely on the self-assembling nature of these components upon hydration described initially in liposomes by Dr Alec Bangham in 1965 *(Bangham, Standish, and Watkins, 1965).* They key principle of NISV formation is the hydration of a solution containing either dissolved or melted vesicle components, upon which rafts comprised of NISV membrane form. After agitation either by mechanical vortexing or sonication, or microfluidic mixing, these rafts fold into spheroid shapes due to the unfavourable interactions with the aqueous medium resulting in repulsion and closing of the spheroid. As the production method and parameters vary, fine-tuning of NISV size and degree of lamellarity is achievable, resulting in NISV that may be small (~100nm), monodisperse, and unilamellar as produced in the microfluidic method, to large (~1500-2000nm) multilamellar vesicles as produced in the melt method. Furthermore, NISV can be modified to accommodate various payloads, such as antibodies, drugs, or RNA for the enhanced delivery of these compounds. For example, NISV modified by the addition of bile salts to the membrane (Bilosomes) have been shown to resist degradation when delivered orally *(Conacher, et al., 2001)*. More recently they have been shown to enhance the efficacy of entrapped antibiotics Levofloxacin and Doxycycline compared to free drug during in vivo *B.*

pseudomallei infection by reducing mortality as well as antibiotic and infection associated weight loss *(D'Elia, et al., 2019)*. Furthermore, modification to the surface of the NISV membrane have resulted in the ability to target NISV and their respective payload to various receptors on target tissues such as NISV surface-modified with glucosamine trafficking to the Glut1 receptor on the blood brain barrier, allowing transmission to the brain of NISV and entrapped antibody via a clathrin-independent, dynamin-dependent endocytic pathway to treat Venezuelan Equine Encephalitic Virus (VEEV) *(Woods, et al., 2020).* Other uses of NISV have also included improving the bioavailability of poorly soluble drugs *in vivo* such as griseofulvin and acyclovir by protecting them from degradation. If poorly soluble in water, drugs may be solubilised in an organic solvent such as DMSO, ethanol, etc., which may be combined with an aqueous buffer and the NISV components via microfluidics, thin film hydration or other appropriate methodology. Residual solvent may be removed using filtration columns or tangential flow filtration, leaving the drug entrapped within the NISV*(Attia, et al., 2007; Jadon, et al., 2009)*. Other applications of NISV have included delivery of DNA in vaccines *(Perrie, et al., 2004)*, and siRNA for cancer therapies *(Obeid, et al., 2017).*

As mentioned previously, the original description of NISV represented the vesicles as protecting entrapped compound from outside conditions and such is true during their applications of drug delivery or incorporation into vaccines. For example, previously NISV have been demonstrated to enhance the immune response to BSA compared to free BSA, and this effect was dependent on the BSA being entrapped within vesicles, not mixed amongst them *(Brewer, and Alexander, 1992).* Furthermore, *in vivo* NISV entrapping HSV-2 antigen have displayed the ability to enhance IgG2a, IL-2, and IFNy levels and afford partial protection in mice against HSV-2 challenge *(Mohamedi, et al., 2000).* The adjuvant abilities of NISV have also been demonstrated using *Toxoplasma gondii,* with soluble tachyzoite antigen (STAg) entrapped within NISV increasing survival of mouse pups when their mother mice were vaccinated with this formulation compared to STAg alone *(Roberts, et al., 1994).*

The NISV formulation described throughout this thesis was first patented as a therapeutic compound in 1997 *(Roberts, et al., 1997).* Before this, NISV had been identified as ideal drug carriers, but had gained interest as a potential therapy of their own - with no entrapped payload. The patent for NISV as a therapeutic

describes the problem with anti-inflammatory treatments of the time, stating that whilst the immune system often initiates inflammatory processes in a pleiotropic manner (many different cytokines being produced by a variety of cells), therapies targeted only single cytokines. This effect was achieved often by direct interaction with the cytokine, or by blocking the receptor from receiving the cytokine as a ligand. As mentioned before, cytokine storm and the multi-faceted processes that generate inflammation cannot be effectively quelled by targeting a single mediator, and thus NISV were proposed as a pleiotropically acting anti-inflammatory. Evidence supplied in the patent that supports this claim was fairly broad, including; reduction in weight loss in mouse models of cachexia induced either by the parasite *Toxoplasma gondii (T.gondii)* or by the peptide FK-565; reduction in the production of pro-inflammatory cytokines TNFα, IL-1, IL-6, IL-8, and IL-12 in J774 macrophages, murine peritoneal macrophages, or Human PBLs; prophylactic dosing of NISV conferring anti-inflammatory effects against LPS challenge for up to 14 days. The size of NISV as a contributing factor towards the anti-inflammatory effects were also investigated, utilising extrusion through polycarbonate membranes and sonication to achieve small 100 and 200nm NISV, demonstrating that larger NISV (400-800nm) NISV were more effective immunomodulators. Whilst NISV were chiefly demonstrated as a promising therapy of their own, their merit as an adjuvant or adjunct treatment was also displayed by the reduction of *T.gondii* cysts in the brains of mice after immunisation with STAg entrapped within NISV. Thus, NISV demonstrate great potential as an immunomodulatory therapy and have continued to be modified and investigated since this initial demonstration.

Work in our laboratory has continually displayed that NISV can effectively modulate the levels of key pro-inflammatory cytokines such as IL-6 in the context of TLR2, TLR3, and TLR4 stimulation. Whilst this work focused mainly on the anti-inflammatory effect of NISV in comparison to their phospholipid-based counterpart liposomes *(McGahon, 2021),* this study aims to explore the notion that NISV possesses both immune enhancing and inflammation-reducing properties in the context of a ssRNA viral infections using TLR7 and TLR8 ligands as a proxy for inflammation induced as a response to an ssRNA virus.

1.9 Aims and Objectives

The overall aim of the studies described herein is to determine to what extent NISV are capable of modulating inflammation induced by activation of the viral ssRNA sensing PRR, TLR7 and TLR8 and to compare this with the effects of dexamethasone. Specific objectives are:

i. To establish a model of ssRNA viral infection using synthetic TLR-specific ligands and bone marrow derived macrophages. Furthermore, it is an aim to determine the effect of large melt method NISV on sentinel cytokines that are implicated in the generation of the inflammatory response to viral ssRNA as an indicator of a wider immune response. Alongside this a further aim is to compare NISV to a conventional anti-inflammatory treatment, dexamethasone. To achieve this, a combination of ELISA assay for cytokine measurements, and viability assays such as alamarBlue to generate EC50 and IC50 curves will be used for non-toxic concentrations of both NISV and dexamethasone. A further aim is to utilise multiplex cytometric bead arrays to provide an overview of multiple cytokines involved in the inflammatory response.

ii. To determine whether NISV produced using the melt method can be modified post-production using extrusion through polycarbonate membranes to yield vesicles of a given size. The aim is to produce small NISV comparable to those generated using microfluidic technologies such as the NanoAssemblr platform. By characterizing the therapeutic effects of these NISV at various sizes, any size dependent differences in NISV immunomodulation will be revealed in various TLR stimulated BMDM. IL-6 and IL-12 in the first instance will be used as indicators of initial effects, before expanding this analysis to a wider milieu of inflammation-associated cytokines.

iii. Survey the metabolic effects of both NISV and dexamethasone on TLR7 and TLR8 stimulated BMDM using LC-MS. An untargeted metabolomics approach will be used to interrogate a wide array of metabolites by matching MS peaks to a curated list of authentic standards and online databases of compounds. The effect of both treatments on energy generation pathways such as glycolysis and the TCA cycle will be investigated, alongside

highlighting the most significant metabolites that are driving variance between experimental groups using multivariate analysis such as OPLS-DA.

iv. To perform transcriptomic analysis on TLR7 and TLR8 stimulated BMDM treated with large melt method NISV or dexamethasone to determine transcription-level differences in pathways affected by these therapies. By investigating pathways and transcription factors associated with regulation of pro-inflammatory gene expression, such as TLR signalling, cytokine/chemokines, NF-kB activity, and NLRP3 activation, the aim is to determine the mechanism by which NISV exert their immunomodulatory effect and highlight areas where NISV display increased anti-inflammatory efficacy when compared with dexamethasone.

2 Materials and Methods

This section contains the general methods used throughout this thesis, with specific deviations from this schema detailed in the relevant chapter.

2.1 Materials

DMEM (Thermo Fisher Scientific, Waltham, MA, USA)

RPMI 1690x (Corning, Corning, NY, USA

FCS (Thermo Fisher Scientific, Waltham, MA, USA)

Trypan blue viability dye (Thermo Fisher Scientific, Waltham, MA, USA)

L-glutamine (Thermo Fisher Scientific, Waltham, MA, USA)

Penicillin-Streptomycin solution (Thermo Fisher Scientific, Waltham, MA, USA)

L929-cells (European Collection of Authenticated Cell Cultures, Salisbury, UK)

PBS (Thermo Fisher Scientific, Waltham, MA, USA)

FACS flow (Thermo Fisher Scientific, Waltham, MA, USA)

Flow cytometry Antibodies (Thermo Fisher Scientific, Waltham, MA, USA)

Monopalmitoyl Glycerol (Sigma Aldrich, St Louis, MO, USA)

Cholesterol (Sigma Aldrich, St Louis, MO, USA)

Dicetyl Phosphate (Sigma Aldrich, St Louis, MO, USA)

Ethanol (Thermo Fisher Scientific, Waltham, MA, USA)

Chloroform (Thermo Fisher Scientific, Waltham, MA, USA)

Methanol (Thermo Fisher Scientific, Waltham, MA, USA)

LPS (Sigma Aldrich, St Louis, MO, USA)

Poly(I:C) (Sigma Aldrich, St Louis, MO, USA)

Imiquimod (Invivogen, San Diego, CA, USA)

TL8-506 (Invivogen, San Diego, CA, USA)

Dexamethasone (Sigma Aldrich, St Louis, MO, USA)

AlamarBlue (Bio-Rad, Hercules, CA, USA)

ELISA Antibodies (Thermo Fisher Scientific, Waltham, MA, USA)

ELISA Recombinant cytokine standard (Biolegend, San Diego, CA, USA)

ELISA PNPP substrate (Merck, Darmstadt, Germany)

Legendplex Cytometric bead arrays (Biolegend, San Diego, CA, USA)

Rneasy mini+ kits (Qiagen, Hilden, Germany)

2.2 Murine stem cell isolation and differentiation into Bone marrow-derived macrophages

Animals were bred under barrier conditions at the University of Strathclyde Biological Procedures unit, Glasgow, UK. 8–12-week-old male BALB/c mice were sacrificed according to schedule 1 humane methods of killing using cervical dislocation set out in the Animals (Scientific Procedures) Act 1986 under project licence PP7699097. Femur and tibia were removed and stored in a sterile bijou until use, typically <1hr. In a sterile biological safety cabinet, the epiphyses of each bone were removed, and bone marrow flushed out using Dulbecco's modified eagle medium (DMEM) with a fine gauge needle and syringe. This was collected in a centrifuge tube fitted with a 40µm cell strainer, which was then centrifuged at 427G for 5 minutes. The liquid component was discarded, and cells were resuspended in 40ml of Mφ media (2% L-glutamine, 2% Penicillin-streptomycin, 20% Foetal calf serum (FCS), 20% L929-cell conditioned media, in DMEM) and 10ml added to 4 petri dishes. These dishes were incubated at 37ºC and 5% CO_2 (Day 0). On day 3, 10ml of Mφ media was added to each dish, and on day 7, 15ml of spent media was removed and replaced with fresh Mφ media. On Day 10, cells were examined by light microscopy to confirm phenotype and adherence after initial determination of identity via flow cytometry, Media was removed and 10ml of chilled PBS added to each plate. After 5 minutes, cells were harvested with a plastic cell scraper and centrifuged at 427G for 5 minutes. Cell pellet was resuspended in complete RPMI 1690x (1% L-glutamine, 1% Penicillin-streptomycin, 10% FCS, in RPMI 1690x). An aliquot of cells was incubated with 0.2% Trypan Blue solution and counted using a haemocytometer. >80% cell viability was

regularly observed. Cells were then added to an appropriate multi-well plate at 1x10^{6}cells/ml and stored in a sterile incubator at 37ºC and 5% CO_2.

2.3 Macrophage confirmation by flow cytometry

Cells seeded at 2x10^{6}cells/ml in 500µl in a 24-well plate were given either 500µl of media or 500µl of 1.5µg/ml LPS. After 24hrs, all media was removed and 1ml chilled PBS added to each well. After 5 minutes, cells were scraped using a pipette tip and added to 1.5ml microcentrifuge tubes placed on ice. An aliquot of cells was killed by placing on a heat block at 95ºC for 5 minutes. Cells were then stained with a live/dead fixable violet cell viability dye and kept on ice in the dark for 30 minutes. Cells were then centrifuged at 300G for 6 minutes and supernatant removed. 1ml of FACS flow was added to each tube and centrifuged as before to wash. Supernatant was removed and cells were stained with a 1/100 dilution of live/dead fixable violet viability dye, anti-CD11b-APC, anti-F4/80-Super Bright 600, anti-CD11c-FITC, and anti-CD86-PE-cy7. Single stains and fluorescence-minus-one samples were also prepared. After another 30-minute incubation on ice in the dark, 1ml of FACS flow was added to each tube and wash step performed as before. Finally, cells were resuspended in 1ml FACS flow and kept at 4ºC in the dark until use. Flow cytometry was performed on an attune NXT acoustic focusing flow cytometer (Thermofisher Scientific, Waltham, MA, USA). A minimum of 30,000 events was recorded for each sample.

2.4 NISV production

Non-Ionic Surfactant Vesicles (NISV) were produced using two main methods, namely the "melt method" and microfluidization. Prior to both production techniques, vesicle components were weighed out and added to either a glass test tube, or glass universal. The components for both methods were the surfactant monopalmitoyl glycerol (DL-α palmitin, MPG), the sterol cholesterol, and the negatively charged surfactant dicetyl phosphate (DCP). These components were combined in the molar ratio of 5:4:1 of MPG:Cholesterol:DCP. For melt method NISV, the components were placed in an oven set to 120ºC until molten, then vortexed for 2 minutes after adding 5ml room temperature PBS.

For microfluidic production of NISV, a benchtop NanoAssemblr Ignite (Precision Nanosystems, Vancouver BC, Canada) was used. Vesicle components were

weighed out as in the melt method and placed in a glass universal. 5ml ethanol (>99%) was added to the NISV components which was then sealed and heated to 60ºC using a water bath. A NanoAssemblr chip was primed following the manufacturer's guidance using PBS as the aqueous phase and ethanol as the solvent phase. Once NISV components were fully solubilised, 3ml of the NISV-Ethanol solution was added to a syringe and placed in the NanoAssemblr, alongside a syringe containing 9ml PBS. Both phases were mixed in a 3:1 ratio of aqueous to solvent phase at a flow rate of 12ml/min. 0.15ml was collected as waste at both the start and end of the production run. Free solvent was removed from the sample using a Vivaspin 20 centrifugal concentrator column with a molecular weight cut-off of 300,000.

For extruded NISV, ranging from around 100nm to 2000nm, NISV were produced as in the melt method. After formation of the NISV stock, the solution was heated to 60ºC using a water bath and then 1ml was extruded through the appropriate polycarbonate membrane installed in a hand mini extruder (Avanti Polar Lipids, Alabaster, AL, USA). This process was performed stepwise, with decreasing pore size to achieve the desired size of vesicle.

NISV size, polydispersity, and charge were measured by dynamic light scattering using a Zetasizer Nano (Malvern Panalytical, Malvern, UK). Samples were diluted appropriately according to manufacturer's guidance to achieve accurate results.

2.5 Cell stimulation

Macrophages were stimulated for 24 hours with the appropriate compound prior to removal of supernatants for analysis. For stimulation of TLR3, TLR4, TLR7, and TLR8, the compounds Poly(I:C), LPS, Imiquimod, and TL8-506 were used respectively. NISV or Dexamethasone was also added at this time to allow co-incubation for 24hrs. All effective concentrations of each compound were determined by non-linear regression for the generation of EC90/IC90 values paired with user experience of the assays. Microplates were stored in a sterile incubator at 37ºC and 5% CO_2 until use.

2.6 AlamarBlue assay

An AlamarBlue assay was performed to determine cell viability/proliferation. After supernatants were removed for use in ELISA, 10% v/v alamarBlue reagent was

added to each well containing BMDM. Plates were incubated in the dark for 4-5hrs, or until sufficient colour change had occurred as assessed by visual inspection. Absorbance was then read using a Spectromax 160x spectrophotometer equipped with Softmax Pro 7 software (Molecular Devices, San Jose, CA, USA). Absorbance values were used to calculate reduction of blue resazurin salt to the red resorufin compound as detailed in the assay manufacturer's instructions.

2.7 ELISA

ELISA was performed on cell supernatants using matched antibody pairs (BD Biosciences, San Jose, CA, USA). ELISA plates were coated with 50ul 1µg/ml of capture antibody, sealed, and stored overnight at 4ºC. Upon use, plates were washed with wash buffer (1% TWEEN in PBS) and patted dry onto paper towels. 200µl blocking buffer (10% FCS in PBS) was added to each well and plates were sealed and incubated at 37ºC for 1 hour. Wash step was repeated as before, and a standard curve was prepared by diluting recombinant ELISA standard for the appropriate cytokine 1:2 with blocking buffer. 30µl of each standard curve concentration was added to wells in duplicate. Cell supernatants were diluted 1:2 with blocking buffer and 30ul added to each sample well. Plates were sealed and incubated at 37ºC for 2 hours. Plates were then washed as before and 50µl 1/1000 dilution in blocking buffer of biotin-conjugated detection antibody was added to each well. Plates were sealed and incubated as before for 1 hour. Plates were then washed as before and 50µl 1/1000 of AKP-streptavidin was added to each well. Plates were sealed and incubated as before for 1 hour. Plates were washed one final time and 50µl 1mg/ml of PNPP substrate was added to each well. Plates were incubated in the dark at room temperature until a sufficient colour change in the standard curve was detected visually and the reaction stopped with 3M sodium hydroxide solution. Plates were then read at 405nm using a spectromax 160x spectrophotometer equipped with Softmax Pro & software.

2.8 Cytometric Bead array

Legendplex multi-analyte bead arrays were used for the simultaneous detection of cytokines in cell supernatants. Assays were performed using filter plates as per the manufacturer's recommendations. Briefly, each well of the filter plate was pre-wet with 100µl of wash buffer for 1 minute and then removed by brief application of a vacuum until well drained. 25µl of assay buffer was added to all wells, with 25µl of

either pre-prepared standard or sample supernatants also added. Cytometric beads were well-mixed by vortex and 25µl added to each well for a total volume of 75µl. Filter plates were then sealed, placed on a plate shaker in the dark, and incubated for 2hrs at room temperature with an oscillation of 500rpm. Filter plates were then drained as before using the vacuum manifold, followed by the addition of 200µl of wash buffer to each well and a repeat of the vacuum draining step. 25µl of detection antibodies were added to each well and the filter plates sealed and incubated as before for 1hr. 25µl of streptavidin-PE was added to each well and the filter plates incubated as before for 30 minutes. Plates was then washed twice as before, and beads were resuspended by the addition of 200µl assay buffer and shaking on the plate reader for 1 minute. Filter plates were then read on an Attune NXT flow cytometer using the autosampler function. Cytokine levels were quantified from raw flow cytometry data using the LEGENDplex software provided as a cloud-based application by the manufacturer of the kit. Populations and fluorescent peaks were gated automatically and then refined by manual adjustment.

2.9 RNA extraction and quality control

RNA was extracted from murine bone marrow-derived macrophages using a Qiagen Rneasy mini kit. Briefly, cells were plated in a 96-well plate with 100µl of cells at $1x10^6$ cells/ml per well. Cells were stimulated with either 1.5µg/ml of Imiquimod, 1.3µg/ml TL8-506. Cells were also treated with either 1.2mM of Melt Method NISV, or 1.67µM of Dexamethasone. After 24hr incubation at 37ºC and 5% CO_2, all supernatant was removed from cells and Rneasy mini kit was used as per the manufacturer's recommendations with some deviations. 100µl cold buffer RLT was added to each well and cells were scraped using a pipette tip. Cells were collected and added to a Qiashredder column placed in a 2ml collection tube which was centrifuged at maximum speed for 2 minutes. 70% ethanol was added to the flow through and 700µl of this mixture was added to a RNeasy spin column placed in a new 2ml collection tube and centrifuged at max speed for 30 seconds. Flow through was discarded, and this step was repeated until all cell-ethanol mixture was processed. 700µl of buffer RW1 was added and centrifuged at max speed for 30 seconds. Flow through was discarded and 500µl of buffer RPE was added and centrifuged at max speed for 30 seconds. Flow through was discarded and this step was repeated increasing centrifugation time to 2 minutes to fully wash the column. Column was dried by placing in a new collection tube and centrifuging at max speed

for 1 minute. Column was placed in a new collection tube and 25µl of RNAse-free water was added directly to the membrane and centrifuged at max speed for 1 minute. Eluted RNA was added back to the membrane and this step was repeated to concentrate RNA in 25µl of elution. Samples were stored at -80ºC between assays.

To determine RNA integrity number (RIN) an Agilent bioanalyzer 2100 (Agilent Technologies, Santa Clara, CA, USA) was used. Samples were loaded onto the RNA Nano gel chip as per the manufacturer's guidance. Electropherograms, peak ratios, and RIN were analysed to determine degree of RNA degradation. A RIN >7 was used as a quality control threshold.

2.10 Transcriptomics

3’-digital gene expression sequencing was performed by Glasgow Polyomics. Libraries were prepared using a Lexogen Quantseq (FWD) kit v2 kit and were sequenced in 1x100bp fragments to a depth of >10 million reads using an Illumina NextSeq 2000 (Illumina, San Diego, CA, USA). Alongside analysis provided by Glasgow Polyomics, data was also analysed using usegalaxy.eu. Raw reads were indexed using by their UMI using UMI-tools, before the read trimming and QC tool trimmomatic was used to discard short reads <20nt, low quality reads <20Phred score, and trim off spacer sequences at start of each read. Reads were aligned to latest reference genome for *mus musculus* mm39 (available from ensembl.org) using HISAT2. After alignment, PCR duplicates were removed using UMI-tools by removing reads with identical UMI and sequence. The programme Featurecounts was used to count reads aligned to exons, discarding reads which mapped to multiple features. This dataset then was used as an input for Deseq2 for differential gene expression by grouping exons into genes and comparing between groups in a case vs control setup. Deseq2 results were annotated using GTF matching mm39 reference genome. Genes were filtered based on adjusted p-value <0.05 (Benjamini and Hochberg method) and fold change absolute value of >1 *(The Galaxy Community, 2022).* For generation of heatmaps outside of the galaxy environment, custom R scripts were used. R packages used included: dplyr, ggplot2, ComplexHeatmap, RColorBrewer, circlize, and colorRamp2.

2.11 Metabolite extraction and metabolomic analysis

Metabolites were extracted from cells stimulated with either Imiquimod (1.7µg/ml) or TL8-506 (1.3µg/ml). NISV (1.2mM) or Dexamethasone (1.7µM) were also added to cell cultures. Extractions were performed following guidance from Glasgow Polyomics. Briefly, in a 96-well plate, cells were seeded at $1x10^6$cells/ml in 100µl. Cells were then stimulated as described previously, to give a total volume of 200µl. After incubation in a sterile incubator at 37ºC and 5% CO_2 for 24hrs. Supernatant was fully aspirated and 100µl per well of a 1:3:1 ratio mixture of Chloroform/Methanol/water at 4ºC was added. Plates were placed on a rocker at 4ºC for 1 hour. Solutions were transferred to clean microcentrifuge tubes and vortexed on a cooled mixer at 4ºC for 5 minutes. Tubes were then centrifuged for 3 minutes at 13,000G at 4ºC and then stored at -80ºC until use.

LC-MS was performed at Glasgow Polyomics using a Dionex UltiMate 3000 RSLC system (Thermo Fisher Scientific, Hemel Hempstead, UK) using a ZIC-pHILIC 5µm Merck Sequant column. Briefly: the column was maintained at 25ºC and samples were eluted with a linear gradient (20mM ammonium carbonate in water, (A), and acentonitrile, (B) over 26 min at a flow rate of 0.3ml/min as follows:

Time/Minutes	%A	%B
0	20	80
15	80	20
17	95	5
26	20	80

Samples were maintained at 5ºC until 10µl were injected into the column. A Thermo Orbitrap QExactive (Thermo Fisher Scientific) was used for mass spectrometry analysis, utilising polarity switching mode. The settings used were as follows:

- Resolution 70,000
- AGC 1e6
- m/z range 70–1050
- Sheath gas 40
- Auxiliary gas 5
- Sweep gas 1

• Probe temperature 150°C

• Capillary temperature 320°C

Raw data was converted and analysed using PiMP (Polyomics integrated Metabolomics Pipeline). Further analysis such as PCA and OPLS-DA was performed using Metaboanalyst 5. REACTOME and KEGG were used for pathway references.

2.12 Statistical analysis

Statistical analysis was performed using Graphpad PRISM 9 and 10, with additional analysis performed using usegalaxy.eu. For a breakdown of the specific tools used in Galaxy, please see the relevant methods section.

3 Chapter 3

Characterising the immunomodulatory effect of Non-Ionic Surfactant Vesicles in comparison to Dexamethasone using Toll-like receptor ligands

3.1 Abstract

NISV have previously been explored as adjuvants and have demonstrated anti-inflammatory properties in TLR4 stimulation models of infection in vitro and in vivo without entrapped payload. The studies documented here aim to further explore the inherent immunomodulatory properties of NISV comprised of mono-palmitoyl glycerol (MPG), cholesterol, and dicetyl phosphate (DCP) produced using the “melt method” in the context of TLR7 and TLR8 stimulation as a proxy for single-stranded RNA (ssRNA) viral infection. Using an L-929 cell conditioned media in our cell culture regimen resulted in a Cd11b++ cd11c- $F4/80_{low}$ bone-marrow derived macrophage (BMDM) population. Characterisation of IL-6 and IL-12 response by BMDM generated by TLR ligands LPS (TLR4), poly(I:C) (TLR3), Imiquimod (TLR7), and TL8-506 (TLR8) revealed EC50 values of 1.298μg/ml (LPS), 6.756-6.851μg/ml (Poly(I:C), 1.584-1.789μg/ml (imiquimod), and 1.339-1.374μg/ml (TL8-506). IC50 of NISV and Dexamethasone analysis using LPS stimulated BMDM IL-6 production revealed values of 1.152mM and 1.67μM respectively. These values were used to study effects of NISV and Dexamethasone on IL-6 and IL-12 production by various TLR stimulated BMDM. A dose dependent reduction in both IL-6 and IL-12 by NISV and Dexamethasone was found when BMDM were stimulated with TLR3 and TLR4 ligands. However, at concentrations previously effective for TLR3 and TLR4 induced IL-12 production, dexamethasone displayed reduced anti-inflammatory effects for TLR7 and TLR8 induced IL-12 production. NISV displayed a dose dependent decrease in IL-12 levels with TLR7 and TLR8, but an increase in IL-6 was observed in TLR8 stimulated cells. Further analysis of cytokines/chemokines using cytometric bead array revealed further differences in NISV effect depending on TLR stimulation, with upregulation of IL-6, IL-27, TNF-α, and MCP-1 by NISV in TLR7 and TLR8 stimulated BMDM but not in TLR3 or TLR4 stimulated BMDM, indicating the ability to of NISV to enhance the pro-inflammatory response in TLR7 and TLR8 stimulated cells. NISV show consistency in upregulation of IL-1α and IL-1β across all TLR ligands. Downregulation of pro-inflammatory cytokines by NISV was generally observed in TLR3 and TLR4 stimulated BMDM greater than those stimulated with TLR7 and TLR8 ligands, whilst Dexamethasone displayed broad downregulation regardless of TLR stimulation. This data suggests that NISV immunomodulatory abilities are somewhat TLR stimulation-specific, with further work needed to investigate the intracellular signalling pathway effects of NISV after TLR ligation.

3.2 Introduction

3.2.1 NISV as an immunomodulator

NISV have previously been demonstrated to exert immunomodulatory effects both *in vitro* and *in vivo*. Initially, characterisation of NISV highlighted their potential as adjuvants, displaying their ability to increase IgG levels in response to entrapped bovine serum albumin (BSA). Furthermore, it was established that the response to the entrapped antigen persisted as long as using Freund's complete antigen (FCA) as adjuvant. Currently, FCA is forbidden for use in humans due to its high toxicity – an aspect not found in NISV. Further study revealed that the previously mentioned induction of IgG generation was specific to BSA entrapped within NISV and was not present when free BSA was mixed with empty NISV and injected *(Brewer and Alexander, 1992;1994).* Despite this, continued study of empty NISV revealed an inherent immunomodulatory effect that was initially described as an anti-inflammatory effect and reported in a patent filed by *Roberts et al.* published in 1997. The formulation of NISV used to display this anti-inflammatory effect was comprised of the surfactant mono-palmitoyl glycerol, the sterol cholesterol, and the charge inducing surfactant dicetyl phosphate combined in the molar ratio of 5:4:1 of MPG:Chol:DCP. **(Fig. 7)**. This formulation produced using the melt method displayed the ability to downregulate IL-6 and TNF-α levels induced by LPS in both human peripheral blood leucocytes and murine peritoneal macrophages *(Roberts, et al., 1997)*. Previous work in our lab has investigated the effect of NISV using both LPS and other TLR ligands such as PAMCSK4 and Poly(I:C), demonstrating that the anti-inflammatory effect of NISV is unchanged when measuring pro-inflammatory "sentinel" cytokines such as IL-6.

Component	Structure
Mono-palmitoyl glycerol	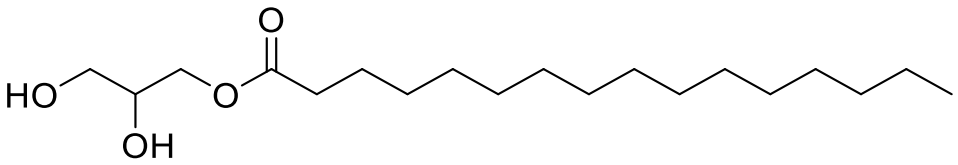
Cholesterol	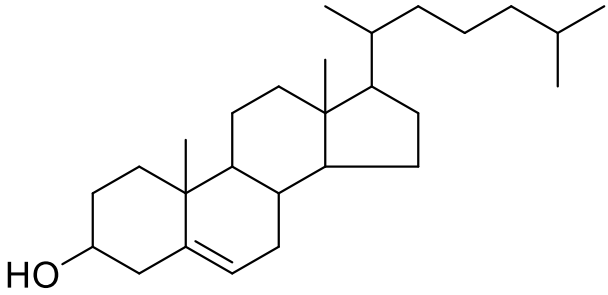
Dicetyl phosphate	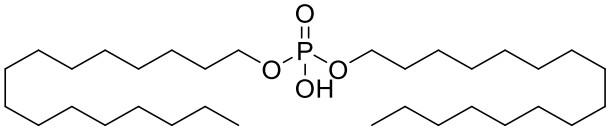

Figure 7. NISV component structure: *Mono-palmitoyl glycerol is a 1-monoglyceride that includes a palmitoyl group as its acyl group and features a single 16-Carbon long tail separated from the hydroxy-containing head group by a carbonyl group linked to an ester bond. Cholesterol is a sterol that is found in mammals, widely distributed in many body tissues and plays a vital role in the structure of animal cell membranes, as well as serving as a precursor component for the biosynthesis of steroid hormones, Vitamin D, and bile acids. Structurally, cholesterol is comprised of four strongly hydrophobic hydrocarbon rings with a weakly hydrophilic hydroxyl group, giving the molecule weak amphipathic properties (Kim, et al., 2023; Goluszko, et al., 2005). Dicetyl phosphate is the dihexadecyl ester of phosphoric acid and is a negatively charged molecule used to prevent flocculation of NISV formulations by imparting a degree of electrostatic repulsion between vesicles (Junyaprasert, et al., 2008). Structures illustrated using Chemdraw Professional V22.2.0*

3.2.2 Interleukin 6

IL-6 is a pro-inflammatory cytokine that was discovered in 1986 and originally termed B-cell stimulatory factor 2 (BSF-2) due to its ability induce antibody production by B-cells *(Hirano, et al., 1986)*. It was later renamed IL-6 after cloning of a protein known as IFN-β2 revealed that it was identical to BSF-2, alongside the same protein being found to function as a hybridoma growth factor *(Kishimoto, 2010).* This highlights the pleiotropic nature of IL-6, and thus, this cytokine is implicated in a variety of inflammatory, autoimmune, and malignant conditions. Structurally, IL-6 is comprised of a four-helix bundle, with a mini helix side chain *(Somers, et al., 1997),* and is a member of a superfamily of helix bundle cytokines that includes IL-27, IL-11, cardiotrophin 1 (CT-1) cardiotrophin-like cytokine (CLC), leukaemia inhibitory factor (LIF), and oncostatin M (OSM). These proteins are grouped upon the basis of their receptor containing the gp130 subunit *(Rose-John, 2018),* which is a membrane bound glycoprotein that acts as a signal transducer *(Taga, et al., 1989).* Alongside IL-6Rα, these subunits form the complex to which IL-6 binds *(Hibi, et al., 1990; Kishimoto, et al.,1992).* IL-6Rα is only expressed on the surface of a limited milieu of cells such as macrophages, neutrophils, and CD4+ T cells, but IL-6Rα also exists as a soluble protein, allowing for both trans- and classical signalling (*Hua, et al., 2017).*

Classical signalling involves binding of IL-6 to surface-expressed IL-6Rα with low affinity, and this complex then binds to the gp130 receptor with high affinity, inducing JAK/STAT signalling transduction for the transcription of IL-6 specific genes *(Reeh, et al., 2019)* This relies upon the expression of IL-6Rα on the cell surface, but for those cells that do not express IL-6Rα, trans- signalling can occur. This requires binding of IL-6 to soluble IL-6Rα which is generated either through partial proteolysis of the membrane bound form by ADAM17, or through alternative mRNA splicing *(Rose-John, 2012).* Once bound, the complex then binds to gp130 which is constitutively expressed on the surface of all cells, allowing the actions of IL-6 to be exerted on non-immune cells. This signalling dichotomy plays a role in the proliferation of inflammation and subsequent resolution, with the initial binding of IL-6 to membrane bound IL-6Rα (classical signalling) causing an increase in local inflammation followed by a quelling that imparts the regenerative tissue healing aspect, whereas IL-6 binding to soluble IL-6Rα seems to sustain the inflammatory

response by binding to a greater number of gp130 molecules on the cell surface. Furthermore, studies have demonstrated that by selectively inhibiting soluble IL-6Rα, inflammation can be reduced whilst the vital infection clearing functions and tissue repair of membrane bound IL-6Rα signalling are unaffected *(Rose-John, 2017; Rose-John, et al., 2023).* Others have also placed IL-6 as a regulator of neuroinflammation, reinforcing the notion that this protein may act in an anti-inflammatory capacity under the correct conditions . Studies have reported that IL-6 can promote the polarisation of M2 macrophages and thus could contribute to an anti-inflammatory effect. Although it should be noted that this is context dependent, as M2 macrophages promote inflammation in allergy and can promote inflammation by working synergistically with Th2 cells *(Casella, et al., 2016).*

Clearly, IL-6 is a multi-faceted cytokine, and therefore functions in a variety of roles in the immune system. Primarily, IL-6 drives the expansion of the immune system and subsequent generation of an inflammatory response. As mentioned previously, this is achieved through induction of the acute phase proteins, expansion of immune cells such as neutrophils, B cells, and activation/polarisation of Mφ, and T cells, for example. These features have made IL-6 an attractive target for inflammation-reducing therapies, thus spawning mAbs that target the cytokine itself (siltuximab) or the IL-6R (tocilizumab). Whilst these treatments are clinically available, non-mAb therapies targeting IL-6 are sparse. However, tocilizumab has been approved for use in cases of severe covid-19 for patients that require mechanical ventilation and are undergoing corticosteroid treatment *(NIH, 2023).* Results of the RECOVERY and REMAP-CAP trials indicate that when used as an adjunct therapy to boost corticosteroid immunosuppression, biologics targeting IL-6 can improve the number of organ support-free days, as well as increase 90-day survival in severe cases of SARS-CoV-2 infection *(RECOVERY, 2021; REMAP-CAP, 2021).*

3.2.3 Interleukin 12

Another cytokine of interest when considering the immune response to viruses is IL-12. Notably, IL-12 is a heterodimeric cytokine, as are the other members of the IL-12 family which also include IL-23, IL-27, and IL-35. IL-12 is comprised of two subunits, namely p35 encoded by the IL-12A gene, and p40 encoded by IL-12B. The p35 (or α-chain) subunit is structurally similar to members of the IL-6 superfamily and comprises a bundle of 4 helices whereas the p40 subunit is structurally similar to soluble type 1 cytokine receptors and comprises 3 β-sheets. *(Vignali, and Kuchroo,*

2012). Together these subunits make up IL-12p70, named for the total molecular weight of the 35kDa, and 40kDa. This heterodimer is the active form of the cytokine and is produced by APCs like DCs and Mφ. Interestingly, IL-12A is constitutively expressed in a number of cell types, with IL-12B only expressed in cells that produce active IL-12p70. Therefore, p40 production is a prerequisite for the synthesis of active IL-12, and as this subunit is only used for IL-12 production rather than for IL-23 or IL-35 etc, it is a specific epitope for IL-12 *(Jalah, et al., 2013).* The p40 subunit may also form homodimers, which were once thought to be inactive, but studies have demonstrated the ability of this molecule to induce iNOS in microglia *(Jana, et al., 2009).* IL-12 exerts its actions by binding to the receptor complex comprised of IL-12Rβ1 and IL-12Rβ2. Structurally IL-12Rβ1 is similar to gp130 used in IL-6 signalling. Also, like IL-6, binding of IL-12 to the receptor initiates signal transduction through the JAK/STAT pathway *(Hu, et al., 2021).*

The main role of IL-12 is activation of CD8+ T cells and NK cells, as well as promoting the Th1 response, bridging the gap between innate and adaptive immunity. Polarisation of CD4+ T cells towards a Th1 phenotype allows for more effective removal of intracellular pathogens such as viruses but may also include bacteria and parasites. To achieve this, Th1 cells amplify the actions of phagocytic cells through the release of IFNy after recognition of antigen presented by MHC I or MHC II. IL-12 also increases the activity of the immune cell specific transcription factor T-bet, which is a potent inducer of IFNy. Thus, a positive feedback loop is established, expanding the cell-mediated immune response for clearance of virally infected cells and free virions *(Guo, et al., 2019; Lazarevic, et al., 2013).*

Figure 8: Intracellular signalling pathways of TLR3, TLR4, TLR7, and TLR8.*TLR4 utilises both MyD88 and TRIF adaptor proteins. Following receptor ligation with LPS, TLR4 dimerises, bringing the intracellular TIR domains into close proximity. TIRAP associates with the TIR, and is phosphorylated by BTK, facilitating the recruitment of the adaptor protein MyD88 to form a complex with IRAK4. Following this, a cascade of autophosphorylation occurs which allows either IRAK1 or IRAK2, and TRAF6 to bind to the TIRAP:MyD88:IRAK4 complex. TRAF6 initiates synthesis of a polyubiquitin chain that provides a scaffold for the TAK1 complex comprised of TAK1 and TAB1-3. The TAK complex can then activate the MAPK signalling pathway which regulates transcription factors like AP-1 and CREB. Alongside this, the TAK also phosphorylates a subunit of the IKK complex, IKKβ. This complex can then degrade IkB, the protein that regulates NF-kB translocation to the nucleus. This allows NF-kB to bind to the appropriate response elements on the DNA and exert its transcriptional activity. This MyD88 dependent signalling cascade is also used by TLR7 and TLR8 exclusively. Alternatively, TLR4 may use the TRIF pathway after internalisation of the receptor. This pathway is also used exclusively by TRIF. TLR4 must use the adaptor protein TRAM to recruit TRIF, whereas TLR3 can recruit TRIF directly. TRIF recruits TRAF3, which serves a similar function to TRAF6 in the MyD88 pathway with activation of the IKK complex for NF-kB activation, but also forms a complex with Ikki and either IRAK4 or TBK. Phosphorylation of these complexes cause translocation of IRF3 and IRF7 to the nucleus for production of type I interferons.*

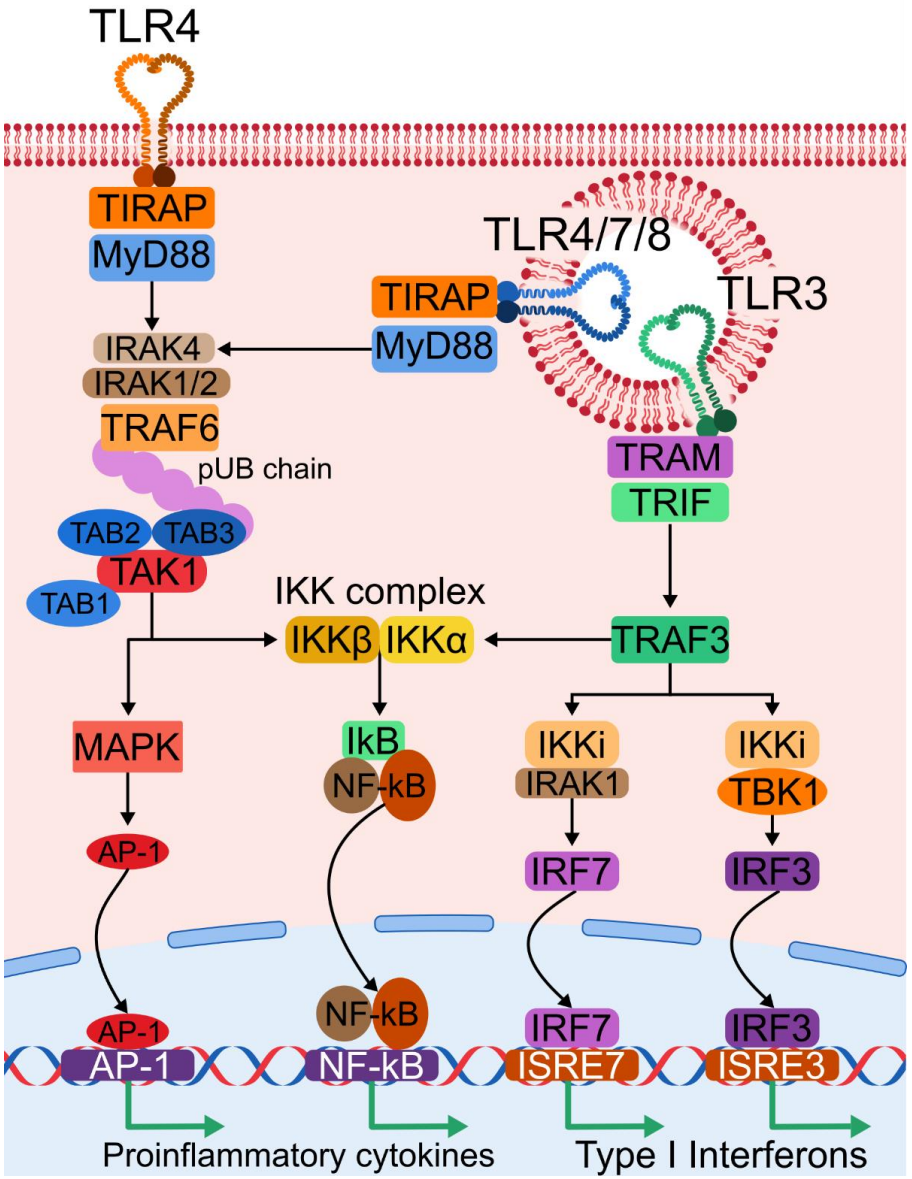

3.2.4 Establishing a Toll-like receptor stimulation model using murine bone marrow-derived macrophages

The experiments detailed in this chapter were performed to determine a robust cell culture and subsequent stimulation with TLR ligand protocol, before investigating the effect of NISV on cytokine levels in comparison to dexamethasone using ELISAs and cytometric bead array. As mentioned above, TLR ligands such as LPS have previously been used to stimulate BMDM before application of NISV, which provides context for NISV immunomodulation in terms of a Gram-negative bacterial infection. To provide context for ssRNA viral infections such as SARS-CoV-2 we opt to use two synthetic ligands for TLR7 and TLR8. Imiquimod is a TLR7-specific ligand imidazoquinoline amine analogue to guanosine and has been shown to elicit MyD88 **(Fig. 8)** and NF-kB signalling in vivo using a TLR7 deficient mouse model. WT mice engaged MyD88 and display NF-kB transcriptional regulation after addition of imiquimod, but this effect is absent in TLR7 negative mice(Hemmi, et al., 2002). For TLR8, we opted to use the potent and TLR8 specific ligand TL8-506, a benzoazepine compound that is an analogue to VTX-233 and strongly activates MyD88 and NF-kB (Lu, et al., 2012) **(Table 1).** By comparing TLR receptor stimulation and the resulting downstream effects we aim to elucidate whether NISV immunomodulation is TLR or adaptor protein specific, alongside whether the location of TLR in the cell plays a role.

Table 1: List of murine toll-like receptors, their natural ligand, and an example of a synthetic ligand.

Toll-like receptor	Recognises	Analogue examples
TLR1/2 heterodimer	Bacterial lipoproteins	Pam3Cys-Ser-Ser
TLR2/6 heterodimer	Diacyl and triacylglycerol moieties	Pam3CSK4
TLR3	dsRNA	Poly(I:C)
TLR4	Lipopolysaccharides	N/A
TLR5	Flagellin	N/A
TLR7	ssRNA	Imiquimod
TLR8	ssRNA	TL8-506
TLR9	CpG DNA	ODN2395
TLR11	Flagellin/profilin	N/A
TLR12	Potentially profilin	N/A

Furthermore, we compare the effect of NISV to dexamethasone due to its frequent use as a potent immunosuppressive drug during the SARS-CoV-2 pandemic. Dexamethasone is a corticosteroid drug that exhibits exclusive glucocorticoid receptor activity and has been demonstrated to decrease patient mortality in severe cases of SARS-CoV-2 infection.

3.3 Aims and Hypothesis

i. Establish an effective bone marrow derived macrophage culture and confirm cell phenotype by flow cytometry. In addition, to determine working concentrations of TLR ligands, NISV, and Dexamethasone for the robust stimulation of cells and subsequent analysis. To achieve this, ELISAs were used to detect sentinel cytokines IL-6 and IL-12 as a measure of TLR ligand activity and the modulation of these cytokines by NISV or dexamethasone as a measurement of treatment for the calibration of future experiments. This provides a model by which to investigate changes in NISV effect in various in vitro infection scenarios.

ii. Corroborate the anti-inflammatory effect of NISV using murine bone marrow derived macrophages stimulated with the TLR3 and TLR4 ligands Poly(I:C) and LPS and expand this to encompass TLR7 and TLR8 using the ligands Imiquimod and TL8-506 respectively. This anti-inflammatory effect will be measured using ELISAs for sentinel cytokines IL-6 and IL-12 and will be compared with dexamethasone. By comparing cells stimulated with different TLR ligands the aim is to elucidate any adaptor protein/intracellular signalling pathway differences in NISV or dexamethasone effect.

iii. Expand the scope of investigation into NISV immunomodulatory effects to include cytokines and chemokines commonly modulated during inflammation and the anti-viral response using cytometric bead arrays. By comparing the effects of NISV or dexamethasone on a greater array of soluble mediators the aim is to determine if there are TLR specific effects of each treatment and expand the notion that NISV can induce both an anti-inflammatory and pro-inflammatory response.

3.4 Results

The results detailed herein explore the immunomodulatory abilities of Melt method NISV and provide a range of effective concentrations of NISV and TLR ligands for use in future study. Following this, experiments were carried out to determine the cytokine profile modulated by NISV in comparison to dexamethasone in various TLR stimulation scenarios using ELISAs and cytometric bead arrays.

3.4.1 Confirmation of cell culture and NISV using flow cytometry and dynamic light scattering respectively

Prior to commencement of stimulation with TLR ligands or treatments, the phenotype of our resulting cell culture was analysed by flow cytometry. The gating strategy used is displayed in **figure 9**. Our analysis found that of live cells, > 95% of cells were CD11b+, with low levels of F4/80 present (10.254%). Cells displayed high levels of CD11c and around half of cells were CD86 positive (44.94%) This indicates that our cell culture conditions resulted in a macrophage culture.

NISV were produced using the melt method and then characterised using a zetasizer to determine size, polydispersity, and zeta-potential on a batch-to-batch basis. This measurement was performed as quality control before each experiment to ensure that NISV fell within the expected parameters for this production method. The mean size of NISV was 1719nm, with an interquartile range of 1501nm to 1887nm. Mean PDI was 0.4248 with an interquartile range of 0.3405 to 0.5240. Mean zeta potential was -28.77mV, with an interquartile range of -32mV to -25.4mV **(Fig.10).** This indicates that despite being produced using a method that relies heavily on operator consistency, melt method NISV can have low batch-to-batch variation.

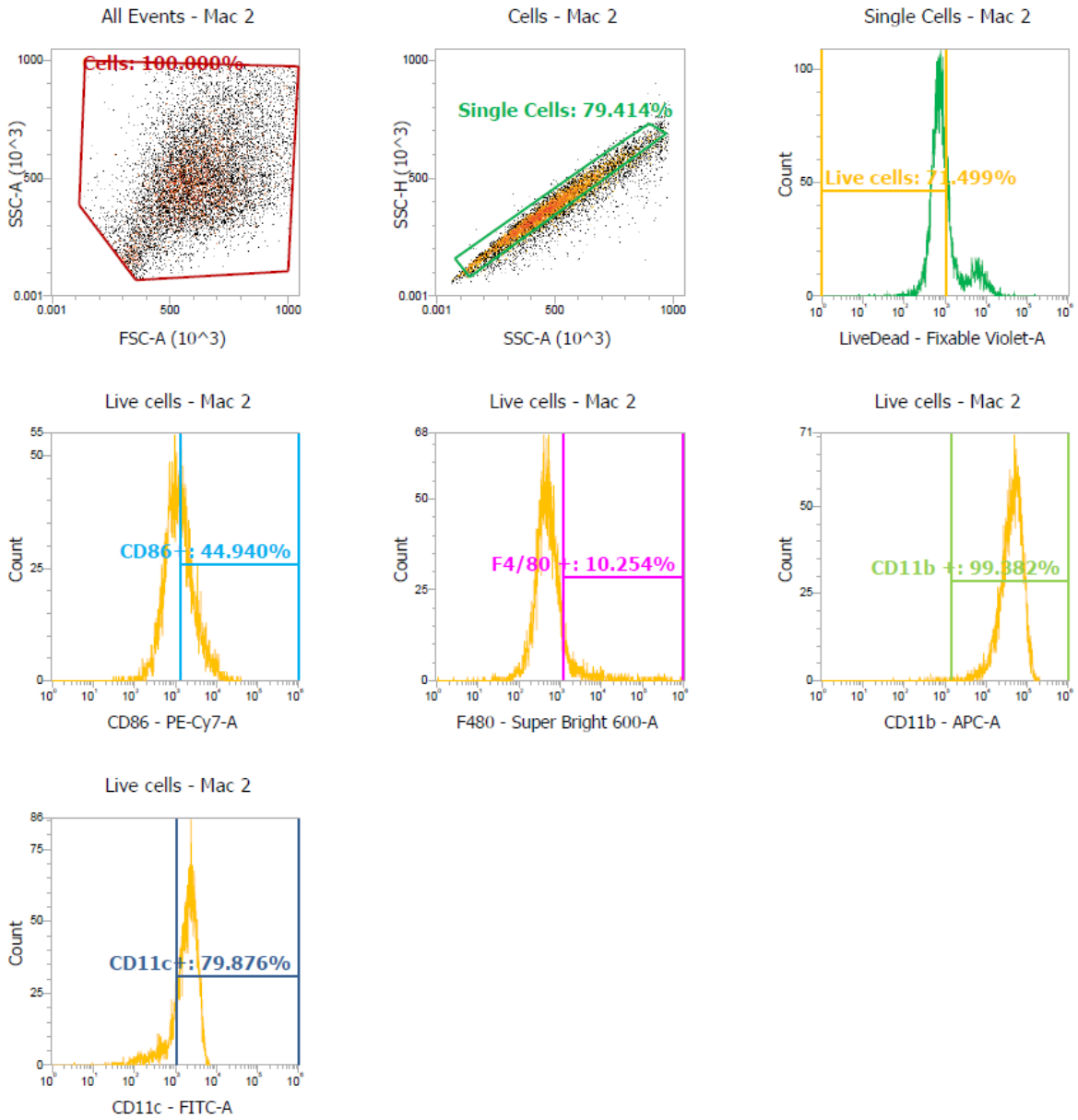

Figure 9: Gating strategy used in cell marker analysis by flow cytometery. *Cells were scraped from their culture dishes and stained for CD11b, CD11c, F4/80, and CD86. A fixable live/dead dye was included in the panel to identify live cells. Target population was gated based on forward scatter and side scatter, with single cells identified by comparing side scatter height and side scatter area. Of these cells, those positive for the fixable dye were excluded and each marker measured using their conjugated fluorophore. Thresholds for positive fluorescent signal were calibrated using unstained cells and single stains used for compensation. Correct compensation was confirmed using fluorescence-minus-1 controls.*

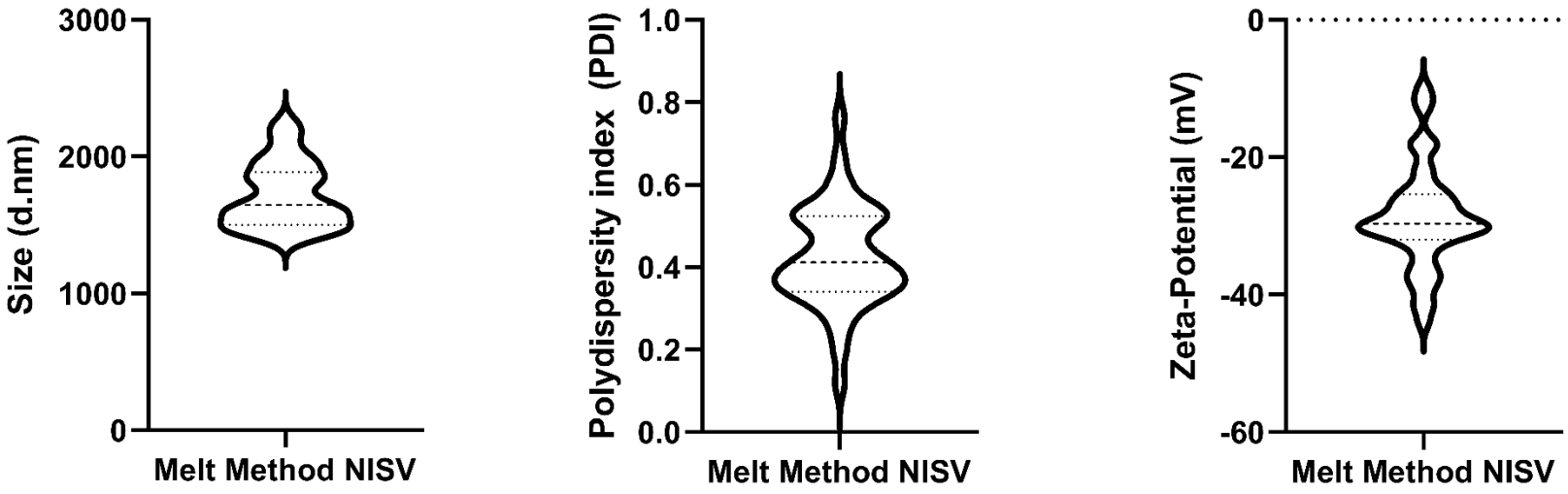

Figure 10: Size, polydispersity, and zeta-potential of NISV produced using the melt method. *Aliquots of NISV produced using the melt method were measured using dynamic light scattering by zetasizer. Each value was generated from 3 runs each consisting of at least 10 measurements. Results displayed here are aggregate of 45 batches/production runs. Violin plots display frequency of values as width of shape, with dotted lines representing median value (bold dotted line) and interquartile ranges (light dotted line). Wider area of shape indicates value of greatest frequency. Size measures the average diameter of each detected particle. Polydispersity index indicates the heterogeneity of the solution, with high PDI revealing samples that contain many different sized particles. Zeta potential measures the membrane charge of each particle as an indicator of stability and ability to resist flocculation.*

3.4.2 TLR ligands are non-toxic to BMDM across a wide range of concentrations and can induce production of IL-6 and IL-12 in a dose-dependent manner.

To determine an appropriate concentration of both TLR ligands and NISV or dexamethasone to use during future studies, BMDM were stimulated with a long dilution series of each TLR ligand and an ELISA for IL-6 and IL-12 production was performed on the supernatants. An alamarBlue cell viability assay was also performed to assess toxicity of each ligand. This assay relies on the ability of metabolically healthy cells to reduce a resazurin salt to resorufin, causing a colour change from blue to purple/pink that correlates with cell number and viability **(Fig. 11).** Even at high concentrations, cell viability did not drop below that of the healthy media alone cells, with some slight increases in alamarBlue reduction found at the top concentration of the TLR ligand dilution. Non-linear regression curves were fitted to the IL-6 and IL-12 ELISA results **(Fig.12, Fig.13).** This allowed the generation of EC50 and EC90 values for LPS, Poly(I:C), imiquimod, and TL8-506. To generate IC50 and IC90 values for NISV and dexamethasone BMDM were stimulated with LPS, and then NISV or Dexamethasone was applied, and curves fit to the resulting data **(Fig. 15).** An alamarBlue assay was also performed to assess toxicity of NISV and Dexamethasone, indicating that at all concentrations assayed, there was no toxic effect on cells **(Fig. 14).** The values generated for all compounds are displayed in **table 2 and 3.**

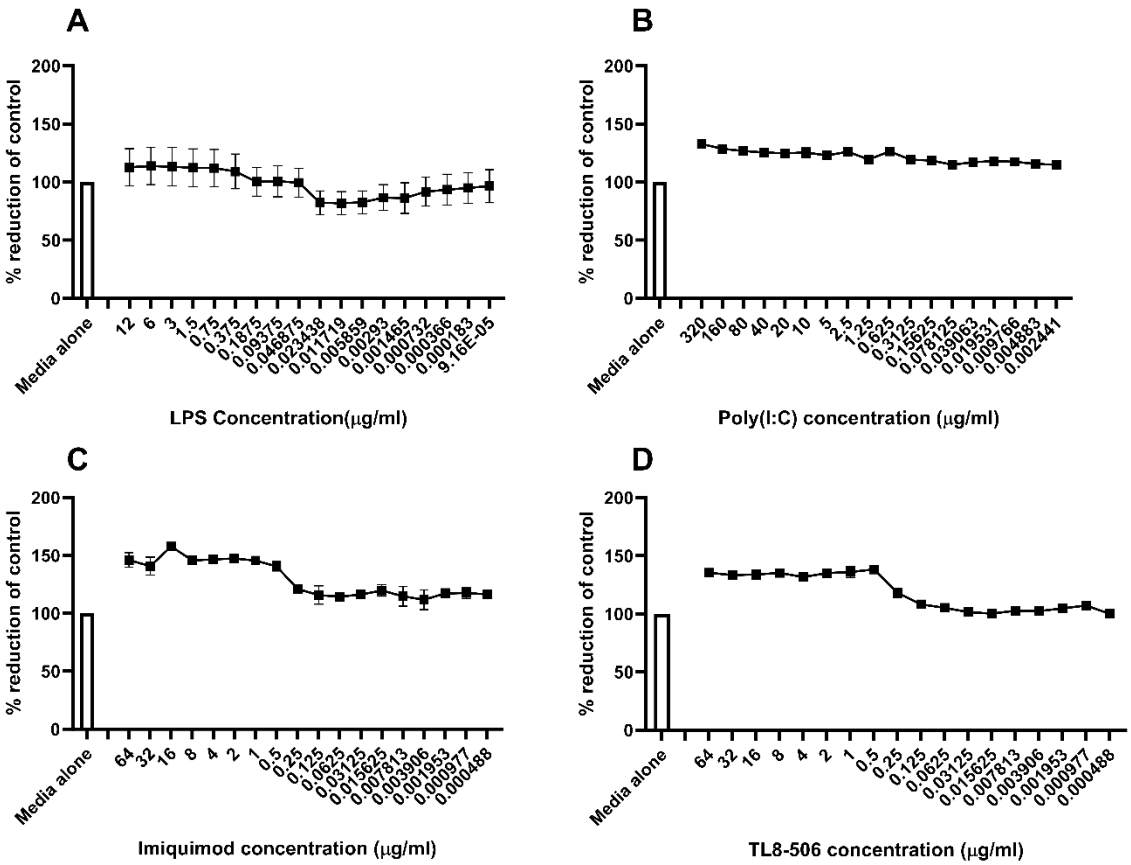

Figure 11: TLR stimulated BMDM viability assessed by alamarBlue assay. *1x10^6 cells/ml were seeded per well into a 96-well plate and stimulated in triplicate with a 1 in 2 serial dilution of either LPS (A), Poly(I:C) (B), Imiquimod (C), or TL8-506 (D) alongside a media alone control. Reduction of alamarBlue is shown as a percentage of healthy untreated media alone cells. Results expressed as mean ± SEM, n=3.*

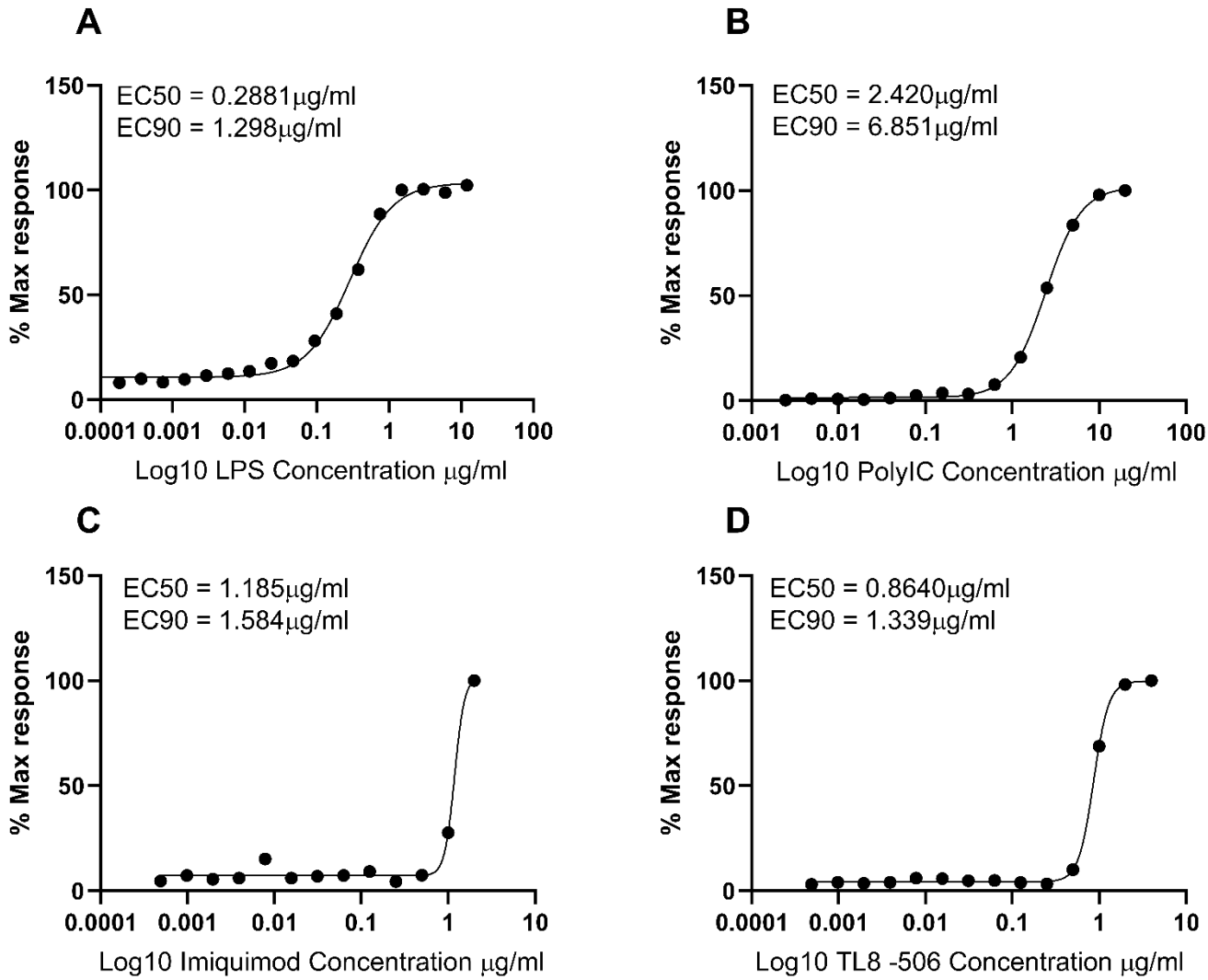

Figure 12: Non-linear regression curves for calculation of EC50/EC90 values using IL-6. *ELISAs for IL-6 production were performed on supernatants from BMDM stimulated with either (A) LPS, (B) Poly(I:C), (C), Imiquimod, or (D) TL8-506. Results expressed as % of max IL-6 response.*

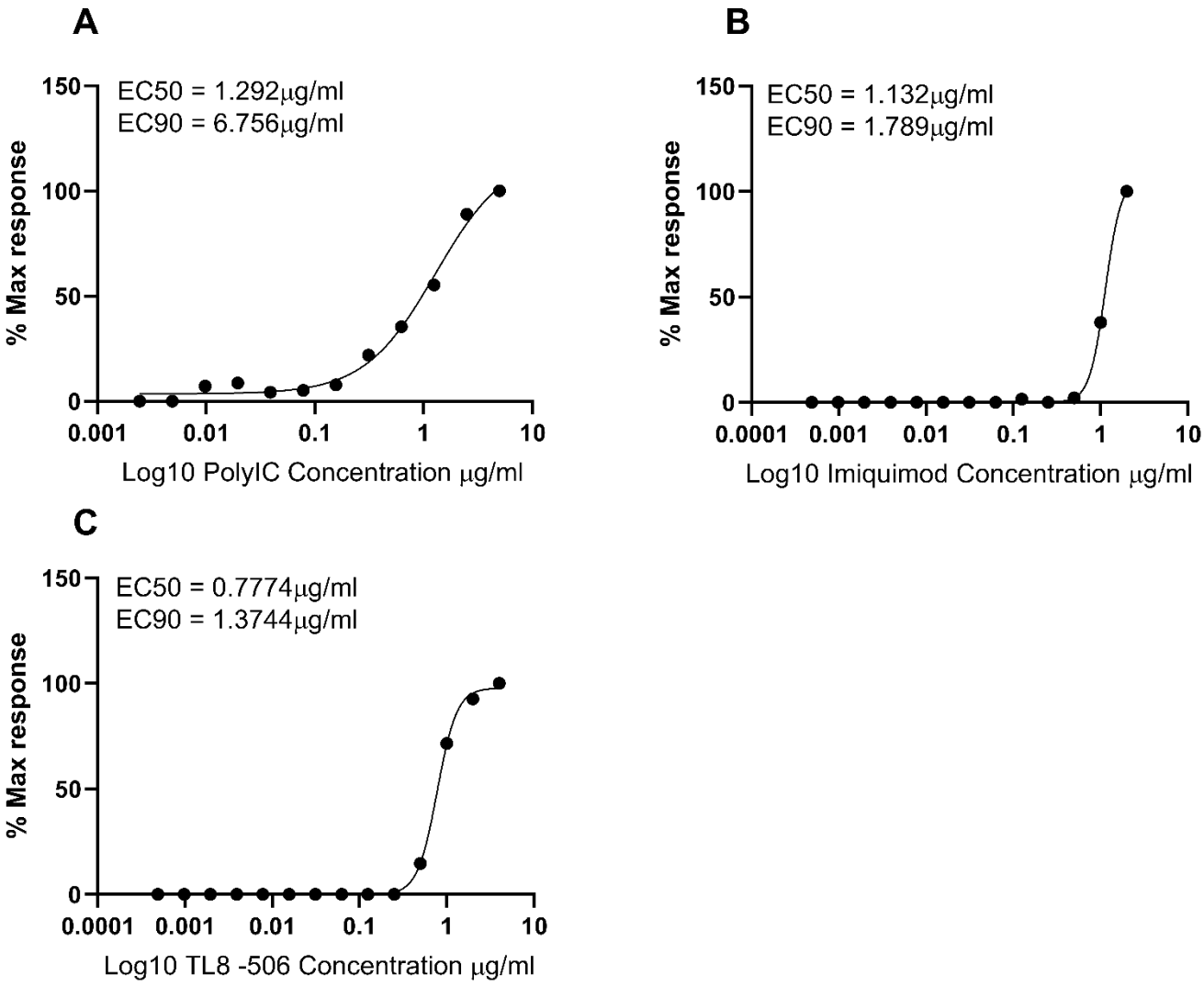

Figure 13: Non-linear regression curves for calculation of EC50/EC90 values using IL-12. *ELISAs for IL-12 production were performed on supernatants from BMDM stimulated with either (A) Poly(I:C), (B), Imiquimod, or (C) TL8-506. Results expressed as % of max IL-12 response.*

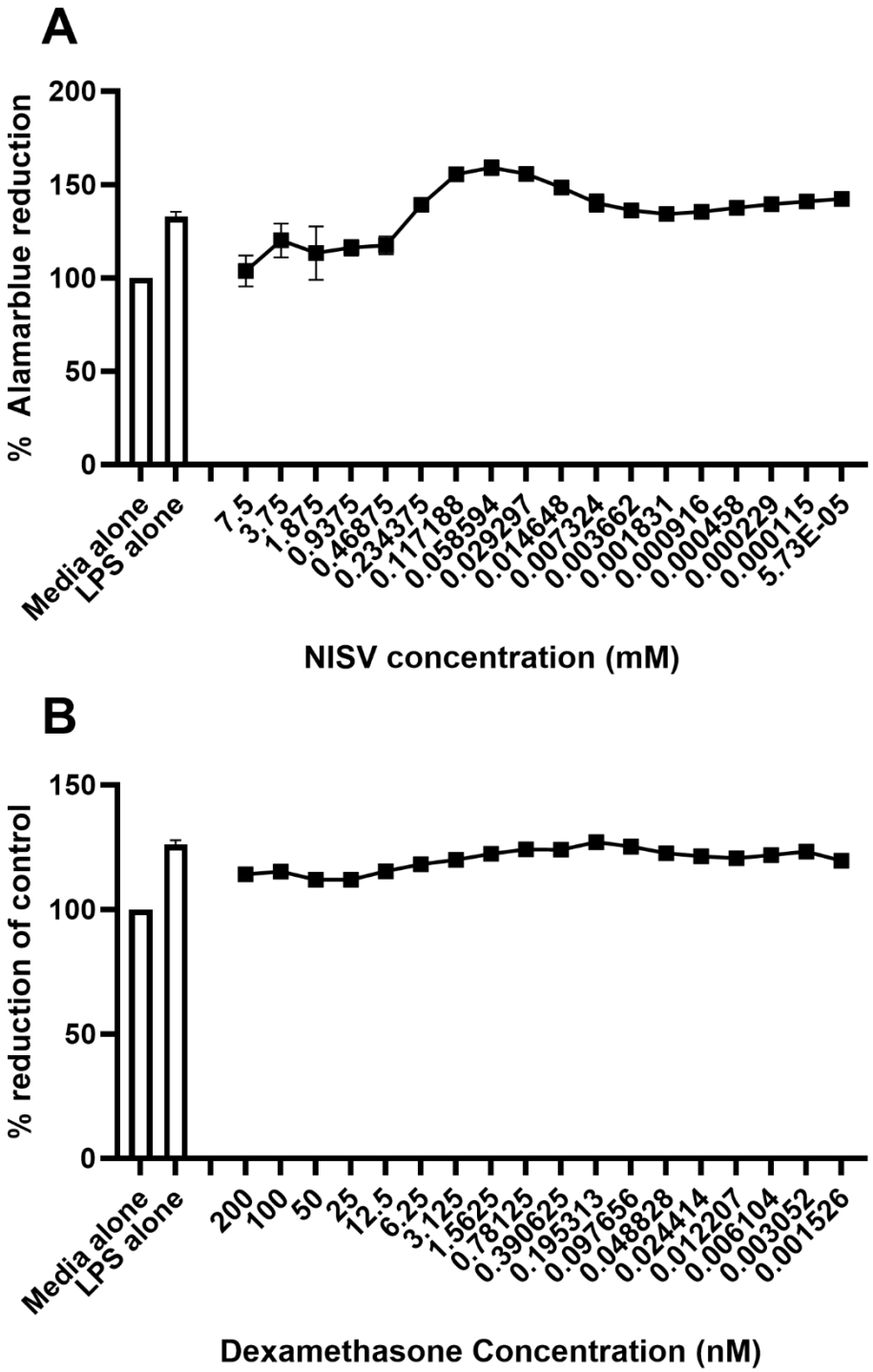

Figure 14: NISV or dexamethasone treated BMDM cell viability assessed by AlamarBlue assay: *1x10^6 cells/ml were seeded per well into a 96-well plate and stimulated in triplicate with 1.3µg/ml LPS. Cells were then treated with a 1 in 2 serial dilution of either NISV (A) or dexamethasone (B), Both a media alone control and LPS alone control were included. Reduction of alamarBlue is shown as a percentage of healthy untreated media alone cells. Results expressed as mean ± SEM, n=3.*

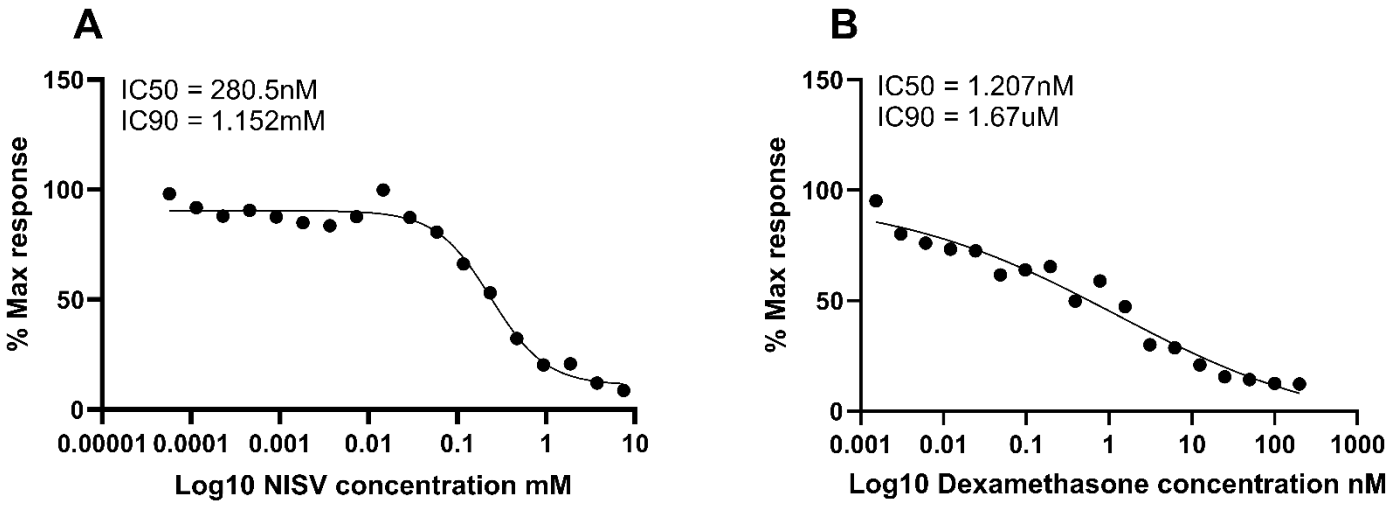

Figure 15: Non-linear regression curves for calculation of IC50/IC90 values using IL-6. *ELISAs for IL-6 production were performed on supernatants from BMDM stimulated with 1.3μg/ml LPS and a 1 in 2 serial dilution of either NISV(A) or dexamethasone(B). Results expressed as % of max IL-6 response.*

Table 2: Summary of EC90 values.

Ligand/Treatment	EC90 (IL-6)	EC90 (IL-12)
LPS	1.298μg/ml	N/A
Poly(I:C)	6.851μg/ml	6.756μg/ml
Imiquimod	1.584μg/ml	1.789μg/ml
TL8-506	1.339μg/ml	1.374μg/ml
LPS + NISV	1.152mM	N/A
LPS + Dexamethasone	1.67μM	N/A

Table 3: Summary of IC90 values

Treatment	IC90 (IL-6)
LPS + NISV	1.152mM
LPS + Dexamethasone	1.67μM

Using the concentrations calculated in the EC/IC50 experiments, ELISAs for IL-6 were performed to preliminarily compare the effect of NISV or dexamethasone on TLR3, TLR4, TLR7, or TLR8 stimulated BMDM. An alamarBlue assay was also carried out to ensure that cell viability was at an acceptable level **(Fig. 16)**, reinforcing the accuracy of results obtained in the ELISA **(Fig. 17)**. In all experiments, both the ligand alone and NISV alone control did not display a reduction in cell viability compared with the media alone cells. However, at 1.67μM, dexamethasone alone displayed around significant decrease in alamarBlue reduction of around 20% when compared to the control cells. This effect was abrogated when dexamethasone was given to cells stimulated with LPS, Poly(I:C), imiquimod, or TL8-506. At all concentrations of NISV or dexamethasone given to TLR stimulated cells, there was no reduction in cell viability compared with media alone cells. This indicates that whilst the dexamethasone alone displayed a small decrease in cell viability, there was no toxic effect present in any stimulation/treatment combination. Examining IL-6 production reveals dexamethasone is a potent inhibitor of IL-6, with very low levels of the cytokine detected at all concentrations of dexamethasone used to treat BMDM regardless of any particular TLR stimulation. In contrast, NISV can reduce IL-6 production from LPS or Poly(I:C) stimulated cells in a dose-dependent manner when compared to the ligand alone control but displays a complex relationship when used to treat imiquimod or TL8-506 stimulated BMDM. Notably, there is a partial decrease in IL-6 levels at the highest concentrations of NISV, with a stimulatory effect on IL-6 appearing at around 0.15mM for both TLR/NISV combinations. This increased level of IL-6 begins to decrease alongside the concentration of NISV, suggesting an optimal concentration, or small effective range of NISV for TLR7/TLR8 IL-6 adjuvancy.

To further explore the effect of NISV in comparison to dexamethasone, we expanded our analysis to include IL-12, alongside using a lower concentration of dexamethasone. To this end, we aimed to identify a concentration of dexamethasone that provided a dose-response curve comparable to that of NISV using the same TLR ligands assayed previously. Again, an alamarBlue assay was carried out examine cell viability, with similar results (not shown) Notably, when beginning our dilution using a reduced concentration of dexamethasone (200nM

instead of 1.67μM), we generated dose-response curves comparable to that of NISV. This effect was observed with both LPS **(Fig. 18)** and Poly(I:C) **(Fig. 19)** stimulated BMDM when measuring IL-6 or IL-12, with the highest concentrations displaying near complete abrogation of each cytokine. However, cell stimulated with the TLR7 agonist imiquimod displayed only a partial reduction of IL-6 when given NISV or dexamethasone **(Fig. 20)**. Whilst this effect does appear to be dose dependent, it is much reduced compared with the effect observed in TLR3 or TLR4 stimulated cells. In contrast to IL-6, NISV displayed a much greater ability to downregulate IL-12 in a dose dependent manner. Dexamethasone, whilst able to reduce the overall level of IL-12 being produced by around 40-60% when compared with the TLR ligand alone, this effect was not dose dependent, indicating specificities with respect to TLR stimulation and dexamethasone dose for the abrogation of certain cytokines. This effect was also observed in TLR8 stimulated cells, with dexamethasone displaying an effective downregulation of IL-6 that lessened as drug concentration lowered, but not with IL-12 **(Fig. 20)**. The effect of NISV on TLR8 stimulated IL-6 production was consistent with our previous assays displaying an initial reduction in IL-6 at the highest concentration (1.5mM) of NISV followed by an increase in IL-6 production, peaking at 0.75mM NISV. When measuring IL-12, this trend was not present, with a classical dose response curve that plateaued at around 0.1875mM and lower (**Fig. 21)**

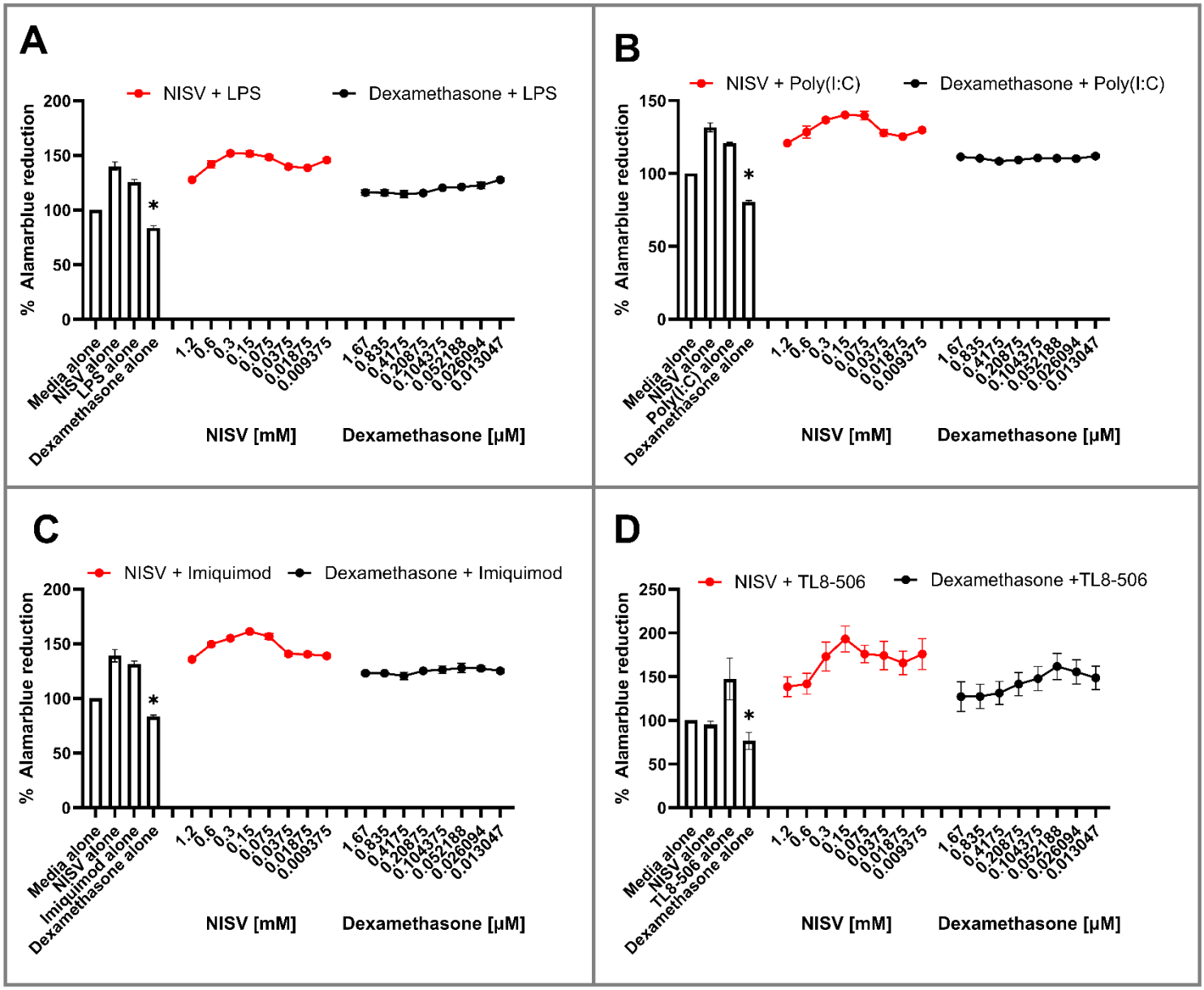

Figure 16: Viability of BMDM after treatment with NISV or Dexamethasone.

*1x10^{6}cells/ml were seeded per well in a 96-well plate and stimulated with either LPS (A), Poly(I:C) (B), Imiquimod (C), or TL8-506 (D). A 1 in 2 serial dilution of either NISV or Dexamethasone starting at 1.2mM or 1.67µM respectively was also added to the BMDM. Control cells were given either media alone, NISV alone, or dexamethasone alone. Reduction of alamarBlue for each group is shown as a percentage of the reduction of the media alone cells. Results are mean ± SEM. n=3. * = p<0.05.*

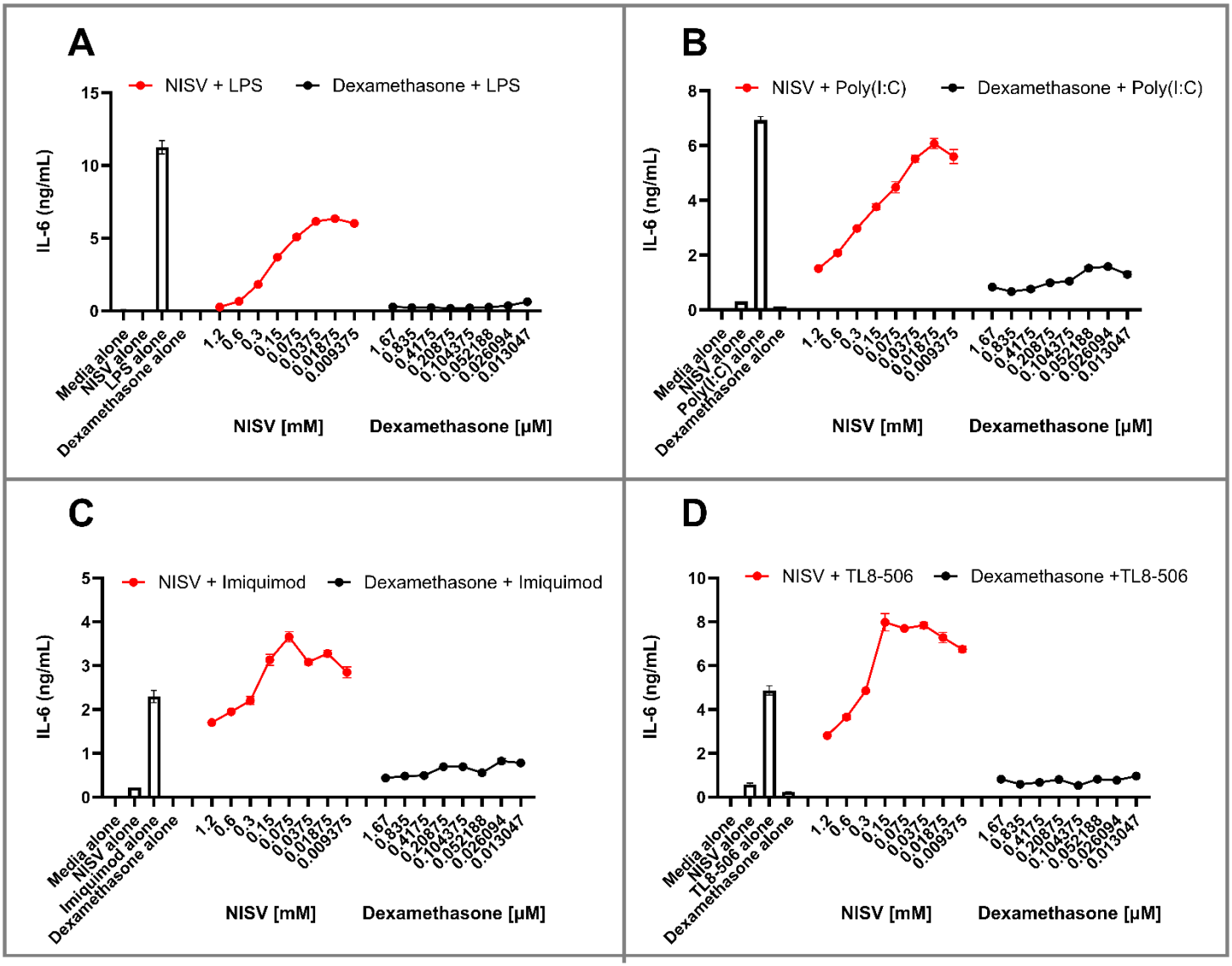

Figure 17: Effect of NISV or Dexamethasone on IL-6 production by TLR stimulated BMDM. *1x10^{6}cells/ml were seeded per well into a 96-well plate and stimulated with either LPS (A), Poly(I:C) (B), Imiquimod (C), or TL8-506 (D). A 1 in 2 serial dilution of either NISV or Dexamethasone starting at 1.2mM or 1.67µM respectively was also added to the BMDM. Control cells were given either media alone, Ligand alone, NISV alone, or dexamethasone alone. Results are mean ± SEM. n=3.*

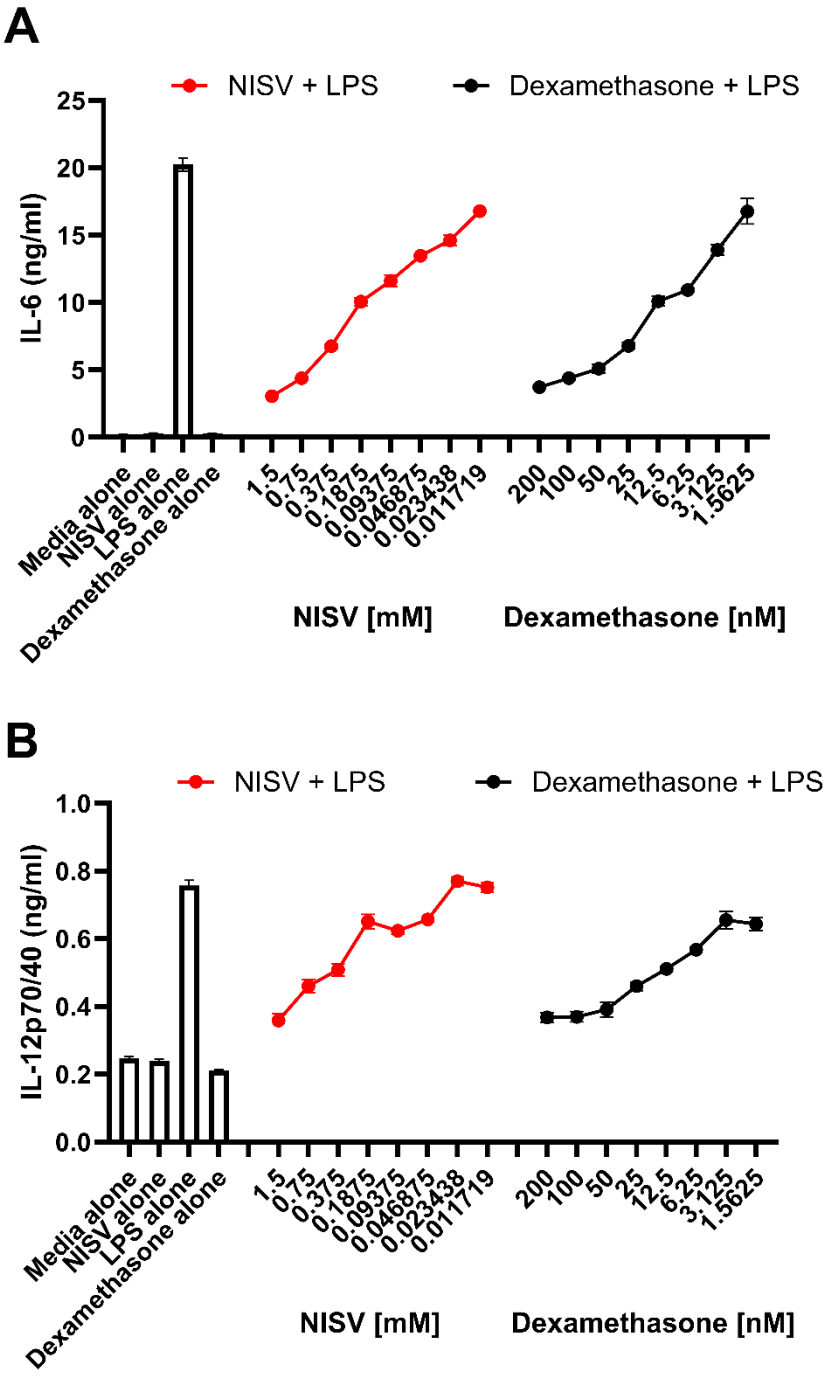

Figure 18: Effect of NISV or low-dose dexamethasone on IL-6 and IL-12 production by TLR4 stimulated BMDM. *1x10^{6}cells/ml were seeded per well into a 96-well plate and stimulated with 1.5µg/ml LPS. A 1 in 2 serial dilution of either NISV or Dexamethasone starting at 1.5mM or 200mM respectively was also added to the BMDM. Control cells were given either media alone, LPS alone, NISV alone, or dexamethasone alone. ELISA for IL-6 (A), and IL-12 (B) used to quantify cytokine levels. Results are mean ± SEM. n=3.*

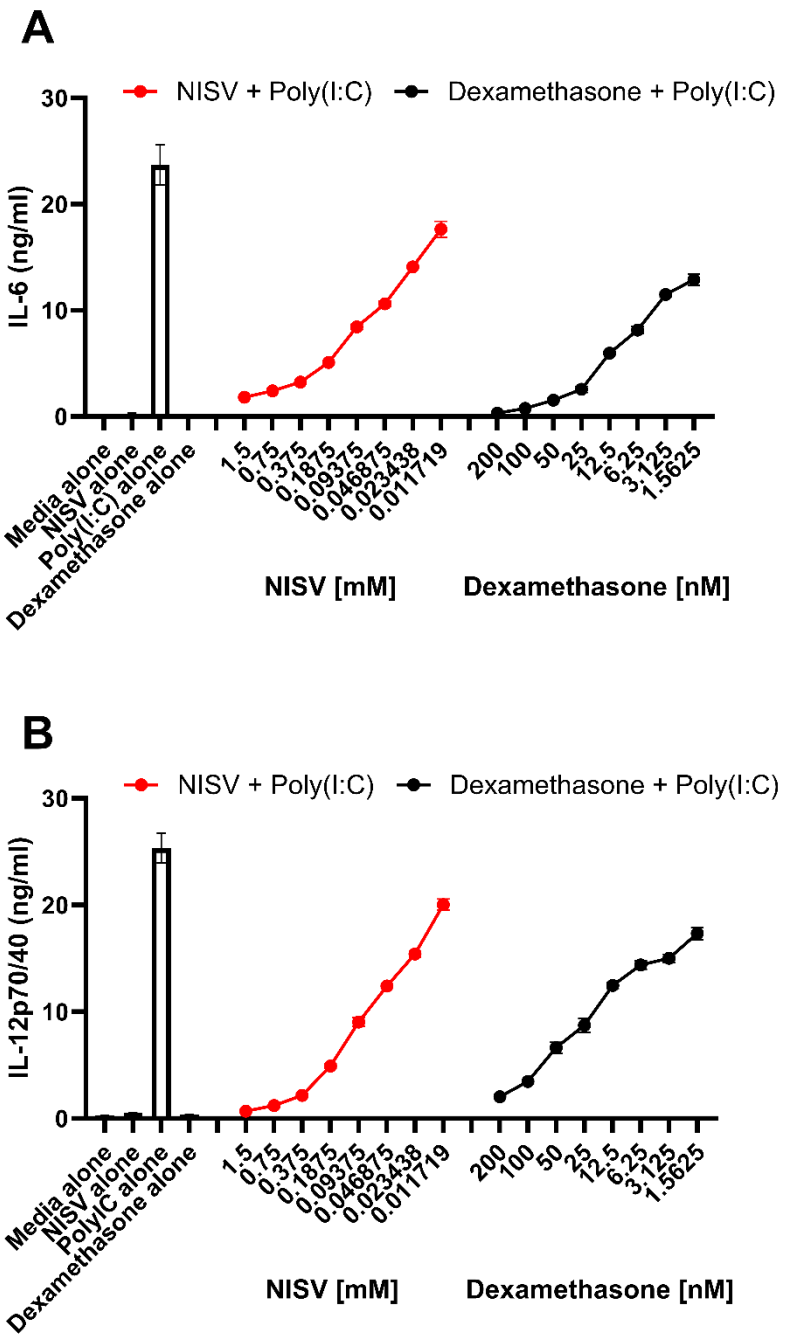

Figure 19: Effect of NISV or low-dose dexamethasone on IL-6 and IL-12 production by TLR3 stimulated BMDM. *1x10^{6}cells/ml were seeded per well into a 96-well plate and stimulated with 7µg/ml Poly(I:C). A 1 in 2 serial dilution of either NISV or Dexamethasone starting at 1.5mM or 200mM respectively was also added to the BMDM. Control cells were given either media alone, Poly(I:C) alone, NISV alone, or dexamethasone alone. ELISA for IL-6 (A), and IL-12 (B) used to quantify cytokine levels. Results are mean ± SEM. n=3.*

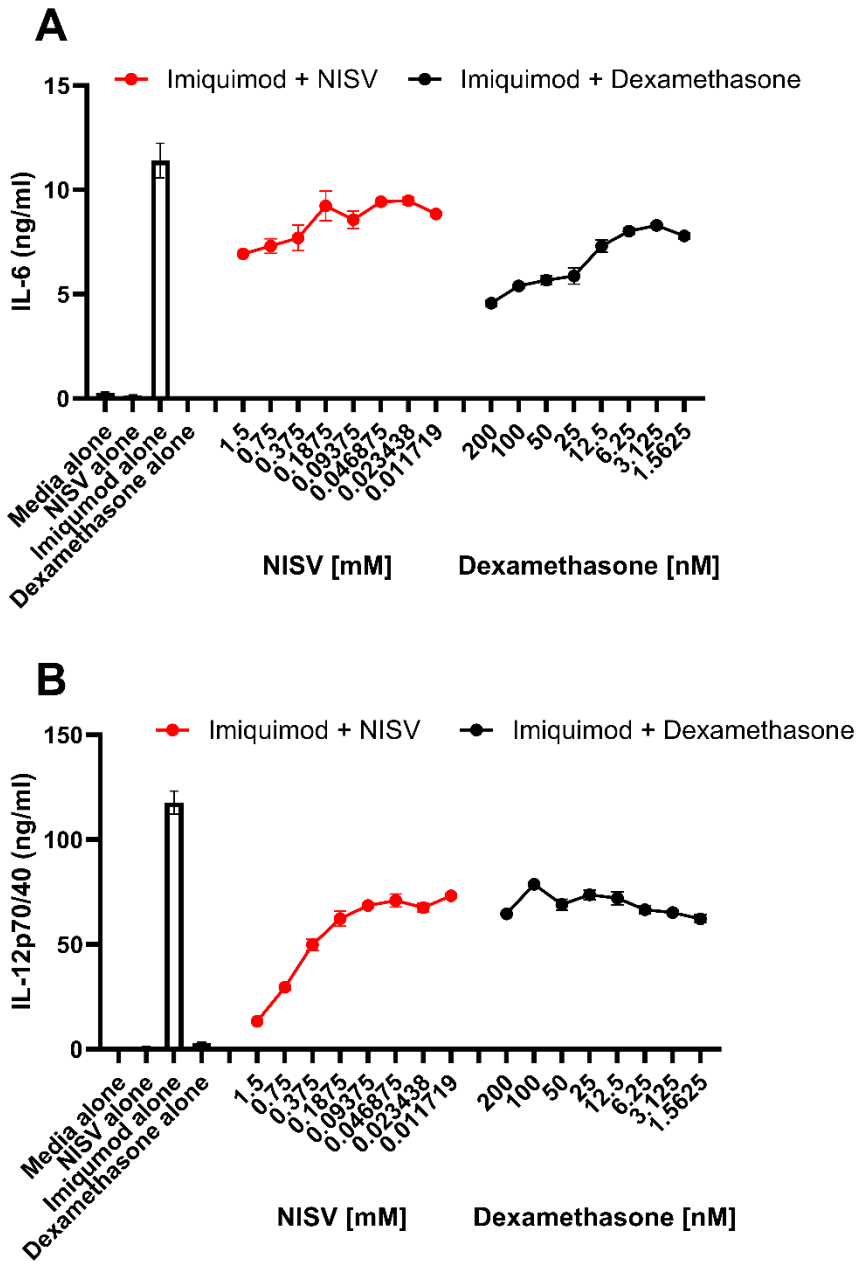

Figure 20: Effect of NISV or low-dose dexamethasone on IL-6 and IL-12 production by TLR7 stimulated BMDM. *1x10^{6}cells/ml were seeded per well into a 96-well plate and stimulated with 1.5µg/ml imiquimod). A 1 in 2 serial dilution of either NISV or Dexamethasone starting at 1.5mM or 200mM respectively was also added to the BMDM. Control cells were given either media alone, imiquimod alone, NISV alone, or dexamethasone alone. ELISA for IL-6 (A), and IL-12 (B) used to quantify cytokine levels. Results are mean ± SEM. n=3.*

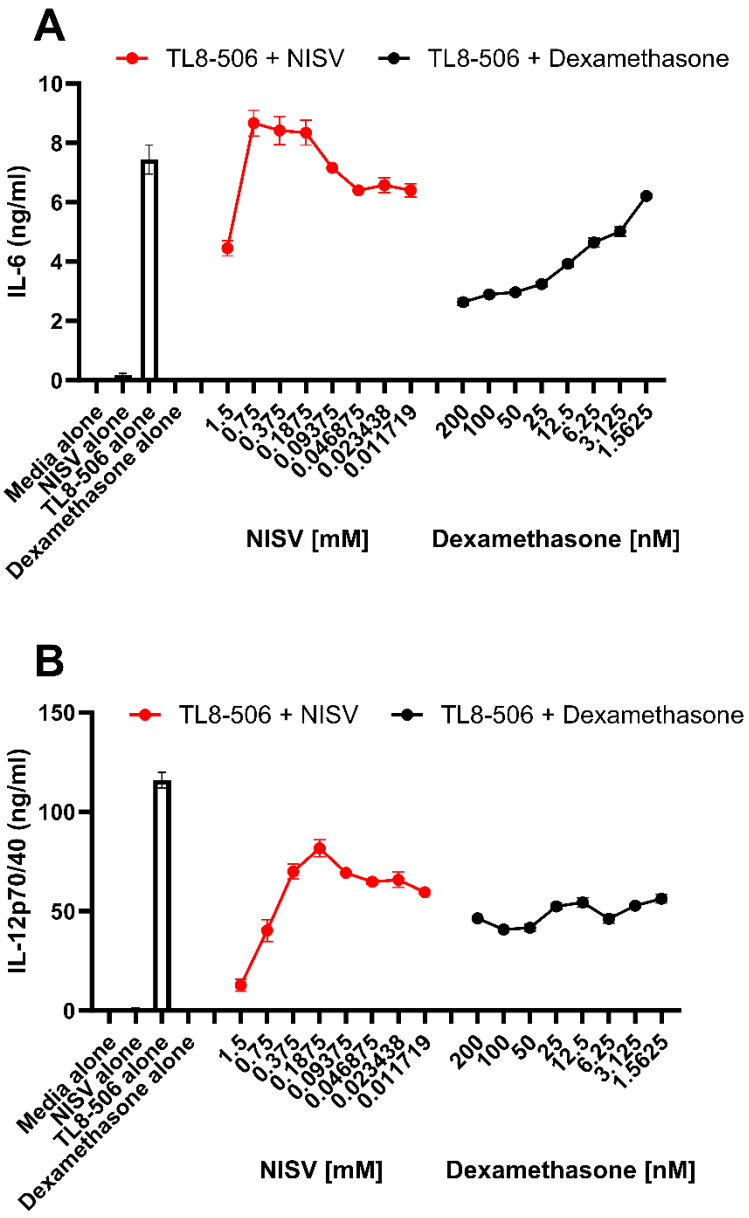

Figure 21: Effect of NISV or low-dose dexamethasone on IL-6 and IL-12 production by TLR8 stimulated BMDM. *1x10^{6}cells/ml were seeded per well into a 96-well plate and stimulated with 1.5µg/ml TL8-506. A 1 in 2 serial dilution of either NISV or Dexamethasone starting at 1.5mM or 200mM respectively was also added to the BMDM. Control cells were given either media alone, TL8-506 alone, NISV alone, or dexamethasone alone. ELISA for IL-6 (A), and IL-12 (B) used to quantify cytokine levels. Results are mean ± SEM. n=3.*

3.4.3 Cytometric bead array analysis

To further investigate the effect of NISV and dexamethasone on a broader range of cytokines, a cytometric bead array was performed. Prior to this, an alamarBlue assay **(Fig. 22)** and ELISA for IL-6 and IL-12 were performed on cell supernatants to ensure the successful stimulation of cells before analysis by bead array. Regardless of TLR ligand stimulation or NISV/Dexamethasone treatment, all cells were viable, with NISV treated cells displaying increased levels of alamarBlue reduction compared with the control. Cytokine levels were consistent with previous assays (not shown).

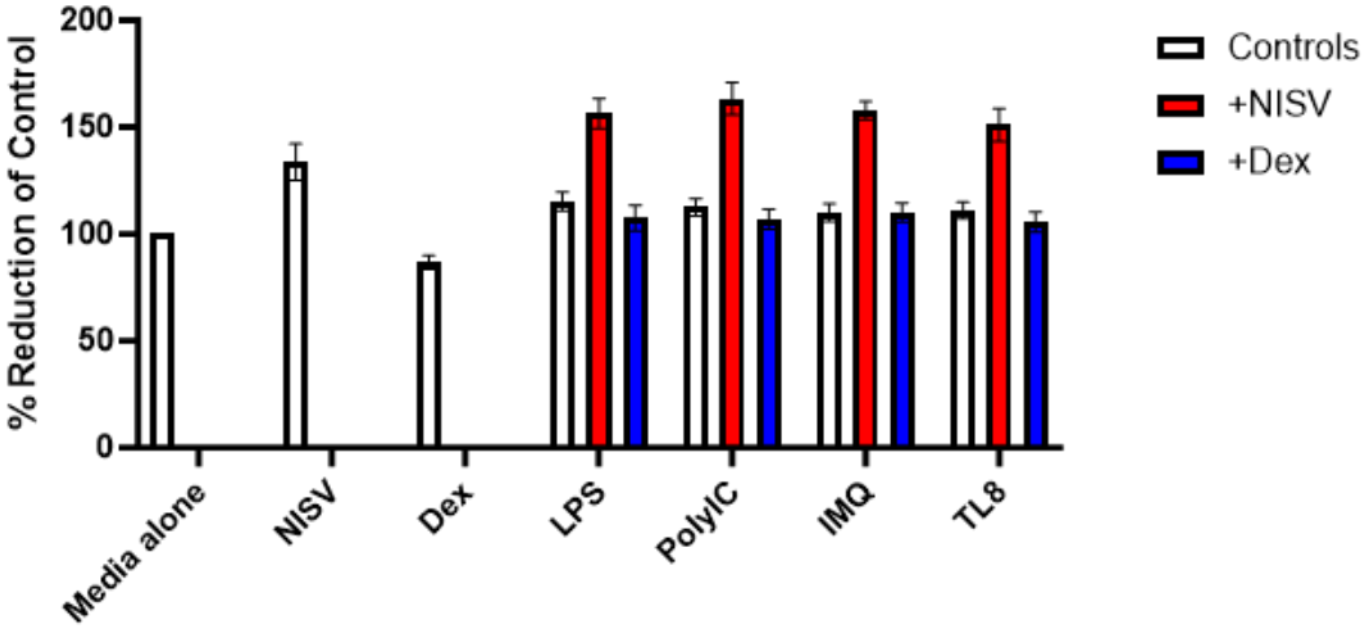

Figure 22: Quality control for cell viability. *BMDM were stimulated with 1.3μg/ml LPS, 6.8μg/ml Poly(I:C), 1.6μg/ml Imiquimod, 1.3μg/ml TL8-506. Cells were then also given either1.2mM NISV or 1.67μM Dexamethasone and an alamarBlue assay was performed to assess cell viability. Reduction of alamarBlue is shown as a percentage of healthy untreated media alone cells. Results expressed as mean ± SEM, n=3.*

Utilising the LEGENDPLEX cytometric bead array assay allows the simultaneous detection of multiple analytes in a sample using monoclonal antibodies conjugated to 2 populations of beads of differing size. Each bead also has a distinct level of APC fluorescence which is used to further differentiate between analytes, which can be determined using a flow cytometer. Combining an inflammation and anti-viral panel allowed the detection of 17 discrete cytokines, chemokines, or other soluble mediators **(Table 4).** Principal component analysis (PCA) plots **(Fig. 23)** were generated to examine sample grouping and the resulting loading plots **(Fig. 24, Fig. 25, Fig. 26, Fig. 27)** used to highlight factors contributing to the greatest variance. Generally, samples displayed good grouping and were either grouped tightly across one principal component if not both. Comparing the loadings of each group, starting with LPS, >70% of total variance was attributed to PC1 (58.17%) and PC2 (26.99%) **(Fig. 24)**. Factors loading onto PC1 at the greatest level included IL-6, TNF-α, RANTES, IP-10, and IL-27 with IL-6 contributing the most. For PC2, there was similar factor loading as displayed with PC1, but this now included an increased contribution from IL-1α and KC (also known as CXCL1). Examining Poly(I:C) **(Fig. 25)**, >70% of variance was attributed to factors loading onto PC1 (71.9%) and included similar cytokines/chemokines as displayed in both PC1 and PC2 of the LPS loading analysis. IL-6, TNF-α, IL-27, KC, RANTES, IP-10, and IL-1α displayed the greatest loading onto PC1 with small contributions from IL-1β, IFN-β and MCP-1. Notably, IP-10 displayed the greatest contribution to PC1 variance. Examining groups containing the TLR7 ligand Imiquimod, PC1 alone accounted for >70% of variance at 81.97% **(Fig. 26)**. Again, IL-6, TNF-α, KC, RANTES feature as contributing greatly, with increased levels of contribution from IL-1α and IL-1β. Furthermore, IP-10 contribution was decreased when compared to that of LPS or Poly(I:C) samples. This trend is repeated with TL8-506 treated samples, with PC1 explaining 77.69% of variance **(Fig. 27)**. Notably, whilst the trend is similar to that of Imiquimod treated samples, there is an increased contribution to variance by the factors IL-1α and TNF-α.

Table 4: Cytokines analysed in cytometric bead array.

IL-23	IL-1α	IL-12p70
TNF-α	MCP-1	IL-6
IL-1β	IL-10	IFN-β
IL-27	IL-17A	RANTES
GM-CSF	KC	
IP-10	IFN-α	

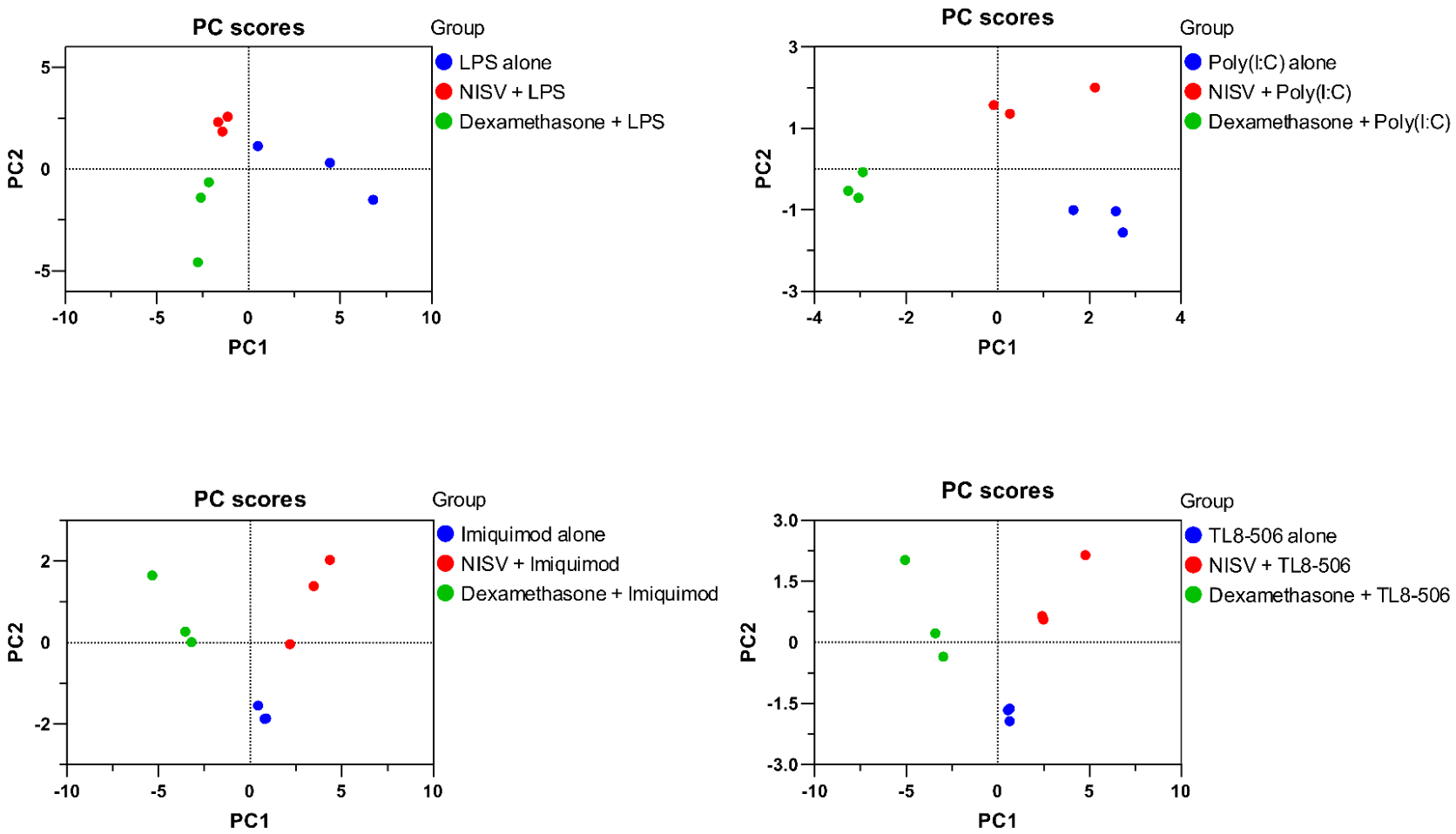

Figure 23: Variance amongst samples used in cytometric bead array. *BMDM stimulated with either LPS (TLR4), Poly(I:C) (TLR3), imiquimod (TLR7), or TL8-506 (TLR8) were treated with either NISV or dexamethasone. Cytokines detected during bead array analysis were used as variables and principal component analysis was performed to assess sample grouping. Principal components selected based on 2 largest eigenvectors*.

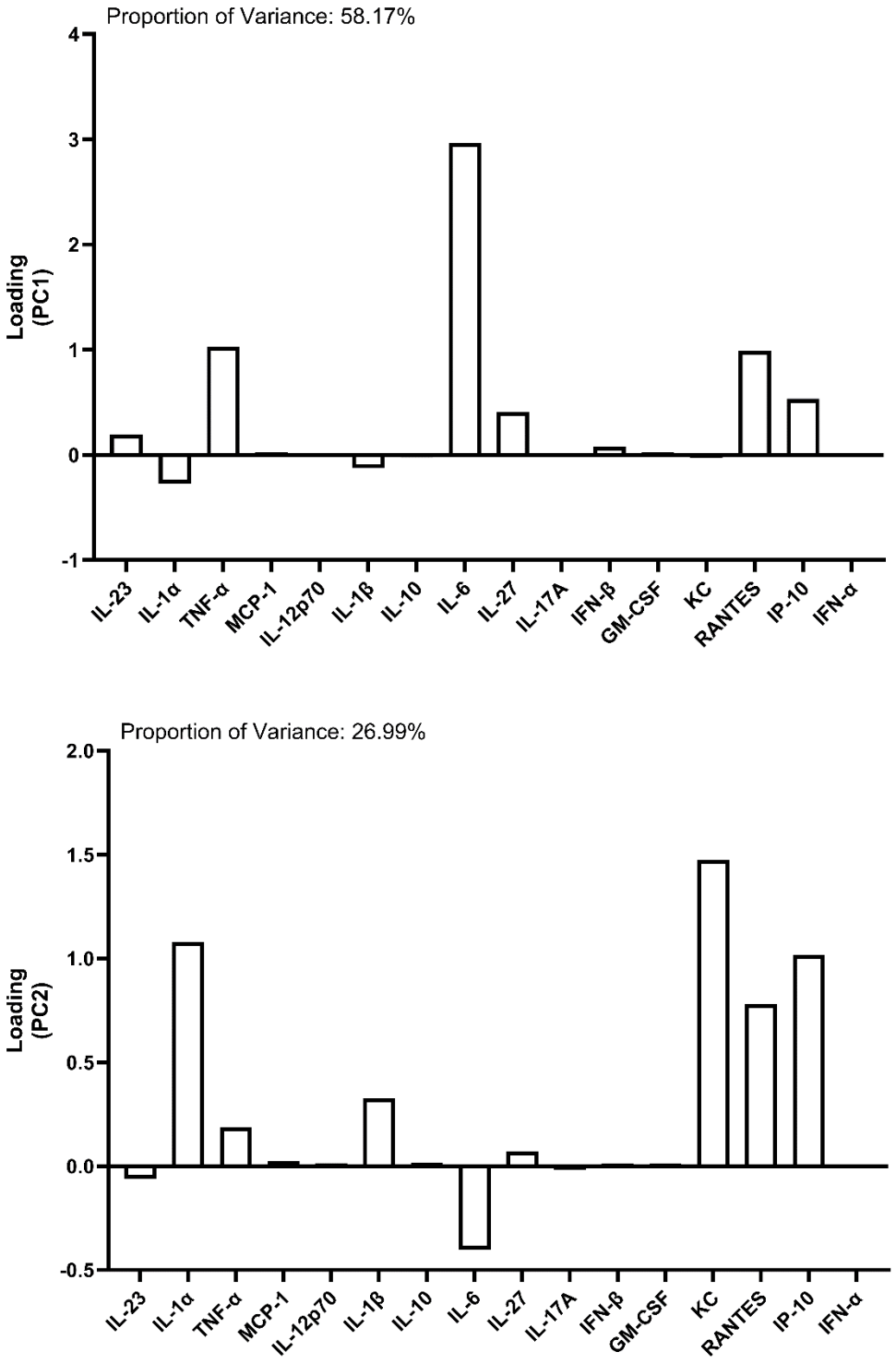

Figure 24: Loadings of factors onto PC1 and PC2 for LPS stimulated samples. *BMDM were stimulated with 1.3μg/ml LPS alone, or with either 1.2mM NISV or 1.67μM dexamethasone. Principal component analysis was performed on cytokine levels quantified using LEGENDPLEX bead arrays. >70% of variance explained by PC1 and PC2 loadings. Bars represent each cytokine's contribution (loading) to driving variance between the groups, which can be both positive or negative modulation.*

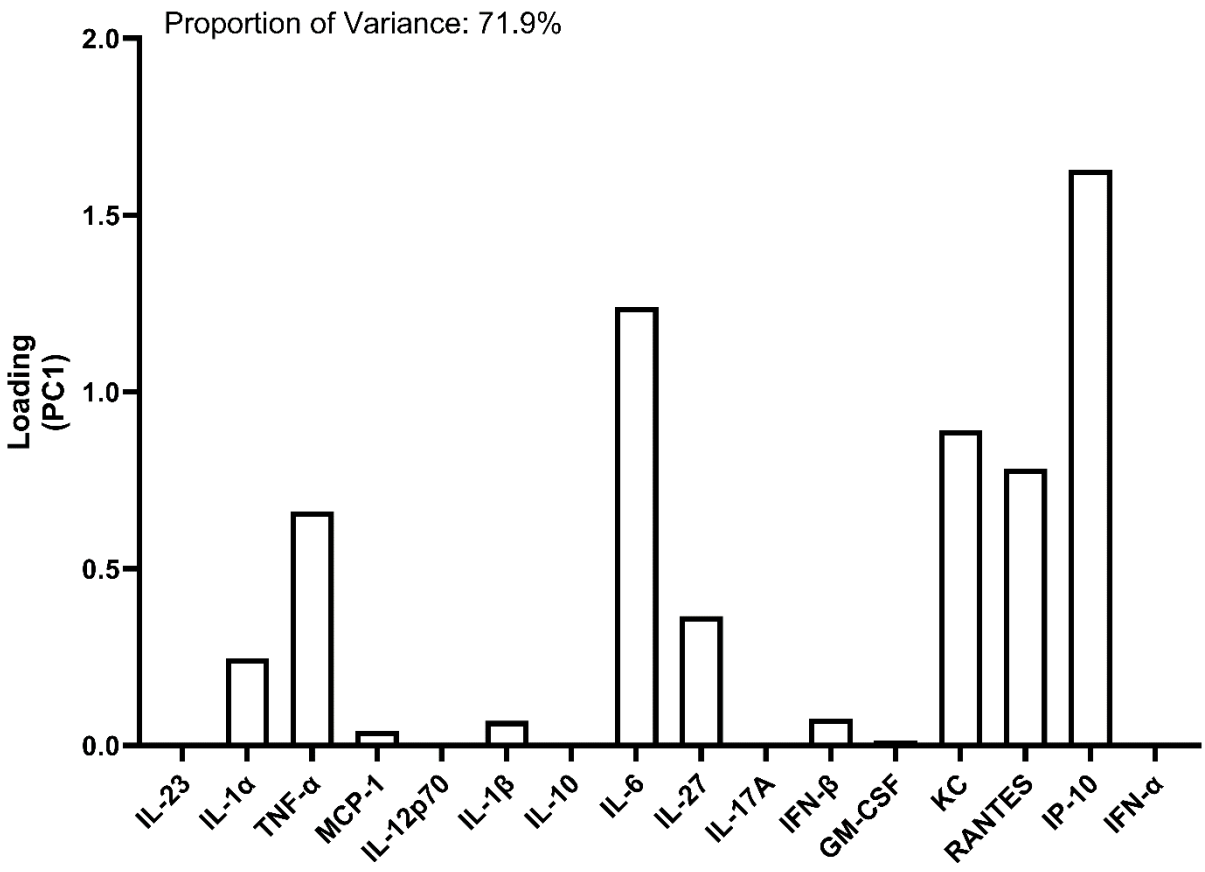

Figure 25: Loadings of factors onto PC1 for Poly(I:C) stimulated samples. *BMDM were stimulated with 6.8μg/ml Poly(I:C) alone, or with either 1.2mM of NISV or 1.67μM dexamethasone. Principal component analysis was performed on cytokine levels quantified using LEGENDPLEX bead arrays. PC1 chosen as it represents >70% of sample variance. Bars represent each cytokine's contribution (loading) to driving variance between the groups, which can be both positive or negative modulation.*

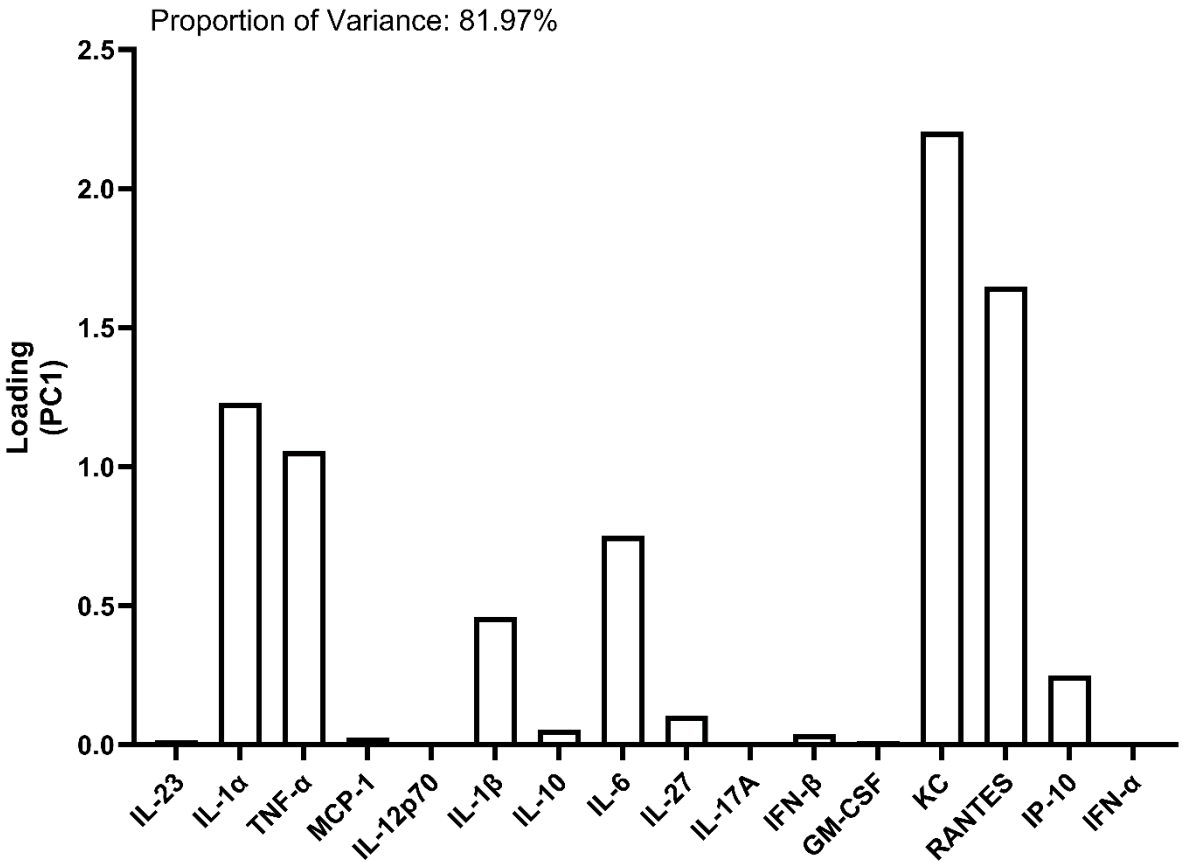

Figure 26: Loadings of factors onto PC1 for Imiquimod stimulated samples. *BMDM were stimulated with 1.6µg/ml imiquimod alone, or with either 1.2mM of NISV or 1.67µM dexamethasone. Principal component analysis was performed on cytokine levels quantified using LEGENDPLEX bead arrays. PC1 chosen as it represents >70% of sample variance.PC1 chosen as it represents >70% of sample variance. Bars represent each cytokine's contribution (loading) to driving variance between the groups, which can be both positive or negative modulation.*

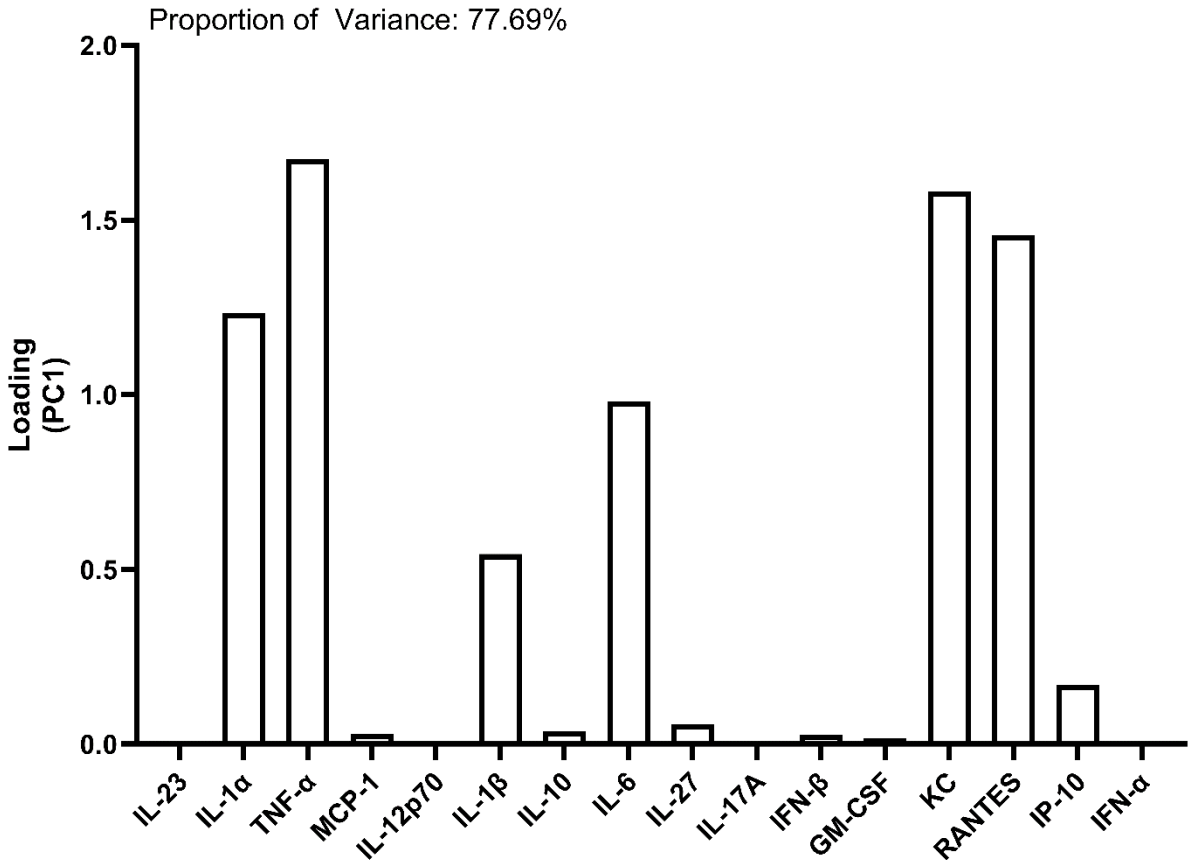

Figure 27: Loadings of factors onto PC1 for TL8-506 stimulated samples.
BMDM were stimulated with 1.3µg/ml TL8-506 alone, or with either 1.2mM of NISV or 1.67µM dexamethasone. Principal component analysis was performed on cytokine levels quantified using LEGENDPLEX bead arrays. PC1 chosen as it represents >70% of sample variance. Bars represent each cytokine's contribution (loading) to driving variance between the groups, which can be both positive or negative modulation.

To further visualise the changes in cytokine/chemokine milieu, heatmaps were generated to compare the change in cytokine/chemokine levels induced by NISV alone or Dexamethasone alone **(Fig. 28)** compared with the control (media alone).

The effect of NISV appears to be mostly slightly stimulatory with an increase in the cytokines in all cytokine assays except MCP-1, IL-12, IL-27, IL-17A, IFN-β, and GM-CSF. Therefore, it is clear that NISV possess immunomodulatory abilities rather than just an anti-inflammatory effect. In contrast, dexamethasone appeared to have less immunostimulatory activity, with only slight increases in IL-1, TNFα, IL-6, KC, RANTES, and IP-10 compared with the media alone control. Notably, there appears to be strong downregulation of IFN-α. Whilst these findings appear contradictory to the effect of dexamethasone, it is likely that cytokine levels were low in both the media alone and dexamethasone alone samples, and thus cytokine detection is influenced by a degree of baseline noise due to the detection limits of the assay.

When comparing the effects of various TLR stimulation on BMDM, we note the general pattern of cytokine upregulation is maintained across all TLR with some minor deviations between TLR7/TLR8 and TLR3/TLR4. In all groups we observe strong production of TNFα and IL-6 (although this effect is greater in TLR3/TLR4), alongside IL-1α, KC, RANTES, and IP-10 upregulation. A particular schism between TLR7/TLR8 and the other TLR stimulated BMDM is the stronger induction of MCP-1 and IL-27 production by TLR3 and TLR4 stimulated BMDM.

Comparing the effect of NISV on cells stimulated with either LPS **(Fig. 29)**, Poly(I:C) **(Fig. 30)**, Imiquimod **(Fig. 31)**, or TL8-506 **(Fig. 32)** reveals that NISV exert both stimulatory and inhibitory effects on cells dependent on the accompanying TLR stimuli. For TLR4 and TLR3 stimulated cells (LPS and Poly(I:C)), pro-inflammatory cytokines such as IL-6, TNF-α, IL-27, were downregulated compared with the ligand alone control. In contrast, this effect was inverse in Imiquimod and TL8-506 (TLR7 and TLR8) stimulated cells, with IL-6, TNF-α, and IL-27 showing increased levels. TLR4 and TLR3 stimulated cells generally experienced downregulation across a greater proportion of the assayed mediators including GM-CSF, RANTES, IFNα, IFN-β, and IL-10. Downregulation of TNF-α was not present in either TLR7 orTLR8 stimulated cells. There were also differences between TLR4 and TLR3 stimulated cells, with MCP-1, IL-12p70, and IL-17A being downregulated in Poly(I:C) + NISV treated samples compared to LPS + NISV treated samples. However, there are common factors between all TLR groups treated with NISV, such as consistent

strong upregulation of IL-1α and IL-1β, and a weaker downregulation of IL-10 and IFN-β.

When examining the effects of Dexamethasone on cytokine/chemokine production in various TLR stimulation scenarios, there is broad downregulation of almost all mediators assayed, and those that are not downregulated are unchanged compared with that of the ligand alone control. There appears to be some differences in the level to which certain cytokines are downregulated by Dexamethasone dependent on the TLR stimuli given to the BMDM. For example, IP-10 is greatly downregulated in TLR7 and TLR8 stimulated cells given Dexamethasone, compared with a smaller degree of downregulation in TLR3 and TLR4 stimulated cells. Both IL-1β and IL-6 are downregulated to a greater extent in TLR8 and TLR3 stimulated cells. Generally, TLR4 stimulated cells displayed the least amount of downregulation conferred upon them by dexamethasone, with little or no change in IL-12p70, IL-10, IL-17A, KC, and RANTES.

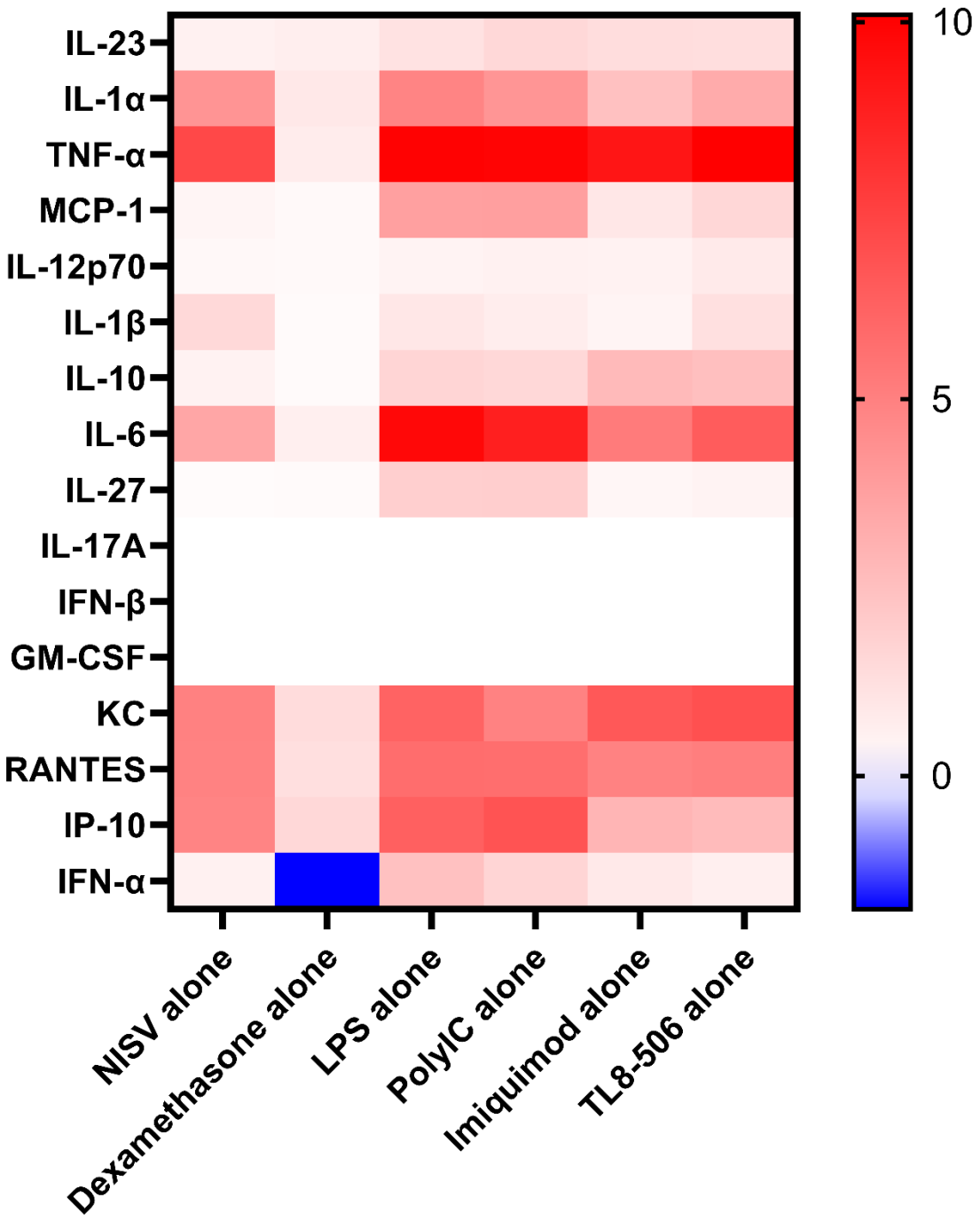

Figure 28: Effect of treatments or stimulation alone on cytokines/chemokines measured by cytometric bead array. *Unstimulated BMDM were treated with NISV alone, dexamethasone alone, or TLR3 (Poly(I:C), TLR4 (LPS), TLR7(imiquimod), or TLR8 (TL8-506) ligands alone and compared with unstimulated BMDM. Log2 fold change was calculated and heatmaps were generated. Results expressed as mean value. n=3.*

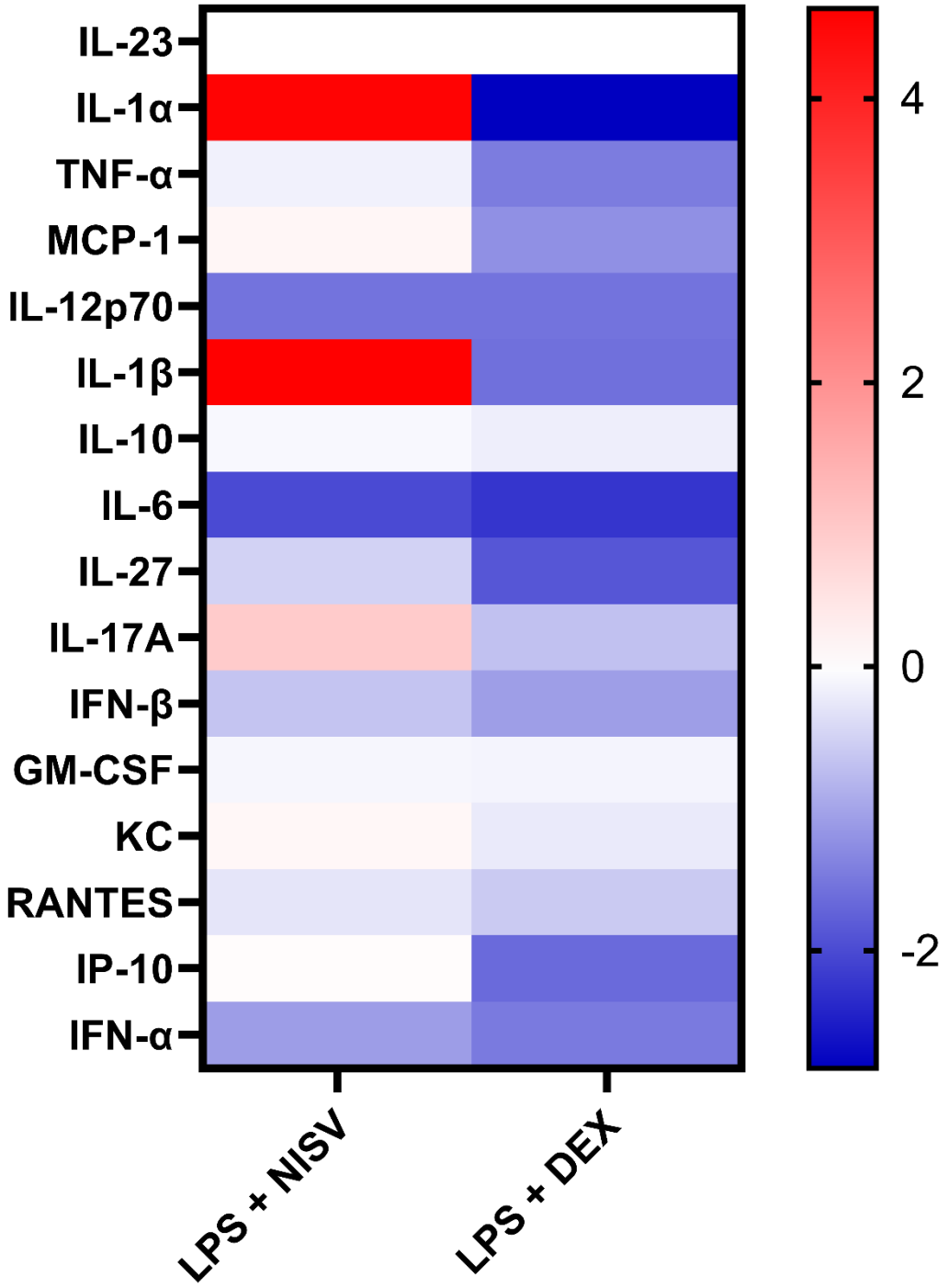

Figure 29: Effect of NISV or dexamethasone on cytokine/chemokine production by LPS stimulated BMDM. *Cells were stimulated with 1.3µg/ml LPS and treated with either 1.2mM NISV or 1.67µM dexamethasone. Log2 fold change was calculated and heatmaps were generated. Results expressed as mean value. n=3*

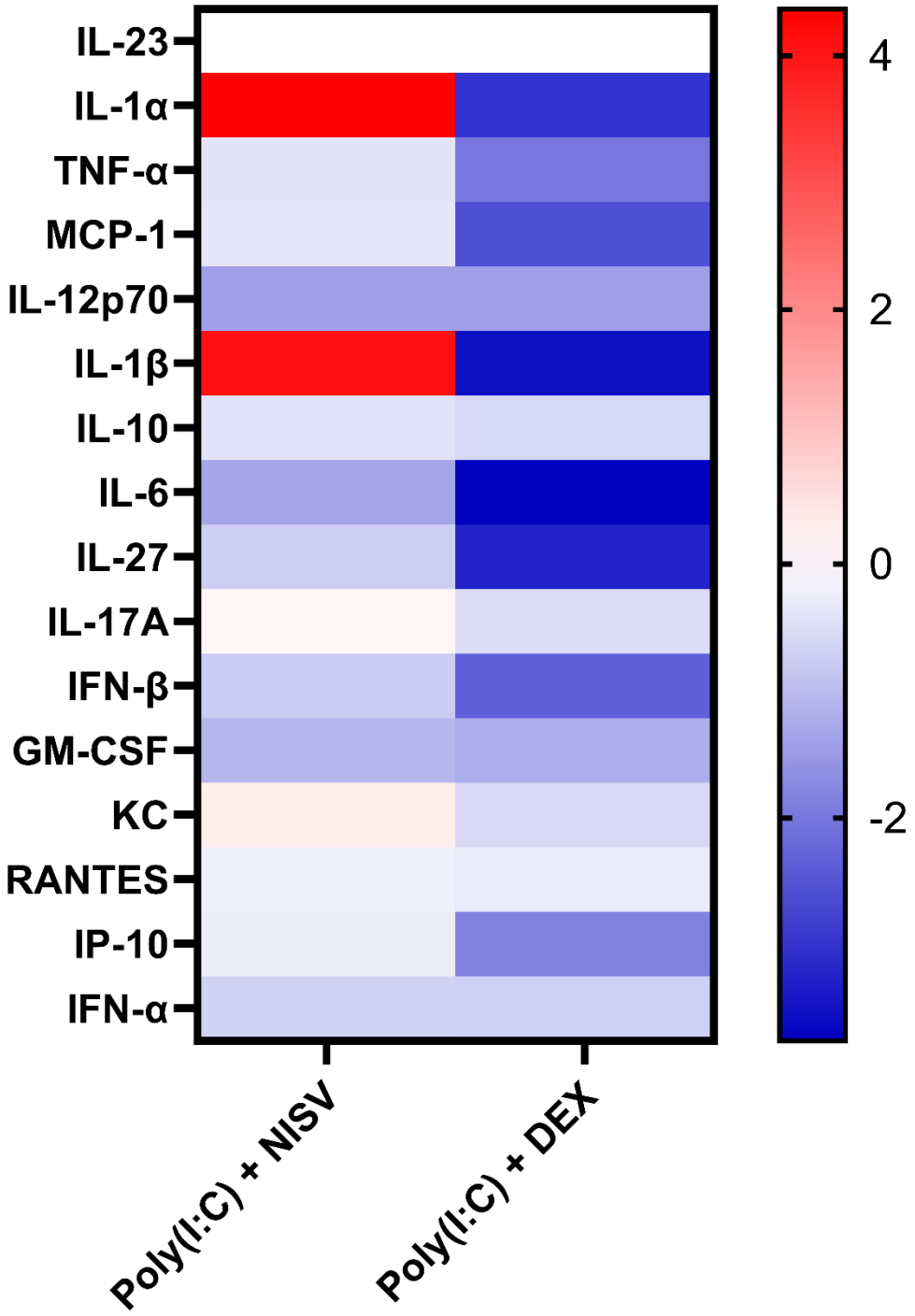

Figure 30: Effect of NISV or dexamethasone on cytokine/chemokine production by Poly(I:C) stimulated BMDM. *Cells were stimulated with 6.8µg/ml Poly(I:C) and treated with either 1.2mM NISV or 1.67µM dexamethasone. Log2 fold change was calculated and heatmaps were generated. Results expressed as mean value. n=3.*

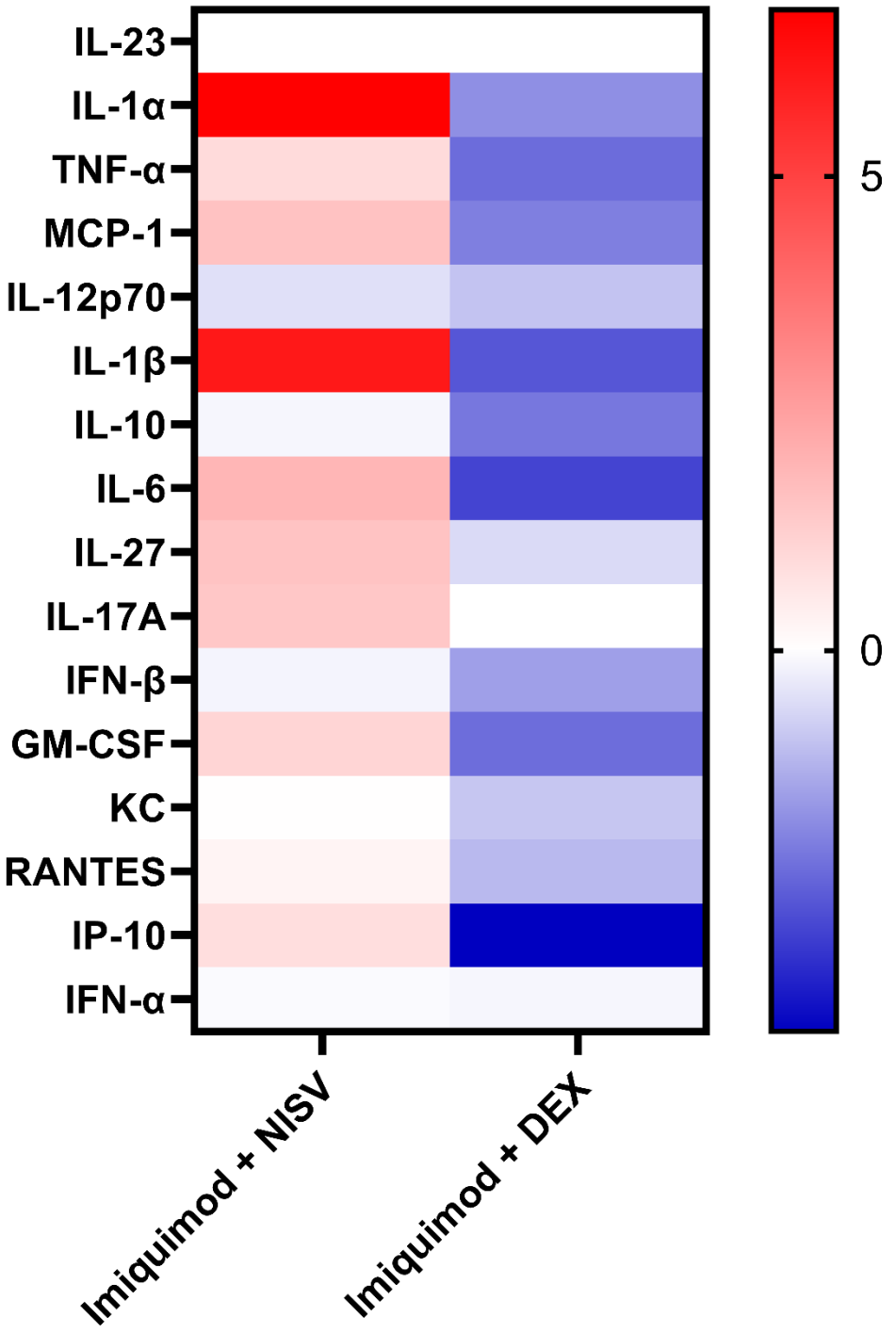

Figure 31: Effect of NISV or dexamethasone on cytokine/chemokine production by imiquimod stimulated BMDM. *Cells were stimulated with 1.6μg/ml imiquimod and treated with either 1.2mM NISV or 1.67μM dexamethasone. Log2 fold change was calculated and heatmaps were generated. Results expressed as mean value. n=3.*

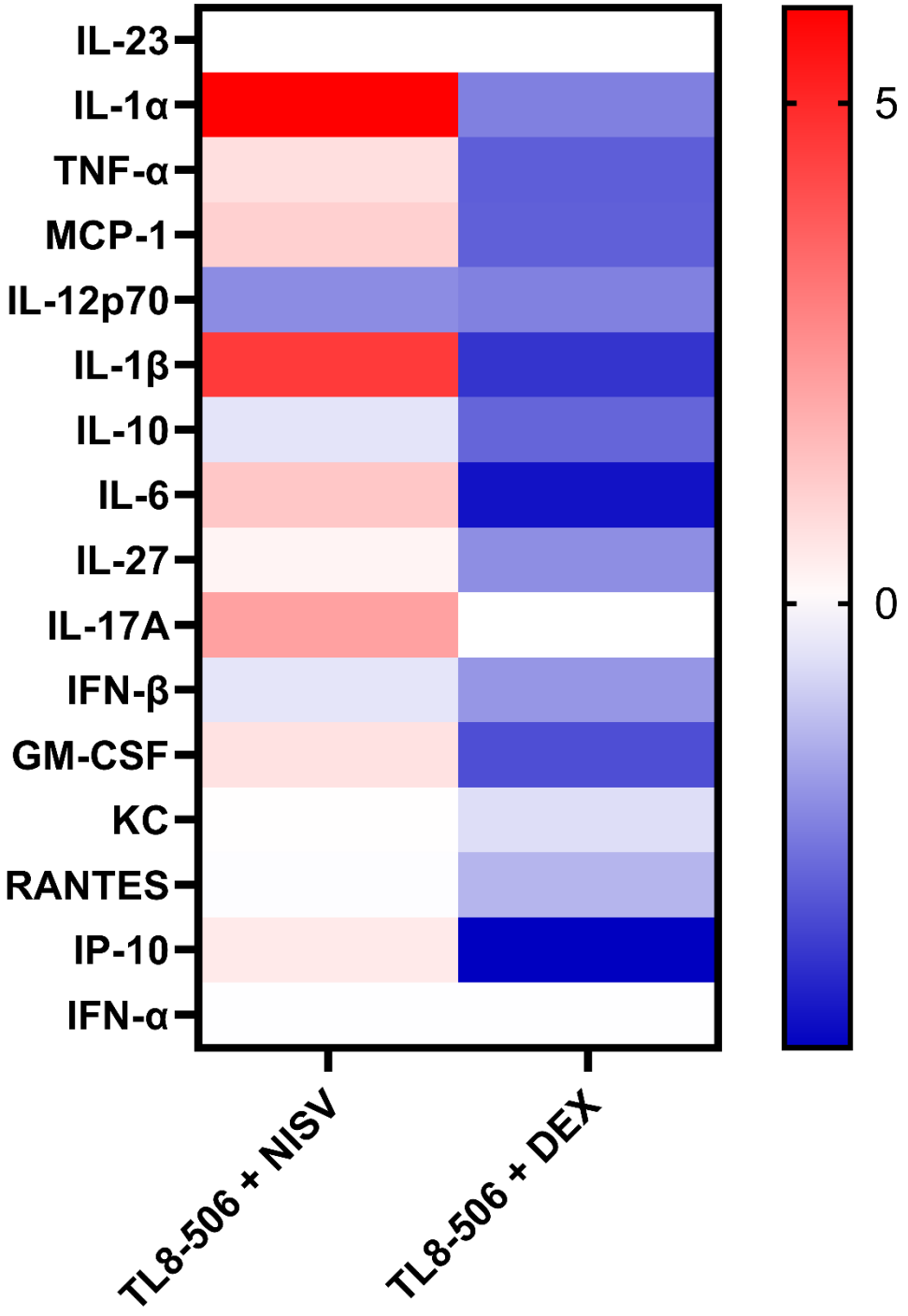

Figure 32: Effect of NISV or dexamethasone on cytokine/chemokine production by TL8-506 stimulated BMDM. *Cells were stimulated with 1.3µg/ml TL8-506 and treated with either 1.2mM NISV or 1.67µM dexamethasone. Log2 fold change was calculated and heatmaps were generated. Results expressed as mean value. n=3.*

3.5 Discussion

To characterise BMDM, not only was flow cytometry used to identify the phenotype of the population but also other factors. For example, cells observed using light microscopy present typical macrophage morphology and display adherence upon maturity. Furthermore, the conditioned L-929 cell media used to differentiate murine stem cells is rich in M-CSF, lending further credence to the identity of our cell population. Whilst the high levels of CD11b indicate a monocyte/macrophages population this marker is also present on neutrophils and eosinophils. Both CD11c and CD86 are not exclusive to macrophages, as they may also be found on the surface of dendritic cells, however, paired with the albeit lower expression of macrophage – specific F4/80 on the cell population, this provides confidence that the cultured cells are macrophages with low levels of DCs potentially also present.

Production of NISV via the melt method generally yields large, heterogenous NISV compared with other established methods of NISV production such as microfluidics. Whilst this method relies heavily on user experience and manual combination of components, these studies have demonstrated that batch-to-batch differences can be quite low. There are 3 defining factors that separate melt method NISV from those vesicular carrier systems in conventional use today: size, heterogeneity of vesicle population, and structure of NISV. Size of NISV has previously been shown to affect localisation within macrophages, with small NISV (<200nm) being trafficked to lysosomes, whereas large NISV (>500nm) did not, and were instead found in the peripheral compartments (ref). Furthermore, small NISV were likely taken up by endocytosis, whereas the larger NISV were taken up by actin-dependent phagocytosis *(Brewer, et al., 2004)*. The effect of NISV size is further explored in chapter 2. Polydispersity is a measure of how homogenous/heterogenous particles are in each suspension and is measured as an index from 0 (fully homogenous) to 1 (fully heterogenous). Due to the manual method of production, the melt method lends itself to higher PDI than more controlled methods of production such as microfluidics or sonication. Whilst current consensus leans towards uniform NISV for applications such as drug delivery where delivering a consistent product is key, the inherently higher PDI of melt method NISV may play a part in their immunomodulatory abilities *(Roberts, et al., 1997).* Whilst uniformity may be a desired characteristic of NISV, the ideal size is debated as both NISV size and structure should be tailored to the application at hand with previous data utilising

liposomes indicating that both large and small liposomes can be used therapeutically *(McAlvin, et al., 2014; Sofou, et al. 2010; Gabizon, et al., 1989; Lopez-Berestein, et al., 1985).*

Cytotoxicity of NISV was measured using the well-established alamarBlue assay. This assay relies on the abilities of functional cell mitochondria to reduce a blue resazurin salt to a red resorufin compound. The degree of colour change can be measured spectrophotometrically and acts as an indicator of cell proliferation or loss of cell viability *(Sherry, et al 1998).* Previous work in our laboratory has revealed that both NISV and TLR stimulation can increase the rate at which resazurin is reduced, which can be explained primarily by an increase in cell metabolism due to increased phagocytosis of particles, or encountering PAMPs, triggering their activation. Furthermore, encountering unincorporated MPG, or NISV broken down during phagocytosis likely generates free surfactant which could have a damaging effect on cells, increasing their metabolic response to NISV *(Inácio Â, S. et al, 2011)*. However, as this assay relies on measuring the absorbance of both colours (570nm for blue and 600nm for red) it should be stated that highly turbid samples such as those containing high concentration of NISV may display a perceived increase in alamarBlue reduction due to absorbance of light by NISV. To accurately calibrate our alamarBlue assays on a plate-to-plate basis, we display the level of reduction as a % of the maximum reduction value ascertained from cells given media alone, which are unstimulated and provides a baseline level of reduction for “healthy” cells. When examining our alamarBlue assays, our results were consistent with the earlier observations of previous lab work in terms of increased metabolism caused by NISV or TLR ligand stimulation. Dexamethasone generally displayed lower levels of alamarBlue reduction which has been demonstrated in other cell types *(Wong, et al., 2009)* which could be attributed to effects on gene transcription and NF-kB, reducing the ability of cells to produce the enzymes necessary to provide reducing agents such as NADH and FADH, or through dexamethasone induced mitochondrial dysfunction *(Luan, et al., 2019; Desquiret, et al., 2008).*

When generating EC values, IL-6 and IL-12 production was measured as a function of TLR stimulation. These cytokines were chosen from both a practical experimental standpoint and grounded in theory. IL-6 is heavily implicated in generation of an inflammatory response, and modulation of this cytokine by NISV has previously been investigated in our lab (ref?). Furthermore, as a well-studied cytokine, the

literature available was abundant. IL-12 was chosen in a similar manner after initial experiments that stimulation of TLR7 and TLR8 may not induce production of IL-6 as strongly as TLR3 and TLR4 stimulation. IL-12 is also important during viral infections as it can activate natural killer cells, enhance Th1 CD4+ T cells, and increase production of IFNy

For TLR3, TLR7, and TLR8, there was little discrepancy between the ability of Poly(I:C), imiquimod, or TL8-56 to induce either cytokine. Whilst induction of IL-6 by LPS was measured and EC values calculated, the ability of LPS to induce IL-12 production was much reduced compared with the other ligands used. Therefore, the IL-12 EC values for LPS were not included as they were deemed unreliable due to low levels of the cytokine produced interacting with the limit of detection and noisy baseline of our assay. Whilst this data displays that the concentrations of ligands used to provoke IL-6 and IL-12 production from BMDM are remarkably similar, further investigation into whether these concentrations are able to optimally induce the maximal response for other cytokines should be undertaken. Whilst this investigation into the cytokine milieu produced under various TLR stimulation utilised the EC90 values generated from these experiments, it is unlikely that this was the optimal concentration for all cytokines assayed in the bead array. Furthermore, whilst the shape of each IL-6 or IL-12 production curve generated from a long dilution series of each ligand was sigmoidal for LPS and Poly(I:C), this was not the case for imiquimod and TL8-506. In contrast, instead of plateauing at a maximal concentration of cytokine production, there was a narrow peak of cytokine production that quickly dropped off as concentration increased. This effect was not due to a loss of cell viability or increased toxicity at high concentrations of the ligand as our viability assay displayed levels of alamarBlue reduction higher than that of the media alone cells. Therefore, to generate EC50/90 values for these ligands, I opted to discount the values after the peak generated by the higher concentrations of imiquimod or TL8-506 and utilise the pseudo-sigmoidal shape of the curve descending from the peak.

To generate IC50s for NISV and Dexamethasone, LPS induced IL-6 production was used as previous work in the lab has well characterised anti-inflammatory properties of NISV using this combination.

The anti-inflammatory actions of NISV on TLR3 and TLR4 stimulated cells demonstrated in this study is consistent with previous observations. Furthermore,

the inhibitory effect of Dexamethasone on TLR3 and TLR4 stimulated cell IL-6 and IL-12 production is not surprising due to its potent action on NF-kB. However, the disparity between these findings and the effect of both NISV and Dexamethasone on TLR7 and TLR8 stimulated cells raise some questions. Firstly, are the actions of NISV and Dexamethasone TLR specific? There are a number of factors that differ between the TLRs studied in this chapter, such as the adaptor protein and signalling pathway activated after ligation, the downstream transcription factors, and the location of the receptor on the cell.

Of the TLR studied, TLR4 uses both TRIF and MyD88 as their adaptor proteins to initiate intracellular signalling. TLR3 exclusively uses TRIF, whereas TLR7 and TLR8 use MyD88 exclusively. Whilst there is some considerable crossover in the downstream signalling of these TLRs, the transcription factors that are generally activated after ligation of the TLR may play a defining role in observed cellular responses and subsequent effects of NISV/dexamethasone. These pathways are further explored in chapter 6 using transcriptomic analysis. A key observation was the adjuvant effect of NISV on TLR7 and TLR8 stimulated cells detected as an increase in IL-6 production. Interestingly, this effect is somewhat replicated with other cytokines such as the “leaderless” IL-1α and IL-1β as seen in the bead array, regardless of which TLR was used to provide cellular stimulation *(Kawasaki, and Kawai, 2014).*

Encoded by the genes IL1A and IL1B, production of IL-1a and IL-1β is not wholly reliant on transcription of genes but instead requires unique processing. For example, IL-1α is produced first as pro-IL-1α and is localised to the cytosol, where it remains as a cell-associated cytokine (*Malik,and Kanneganti, 2018).* Pro-IL-1α is biologically active and may be cleaved by calpain to generate IL-1α. There are key differences in the biological processes of these two forms of IL-1α. The pro-protein can act as an intracellular alarmin as well as binding chromatin. This causes pro-IL-1α to be sequestered and can act as a regulatory measure in the inflammatory loop of IL-1α signalling. Pro-IL-1α may also be trafficked to the outer surface of the plasma membrane where it can be cleaved to produce IL-1α and initiate inflammatory signalling between cells. Cleavage of the pro-protein whilst it resides within the cell can yield mature IL-1α that is released upon cell necrosis, acting as an inflammatory signal. Despite these differences both pro-IL-1α and IL-1α bind to

the same receptor (IL-1R1) and can thus induce comparable biological effects *(Afonina, et al., 2015).*

In contrast, pro-IL-1β is biologically inactive and must be cleaved by the IL-1 converting enzyme (ICE) also known as capase-1. Another difference between IL-1β and IL-1α is that IL-1β is not cell-associated or constitutively expressed, instead secretion is induced by cells in response to PRR ligation or DAMPs. Despite this, the function of secreted IL-1β and IL-1α is largely the same, both binding to IL-1R1 and exerting signal transduction through TIR domains, like that of the TLRs.

Release of both IL-1α and IL-1β does not follow the canonical protein secretion pathway e.g.. expression, trafficking to the ER for folding, and budding from the Golgi for exocytosis. Instead, the action of caspase 11 has been implicated in the initiation of pyroptosis and thus pro-inflammatory cell lysis and release of cell contents into the extracellular space. Studies have demonstrated that pore formation mediated by gasdermin D is critical for this process. Gasdermin D must also be proteolytically cleaved, either by caspase 11 or caspase 1 (similar to IL-1β) to initiate pyroptosis and subsequent release of IL-1α/β. This method of pyroptosis mediated by gasdermin D is regulated in part by the non-canonical NLRP3 inflammasome Interestingly, it has been shown that gasdermin D is critical for lethal sepsis in mice and thus investigation into the ability of NISV to alter this pathway may yield insight into more focused therapeutic applications of this treatment *(Kayagaki, et al., 2015).*

Our data also demonstrated an interesting interaction of dexamethasone and TLR7/TLR8 stimulated cells. At concentrations of the drug that were previously effective at reducing IL-6 and IL-12 production in TLR3 and TLR4 stimulated cells, we noted a reduction in the effectiveness of dexamethasone, particularly with IL-12 production, in TLR7 and TLR8 stimulation scenarios. Whilst a degree of cytokine downregulation was present, the classical dose-response curve that was previously demonstrated was absent, being replaced with a plateau at around 50% of total IL-12 production as measured against the ligand alone control. Previous studies have demonstrated that in cases of systemic lupus erythematosus (SLE), chronic activation of TLR7 by self-RNA confers a degree of glucocorticoid resistance, reducing the effectiveness of drugs like dexamethasone. As dexamethasone exerts effects through interactions with NF-kB, alternative transcription factors activated during TLR7 and TLR8 ligation may allow IL-12 to be produced despite the effects of dexamethasone *(Guidducci, et al., 2015).*

Dexamethasone also displayed much broader downregulation of cytokines assayed in the cytometric bead array, which was generally consistent across all TLR stimulation scenarios. Unlike NISV, the mechanism by which dexamethasone exerts its anti-inflammatory effect is well studied, and thus the similarity observed in cytokine modulation could be attributed to a common mechanism exploited by dexamethasone such as NF-kB disruption or simply binding to the GR. To further investigate this, blockade of GR binding may be used to determine the specific route of action of dexamethasone. It was noted that whilst the pro-inflammatory cytokines such as IL-6, TNFα, and IL-1α/β are downregulated in dexamethasone treated cells, there is also a decrease in cytokines that have anti-inflammatory effects. such as a decrease in IL-10 production. Studies have demonstrated that dexamethasone may have a biphasic effect on IL-10 production with high doses (such as in our study) inhibiting IL-10 production, and low doses stimulating IL-10 production *(Franchimont, et al., 1999; Mozo, et al., 2004).*

4 Chapter 4

Evaluating the effect of size on the immunomodulatory abilities of NISV

4.1 Abstract

NISV are a modifiable platform technology that can be produced using a variety of methods. Conventional NISV production techniques favour small, homogenous suspensions of vesicles to facilitate efficient delivery and uptake by cells. Production of NISV at the nanoscale (~100nm) level is achievable through the use of microfluidic techniques, streamlined by the use of equipment such as the NanoAssemblr Ignite. To evaluate the immunomodulatory abilities of these MPG:Chol:DCP vesicles and examine whether size is a critical factor for the efficacy of NISV, ELISA and cytometric bead arrays were utilised to quantify cytokine production from TLR stimulated BMDM treated with NISV of various sizes as an indicator of the immune response. Production and validation of the physical characteristics of NISV were made using the melt method, sequential extrusion through polycarbonate membranes (PCM), and using the NanoAssemblr platform. A simple method for generation of smaller vesicles from melt method NISV using a hand extruder is detailed. After production of NISV, a zetasizer was used to accurately characterise the size of each NISV preparation. The resulting NISV retained a negative charge and displayed a reduction in PDI that correlated with the sequential extrusion through membranes. To evaluate the effect of these different sized NISV, the quantification of IL-6 and IL-12 as sentinel cytokines was used as a marker of immunomodulation. Subsequent IC50 values generated from this data were used to compare the potency of NISV at various sizes, revealing TLR specific effects of NISV of different sizes, and an increase in toxicity induced by smaller NISV. Through further analysis of common inflammation cytokines and chemokines, it was demonstrated that size does not drastically alter the pattern of immunomodulation imparted by NISV but does increase the potency. This chapter provides a foundation for future characterisation of specific interactions with NISV of a determined size and various TLRs. To continue this investigation, future work may utilise imaging to study uptake or -omic technologies to discern the minutiae of size-dependent NISV immunomodulation at the transcriptional level or asses wider metabolic changes imparted by large vs small NISV.

4.2 Introduction

4.2.1 Origins of production methods

As a platform technology, NISV possess the potential for modifications to their physical structure which can be achieved through a variety of methods and formulae additions. Previously, it has been demonstrated that NISV (and liposomal systems to which NISV are a synthetic analogue) can be produced using different manufacturing methods ranging from small-scale laboratory techniques to “bulk” industry-scale technologies. Many of the techniques used for the production of NISV originate in liposomes. Initially, liposomes were discovered by Alec D Bangham in 1965, and produced using what would become known as the thin film hydration method (TFH). This method stems from Bangham’s initial discovery that a dried layer of lipids would spontaneously form a “fire balloon” shape upon hydration with water. TFH requires the lipid components to be solubilised in an organic solvent such as chloroform which is then slowly evaporated under a vacuum at 30ºC until a thin film of lipids remains. This is then hydrated with an aqueous solution and forms vesicles around 10-100nm in diameter (Bangham, et al., 1965). Other methods include the ethanol/ether injection methods first established by Batzri and Korn in 1973 (Batzri, and Korn, 1973), which involves solubilising the lipid components in an organic solvent such as ethanol, or in ether, and then injecting the solution into aqueous media using a very fine gauge needle and syringe. This generates small evenly dispersed vesicles but is also a lengthy process. A review of the most popular vesicle preparation methods is available from Meure, et al *(Meure, et al., 2008)*

4.2.2 Thermodynamics and self-assembly of NISV

Despite the many options for the production of NISV, a core concept that characterises the spontaneous self-assembly of vesicles is Gibbs free energy *(Gibbs, 1873).* This concept of thermodynamics describes the energy available in a closed system, with Gibbs free energy specifically combining both enthalpy and entropy into a single equation. Thus, the Gibbs free energy of a thermodynamic reaction

e.g., vesicle formation and can be defined by the equation:

$$G = H - TS$$

Where:

G = Gibbs free energy

H= Enthalpy

T= Temperature

S = Entropy

The resulting value or change in Gibbs free energy ($\Delta\mathrm{G}$) describes the reaction. A negative $\Delta\mathrm{G}$ value describes a spontaneous reaction, as the system becomes ordered, and the free energy decreases. Applying a basic understanding of Gibbs free energy to the production of NISV via the melt method we can visualise that NISV components in room temperature buffer have low enthalpy i.e.low total heat content of the system. By increasing both the temperature and entropy through heating of the NISV and applying agitation, we encounter the following situation:

$$G = H_{low} - T_{high} * S_{high}$$

Thus, providing a negative value of $\Delta\mathrm{G}$, indicating a spontaneous reaction – the self-assembly of NISV. Furthermore, the structural stability of NISV is supported by the reduction in Gibbs free energy. Before formation, the hydrophobic hydrocarbon groups of the free surfactant would not interact with water molecules, therefore restricting their movement – a decrease in entropy. When NISV are formed, the hydrophobic groups are sequestered within the bilayer membrane, reducing their interaction with water molecules. This allows for greater freedom of movement of water molecules and therefore an increase in entropy which ultimately maintains the low level of free energy in the system *(Eibl, 1984; Sych, et al., 2018).*

Aside from the thermodynamic requirements for NISV formation, production of a vesicle suspension often relies upon a number of production steps common to most methods. There are typically 4 key steps in preparing a functional suspension of vesicles for therapeutic application: liquification of vesicle components, which can be achieved through heating to a molten suspension, or solubilisation in an organic solvent; purification of the suspension to remove unreacted components, un-entrapped payload, or excess harmful solvents; Quality control and characterisation

of the physical parameters, typically determined using dynamic light scattering; and post-production modifications, such as extrusion or sonication to reduce the heterogeneity or size of the vesicles in the preparation *(Christian Isalomboto, et al., 2018; Akbarzadeh, et al., 2013).*

Whilst many of these methods can be scaled-up for industrial production, a platform with potential for mass-production of NISV is the NanoAssemblr from Precision Nanosystems. This platform utilises controlled microfluidic mixing on a chip to generate consistent vesicle suspensions quickly, using minimal amounts of liquid. Furthermore, this system can be easily scaled up from preclinical lab applications to full-scale manufacturing and clinical applications, as well as acting as a deployable nanomedicine production system for areas without the manufacturing infrastructure already in place *(Gdowski, et al., 2018).*

4.2.3 Desirable characteristic of clinical NISV

Examining the current landscape of treatments that utilise liposomes or similar vesicular delivery systems, such as Abeclet, DaunoXome, Doxil, Epaxal, and Myocet, 80-100nm vesicle are used often *(Carugo, et al.,2016).* Vesicle size is a determining factor for distribution, retention, and clearance of liposomes/NISV, with various organs able to filter out particles of different sizes. For example, particles less than 5nm can be cleared by the kidneys *(Liu, et al., 2013)*, whereas particles in the range of 6nm to 100nm can be cleared by the liver (Zhang, et al., 2016). Vesicle size may also dictate the route of delivery. For example, whilst it is unlikely that a suspension of NISV would contain vesicles >5μm using these production methods, any agglomeration, loss of stability, or loss of charge may generate larger particles in the suspension. This is particularly true for large NISV (>1000nm) in more heterogenous suspensions such as those produced using the melt method. For inhaled routes, this could cause particles to become sequestered in the capillaries of the lung (5-10μm diameter) *(Nemmar, et al., 2002; Kutscher, et al.,2010).* Furthermore, through intravenous injection, small emboli may form in capillaries, obstructing the flow of blood. Therefore, it is clear that vesicle size is a critical factor in payload-delivery situations, but size also affects the drug loading, and targetting capabilities of NISV. Smaller NISV also have a much-increased surface area-to-volume ratio, and it is well known that particles in the nano-scale benefit from this effect than those in the micro-scale, as this may increase the ability to entrap drugs within the membrane, increase bioavailability through increased interface with

tissues, or increase the ability of compounds on the surface of the vesicle to interact with a greater area *(Danaei, et al., 2018).*

Evidence also suggests that a negative charge is a desired characteristic of nanoparticles, with positively charged nanoparticles (e.g., +30mV) being cleared by phagocytes quicker than those with a negative charge. As serum proteins are negatively charged, it is likely that NISV with -30mV can be overlooked by patrolling phagocytes, whereas positively charged particles are more apparently foreign and therefore preferentially engulfed *(Trac, and Chung, 2021).* However, the converse is true, and NISV could be targeted to phagocytes by imparting them with a positive charge.

In terms of how heterogenous a vesicle suspension may be, or conversely how homogenous, this can be examined using a polydispersity index. Generally, clinical applications of liposomes or NISV desire a low PDI, generally around 0.2 or lower, with upper limits of around 0.3 *(Xu, et al., 2022).* Low PDI can also provide a higher cellular delivery dose of entrapped drugs than high PDI particle suspensions *(Johnston, et al., 2018).*

To investigate whether the differences of nano-scale and micro-scale vesicles extends to the immunomodulatory effects of NISV, we utilise the post-production method of size control known as extrusion *(MacDonald, et al., 1991).* This technique uses polycarbonate membranes of fixed pore size inserted into a gas-tight apparatus with attached syringes. By heating the NISV suspension to 60ºC to reach the phase transition from the gel-like solid phase, to the more malleable liquid phase, NISV can be repeatedly passed through pores to decrease their size. This technique has been widely used to create small, relatively monodisperse populations of nanoparticles such as liposomes. Whilst this technique has been explored by others to achieve desirable size for drug delivery, my interest is to evaluate the effectiveness of extrusion to produce small NISV from the melt method, and how this might affect the immunomodulatory properties displayed in chapter 3.

4.3 Aims and Hypothesis

This chapter aims to:

i. Generate NISV using multiple production methods and validate physical characteristics and immunomodulatory actions. NISV will be made using the melt method as before but will also be extruded through polycarbonate membranes of various sizes to produce NISV of sequentially smaller diameter, bridging the gap between the large melt method NISV and the small NanoAssemblr NISV. The toxicity and immunomodulatory abilities of these NISV will be examined using AlamarBlue cell viability assays, and ELISA for two sentinel cytokines: IL-6 and IL-12. By eliciting production of these cytokines with various TLR ligands, the aim is to determine if size is a critical parameter for immunomodulation, and any subsequent TLR + size specific differences.

ii. Evaluate the effects of NISV of different sizes over a broad cytokine milieu, with a focus on soluble mediators involved in the generation or resolution of inflammation using a cytometric bead array. NISV of different sizes may be taken up by different mechanisms, which could also influence ligand interaction with TLR dependent on the location of the receptor (surface or endosomal). Furthermore, NISV size may change the volume of NISV being ingested by macrophages influencing the magnitude of immunomodulation. Evaluating a range of cytokines and chemokines, an aim is to determine if size alone can affect the cytokine profile of TLR stimulated BMDM to either promote or reduce inflammation and evaluate how this may affect the immune response in a viral infection scenario.

4.4 Results

The experiments detailed here were undertaken to investigate whether size was a critical factor for the immunomodulatory abilities of NISV.

4.4.1 Melt method NISV are easily extruded to sub-100nm sizes

To bridge the gap in vesicle size between those produced using the melt method, and those produced using the NanoAssemblr, we first produced a large batch of melt method NISV which were then extruded stepwise through polycarbonate membranes using a hand extruder. Prior to extrusion, melt method NISV were measured by DLS to confirm size, polydispersity, and zeta-potential as a quality control. This step was repeated after the extrusion to evaluate the physical characteristics of each NISV fraction produced at each step of the extrusion.

As pore size decreased, NISV size also decreased, until a plateau was reached at the 200nm pore size, whereby the size change between NISV produced using a 200nm membrane did not significantly differ from those produced using a 100nm membrane. This trend was somewhat replicated when examining PDI, but with 3 groups emerging from the data. Non-extruded, 1000nm PCM NISV, and NanoAssemblr produced NISV displayed a PDI of around 0.5, with the next group, NISV extruded through an 800nm and 400nm PCM displayed a PDI of around 0.3. As the size of the membrane lowered again, 200nm PCM and 100nm PCM NISV displayed a PDI of around 0.1. The zeta potential for all NISV remained between -15mV and -30mV with no pattern observed **(Fig. 33)**. **Table 5** displays a summary of the numerical values obtained from zetasizing each NISV suspension, including the mean size resulting from extrusion through each membrane. These data demonstrate that extrusion is a simple and low-cost method for the post-production modification of NISV with decreasing PDI whilst retaining the desired negative charge.

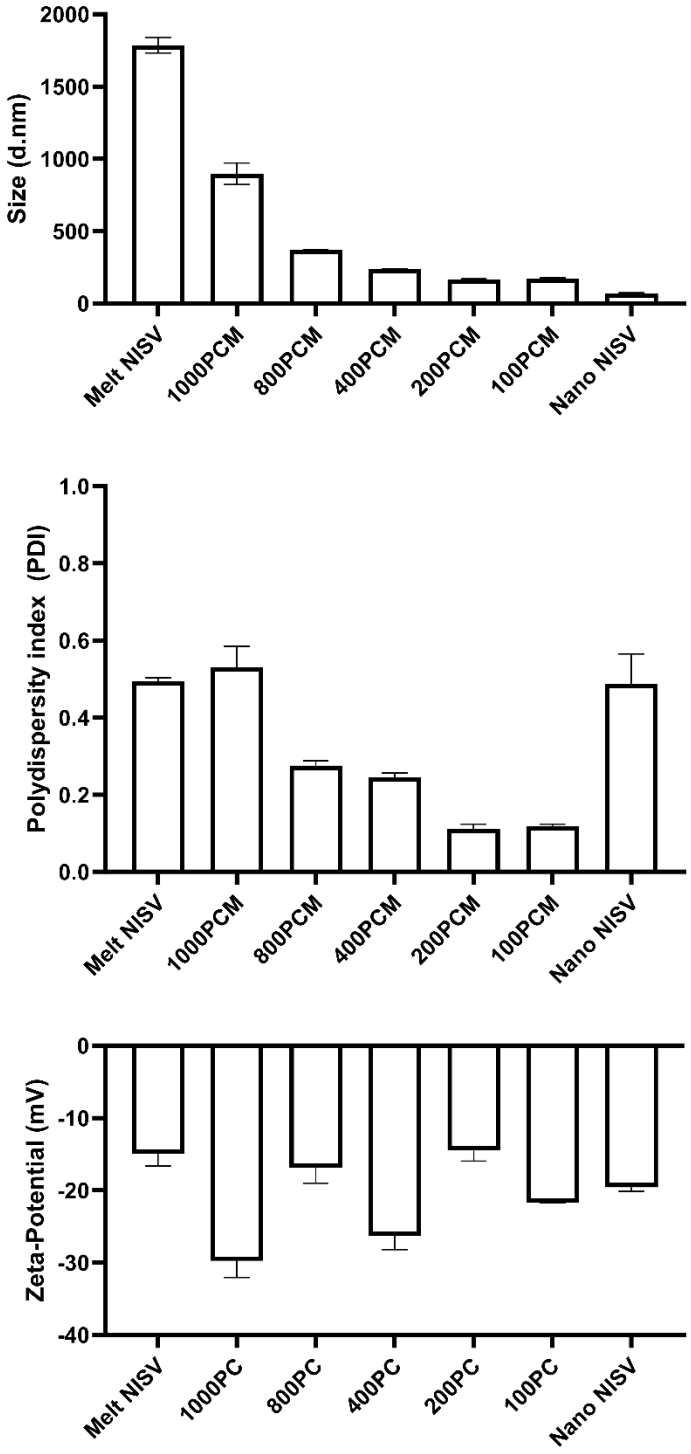

Figure 33: Physical characteristics of extruded NISV measured by Zetasizer. *Melt method NISV were extruded through polycarbonate membranes at 60ºC. Pore size for each membrane is included, alongside a non-extruded melt method produce NISV suspension, and NISV made using a NanoAssemblr. Results expressed as mean ± SEM. n=3.*

Table 5: Summary of key physical features of NISV by production method

NISV production method	Size (d.nm)	Polydispersity Index	Zeta-potential (mV)
Melt method (non-extruded)	1785.667 ± 53.561	0.494 ± 0.100	-15.000 ± 1.644
1000PCM extrusion	896.467 ± 74.601	0.531 ± 0.054	-29.767 ± 2.282
800PCM extrusion	370.133 ± 4.029	0.276 ± 0.012	-16.833 ± 2.195
400PCM extrusion	236.767 ± 0.767	0.245 ± 0.011	-26.333 ± 1.866
200PCM extrusion	167.533 ± 3.11	0.111 ± 0.013	-14.500 ± 1.453
100PCM extrusion	173.967 ± 2.174	0.119 ± 0.004	-21.700 ± 0.058
NanoAssemblr	70.630 ± 3.697	0.487 ± 0.078	-19.600 ± 0.586

After characterisation of NISV, some groups were discarded to streamline analysis as the difference in size between certain extruded groups was not significant. The sizes used were that of the non-extruded NISV at ~1700nm, those resulting from the 1000nm, and 400nm PCM at ~900nm and ~230nm respectively, and those produced by microfluidics using the NanoAssemblr at ~70nm. To determine any toxic effect imparted by a reduction in NISV size, alamarBlue assays were used. Non-extruded ~1700nm NISV were non-toxic at all concentrations assayed, regardless of TLR stimulation **(Fig. 34)**. However, for all other sizes, and regardless of TLR stimulation, extruded NISV at sizes ~900nm and ~230nm, and 70nm NanoAssemblr NISV displayed increased toxicity at concentrations above 0.375mM. Whilst the anti-inflammatory effect is maintained, the increase in toxicity narrows the therapeutic window for small NISV as a potential immunomodulator. In future analyses, a dotted box indicates where concentrations were toxic for these groups.

4.4.2 NISV ability to inhibit IL-6 and IL-12 in TLR-stimulated macrophages is retained after post-production extrusion

Examining NISV's effect on modulation of IL-6 or IL-12 production from TLR stimulated BMDM at different sizes by ELISA **(Fig. 35, Fig. 36, Fig. 37, Fig. 38)** revealed that for LPS, a dose-dependent decrease in IL-6 production was observed regardless of NISV size or production method **(Fig. 35).** Discounting toxic concentrations above 0.375mM for ~900nm, ~230nm, and ~70nm NISV, this effect is still significant. IL-12 production from LPS stimulated BMDM was low compared to other groups, and a noisy baseline combined with a lack of assay sensitivity caused this data to be unreliable. A similar trend of dose-dependent downregulation of IL-6 was found in TLR3 stimulated BMDM regardless of NISV size, with NISV also able to downregulate IL-12 in a dose-dependent manner **(Fig. 36)**. When examining modulation of TLR7 induced IL-6 production with NISV **(Fig. 37)**, there was no significant downregulation observed at non-toxic concentrations, with IL-6 levels rising significantly to above that of the imiquimod alone control at all sizes. In contrast, IL-12 was significantly downregulated at the highest non-toxic concentrations for all NISV sizes. However, ~230nm and ~70nm NISV at concentrations below 0.09375mM induced an increase in IL-12 production greater than that of the ligand alone. TL8-506 stimulated cells **(Fig. 38)** given ~1700nm NISV displayed a dose dependent downregulation of IL-6, which was absent at the non-toxic concentrations of ~900nm NISV, and an increase in IL-6 was noted at the non-toxic concentrations of ~230nm and ~70nm NISV. The trend of IL-12 modulation

observed in imiquimod stimulated cells was also observed in TL8-506 stimulated cells with significant reduction in IL-12 production compared with the control for all samples at non-toxic concentrations regardless of size. Also, as with TLR7 stimulated cells, concentrations of ~230nm and ~70nm NISV below 0.09375mM induced an increase in IL-12 levels greater than that of the TL8-506 alone control. These data indicate that whilst the pattern of immunomodulation is generally not changed at different sizes of NISV, the ability to achieve an immunomodulatory effect may sometimes be lost as smaller NISV become more toxic.

Figure 34: toxicity of extruded NISV assessed by alamarBlue assay. *Cells were stimulated with either A) LPS, B) Poly(I:C), C) Imiquimod, or D) TL8-506, and a treated with a 1 in 2 serial dilution of NISV at extruded to generate various sizes. Results expressed as mean ± SEM.* Values marked with * are significantly lower than the media alone control. * = p <0.05

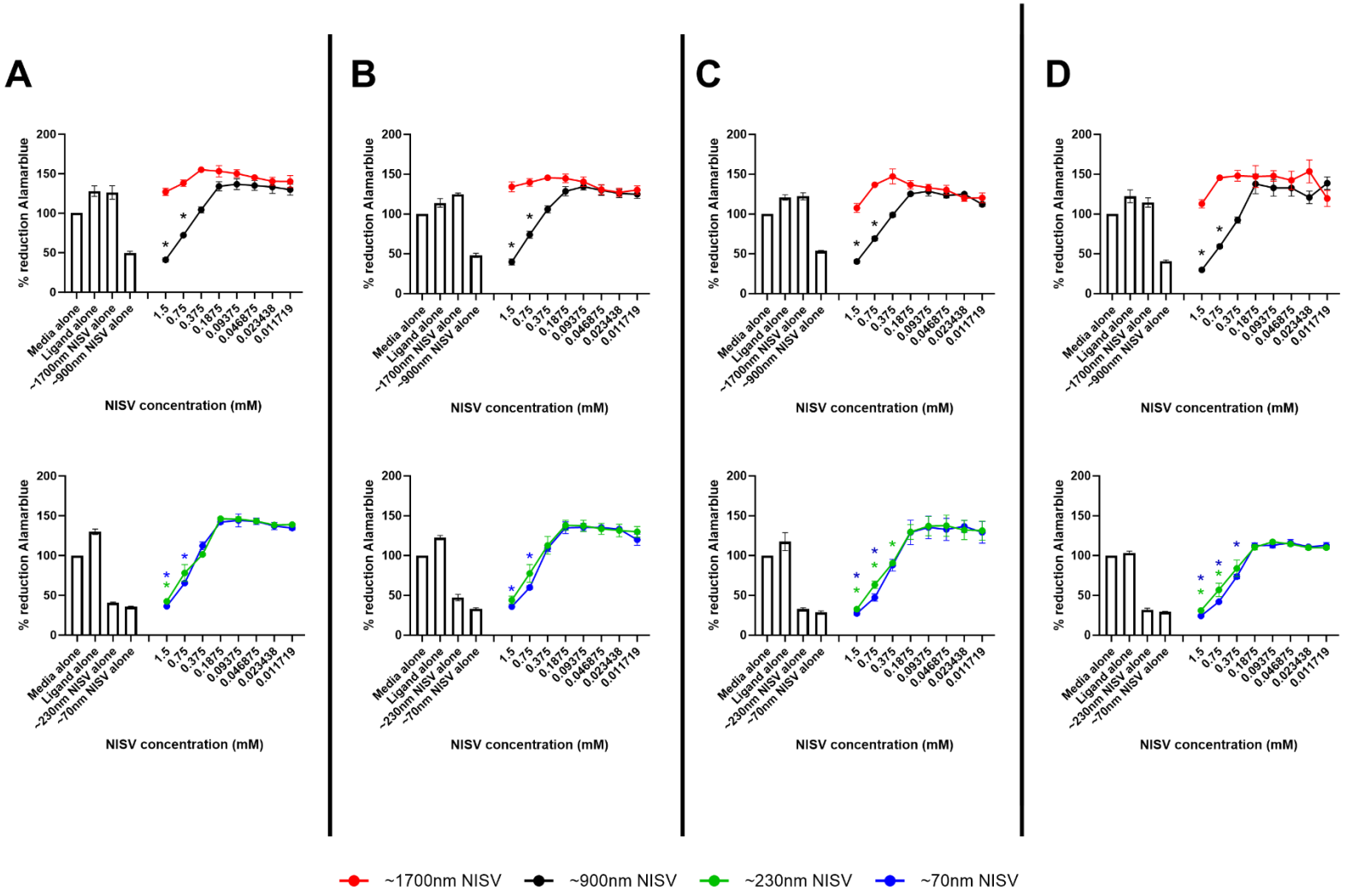

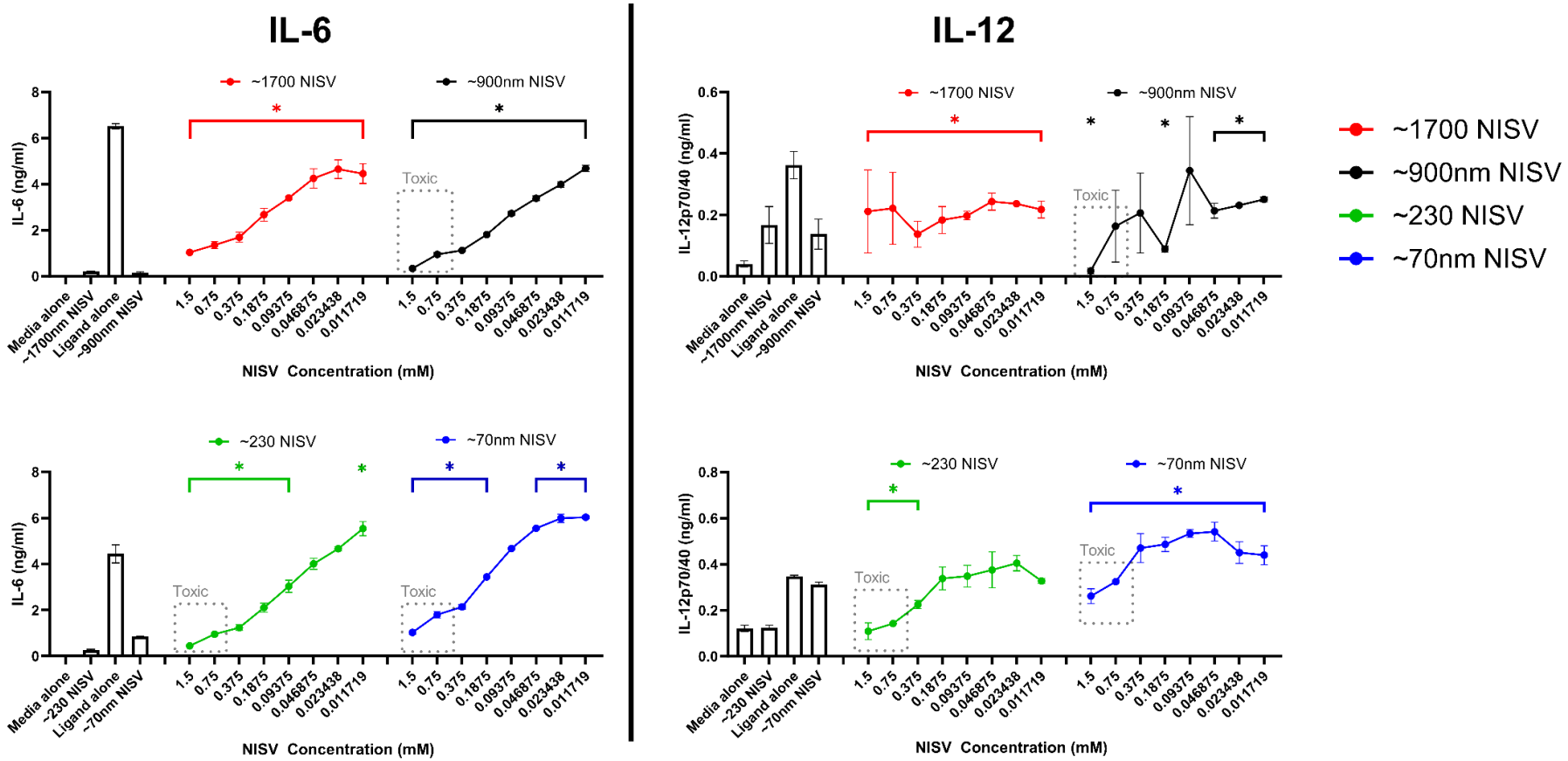

Figure 35: Modulation of LPS induced BMDM IL-6 and IL-12 production by NISV extruded to various sizes. *BMDM stimulated with LPS were treated with 1.5mM of NISV serially diluted 1:2. 1700nm NISV and 70nm NISV were not extruded, whereas all other sizes were. Cytokine levels quantified by ELISA. Dotted box indicates toxic concentrations. Results expressed as mean ± SEM, n=3. Values marked with * are significantly different from ligand alone control. * = p<0.05*

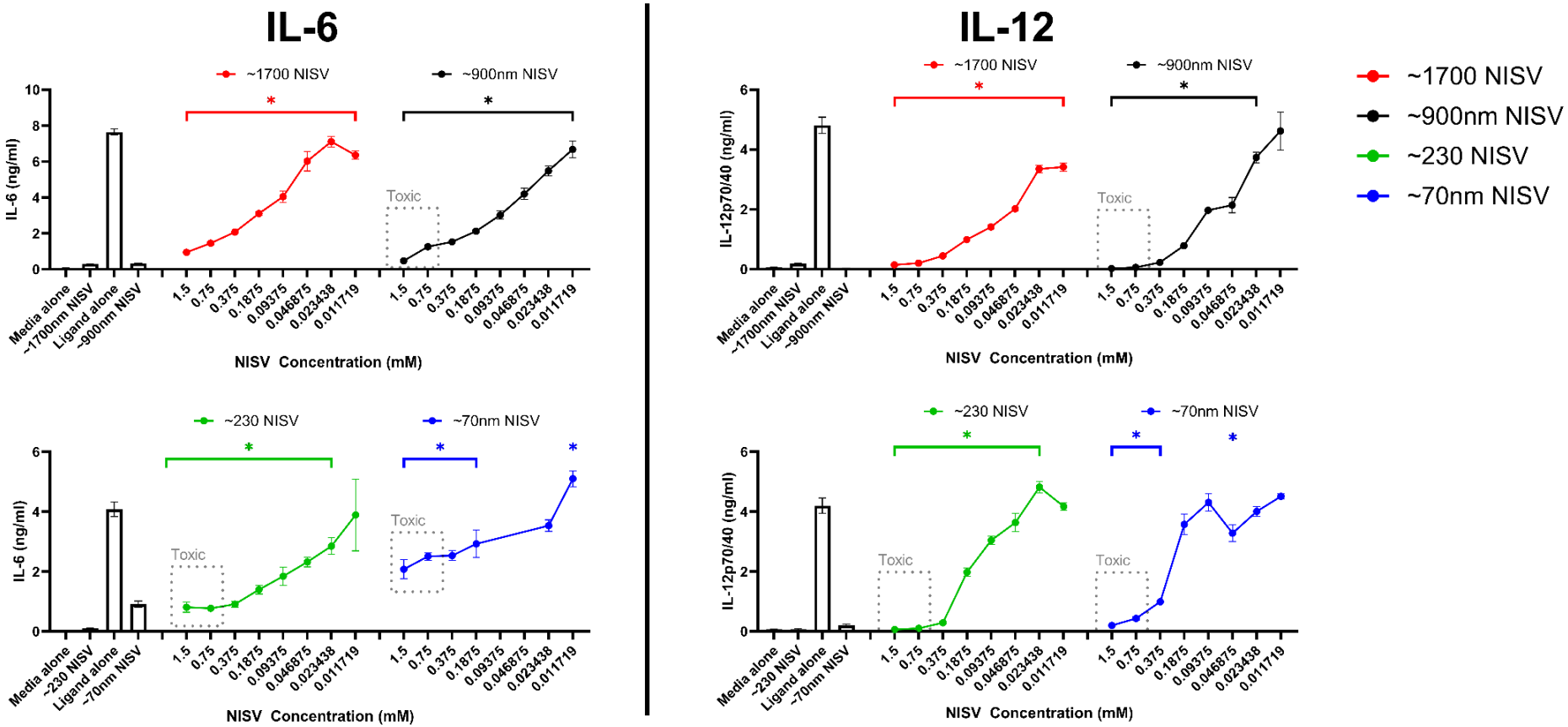

Figure 36: Modulation of Poly(I:C) induced IL-6 and IL-12 production by NISV extruded to various sizes. *BMDM stimulated with Poly(I:C) were treated with 1.5mM of NISV serially diluted 1:2. 1700nm NISV and 70nmNISV were not extruded, whereas all other sizes were. Cytokine levels quantified by ELISA. Dotted box indicates toxic concentrations. Results expressed as mean ± SEM, n=3. Values marked with * are significantly different from ligand alone control. * = p<0.05.*

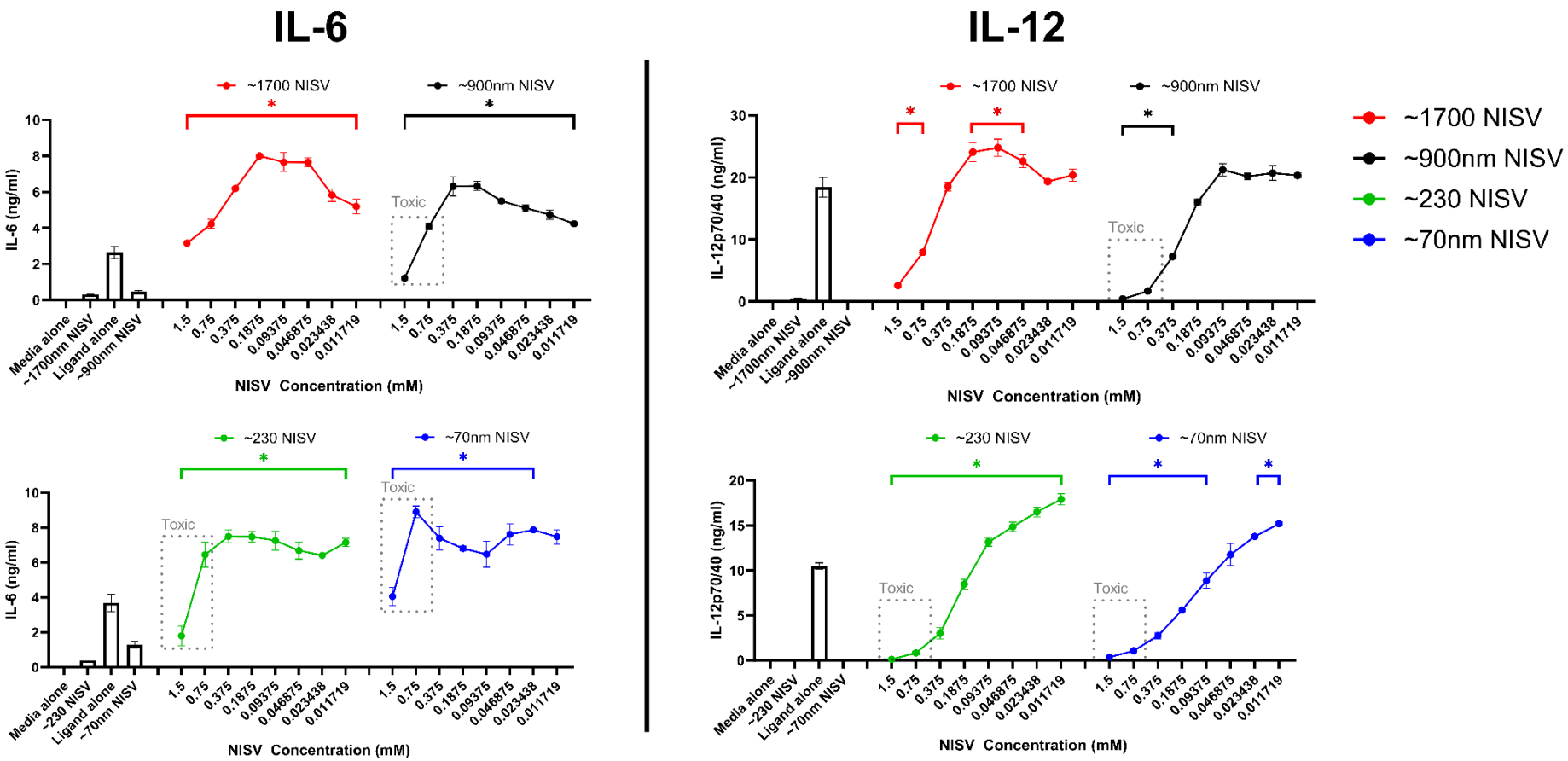

Figure 37: Modulation of imiquimod induced IL-6 and IL-12 production by NISV extruded to various sizes. *BMDM stimulated with Imiquimod were treated with 1.5mM of NISV serially diluted 1:2. 1700nm NISV and 70nmNISV were not extruded, whereas all other sizes were. Cytokine levels quantified by ELISA. Dotted box indicates toxic concentrations. Results expressed as mean ± SEM. Values marked with * are significantly different from the ligand alone control. * = p<0.05.*

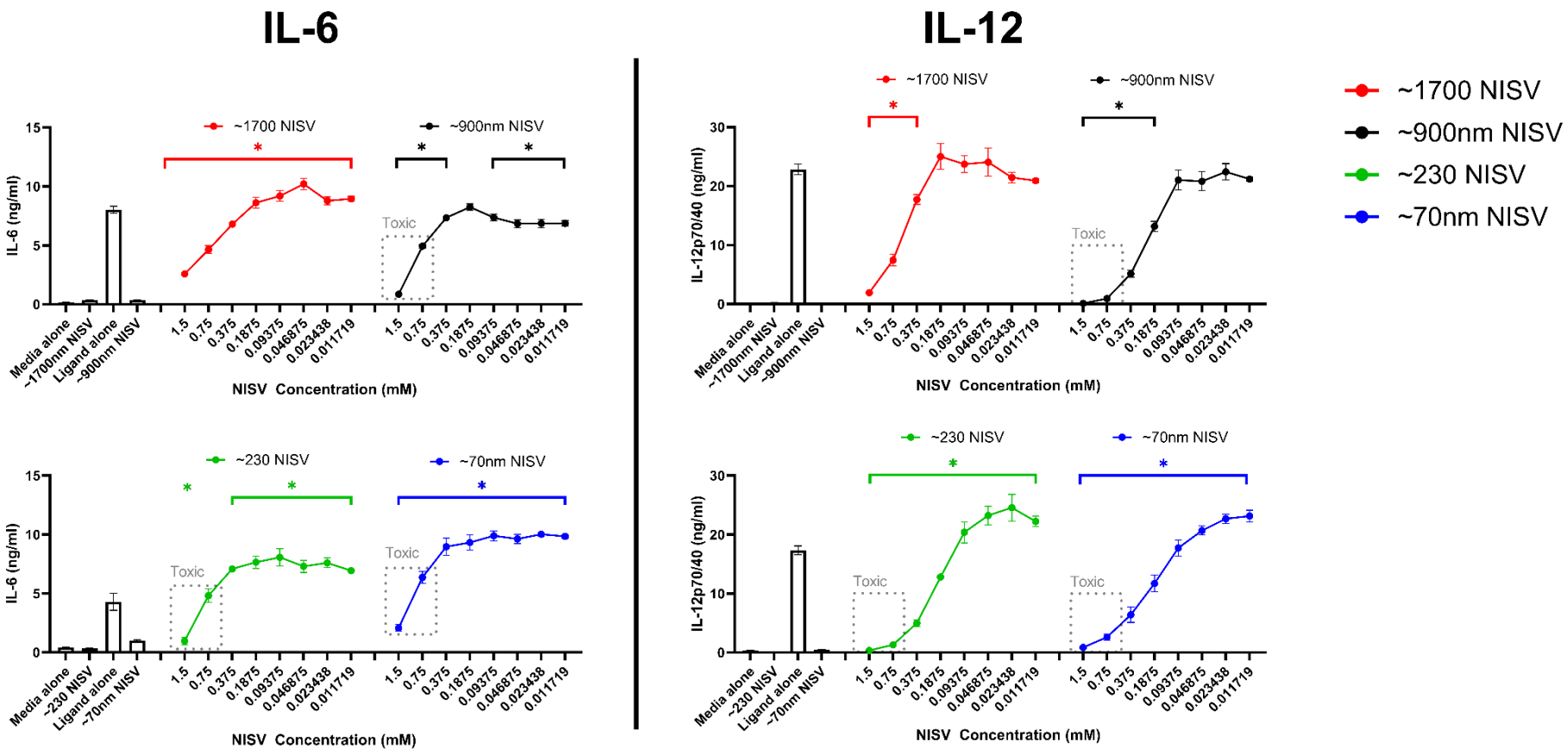

Figure 38: Modulation of TL8-506 stimulated IL-6 and IL-12 production by NISV extruded to various sizes. *BMDM stimulated with TL8-506 were treated with 1.5mM of NISV serially diluted 1:2. 1700nm NISV and 70nm NISV were not extruded, whereas all other sizes were. Cytokine levels quantified by ELISA. Dotted box indicates toxic concentrations. Results expressed as mean ± SEM. Values marked with * are significantly different from ligand alone control.*

To compare the potency of NISV able to generate a dose-response interaction, IC50 values were generated where possible. As some combinations of NISV/TLR/cytokine did not generate sigmoidal curves, only those that could have a reliable curve fit were included in this analysis.

NISV reduction of LPS induced IL-6 production **(Fig. 39)** was most potent in at ~900nm and ~230nm with similar IC50s at 0.07224mM and 0.07027mM respectively. This was followed by 70nm NISV, with the largest NISV the least potent. For IL-6 and production induced by Poly(I:C) stimulation **(Fig. 40, Fig. 41)**, NISV potency increased as size decreased, although the difference between the smaller sizes of NISV at ~900nm and ~230nm was small, there was a greater increase in potency between ~1700nm NISV and these smaller extruded preparations. As the smallest size at ~70nm did not produce a reliable curve it was omitted from this analysis. When comparing this to the effect of Poly(I:C) induced IL-12 production, there was very little difference between each size of NISV. This may indicate that induction of certain cytokines is more efficiently achieved by different sizes of particles.

The potency of NISV in reducing IL-12 production by imiquimod stimulated cells appears to be size dependent **(Fig. 42)** Excluding toxic concentrations of smaller NISV, we observed a correlation between a decrease in NISV size and increase in potency. A similar trend was observed in TL8-506 stimulated cells treated with decreasing sizes of NISV **(Fig. 43)**, although the increase in potency was much smaller than in imiquimod stimulated cells.

These data indicated that the ability of NISV to modulate IL-6 and IL-12 production is not affected by NISV size – they still retain the ability to alter cytokine levels in the same pattern, but the potency of NISV effects may be increased by decreasing vesicle size.

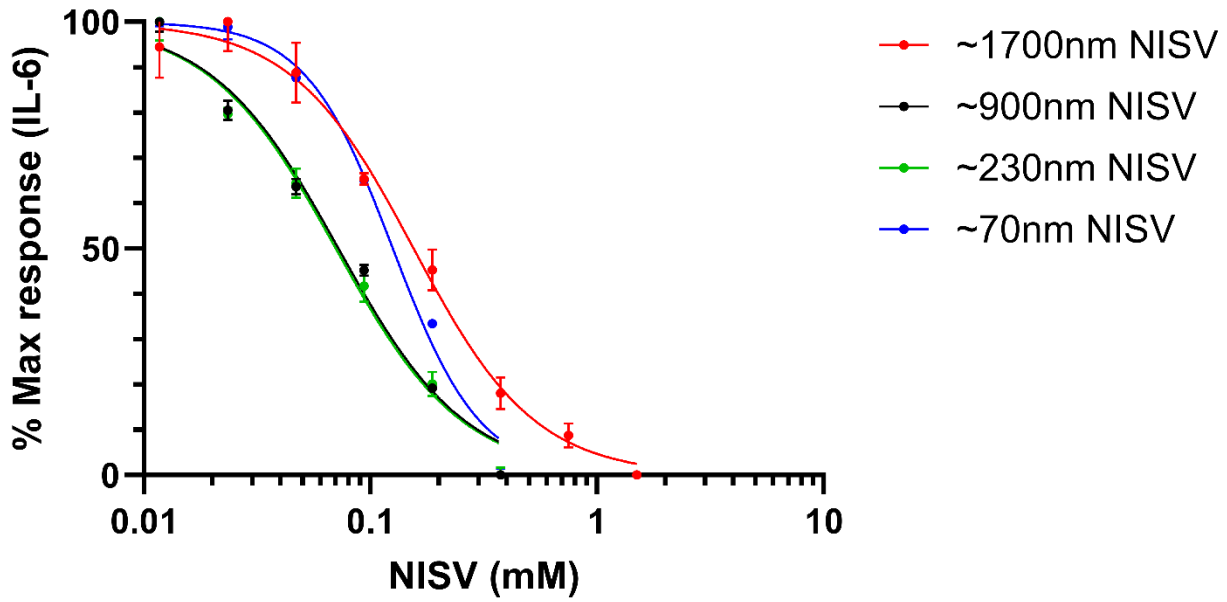

	~1700nm NISV	~900nm NISV	~230nm NISV	~70nm NISV
IC50	0.1550	0.07224	0.07027	0.1255

Figure 39: Comparison of IC50 values of NISV ability to reduce LPS-induced IL-6 production. *IL-6 levels quantified by ELISA were normalised and expressed as a percentage of the maximal cytokine level for each size. Variable slope non-linear regression curves were fit to the data and relative IC50 values calculated.*

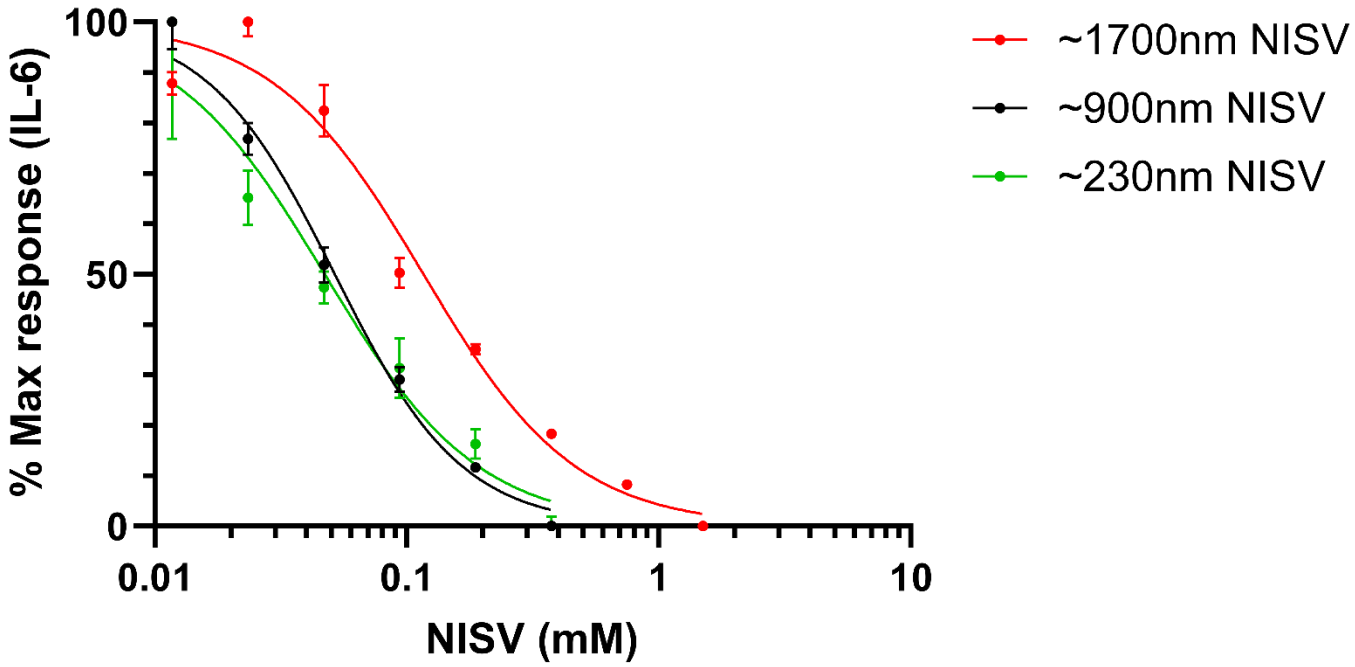

	~1700nm NISV	~900nm NISV	~230nm NISV
IC50	0.1165	0.05179	0.04722

Figure 40: Comparison of IC50 values of NISV ability to reduce Poly(I:C)-induced IL-6 production. *IL-6 levels quantified by ELISA were normalised and expressed as a percentage of the maximal cytokine level for each size. Variable slope non-linear regression curves were fit to the data and relative IC50 values calculated.*

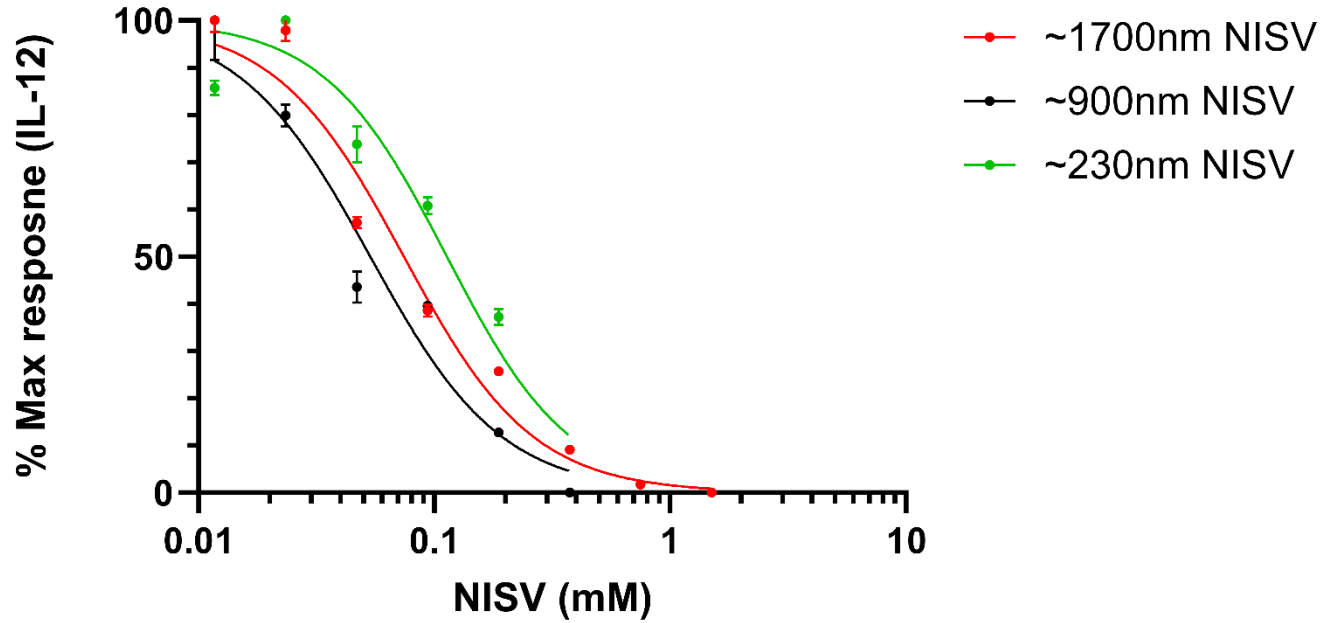

	~1700nm NISV	~900nm NISV	~230nm NISV
IC50	0.07432	0.05352	0.1131

Figure 41: Comparison of IC50 values of NISV ability to reduce Poly(I:C)-induced IL-12 production. *IL-12 levels quantified by ELISA were normalised and expressed as a percentage of the maximal cytokine level for each size. Variable slope non-linear regression curves were fit to the data and relative IC50 values calculated*

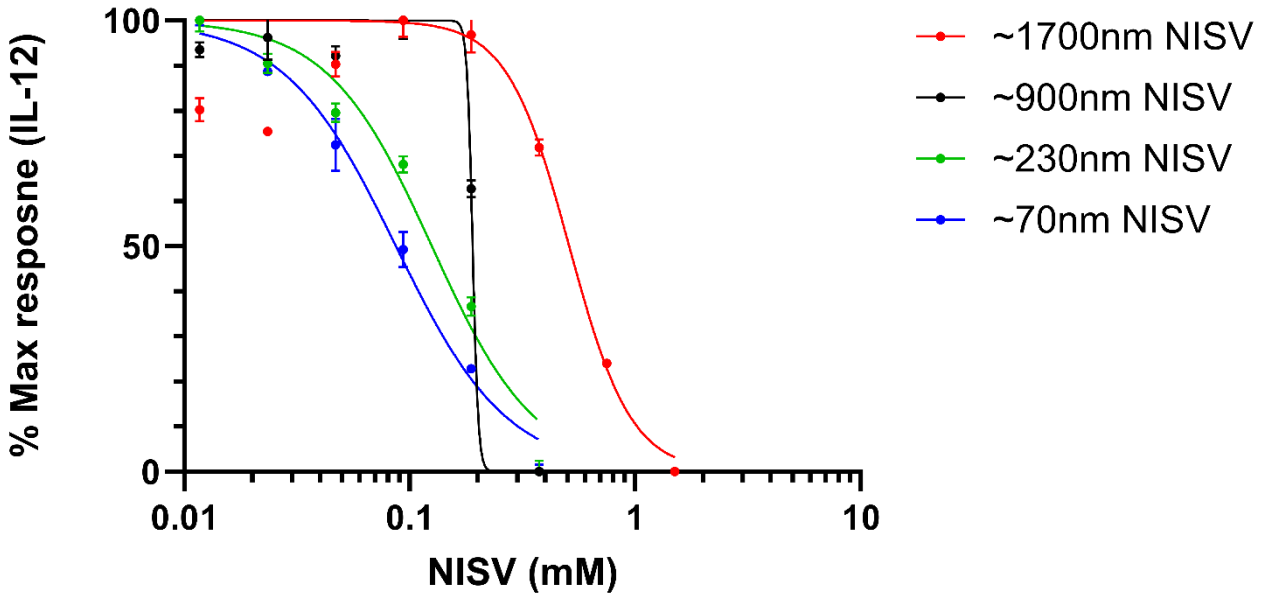

	~1700nm NISV	~900nm NISV	~230nm NISV	~70nm NISV
IC50	0.5100	0.1903	0.1254	0.08688

Figure 42: Comparison of IC50 values of NISV ability to reduce Imiquimod-induced IL-12 production. *IL-12 levels quantified by ELISA were normalised and expressed as a percentage of the maximal cytokine level for each size. Variable slope non-linear regression curves were fit to the data and relative IC50 values calculated.*

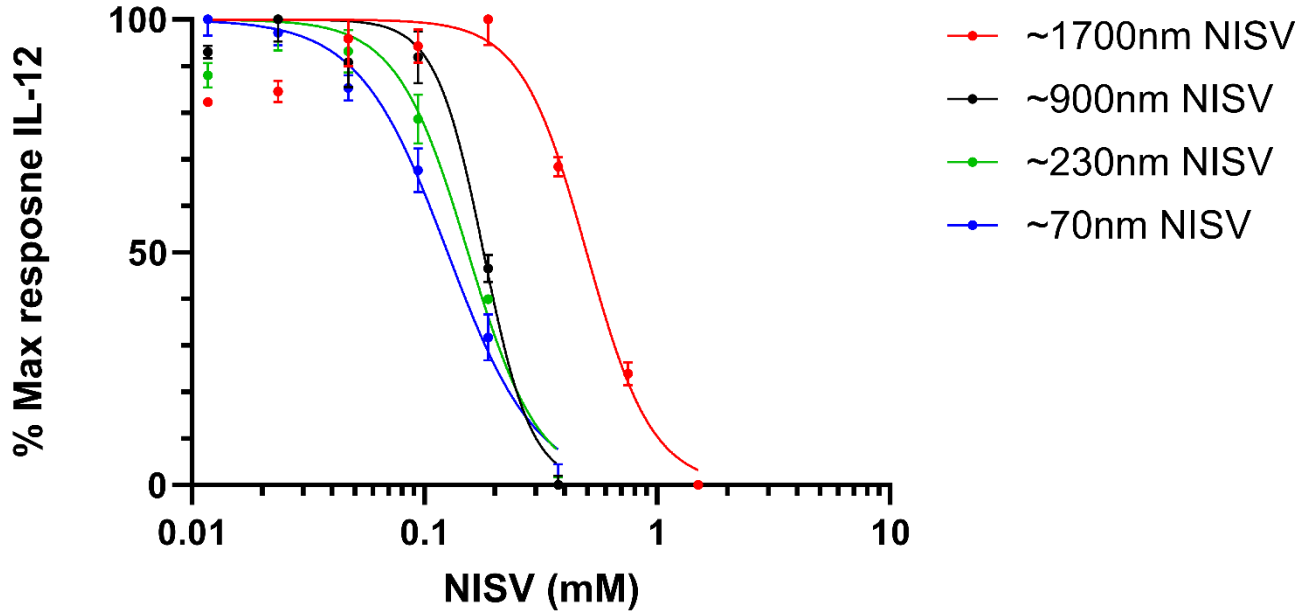

	~1700nm NISV	~900nm NISV	~230nm NISV	~70nm NISV
IC50	0.4970	0.1792	0.1536	0.1255

Figure 43: Comparison of IC50 values of NISV ability to reduce TL8-506-induced IL-12 production. *IL-12 levels quantified by ELISA were normalised and expressed as a percentage of the maximal cytokine level for each size. Variable slope non-linear regression curves were fit to the data and relative IC50 values calculated.*

4.4.3 Changing NISV size alters effect on cytokine in a TLR specific manner

To further investigate whether size affects the induction of inflammation related cytokines and chemokines, we selected 3 sizes to compare using cytometric bead array. Prior to cell stimulation, the physical characteristics of NISV produced for this experiment were quantified by Zetasizer. Pilot studies indicated that there would be little difference between the sizes regardless of TLR ligand, and thus only LPS and imiquimod were used to stimulate BMDM. LPS was chosen as it has been well characterised in both the literature and in our laboratory, and imiquimod was chosen to evaluate the effect of NISV on an intracellular viral-sensing TLR.

Melt method NISV that were not extruded displayed sizes of around 1430nm with a PDI of 0.519 **(Fig. 44)**. These NISV were also sufficiently negatively charged at –29.900mV. From this suspension, NISV were extruded through a 1800nm PCM, followed by a 100nm PCM. The first extrusion step produced NISV that were ~608nm in size, with a lower PDI than that of the non-extruded NISV at 0.307. These NISV were also negatively charged as expected, with a zeta-potential of -32.600mV. NISV extruded through a 100nm PCM were ~130nm in size, with a much lower PDI of 0.078, and a zeta-potential of -26.200mV.

Prior to the cytometric bead array, cells were stimulated with LPS or imiquimod and either the ~1430nm, ~610nm, or ~130nm NISV. We evaluated the toxicity of each NISV + TLR ligand combination by alamarBlue assay, followed by an ELISA for IL-6 to ensure correct stimulation. Examining the toxicity of either the ligand alone, NISV alone, or NISV and ligand combinations, we observed no significant decreases in alamarBlue reduction in any group **(Fig. 45)**. IL-6 ELISA results were consistent with previous data indicating no errors during stimulation.

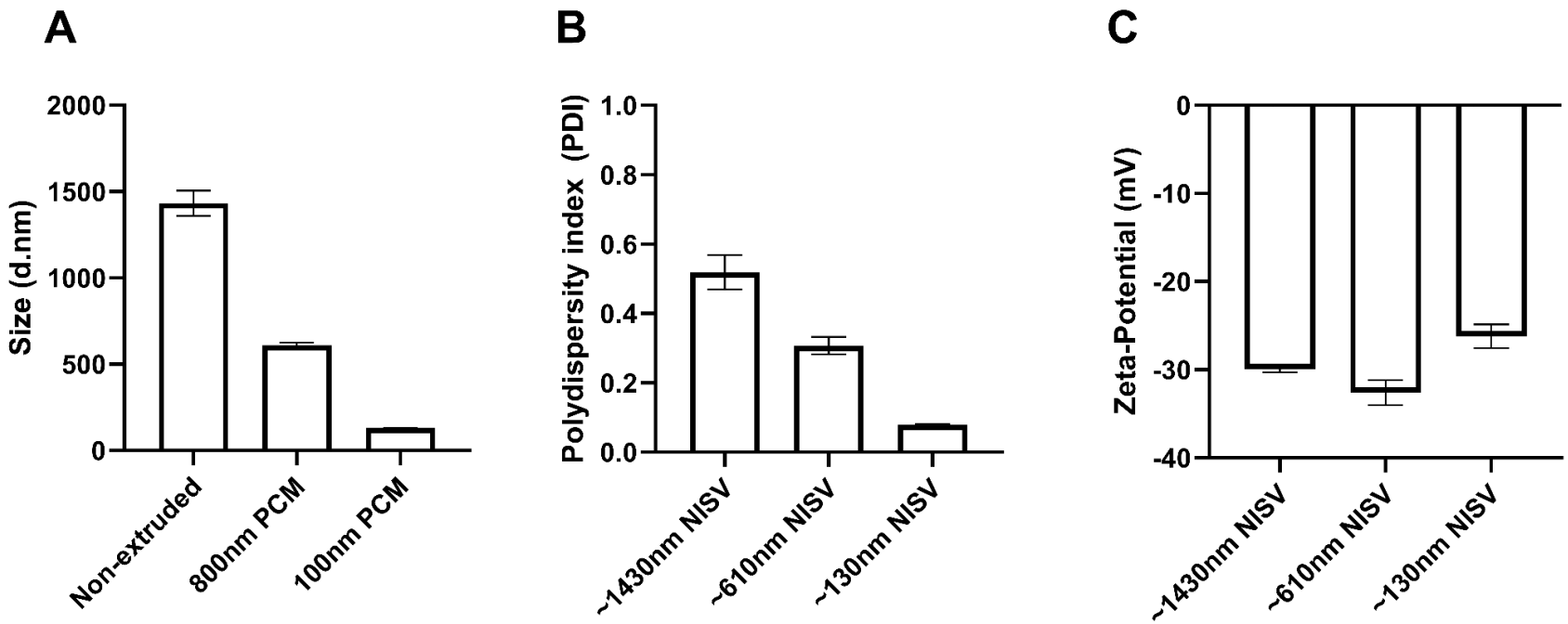

Production method	Size (d.nm)	Polydispersity Index	Zeta-potential (mV)
Non-extruded melt method	1432 ± 73.323	0.519 ± 0.050	-29.900 ± 0.0379
Melt method + 800nm PC membrane	608.133 ± 15.474	0.307 ± 0.025	-32.600 ±1.422
Melt method + 100nm PC membrane	130.400 ± 0.945	0.078 ± 0.002	-26.200 ± 1.365

Figure 44: Physical characteristics of extruded NISV measured by Zetasizer. *Melt method NISV were extruded through 800nm and 100nm polycarbonate membranes at 60ºC. A non-extruded melt method NISV suspension was also characterised. Results expressed as mean ± SEM, n=3.*

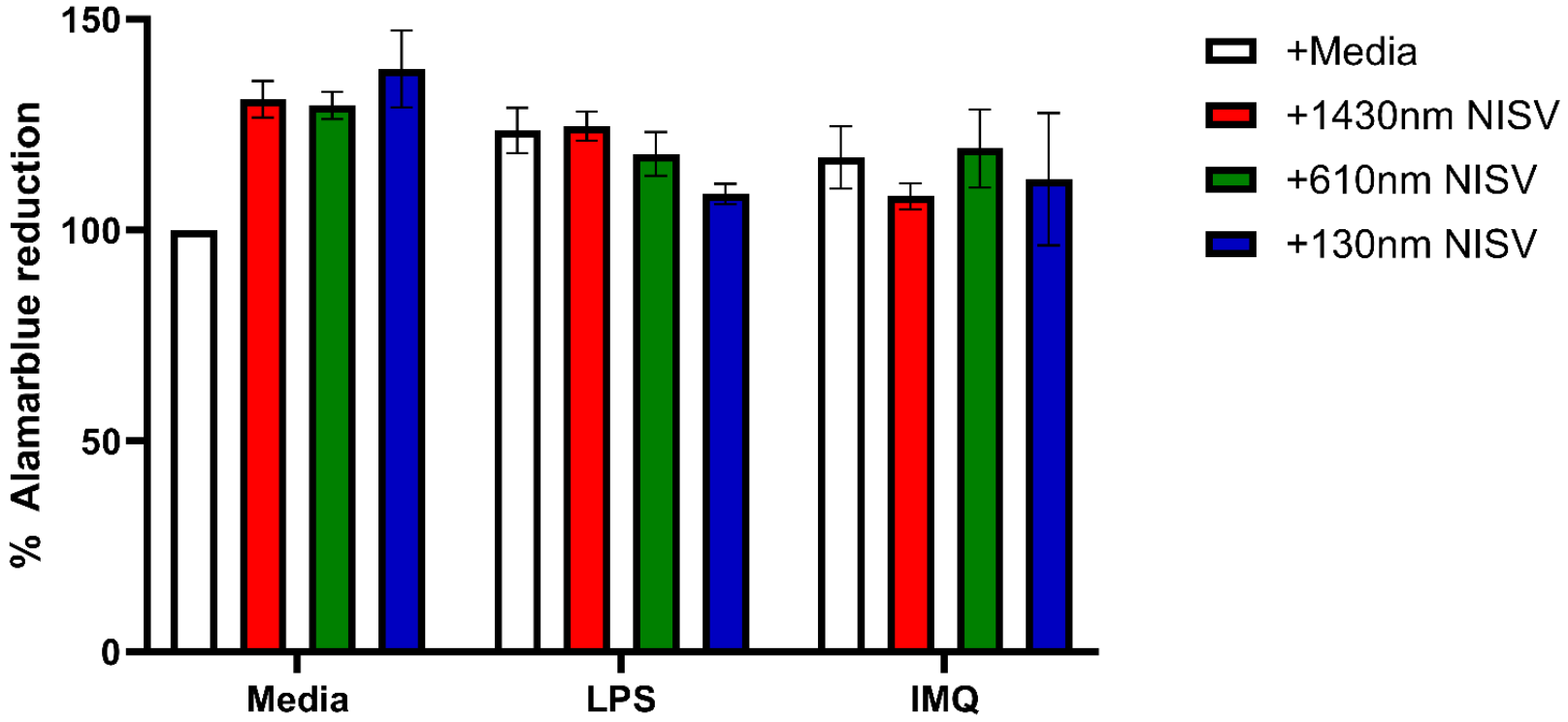

Figure 45: Extruded NISV effect on TLR stimulated BMDM viability assessed by alamarBlue assay. *cells were stimulated with either 1.3µg/ml LPS or 1.6 µg/ml Imiquimod. Cells were treated with 0.375mM of non-extruded ~1430nm NISV, or extruded NISV sized either ~610nm or ~130nm. Results expressed as mean ± SEM, n = 3.*

A cytometric bead array was then performed on supernatants from these cells, to provide a wider examination of the effects of NISV size on a broad spectrum of cytokines/chemokines involved in the inflammatory response.

PCA plots were used to quality control sample grouping, with samples generally clustering well along one principal component, if not both **(Fig. 46).** From PCA, loading plots identified IL-6 and TNFα contributing the greatest to variance between stimulated cells and stimulated cells treated with NISV.

To visualise changes in the pattern of cytokine/chemokine production between different sizes of NISV, heatmaps were generated using the Log2 fold change (Log2FC) of NISV alone vs media alone, or NISV + ligand vs the ligand alone control. Consistent with previous data, NISV alone increased IL-6 and TNFα production compared with unstimulated cells **(Fig.47)**. This effect was present in all sizes of NISV, although cytokine upregulation was greatest with ~1430nm NISV, and displayed a decrease in both IL-6 and TNFα upregulation as NISV size decreased. Alongside this, other apparent size-dependent effects were the strong downregulation of IL-10 present with large NISV alone, and the induction of IL-1α and IL-1β production by the smallest NISV.

The effect of NISV on LPS stimulated BMDM was mostly consistent with previous experiments **(Fig. 48).** As observed previously, both IL-1α and IL-1β were upregulated by NISV, with ~130nm NISV increasing IL-1α levels more potently than other sizes. Generally, NISV displayed anti-inflammatory effects by decreasing IL-6, IL-27, and TNFα levels, with either little or no effect on MCP-1, IL-12p70, IL-10, IL-17A, GM-CSF, IL-23, and IFNβ. In contrast, the pattern of NISV immunomodulation differs when used to treat imiquimod induced cytokine/chemokine production **(Fig.49).** As before, IL-1α and IL-1β were upregulated in all sizes of NISV, but ~130nm NISV greatly increased the levels of these cytokines compared with imiquimod alone. Unlike the effect of NISV on LPS stimulated BMDM, there was generally an increase in pro-inflammatory cytokine production observed, with TNFα and IL-27 increasing after treatment with all sizes of NISV. Examining IL-6 reveals disparity between NISV ~1430nm in size and those at ~610nm and ~130nm. The larger, non-extruded NISV retain the adjuvant effect demonstrated previously by increasing the levels of IL-6, whereas both smaller sizes strongly downregulate IL-6 compared to cells stimulated with imiquimod alone. This effect was greater in ~130nm NISV.

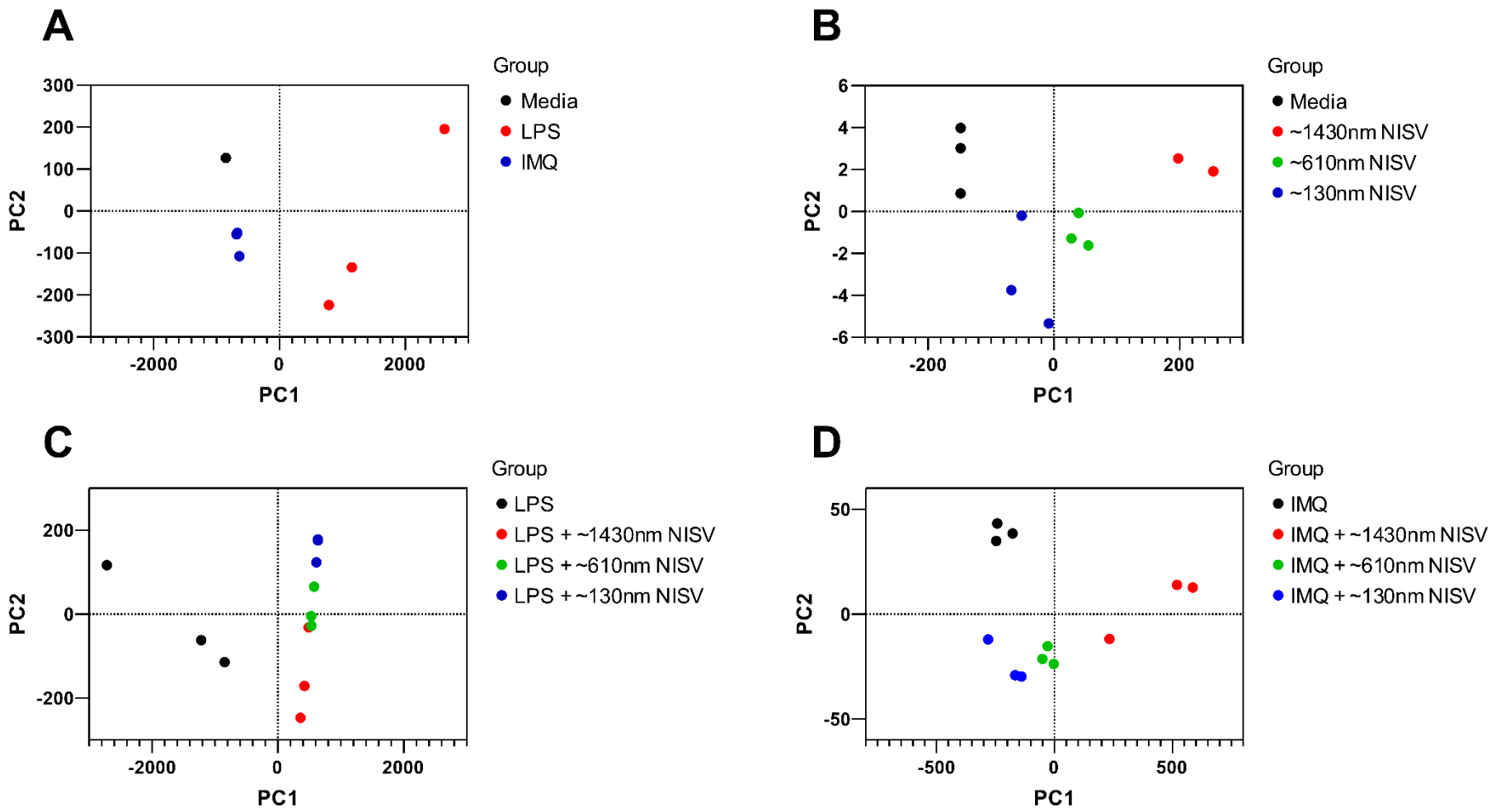

Figure 46: PCA scores comparing distribution of variance amongst samples used in cytometric bead array. *Principal components selected based on 2 largest eigenvectors. (A) control samples stimulated with either media, LPS, or imiquimod alone, (B) unstimulated cells treated with 3 sizes of NISV, (C) LPS stimulated cells treated with 3 sizes of NISV, (D) imiquimod stimulated cells treated with 3 sizes of NISV.*

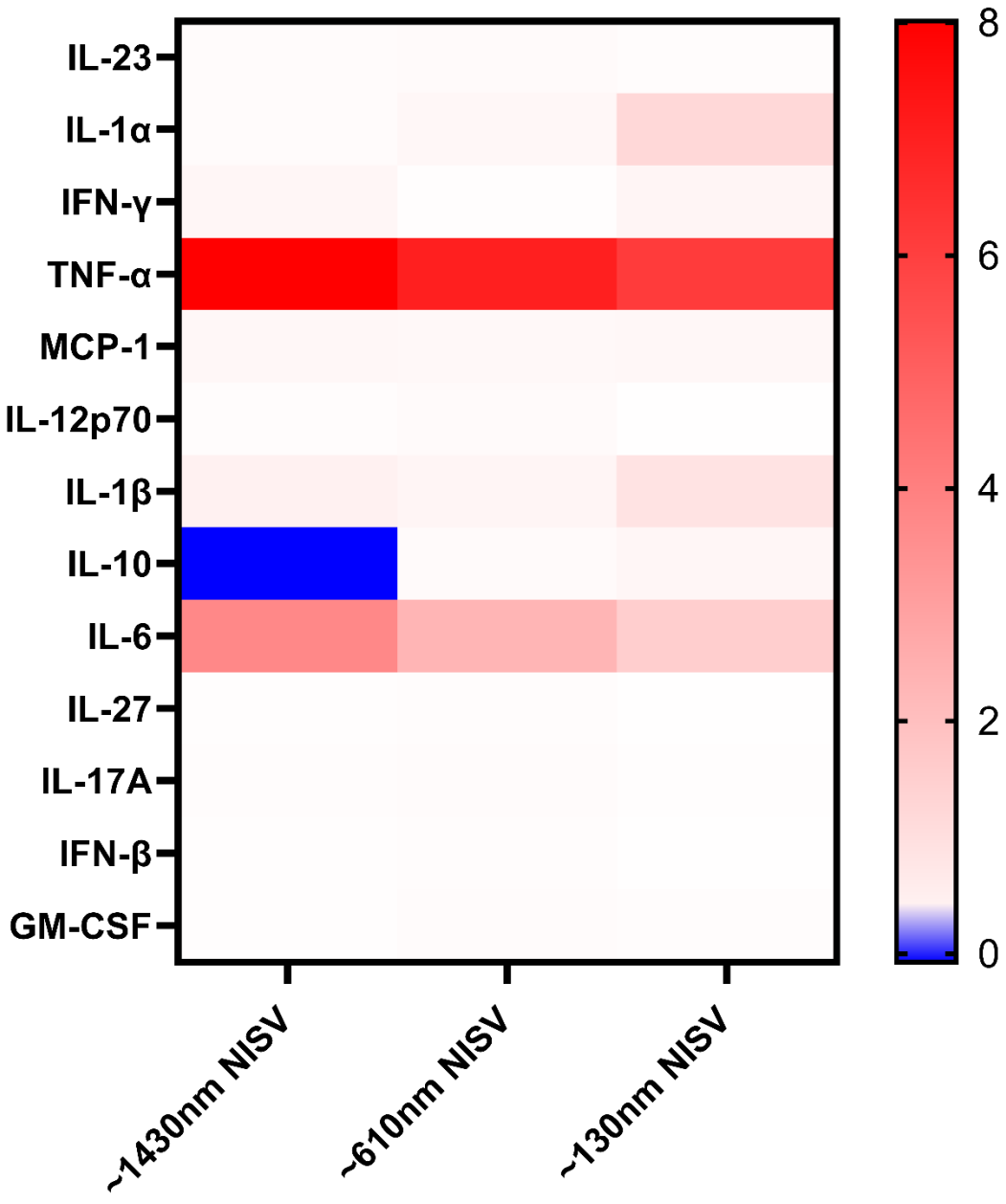

Figure 47*:* Heatmap comparing the effect of different sizes of NISV on cytokine/chemokine production by unstimulated BMDM. *Effect of NISV was calculated as Log2 fold change compared with the control media alone. Red values indicate an increase in cytokine/chemokine level compared with the control, white values indicate no change, and blue values indicate a decrease in cytokine/chemokine level compared to the control. Values are expressed as mean of n=3.*

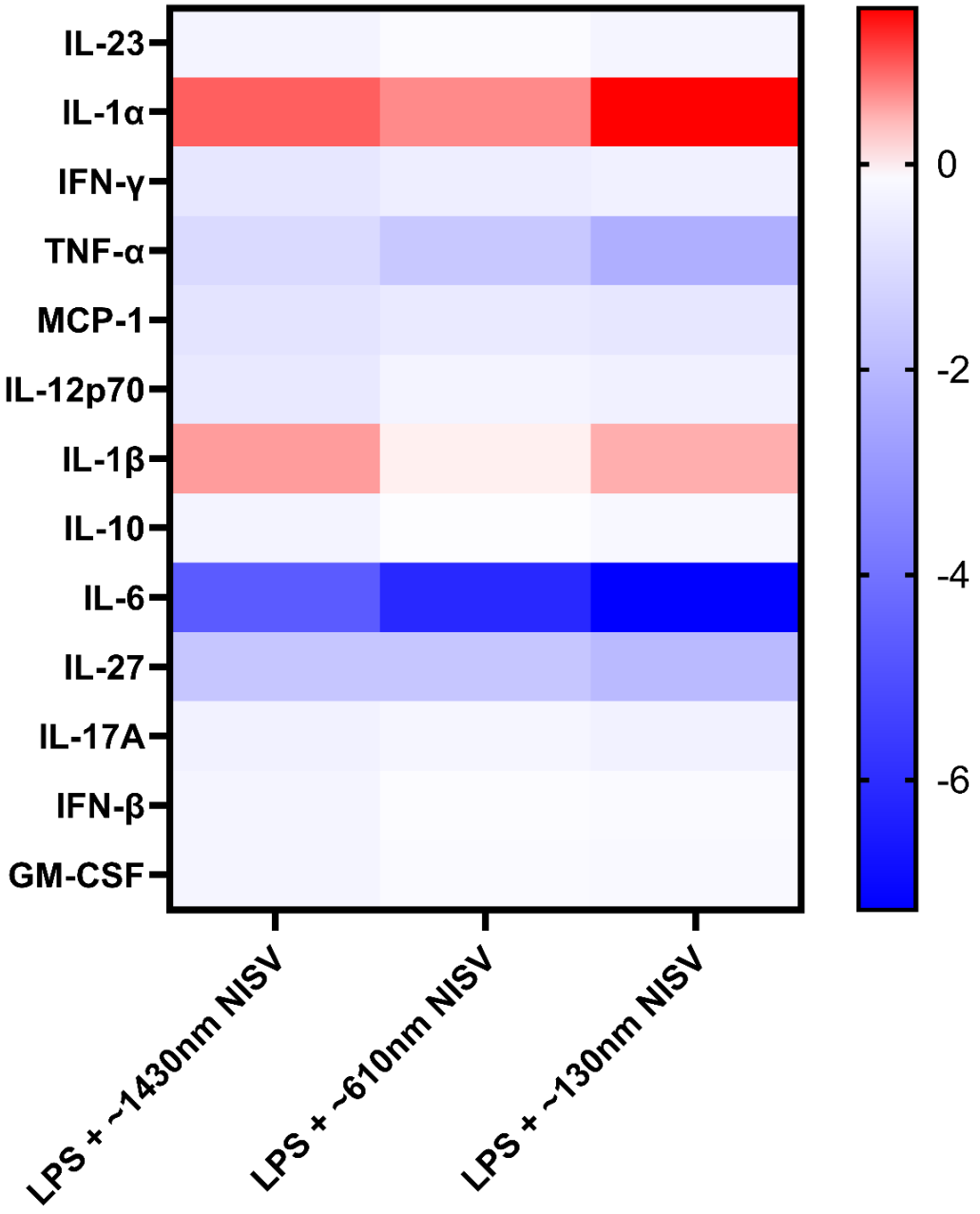

Figure 48: Heatmap comparing the effect of different sizes of NISV on cytokine/chemokine production by LPS stimulated BMDM. *Effect of NISV and LPS was calculated as Log2 fold change compared with the control ligand alone. Red values indicate an increase in cytokine/chemokine level compared with the control, white values indicate no change, and blue values indicate a decrease in cytokine/chemokine level compared to the control. Values are expressed as mean of n=3.*

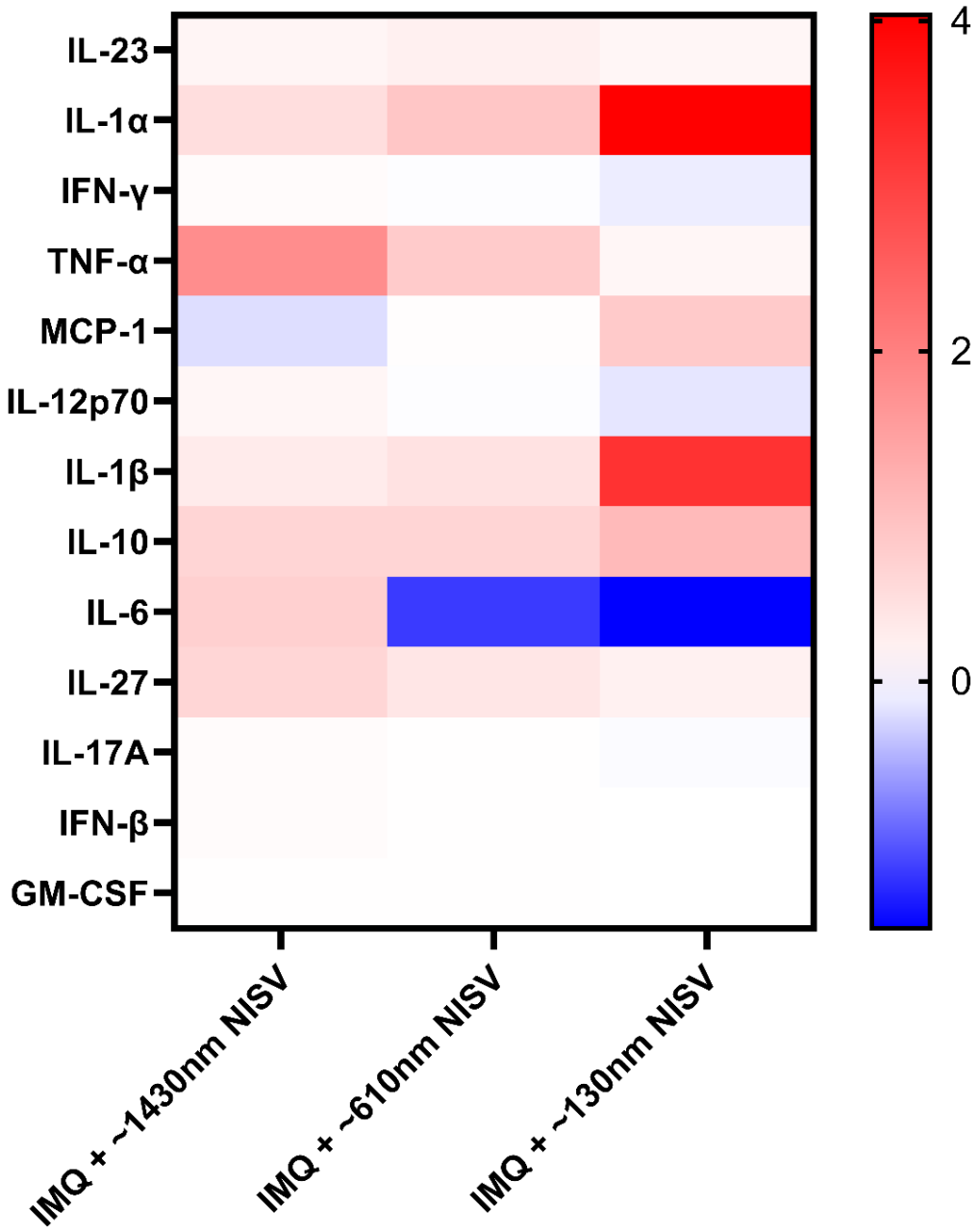

Figure 49: Heatmap comparing the effect of different sizes of NISV on cytokine/chemokine production by imiquimod stimulated BMDM. *Effect of NISV and imiquimod was calculated as Log2 fold change compared with the control ligand alone. Red values indicate an increase in cytokine/chemokine level compared with the control, white values indicate no change, and blue values indicate a decrease in cytokine/chemokine level compared to the control. Values are expressed as mean of n=3.*

4.5 Discussion

Our studies indicate that whilst size does not greatly alter the immunomodulatory effect of NISV, a decrease in size does contribute to increased toxicity and potency. Furthermore, the effect of vesicle size appears to change depending on the TLR stimulation applied to macrophages.

The effect of size has been previously explored using liposomes and NISV alike. Larger vesicles have been demonstrated to experience quicker uptake by macrophages in a study by Epstein, et al., as 600nm liposomes were taken up quickly over 1hr, with near 100% uptake at this time point. As liposome size decreased, uptake rate decreased, with the smallest liposomes at 80nm only reaching the same level of uptake as large liposomes at 48hrs, with only 60% uptake at 1hr *(Epstein, et al., 2010).* Conversely to this, studies have indicated that in other cells such as Caco-2 cells (colon cancer cells), the smallest liposomes at ~40nm experienced a 12-fold increase in uptake compared with the largest liposomes at ~270nm *(Andar, et al., 2014).* This disparity indicates that cell type may be a determining factor in the size preference for efficient vesicle uptake. Macrophages have been previously demonstrated to utilise phagocytosis for the uptake of >500nm particles which requires actin rearrangement and is usually independent of clathrin and caveolin. This correlates with uptake of bacteria, whereas methods such as pinocytosis and receptor-mediated endocytosis are used for smaller particles and solutes, such as viruses or macromolecules *(Aderem, and Underhill, 1999).* Further studies have demonstrated that size, shape, and surface charge influence phagocytosis, with the optimum uptake occurring with particles between 1μm-3μm, which is the size range for many bacteria. Alongside this, the shape of the particle affects phagocytosis, with spheres faring poorly compared with oblate ellipsoids *(Lu, et al., 2010)*.

After phagocytosis, size may also influence trafficking of NISV to cellular compartments. It has been demonstrated that whilst uptake was similar for NISV of different sizes (i.e., 155nm and 560nm NISV – below and above the phagocytic threshold), vesicles localised to different cellular compartments. Small NISV were found to localise to perinuclear lysosomes, whereas large NISV were found in peripheral compartments, distinct from lysosomes. Furthermore, it was demonstrated that small NISV were taken up by endocytosis, and large NISV by phagocytosis. This reveals that whilst the ability to uptake NISV is likely not affected by size, the mechanisms of uptake, as well as the internal destination and therefore fate of the vesicles is influenced by size *(Brewer, et al., 2004).*

Outside of size, other features such as surface charge may also affect the ability of macrophage to phagocytose particles. Studies have demonstrated that particles with a

charge, regardless of whether this is positive or negative, are more efficiently engulfed than neutral particles. Alongside this, particle rigidity, largely imparted by the inclusion of cholesterol into the membrane, plays a role in uptake. Particles that are more malleable are more difficult to engulf, and therefore experience lower uptake than more rigid particles *(Paul, et al., 2013).* Relating to particle rigidity is the observation that NISV that have been passed through an extruder do not display sizes accurate to exact pore size used. However, this feature of NISV has been discussed previously, particularly in the original patent which discussed the therapeutic potential of this NISV formulation *(Roberts, et al., 1997).* In part, the elasticity of NISV may be a factor in this effect, as they are likely squeezed through the membranes and partially return to their original dimensions. Subsequent passes through the membrane, may alter this interaction, but in the interest of consistency NISV were passed through each polycarbonate membrane 10 times.

These observations combined with the previous work stated above provide three main explanations of the data presented herein:

Firstly, smaller NISV, and vesicles subject to extrusion exhibit both higher toxicity and generally greater potency than larger NISV subject to no post-production modifications. By comparing production method, i.e., microfluidic production vs melt method + extrusion. My current hypothesis is that free surfactant, i.e., unreacted NISV components or, in the case of extruded NISV, surfactant sheared from NISV as they decrease in diameter is interacting with the cells. Surfactants have previously been well characterised as toxic to cells due to their ability to interact with both the cell membrane, as well as entering the cytoplasm and disrupting cell organelles. Whilst other surfactants such as anionic, and cationic surfactants appear to be more toxic, non-ionic surfactants still retain this deleterious feature *(Grant, et al., 1992).* Whilst the negative effects of surfactant exposure tends to be greater in polarised cells such as that of epithelial cells, non-polarised cells such as the macrophages used in this study still experience surfactant toxicity through similar mechanisms *(Inácio Â, et al., 2011).* Subsequent experiments to characterise the free surfactant using a tangential flow filtration unit to purify NISV, removing all solvent and unreacted material appears to have rectified the drop in cell viability observed when BMDM are treated with small NISV alone (not shown).

Secondly, it was observed that smaller NISV are generally more potent than large NISV. A simple explanation may be that due to the smaller size, a greater amount of NISV enter the cell during engulfment. Whilst increased NISV uptake will eventually lead to increased surfactant within the cell due to breakdown of the vesicle, it has been previously demonstrated that surfactant alone does not confer the immunomodulatory properties,

instead this requires the organisational structure of an NISV to achieve the effect *(McGahon, 2021).* Interestingly, the mechanisms of particle uptake are likely diverse in the present study as the small particles <100nm are taken up efficiently by clathrin-mediated mechanisms. This is due to the physical constraints of the clathrin lattice that is used to engulf particles *(Baranov, et al., 2021)*. Particles greater than this size, but smaller than 500nm may be taken up by alternative endocytic mechanisms such as caveolin-mediated endocytosis. Furthermore, as mentioned previously, particle size can affect intracellular localisation, and thus small NISV may be more efficiently trafficked to lysosomes. Previous work in our lab has demonstrated that individual components e.g., MPG, Cholesterol, or DCP do not exert the same effects as NISV in terms of immunomodulation *(McGahon, 2021)*, which implies that the structural organisation of NISV is required for this effect. Thus, greater uptake of small NISV (which have a greatly increased surface area to volume ratio) does not exert effects purely from a greater accumulation of NISV components in the endosome or lysosome. As the mechanism of NISV immunomodulation remains unknown, it is unclear whether there is an ideal location to which NISV traffic, or uptake method to enhance these immunomodulatory effects.

Finally, whilst the overall pattern of cytokine/chemokine induction altered by NISV is generally unaffected when changing the size of NISV, there are some discrepancies when examining the effect of vesicles on imiquimod stimulated cells. For example, small ~130nm NISV induce IL-1α and IL-1β much more potently than both larger sizes. A potential mechanism explaining this effect could be purely physical. As mentioned previously, free surfactant generated during extrusion may cause damage to the membrane of cells, and thus when the NLRP3 inflammasome is activated upon TLR ligation, gasdermin D is proteolytically cleaved by caspase 11 and thus can initiate pore formation for release of IL-1 cytokines that are stored in the cytosol. Potential weakening of the plasma membrane by small NISV or free surfactant could increase pore size or reduce the integrity of the hole, allowing greater release of these cytokines *(Kayagaki, et al., 2015; Devant, and Kagan, 2023).* Alongside this, vesicles extruded to ~610nm and ~130nm were able to potently downregulate imiquimod induced IL-6 production, whereas NISV sizes ~1430nm slightly increased the levels of IL-6. It should be noted that all sizes of NISV can increase IL-6 without TLR stimulation, and thus the addition of TLR stimulation causing the inverse effect is peculiar.

One question provided in this chapter is whether the change in potency of NISV of different sizes is statistically significant. To further investigate this aspect, more accurate calibration of IC50 curves, coupled with at least n=3 replicates would be required to assess this *in vitro.*

However, whether the difference in potency is physiologically relevant is debatable, and *in vivo* studies would be required to further finalise this observation.

5 Chapter 5

Characterising the effect on cellular metabolism imparted by NISV or dexamethasone in TLR7 or TLR8 stimulated BMDM

5.1 Abstract

Cellular metabolism is closely interwoven with induction of the immune response and can be modified by pathogens such as viruses to enhance their survival within the host. Key pathways related to energy generation, macromolecule synthesis, and catabolism/recycling of substrates are often altered upon infection and can be further modified by the immune system. Altered metabolism and dysregulation of typical functioning is prevalent in a slew of malignancies including cancer and diabetes, with the latter exacerbating viral infections such as SARS-CoV-2. Focusing on the metabolic effects of this virus, we aim to investigate the effect of both NISV or dexamethasone on metabolism in a TLR7 or TLR8 stimulated BMDM model. Bone marrow derived macrophages (BMDM) were stimulated with either the TLR7-specific ligand imiquimod, or the TLR8-specific ligand TL8-506. Cells were then treated with a single concentration of melt method NISV, or dexamethasone determined via earlier IC50 experiments. After 24hrs, a cold chloroform:methanol:water (1:3:1) extraction was used to collect metabolites from cells. Metabolite extracts were then analysed by LC-MS and peaks matched to internal authentic standards or identified using publicly available databases based on mass-charge ratio and retention time. By examining energy generation pathways such as glycolysis and TCA cycle light was shed on the ability NISV or dexamethasone to alter energy metabolism, as well as identify key metabolic pathways altered by each treatment in comparison to cells given TLR stimulation and no treatment. PCA and OPLS-DA was also utilised to identify significant metabolites and pathways that are altered by NISV treatment. The data demonstrates that whilst the effects of NISV on bioenergetic pathways such as glycolysis are minor, NISV can cause an increase in phospholipid production and exert differential effects on macrophage itaconate production dependent on the specific TLR activated. It was also demonstrated that in terms of Warburg effect-like changes, dexamethasone and NISV exhibit a similar pattern of metabolic perturbations dependent on whether TLR7 or TLR8 is activated and show a reversal in fatty acid regulation with both treatments.

5.2 Introduction

Maintenance of cell homeostasis relies upon a variety of bioenergetic processes that supply both the energy and building blocks for the generation of proteins, nucleic acids, fatty acids and other macromolecules required for typical cell function. Ensuring nominal metabolic functioning in immune cells is essential for an effective response to damage or infection, alongside metabolic plasticity allowing interchange of carbon between substrates and metabolic intermediates. Alterations to this normal functioning can arise from changes or detected perturbations to the local environment, such as trauma and generation of DAMPs, cell death, pathogen invasion and generation of PAMPs, or through signalling from other cells through cytokines and chemokines *(O'Neill, and Pearce, 2016; Cheng, et al., 2014)*. Metabolism is an extremely broad topic, with the Kyoto Encyclopedia of Genes and Genomes (KEGG) annotating greater than 19,136 metabolites or chemicals, and 11,965 reactions that are biologically relevant to metabolism. Therefore, this chapter will focus on key pathways that play a central role in macrophage immunometabolism, namely glycolysis and the TCA cycle, alongside investigating the emerging significant metabolites as determined by dimensionality reducing statistical analyses such as OPLS-DA. Furthermore, I shall focus on these pathways in the context of a ssRNA viral infection and examine some of the metabolic mechanisms exploited by viruses to achieve successful infection and dissemination within the host.

5.2.1 Macrophage metabolism under normoxic conditions

The metabolic requirements and therefore metabolic processes occuring in cells vary depending on the role and functions of the particular cell. When discussing the metabolism of immune cells such as Mφ or DCs, the processes that contribute to their nominal functioning can be termed immunometabolism. Particularly for these cells, glycolysis, TCA cycle, and fatty acid metabolism is important. Like all cells, Mφ undergo respiration which typically begins with the breakdown of glucose acquired primarily from the breakdown of food, or alternatively through glycogenolysis or gluconeogenesis in the liver. To facilitate entry of glucose into the cell, glucose transporters such as GLUT1 are used. Although there are 14 GLUT proteins identified in humans, GLUT1 is the primary glucose transporter used by pro-inflammatory macrophages *(Thorens, and Mueckler, 2010).* Once glucose enters the cell cytoplasm via this mechanism, glycolysis occurs. This process involves enzymes that break down glucose into compounds that can be used as intermediates in the synthesis of other macromolecules by various metabolic pathways. Alongside this glycolysis generates 4 molecules of ATP from one molecule of glucose (a net gain of 2 ATP as there is an investment of 2 ATP to phosphorylate glucose by hexokinase and trap it inside the cell). The

Coenzyme NADH is also generated during glycolysis and is used in downstream pathways as an electron carrier to generate further ATP. A full explanation of glycolysis is available in **figure 50**

An important aspect of macrophage metabolism is the production of nitric oxide (NO) and related compounds that can exert anti-pathogen effects, mediate inflammation, and regulate other cells of the immune system. Production of NO by macrophages is dependent on enzymes that vary within the spectrum of M1 to M2 macrophages. The canonical NO production pathway in M1 macrophages relies upon expression of the enzyme nitric oxide synthase (NOS) and results in the conversion of arginine to NO and citrulline which may be recycled for further NO production through transamination and the interaction of aspartic or glutamic acid with citrulline. M2 macrophages are also involved in arginine metabolism but utilise arginase to generate ornithine and urea *(Rath, et al., 2014).* This effect serves to deplete arginine and disrupt the ability of macrophages to generate NO and therefore inflammation, as well as providing feedstock for proline synthesis. Furthermore, arginine has been shown to be utilised during macrophage proliferation, and thus depleting this amino acid serves to limit macrophage expansion *(Yeramian, et al., 2006).* Thus, polarisation of macrophages displays strong perturbations in metabolism, with measurement of key metabolites such as arginine, ornithine, citrulline, and proline providing a valuable indicator of whether a treatment may elicit an inflammatory phenotype, or a tissue repair and homeostasis phenotype. The ability of a treatment to direct macrophage metabolism towards the desired outcome would be a boon when considering pathologies resulting from viral infection or the generation of sepsis due to the key role macrophages play in directing the immune response *(Wang, and Wang, 2023)*

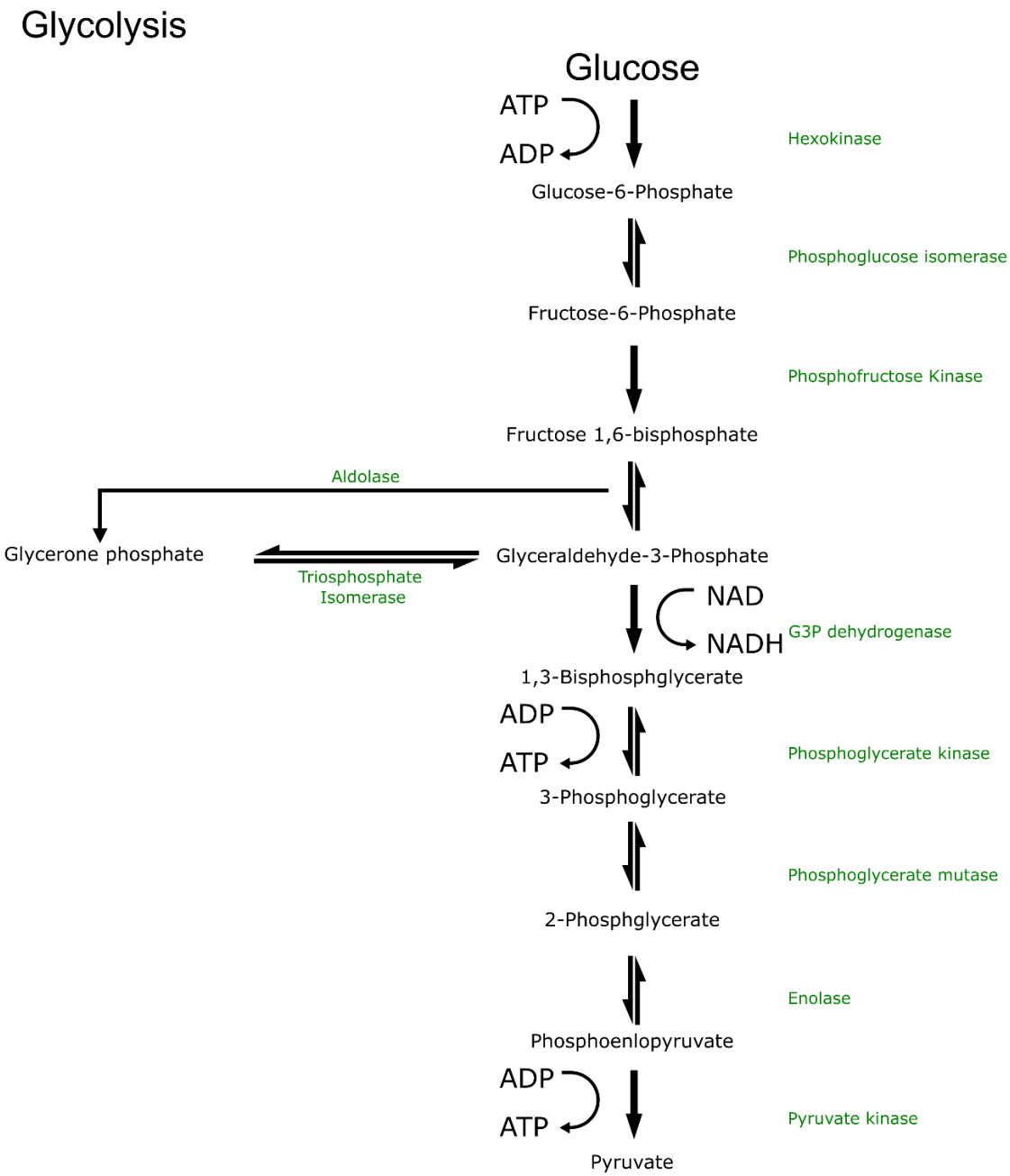

Figure 50: Metabolites and enzymes involved in the Glycolysis pathway. *After entry into the cell via GLUT1, 2 molecules of ATP are invested to provide energy to hexokinase, phosphorylating glucose to glucose-6-phosphate. This is then reversibly isomerised by phosphoglucose isomerase into fructose-6-phosphate, and then phosphorylated further by phosphofructose kinase to give fructose 1,6-phosphate. At this point, aldolase acts upon Fructose 1,6-bisphosphate to irreversibly split the aldol into glycerone phosphate and reversibly into glyceraldehyde-3-phosphate (G3P). Glycerone phosphate may be rapidly reversibly isomerised into G3P by the isomerase triosphosphate isomerase. G3P is then oxidised by G3P dehydrogenase and the coenzyme NAD which acts as a reducing agent to accept the electron, generating 1,3-bisphosphoglycerate. This is then phosphorylated by phosphoglycerate kinase to produce 3-phosphoglycerate, with the phosphate group forming ATP from ADP. Phosphoglycerate mutase then produces 2-phosphoglycerate from 3-phosphoglycerate, which is then converted to phosphoenolpyruvate by enolase. Finally, pyruvate kinase phosphorylate phosphoenolpyruvate to generate pyruvate, with ATP being formed from ADP and the phosphate group lost from phosphoenolypyruvate. Overall, 2 molecules of ATP are invested, and then 4 molecules of ATP and 2 molecules of NADH are produced during glycolysis (Patil, et al., 2022).*

5.2.2 Tricarboxylic acid cycle and oxidative phosphorylation

Pyruvate produced during glycolysis then travels from the cytoplasm to the intermembrane space of mitochondria by a voltage dependent anion channel (VDAC) and, using transmembrane proteins such as mitochondrial pyruvate carrier (MPC), is transported to the mitochondrial matrix. Pyruvate then undergoes a series of cyclic reactions mediated by enzymes that result in the generation of 6 molecules of NADH and 2 of FADH2 which are required for the generation of ATP in the electron transport chain (ETC), acting as electron donors. A full explanation of the TCA cycle is provided in **figure 51** Whilst the TCA cycle does not directly utilise molecular oxygen, without it the cycle cannot refresh as the electron donors mentioned previously (NADH and FADH2) require the functioning of the oxygen dependent ETC to oxidise back to NAD+ and FAD+.

The ETC occurs in the intermembrane space of the mitochondria and involves two electron transport pathways that results in the pumping of protons into the mitochondrial membrane which allows the generation of ATP. This is the ultimate goal of the oxidative phosphorylation pathways and provides the high energy yield needed for typical homeostasis. The two main pathways in the ETC include either the use of NADH and the complexes I, III, and IV, or succinate and complexes II, III, and IV. Both substrates are primarily produced in the TCA cycle. As ETC relies on molecular oxygen as a final electron acceptor, the ability to generate energy in an efficient manner (i.e., not relying on increased glucose consumption for 2 net ATP yield in glycolysis) demands aerobic conditions *(Zhao, et al., 2019).*

Outside of energy generation, branches of the previously mentioned pathways contribute to the production of metabolic intermediates used in the production of nucleotides, amino acids, fatty acids. For example, acetyl CoA generated in the TCA cycle is also used in fatty acid synthesis by conversion to malonyl CoA by acetyl CoA decarboxylase *(Wakil, et al., 1983; Chu, et al., 2021).* Offshoots of glycolysis such as the PPP use glucose-6-phosphate to generate pentoses and ribose-5-phosphate, precursors to nucleotide and amino acid synthesis *(Stincone, et al., 2015).* Alongside general metabolic redirection, these pathways have been identified as important during viral infection as host metabolic processes provide the building blocks and biochemical substrates needed for viral replication and assembly *(Sanchez, and Lagunhoff, 2015).*

TCA Cycle

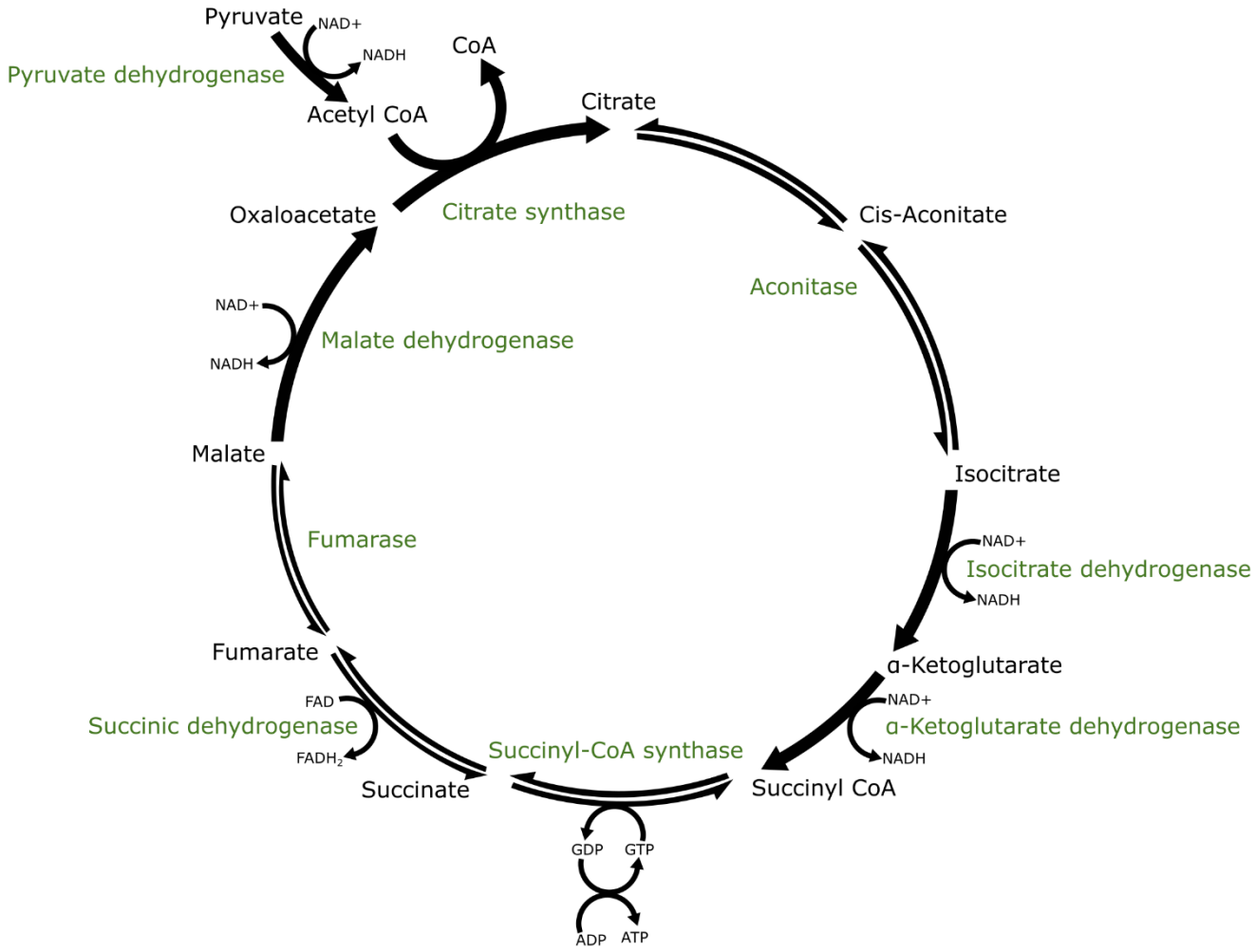

Figure 51: Metabolites and enzymes involved in the TCA cycle. *After generation of pyruvate from glucose during glycolysis, the multi-enzyme complex pyruvate dehydrogenase irreversibly oxidises pyruvate to form acetyl CoA, releasing NADH as a byproduct. Citrate synthase then produces citrate by combining oxaloacetate with the acetyl moiety of acetyl CoA in a condensation reaction. Citrate is then reversibly converted to the isomer isocitrate by aconitase using the intermediate cis-aconitate. A series of oxidation reactions convert isocitrate to α-ketoglutarate, and then succinyl CoA, reducing NAD+ to NADH in the process. Succinyl-CoA synthase then reversibly catalyses the production of succinate, resulting in the generation of ATP or GTP from either ADP or GDP respectively. Succinate is then oxidised to fumarate by succinic dehydrogenase, reducing FAD+ to $FADH_2$. Fumarase catalyses the reversible hydration or dehydration of fumarate to malate, with malate finally being oxidised to produce oxaloacetate. This also produces NADH and begins the TCA cycle once more (Arnold, and Finley, 2023; Kang, et al., 2021; Phillips, et al., 2009; Krebs, and Johnson, 1937).*

5.2.3 Metabolic dysregulation

During a viral infection, multiple factors contribute to changes in metabolic function. As viruses can be considered obligate intracellular parasites, the ability to replicate their genome, produce viral proteins, and ultimately generate new virion for further dissemination relies upon the metabolic pathways and cellular machinery of the host. Therefore, virally infected cells exhibit altered metabolism that often favours the pathogen. Depending on the virus, prospective cells for infection are typically quiescent and upon infection an increase in metabolic activity is observed. Whilst this schema may be true for many viruses, pathogens like HIV preferentially infect cells that have increased levels of metabolic activity e.g., activated CD4+ T cells vs their dormant subsets *(Kang, and Tang, 2020).* To provide energy for the biosynthetic processes that are required by the virus, energy metabolism is often altered, with an increase in glycolysis observed. Notably, there is a preference for glycolysis even in aerobic conditions, and although inefficient compared with normoxic respiration, is thought to more quickly provide a burst of energy production compared with lengthy oxidative phosphorylation. This feature is also present in cancer cells and is termed the Warburg effect *(Vander Heiden, et al., 2009).* Alongside increased energy metabolism, a switch from fatty acid oxidation to fatty acid synthesis is often observed, particularly in the case of enveloped viruses as they require fatty acids for the generation and stability of their outer lipid membrane, alongside the utilisation of lipids for membrane remodelling. By altering the local membrane architecture, lipids can act as a scaffold for viral replicases, as well as providing protection for viral proteins and nucleotides, slowing detection of these viral motifs by the cell (*Heaton and Randall, 2011).* This further reinforces the idea that altered cellular metabolism can perturb the ability of the immune system to mount a timely and effective response.

Despite the efforts of viral pathogens to avoid detection, an eventual anti-viral response can contribute to alterations in local cellular metabolism and reverse some metabolic influences of the virus. Release of type I and II IFNs are associated with an anti-viral response. Type I includes IFNα subsets (of which there are 13 in humans) and IFNβ, whereas type II IFNs comprise only IFNy. These cytokines bind to receptors on most cells (IFNAR for type I IFNS, IFNGR for type II IFNS), and exert their effects through initiating transcription of interferon stimulatory genes (ISGs) of which there are greater than 300. The effects of these genes can be varied and include effects such as the suppression of sterol regulatory binding protein-2 (SREBP) (a negative regulator of cholesterol) to increase cholesterol biosynthesis and therefore deprive viruses of lipid, or increased production of Cholesterol 25-hydroxylase (CH25H) which converts cholesterol to 25-hydroxycholesterol (25HC), disrupting viral membrane fusion *(Platanias, 2005; Sumbria, et al., 2020).*

Altered metabolism is not unique to viral infections and is implicated in a variety of disease states and conditions. Of particular relevance is cancer, with many contributions to our understanding of altered metabolism stemming from the study of tumours. Skewed metabolism in cancer cells is well documented, as metabolic restructuring occurs to promote rapid cell growth and sustain the cell in a harsh microenvironment. Namely, an increase in glucose consumption compared with surrounding unaffected cells is observed, alongside a tendency to metabolise glutamine for the synthesis of fatty acids. In contrast to the effects of IFNs mentioned earlier, mTORC pathways induced in cancer cells increase the actions of SREBP-1 (a positive regulator of cholesterol), therefore increasing cholesterogenic processes to provide cholesterol for rapid cellular growth *(Peterson, et al., 2011).* Cancer cells may also use the PPP to generate nucleotides and NADPH to further fuel the production of macromolecules needed for their proliferation *(Schiliro, and Firestein, 2021).*

Another prevalent condition resulting from altered metabolism is diabetes. Again, glucose metabolism is implicated in the pathogenesis of this disease. Chiefly, inability to produce insulin at sufficient levels has been linked to dysregulation of glycolysis and subsequently low ATP production in the mitochondria. A key factor in this paradigm is the availability of NADH as a reducing agent required for ATP production in the mitochondria, which controls the ATP sensitive K^+ channels through which insulin is secreted in pancreatic β cells. Studies have demonstrated that by inhibiting mitochondrial metabolism or mitochondrial coupling agents such as glutamate, citrate, and NADH, the release of insulin stimulated by glucose is reduced *(Haythorne, et al., 2019; Prentki, et al., 2013)*. Whilst the focus of this thesis is viral infections, it cannot be understated that a treatment that modulates cellular metabolism could be of potential use in other malignancies with metabolic dysfunction at their core.

5.2.4 The Warburg effect

Named for the observation that tumour cells undergo aerobic glycolysis, published by Otto Warburg in 1927, the Warburg effect has been most studied in the field of oncology. It was understood that cancer cells could survive in an oxygen-deprived environment given that they were supplied with glucose, thus implying an alternative method of energy production available to tumour cells outside of normoxic respiration *(Warburg, et al., 1927).* Aerobic glycolysis is a common feature of many viruses and is marked by low levels of intracellular glucose, higher levels of lactic acid, increased GLUT expression, increased pyruvate dehydrogenase kinase (PDK), and increased hexokinase expression *(Burns, and Manda, 2017).* Understanding these biomarkers in the context of the Warburg effect, and the

subsequent effect of NISV, dexamethasone, or alternative compounds can provide insight into a potential therapeutic mechanism which can be exploited to improve treatment efficacy.

Upregulation of GLUT expression allows cells to meet the increased demand for glucose by increasing sugar flux. Concomitantly, increased expression of hexokinase converts glucose into G6P which can be used in the PPP, fuelling nucleotide production. This step also allows increased generation of NADPH through the oxidative branch of the PPP, which pairs with low NADH generation from reduced TCA cycle functioning to skew cellular metabolism towards anabolic reactions *(Chen, et al., 2019).* This decrease in TCA cycle functioning is contributed to by increased PDK expression, which phosphorylates PDH, decreasing the conversion of pyruvate to acetyl-CoA, effectively depleting the feedstock of the TCA cycle *(Zhu, et al., 2020).* Abundance of NADPH is a double-edged sword for viruses, as NADPH acts as a reducing agent for the production of cholesterol through the mevalonate pathway, alongside acting as a cofactor in lipid biosynthesis *(Chandel, 2021).* However, NADPH is also used in the generation of reactive oxygen species as an electron donor which creates a hostile environment for viruses *(Canton, et al., 2021).*

5.2.5 Sars-Cov-2 infection and metabolism

Whilst the study of SARS-CoV-2 has been intense due to the recency of the outbreak, there may be gaps in our knowledge of the virus' effect on cellular metabolism. In such cases, observations made during the examination of other ssRNA respiratory viruses have provided potential insights into the metabolic restructuring upon SARS-CoV-2 infection. To begin, a brief review of our current understanding of SARS-CoV-2 in the context of metabolism.

During SARS-CoV-2 life cycle, altered cellular metabolism contributes to pervasiveness of the virus or is a consequence of viral metabolic manipulation. Studies on viral entry have implicated a number of metabolites and pathways in facilitating increased susceptibility to SARS-CoV-2 infection. As mentioned in relation to cancer, lipids are of vital importance. Abnormal levels of lipids have been observed co-localising with the N protein of SARS-CoV-2 in the lungs of patients, alongside single-cell RNA seq studies displaying great alterations to lipid patterns in patients with severe COVID-19 *(Zhao, et al., 2022).* Outside of envelope production, lipid rafts on the surface of cells may facilitate viral entry and thus therapies that upregulate CH25H disrupt these rafts and inhibit viral entry, similar to the effect of IFNs *(Wang, et al., 2020).* Viral entry may also be increased through upregulation of ACE2 brought on by high glucose levels. Notably, this correlates with diabetes patients displaying increased susceptibility to SARS-CoV-2 infection and increased risk of severity *(Vargas-Rodriguez, et al., 2022).*

During replication, lipid and glucose metabolism are once more implicated alongside the PPP, and fatty acid synthesis. Lipid droplets, cellular organelles that act as lipid storage and regulators of lipid homeostasis are involved in the replication cycle of many viruses. Inside the hydrophobic core of the phospholipid monolayer, triacylglycerols, cholesteryl esters and enzymes involved in lipid metabolism reside *(Olzmann, and Carvalho, 2019).* Researchers have demonstrated that the N-protein of SARS-CoV-2 can upregulate diacylglycerol acyltransferase (DGAT) to generate triacylglycerol from diacylglycerol and fatty acyl-CoA to promote lipid droplet formation *(Yuan, et al., 2021).* Increased lipid production can promote formation of viral replication complexes and provide the substrate required for virus particle production *(Zhang, et al., 2019).* Inhibition of fatty acid synthesis by inhibition of fatty acid synthase (FASN) can inhibit SARS-CoV-2 replication by depleting the substrate needed to generate these lipid droplets and thus reduce capacity for lipid metabolism. Whilst this requires further study in the context of SARS-CoV-2, other +ssRNA viruses such as Dengue virus utilise FASN as part of their replication complexes, highlighting this route as a potential therapeutic target *(Heaton, et al., 2010).*

Increased glycolysis provides substrates for nucleotide synthesis through increased production of G6P which fuels the PPP for production of ribose-5-phoshphate required for synthesis of nucleotides. To further this notion, increased levels of the first enzyme in the PPP, G6P dehydrogenase, has been found in the lungs of COVID-19 patients *(Santos e Silva, et al., 2021; Chen, et al., 2023)*. Studies have investigated the potential of PPP as a target for SARS-CoV-2 therapy; by depleting hexokinase and phosphoglucose isomerase using 2-Deoxy-glucose, alongside inhibition of the enzyme transketolase, both the oxidative and non-oxidative path towards ribose-5-phosphate is downregulated. Thus, SARS-CoV-2 RNA synthesis was abrogated *(Bojkova, et al., 2021).*

5.3 Aims and hypothesis

This chapter aims to:

i. Utilise an untargeted metabolomics method to evaluate any major perturbations in macrophage metabolism imparted by NISV or dexamethasone treatment after TLR7 or TLR8 stimulation. By utilising dimensionality reducing statistical analyses such as PCA and OPLS-DA, the aim is to highlight the significantly changed metabolites that are driving variance between TLR stimulated BMDM and those same BMDM treated with NISV or dexamethasone.

ii. Investigate metabolic pathways involved in bioenergetic processes such as glycolysis and the TCA cycle. By closely examining the effects of NISV or dexamethasone on these pathways in TLR stimulated BMDM, the aim is to determine any detrimental effects of NISV or dexamethasone that could have implications when used as a treatment for viral infection induced sepsis. As these pathways are often altered in a variety of malignancies outside of viral infections, such as cancer, we also consider the exacerbation of the Warburg effect as an indicator of NISV or dexamethasone appropriateness as a treatment.

5.4 Results

To investigate the effect of NISV on the metabolic processes of cells, BMDM were stimulated with either the TLR7 ligand imiquimod, or the TLR8 ligand TL8-506 at their EC90 concentrations determined in earlier experiments. The cells were then treated with either NISV or dexamethasone, at IC90 concentrations, similarly determined earlier. After 24hrs stimulation, a cold chloroform:methanol:water extraction was performed on the cells and extracts were analysed by LC-MS. The physical properties of the NISV used in this experiment, as characterised by a Zetasizer are consistent with previous experiments: NISV were between 1.5-2μm with a modest PDI, and sufficient negative charge of around -30mV **(Fig. 52)**.

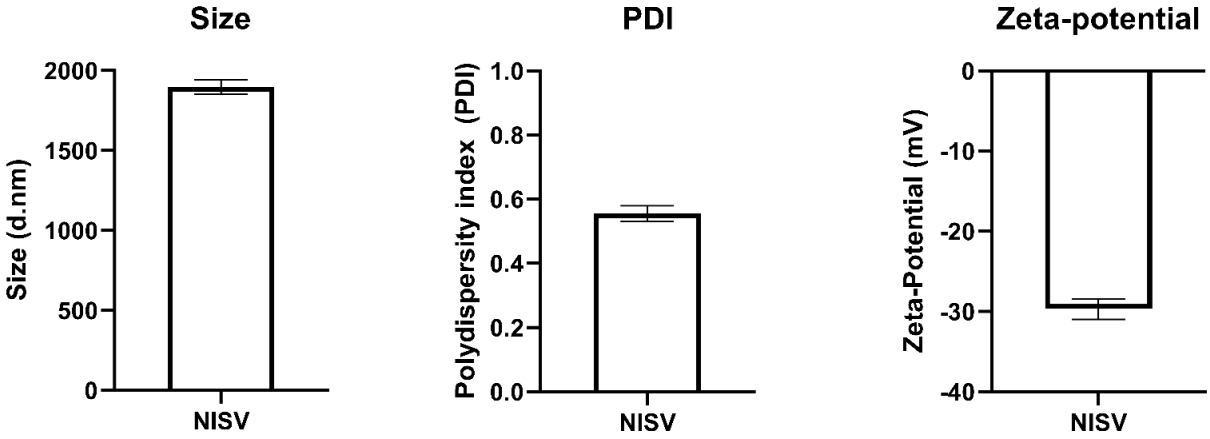

Size (d.nm)	Polydispersity Index (PDI)	Zeta-potential (mV)
1897 ± 45.310	0.555 ± 0.025	-29.700 ± 1.290

Figure 52: Physical characteristics of NISV used in metabolomics and transcriptomics experiments. *Size, PDI, and Zeta-potential measured by dynamic light scattering using a Zetasizer. Results expressed as mean ± SEM, n = 3.*

5.4.1 NISV or dexamethasone treatment does not severely affect overall metabolism

After LC-MS detection of metabolites, volcano plots were then generated to examine the significantly upregulated or downregulated metabolites that were putatively annotated or identified. Stimulation alone and treatment alone cases were compared wih the media alone control, e.g. TLR7 alone stimulation vs media alone cells, or NISV alone treatment vs media alone cells. For TLR stimulated cells + treatment, this was compared with the appropriate TLR alone control. Generally, the effect of NISV or dexamethasone alone displayed the least significant changes, whereas groups that included TLR stimulation and either NISV or dexamethasone displayed the greatest change in metabolites **(Fig. 53).**

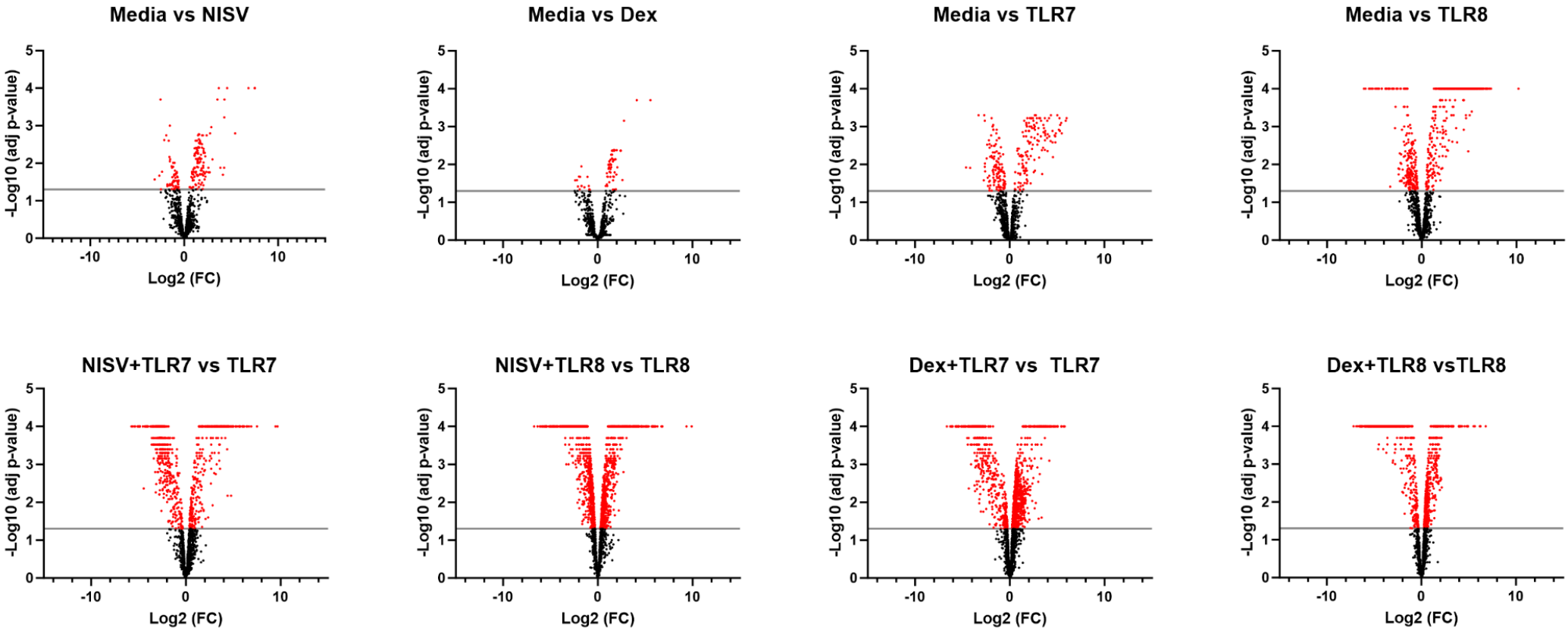

Figure 53: Volcano plots displaying significant differences in NISV or Dexamethasone treated TLR7 or TLR8 stimulated BMDM. *Metabolomic analysis was performed on extracted samples from BMDM stimulated with either 1.6µg/ml Imiquimod (TLR7) or 1.3µg/ml TL8-506 (TLR8), and then treated with 1.2mM NISV or 1.6µM of dexamethasone. Controls included were unstimulated cells (Media) or those NISV alone, dexamethasone alone, imiquimod alone, or TL8-506 alone where appropriate. Values in red = significant. Significance cutoff at adjusted p value <0.05 using false discovery rate.*

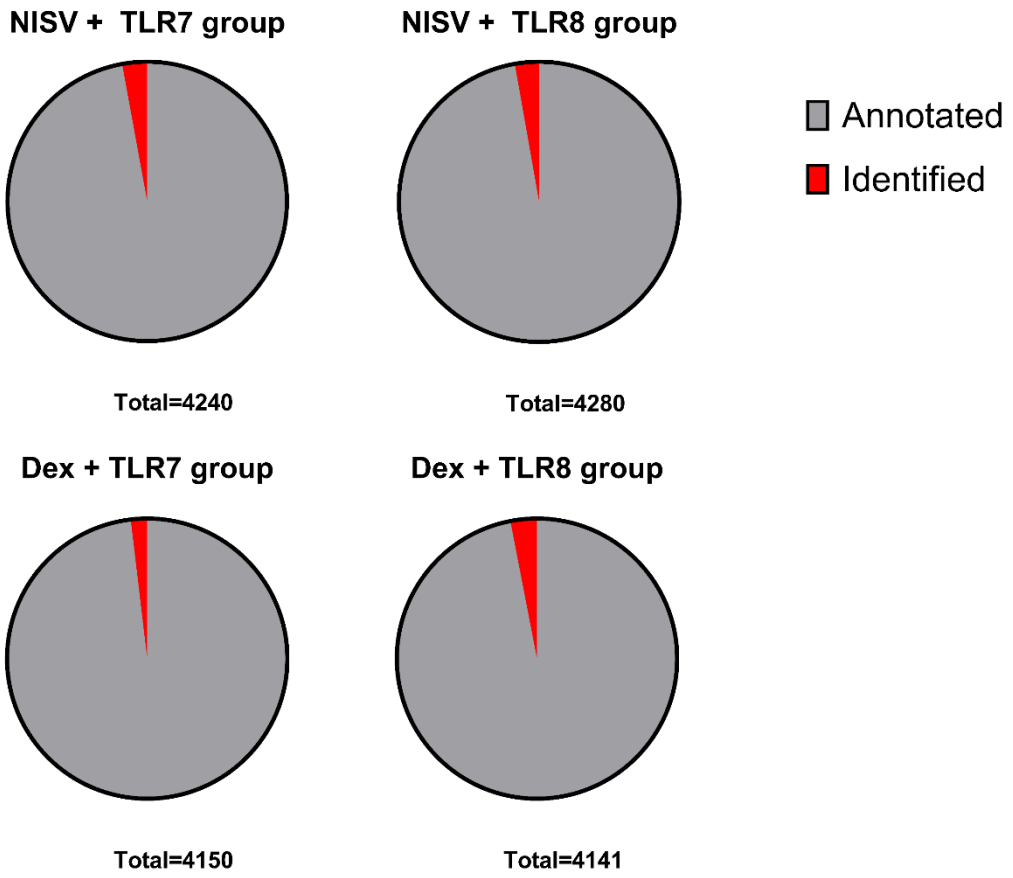

Figure 54: Metabolites identified in each comparison group.

From total LC-MS peaks, peaks were matched to a known authentic standard or putatively annotated by peak-matching using publicly available databases such as HMDB and KEGG. According to the metabolomics standards initiative, these detected compounds were deemed either "identified" – matching a standard accurately identifying a single metabolite or "annotated" - matching the LC-MS features of metabolites described in the MS databases but could match multiple metabolites.

Samples were analysed in 4 main comparison groups with the relevant controls: NISV+TLR7 stimulation, NISV + TLR8 stimulation, dexamethasone + TLR7 stimulation, and dexamethasone + TLR8 stimulation. According to the metabolomics standard initiative (MSI), peaks were deemed identified (matching an authentic standard) or annotated (one peak could potentially match multiple metabolites), representing level 1 and level 2 identification, respectively **(Fig. 54)**. For NISV + TLR7 analysis, 4,240 peaks were detected and assigned to metabolites, with 4118 annotated and 122 identified. For NISV + TLR8, 4280 total peaks were assigned, with 4161 annotated and 119 identified. For dexamethasone + TLR7, 4182 peaks were identified with 4072 annotated and 78 identified. Finally, dexamethasone +TLR7 displayed 4142 total peaks, with 4015 annotated and 126 identified.

Alongside automatic annotation based on internal standards used during LC-MS and multiple metabolic database queries, peaks were manually annotated based on suggested confidence values and inference about the feasible origin of each compound where appropriate. For example, for a given peak, suggested compounds that were only found in plants or other sources not explained by the experimental design were disregarded and the pool of potential compounds narrowed down. To provide robust analysis, only identified compounds were used for direct comparison, with putatively annotated compounds used to support this data after manual scrutiny of potential annotation.

Firstly, PCA was used to quality check sample grouping both when all metabolites were considered e.g... identified compounds and putatively annotated compounds **(Fig. 55 - 56).** When examining all metabolites detected, there was generally good grouping of replicates particularly in the NISV experimental groups indicating high accuracy and reproducibility. NISV samples were also separated well, indicating distinct effects imparted by each combination of stimulation and treatment. Comparing this to all metabolites detected in the dexamethasone groups reveals that whilst samples displayed fairly tight grouping, there was less distinct separation between groups. To provide robust analysis, and streamline the processing of these large datasets, we chose to utilise only identified metabolites when exploring metabolic pathways affected by each treatment. Tight grouping of the treatment groups provided the opportunity for robust comparison using orthogonal partial least squares-discriminant analysis (OPLS-DA) to highlight metabolites of importance for metabolic pathway probing.

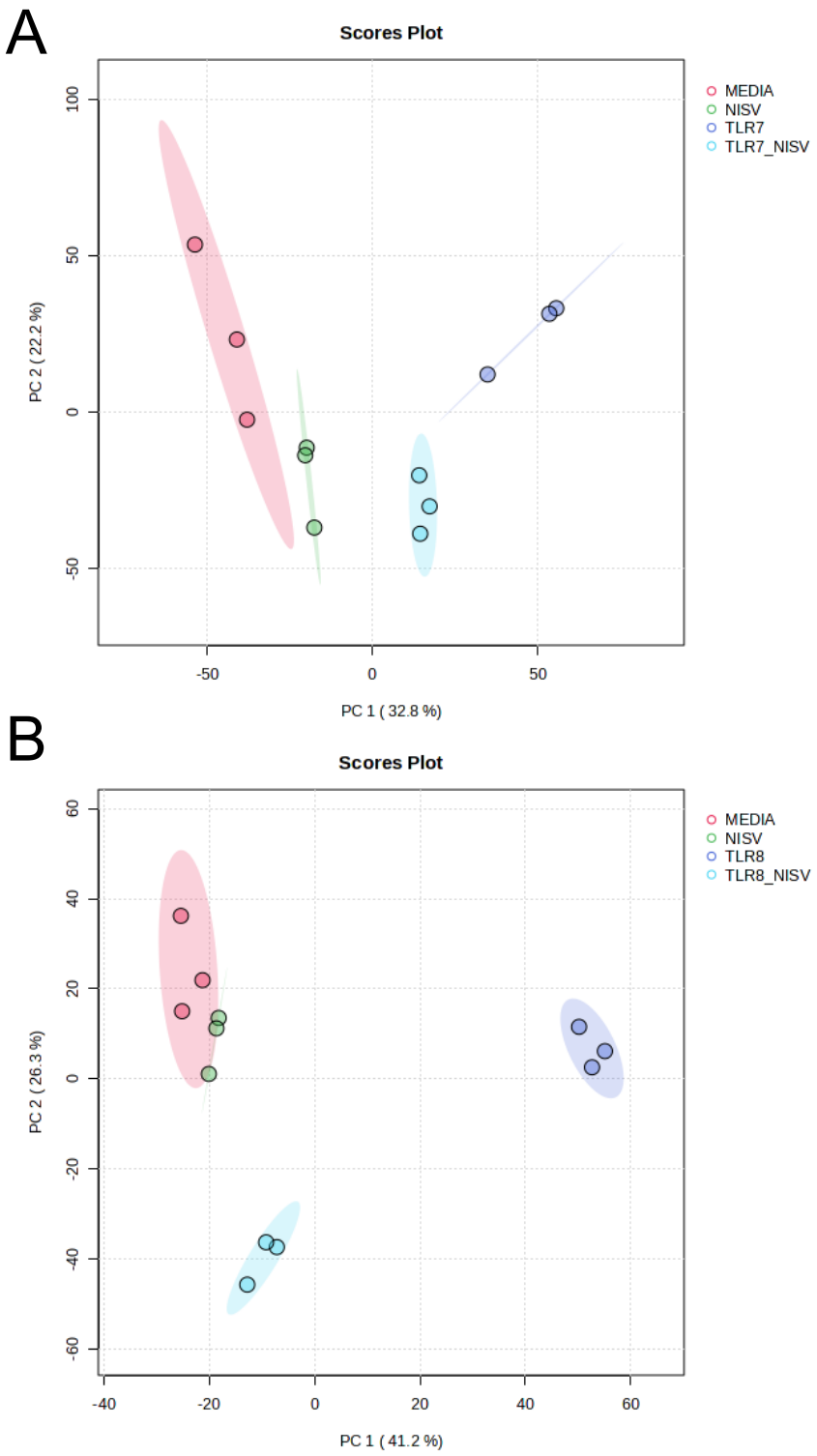

Figure 55: PCA plots displaying sample grouping by all metabolites for TLR stimulated BMDM treated with NISV. *Principal component analysis was used to compare LC-MS peaks denoting all potential metabolites in each group, followed by only LC-MS peaks matching an authentic standard. (A) TLR7 stimulated cells + NISV all metabolites, (B) TLR8 stimulated cells + NISV all metabolites. Coloured areas represent 95% confidence interval for each group. Components selected on largest % variance explained.*

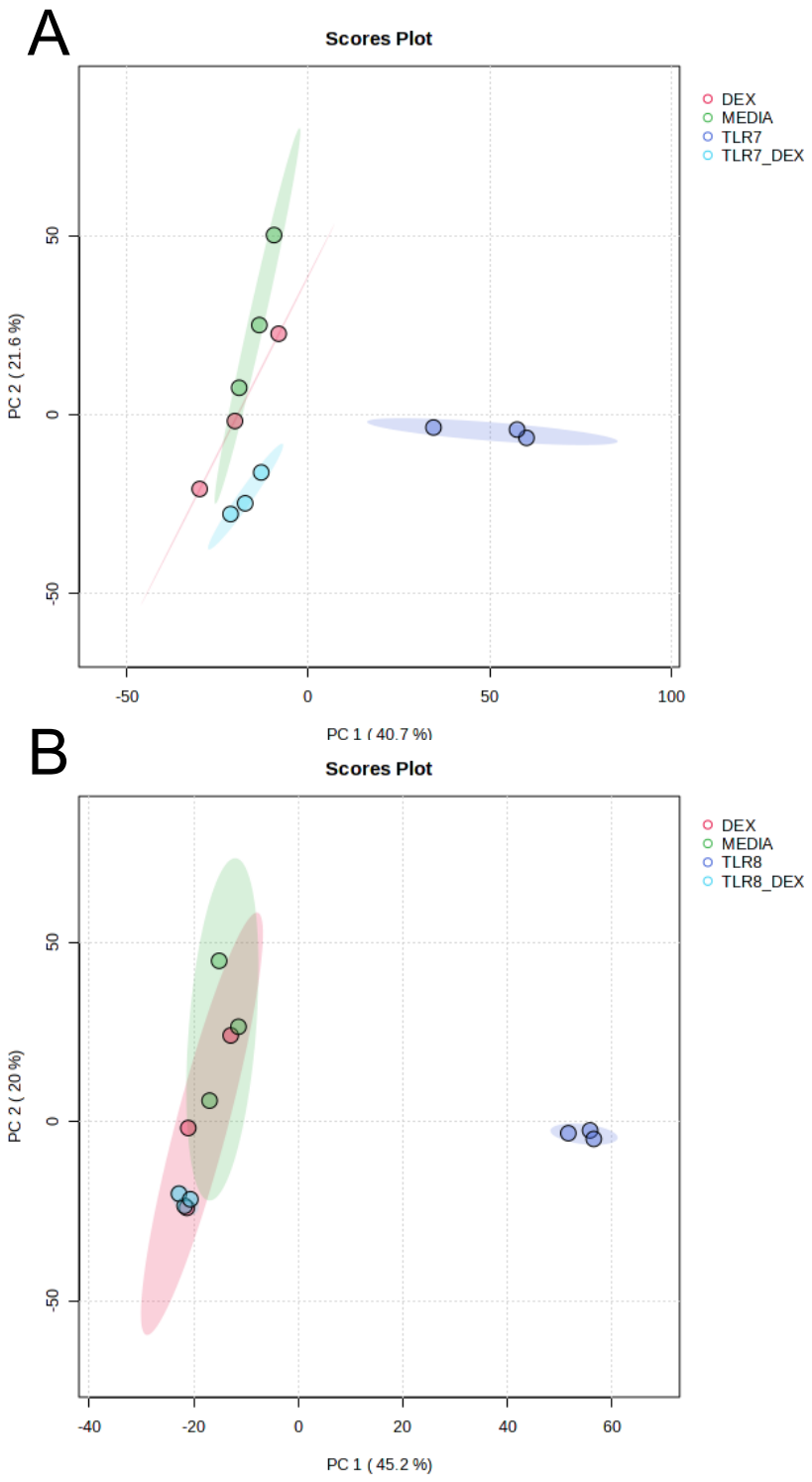

Figure 56: PCA plots displaying sample grouping by all detected metabolites for TLR stimulated BMDM treated with dexamethasone. *Principal component analysis was used to compare LC-MS peaks denoting all potential metabolites in each group, followed by only LC-MS peaks matching an authentic standard. (A) TLR7 stimulated cells + dexamethasone all metabolites, (B) TLR8 stimulated cells + dexamethasone all metabolites. Coloured areas represent 95% confidence interval for each group. Components selected on largest % variance explained.*

OPLS-DA requires comparison between only two groups and considers the group status. This can create a false positive and force separation between groups, and thus it is advised to use PCA to determine if there is good group separation prior to OPLS-DA. This data is provided in **appendices 1 and 2.** As we observed good grouping of samples and separation between the NISV + TLR vs TLR alone and Dex + TLR vs TLR alone groups, we proceeded to utilise OPLS-DA and generate a list of VIP metabolites.

5.4.2 NISV treatment affects phospholipid synthesis and itaconate

Examining the effect of NISV on TLR7 or TLR8 stimulation reveals common metabolites to both groups (**Fig. 57).** Intermediates involved in phospholipid synthesis, choline phosphate and ethanolamine phosphate, are decreased in both groups vs the ligand alone control, highlighting the ability of NISV to affect production of phosphatidylcholine (PC) or phosphatidylethanolamine (PE). These phospholipids are the most abundant molecules that comprise the membranes of macrophages, and although putatively annotated, are generally upregulated in our data, explaining the decrease in intermediates as a conversion to both PC and PE. Furthermore, malonate is upregulated in both groups, which is an intermediate in the production fatty acids that are an essential requirement for phospholipid synthesis.

In terms of energy metabolism, upregulation of both phosphoenolpyruvate and cis-aconitate feature in both groups. Phosphoenolpyruvate is produced during glycolysis and is part of the production of the essential TCA feedstock acetyl-CoA via conversion to pyruvate. From acetyl-CoA, citrate, and then cis-aconitate is produced. Notably, another metabolite common to both groups, itaconate is produced from cis-aconitate as part of C5 dibasic acid metabolism. Itaconate is involved in regulation of inflammation in macrophages, through inhibitory actions on succinate dehydrogenase, KEAP1, and ATF3. The downstream effects of KEAP1 alkylation by itaconate increases the activity of NRF2, an anti-inflammatory transcription factor, whereas itaconate increases the activity of IκBζ via ATF3, blocking NF-kB binding to DNA. Interestingly, itaconate is increased by NISV in TLR7 stimulated cells, but decreased in TLR8 stimulated cells.

Other metabolites found in both VIP are malonate, 2-hydroxyglutarate, and N-acetylglutamine. 2-hydroxyglutarate levels are increased in NISV treated samples and is also involved in C5 dibasic acid metabolism. Accumulation of this metabolite may indicate acidic pH and can have toxic effects on cells. N-Acetylglutamine is down regulated and involved in initiation of the urea cycle and can activate the enzyme CPSI which produces citrulline from carbamyl phosphate.

Metabolites unique to TLR7 + NISV include those involved in ascorbic acid synthesis: L-gulono-1, 4-lactone and oxalate. As a precursor intermediate of ascorbic acid synthesis, L-

gulono-1,4-lactone is upregulated, alongside increased levels of the breakdown product of ascorbic acid, oxalate, NISV may increase ascorbic acid production.

Another interesting pair of compounds identified in the VIP list includes both uridine and D-ribose. Studies have demonstrated that scavenging of D-ribose from uridine breakdown can support glycolysis when nutrients are limited.

TLR8 + NISV effect includes effects on various nucleosides such as decreases orotidine and inosine, with increases in xanthine – a purine degradation product. There is also a decrease in α-ketoglutarate, and an increase in 2-methylcitrate. The lower levels of α-ketoglutarate observed could indicate effects on arginine metabolism, ascorbic acid synthesis, and amino acid metabolism. 2-methylcitrate is involved in propanoate metabolism and is an intermediate in the production of succinate, with slightly lower succinate concentrations detected in TLR8 stimulated cells treated with NISV.

5.4.3 Dexamethasone affects arginine biosynthesis

The above approach was also used to examine the effect of dexamethasone on both TLR7 and TLR8 stimulated cells, and OPLS-DA VIP plots produced **(Fig. 58).** Notably, when examining the effect of dexamethasone on TLR7 stimulated, all 15 VIP metabolites are upregulated, whereas with dexamethasone + TLR8 stimulation there is a mix of both increased and decreased compounds vs the TLR8 alone control.

Beginning with dexamethasone + TLR7 effects, there are a number of compounds that also feature in the NISV VIP lists such as choline phosphate, malonate, and L-Gulono-1,4-lactone. Whilst malonate and L-Gulono-1,4 -lactone are similarly increased in NISV + TLR7 samples, choline phosphate is downregulated, contrasting with the effect of dexamethasone. One group of compounds that has emerged from the dexamethasone + TLR7 VIP list is those involved in arginine biosynthesis: L-Ornithine, L-Citrulline, and L-Arginine, all of which are increased vs TLR7 alone samples. Examining other metabolites involved in this pathway such as α-ketoglutarate, glutamate, and N-acetylglutamate reveals that these compounds are also upregulated. Alongside this trans-4-Hydroxy-L-proline is also included in the VIP list, which is produced downstream of ornithine from the also increased L-proline.

Another group of upregulated compounds present in the VIP list includes L-leucine, and L-isoleucine. These compounds are produced from pyruvate via a series of intermediates and are involved in the production of branched chain amino acids. This effect is also noted in dexamethasone treated TLR8 stimulation, with an increase in L-Valine from the same pathway present in the VIP list.

Further examination of dexamethasone + TLR8 reveals metabolites patterns observed in earlier analysis such as decreased itaconate, decreased α-ketoglutarate (NISV + TLR8), and increased ornithine (Dexamethasone + TLR7). Notably, both 2-phospho-D-glycerate and 3-phospho-D-glycerate are decreased, which may indicate decreased glycolytic activity.

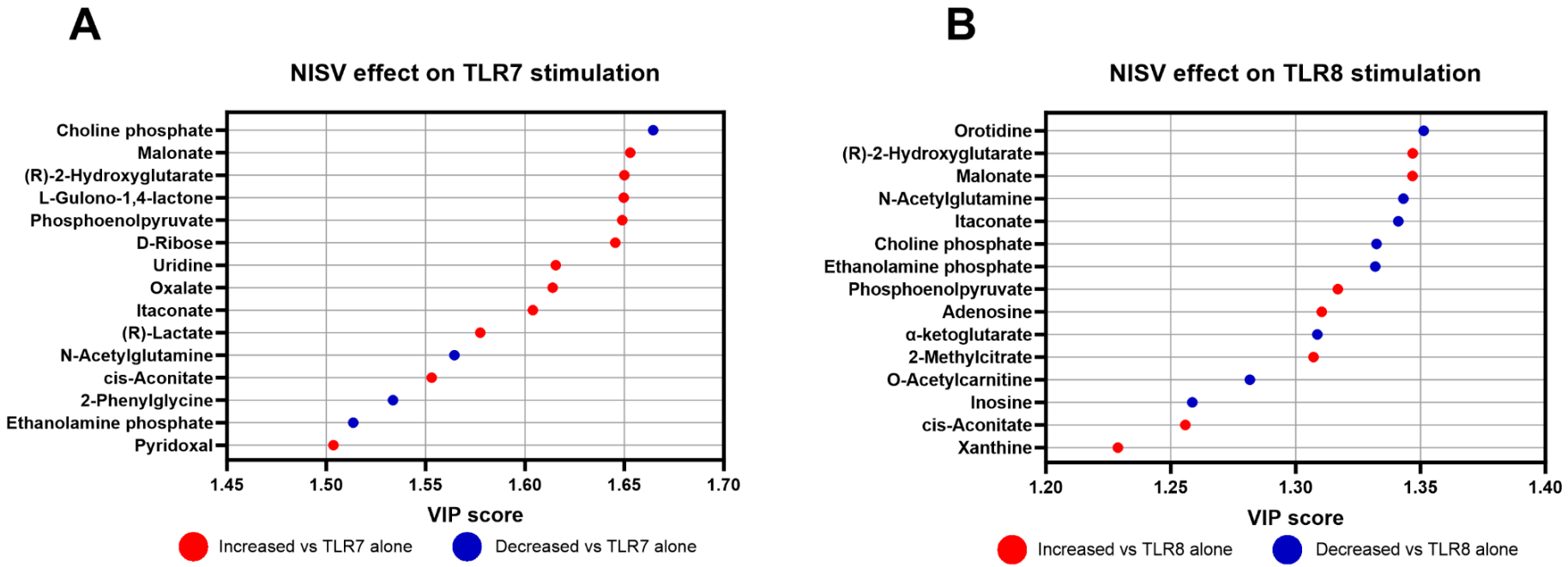

Figure 57: OPLS-DA VIP comparing effects of NISV on metabolism of TLR stimulated BMDM. *Plots display top 15 metabolites that are altered by NISV treatment as determined by OPLS-DA. Red symbols indicate an increase compared with the ligand alone control, blue symbols indicate a decrease compared with the ligand alone control. (A) Effect of NISV on TLR7 stimulated BMDM, (B) effect of NISV on TLR8 stimulated BMDM.*

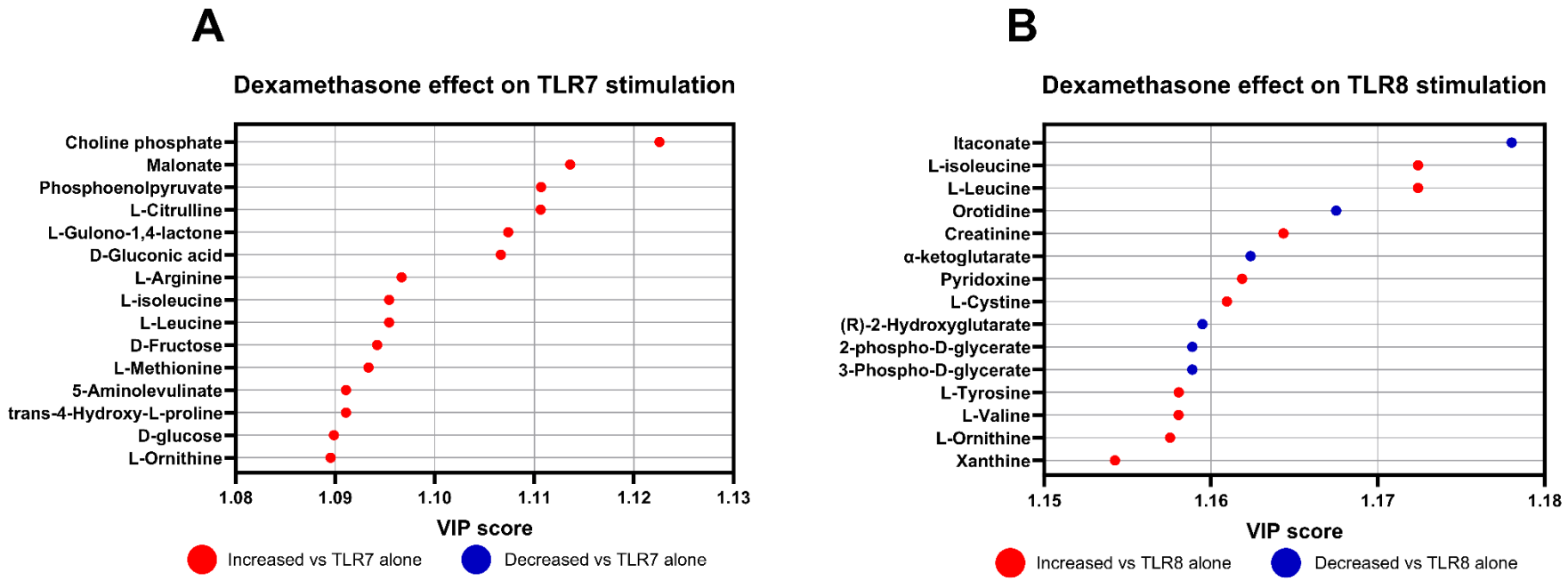

Figure 58: OPLS-DA VIP plots identifying metabolites altered by Dexamethasone treatment. *Plots display top 15 metabolites that are altered by dexamethasone treatment as determined by OPLS-DA. Red symbols indicate an increase compared with the ligand alone control, blue symbols indicate a decrease compared with the ligand alone control. (A) Effect of dexamethasone on TLR7 stimulated BMDM, (B) effect of dexamethasone on TLR8 stimulated BMDM*

5.4.4 NISV and TLR stimulation strongly upregulates phosphoenolpyruvate and can restore bioenergetic pathways to that of pre-stimulation levels

After overview of these groups, I chose to investigate Glycolysis and the TCA cycle, as these pathways are generally modulated during infection and activation of cells. Dissecting any effects on glycolysis may provide insight into the Warburg effect, and how NISV may contribute to this. To provide a more complete picture of each pathway, annotated compounds were manually scrutinised before inclusion with the identified compounds.

First, examining the effects of NISV and TLR7 stimulation on glycolysis **(Fig. 59)** reveals that unstimulated cells given NISV upregulate pyruvate compared with the media alone control, and to a greater degree than TLR7 stimulated cells. Furthermore, the addition of NISV to TLR7 stimulated cells also significantly increases pyruvate compared with TLR7 stimulation alone. TLR7 stimulation alone does not significantly increase pyruvate compared with unstimulated cells. NISV treatment alone also increases the level of 3-phospho-D-glycerate compared with TLR7 stimulated cells. However, both TLR7 stimulation and NISV treatment alone increase the level of glycerone phosphate, but this effect is not observed when TLR7 stimulated cells are treated with NISV. The combination of TLR7 stimulation and NISV also displayed a significant increase in phosphoenolpyruvate, with this metabolite absent from all other groups. Concerning aerobic glycolysis such as that of the Warburg effect, a decrease in lactate levels was found in TLR7 stimulated cells, which was reversed to control levels by the addition of NISV. These data indicate that NISV can reverse effects on TLR7 stimulated BMDM and by increasing pyruvate and lactate to pre-stimulation levels.

The trends observed for phosphoenolpyruvate and pyruvate in TLR7 stimulated cells were also found in TLR8 stimulated cells **(Fig. 60)**. In contrast, TLR8 stimulation greatly increased the levels of glycerone phosphate compared with all other groups. This effect was also observed with an increase in fructose 1,6-bisphosphate, and a similar trend was observed for lactate, with NISV having no reduction on lactate levels in TLR8 stimulated cells. Compared with the effect of NISV on lactate in TLR7 stimulated cells, the inability of NISV to reduce lactate levels to that of pre-stimulation levels indicates that there may be alternative metabolic requirements induced by ligation of each TLR

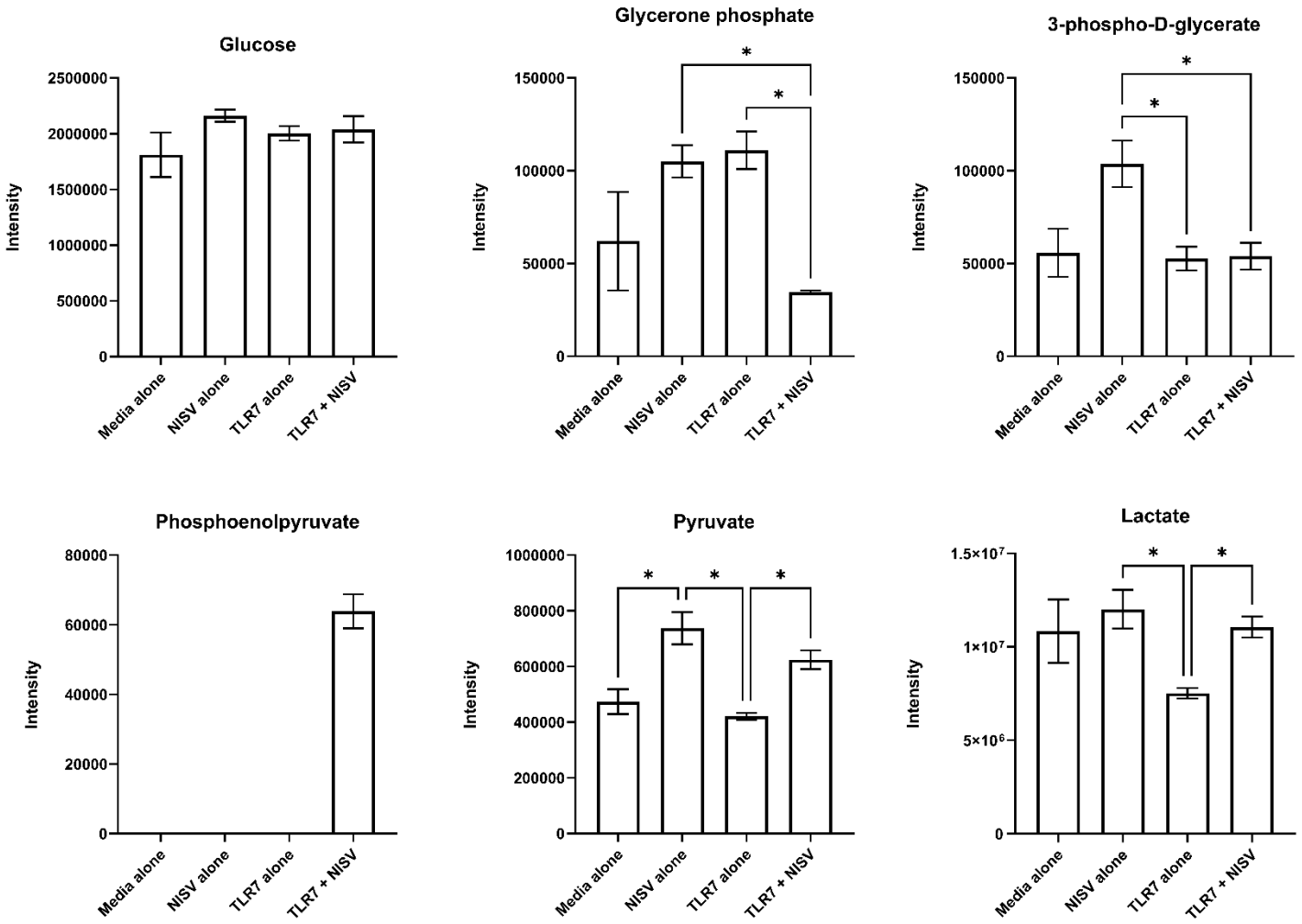

Figure 59: Detected metabolites of the glycolysis from BMDM pathway stimulated with the TLR7 agonist imiquimod and treated with NISV. *Metabolites from cells treated with either media alone, NISV alone, imiquimod (TLR7) alone, or NISV and imiquimod were extracted and the peak intensities measured using LC-MS. Significance between groups was determined using a pairwise t test with Welch's correction. * = $p<0.05$, $n=3$.*

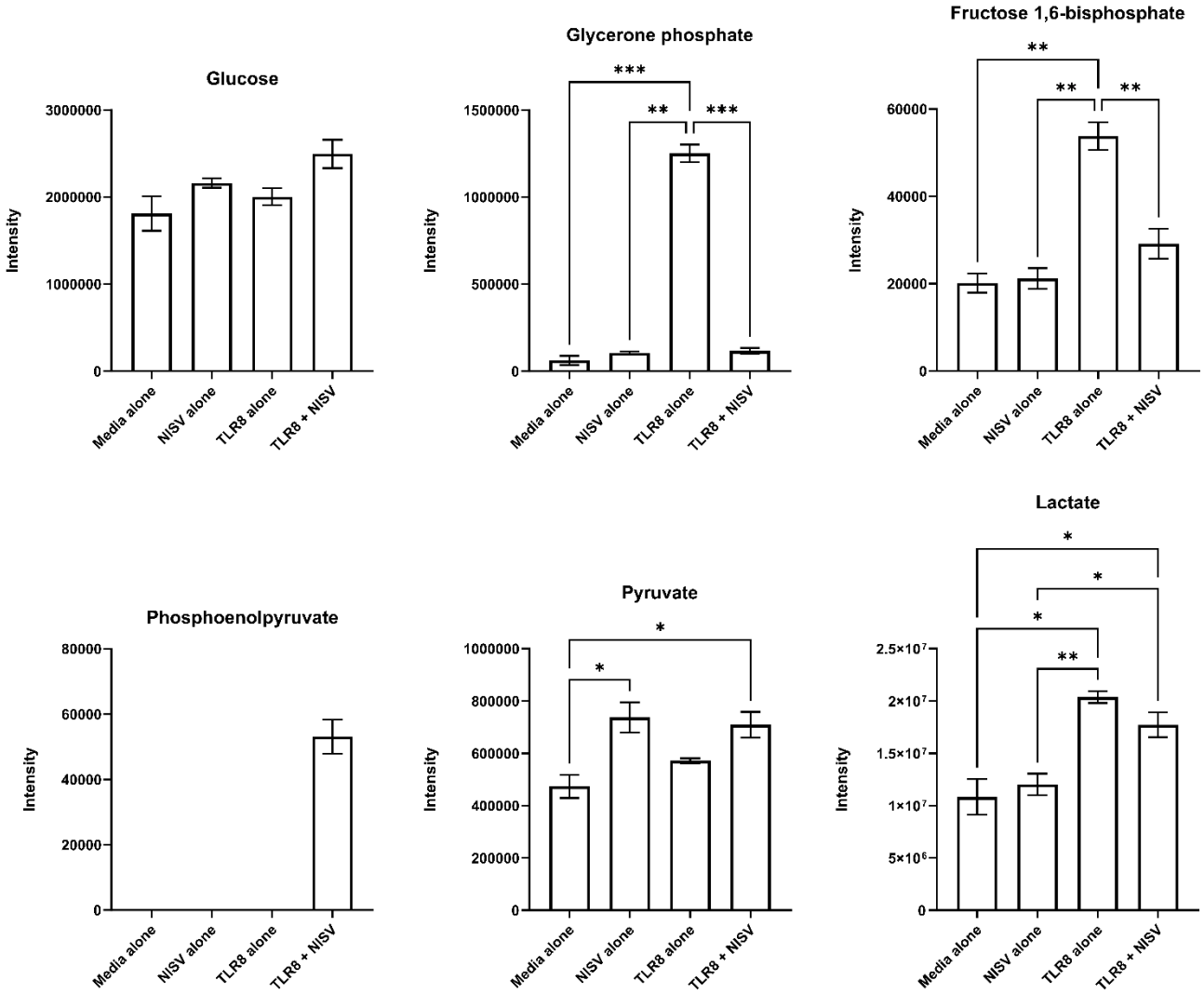

Figure 60: Detected metabolites of the glycolysis pathway from BMDM stimulated with TLR8 agonist TL8-506 and treated with NISV. *Metabolites from cells treated with either media alone, NISV alone, TL8-506 (TLR8) alone, or NISV and TL8-506 were extracted and the peak intensities measured using LC-MS. Significance between groups was determined using a pairwise t test with Welch's correction. * = p<0.05, **=p<0.01, *** =p<0.001, n=3.*

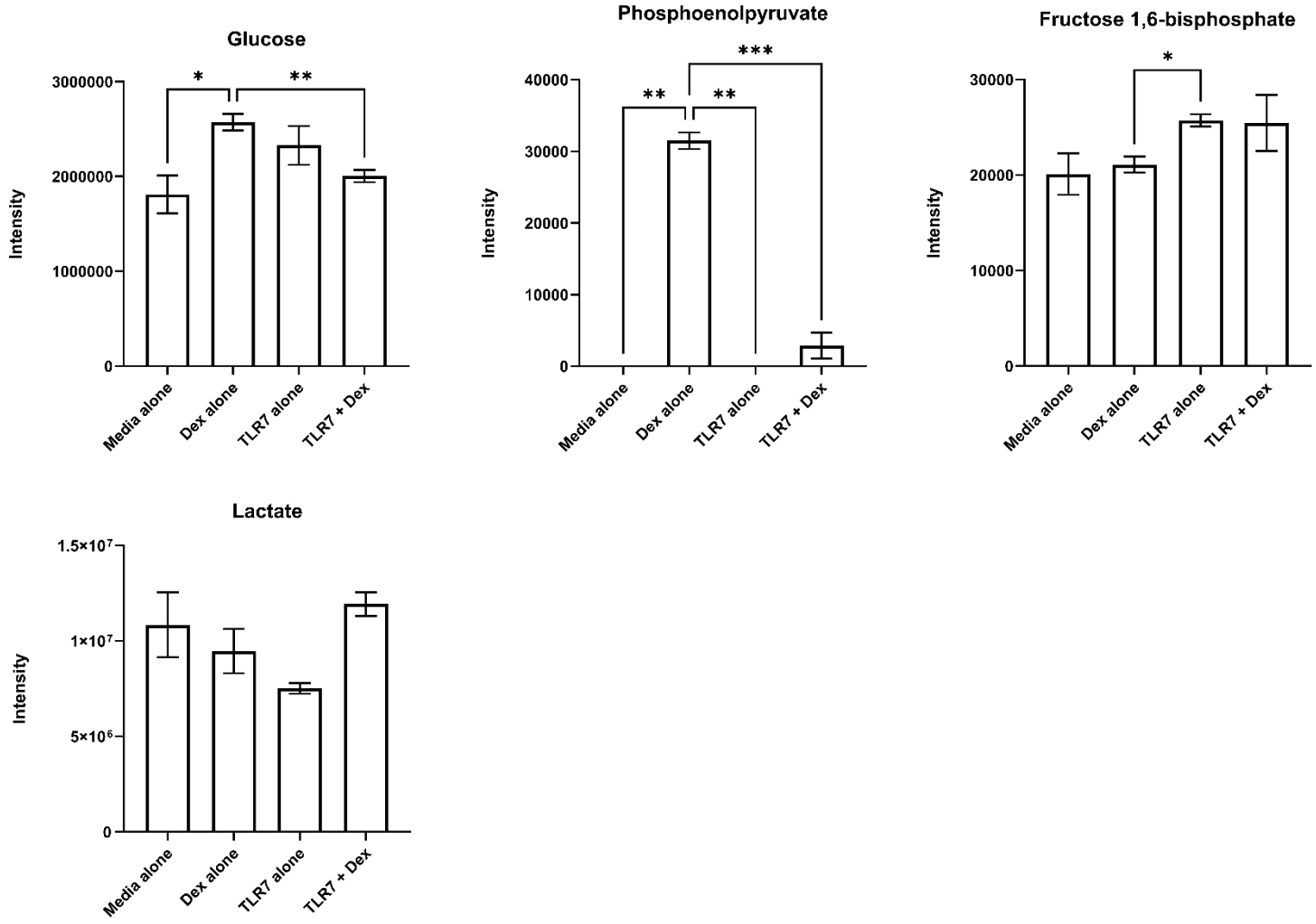

Figure 61: Detected metabolites of the glycolysis pathway from BMDM stimulated with the TLR7 agonist imiquimod and treated with dexamethasone. *Metabolites from cells treated with either media alone, dexamethasone alone, imiquimod (TLR7) alone, or dexamethasone and imiquimod were extracted and the peak intensities measured using LC-MS. Significance between groups was determined using a pairwise t test with Welch's correction. * = p<0.05, **=p<0.01, *** =p<0.001, n=3.*

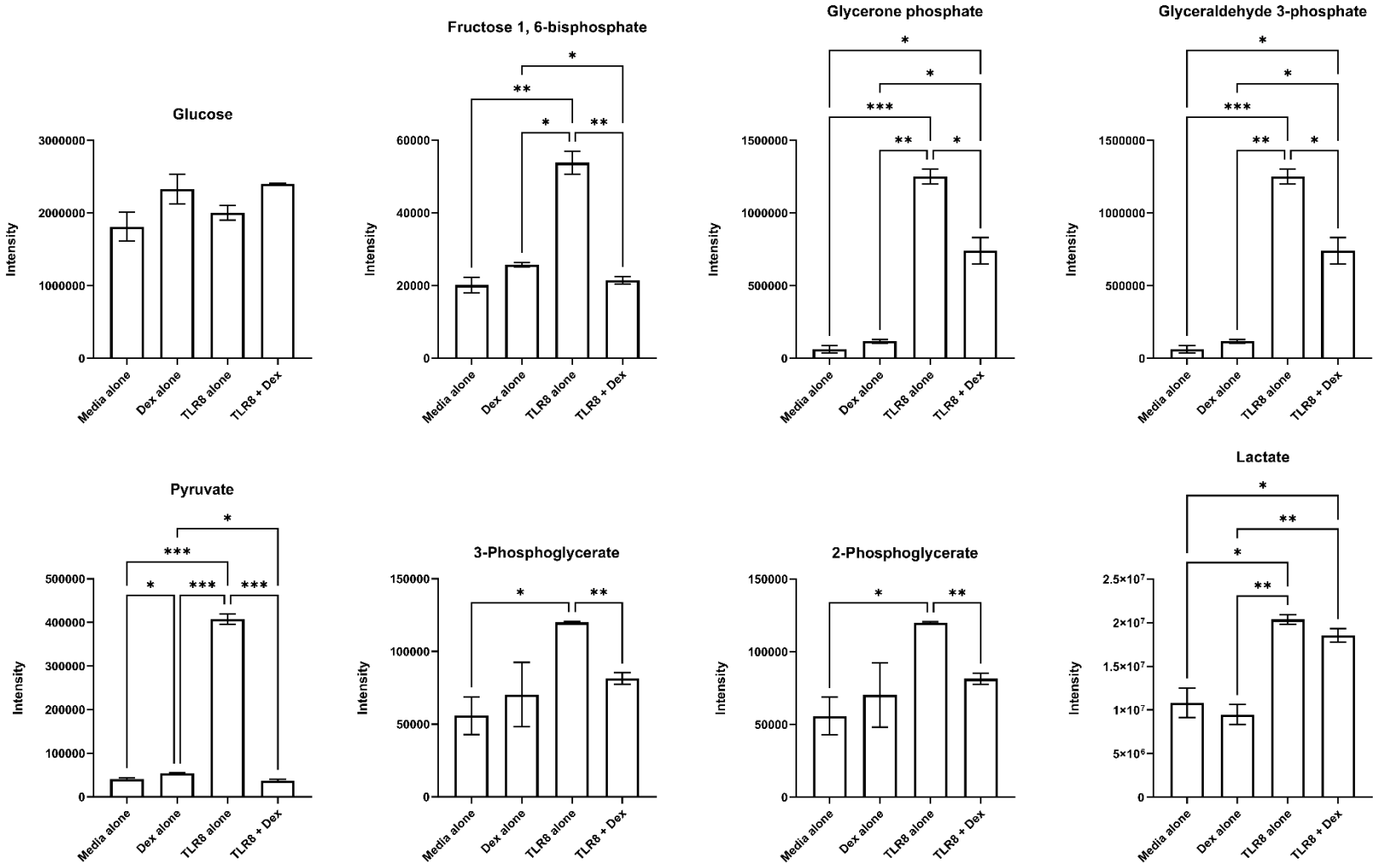

Figure 62: Detected metabolites of the glycolysis pathway from BMDM stimulated with the TLR8 agonist TL8-506 and treated with dexamethasone. *Metabolites from cells treated with either media alone, dexamethasone alone, Tl8-506 (TLR8) alone, or dexamethasone and TL8-506 were extracted and the peak intensities measured using LC-MS. Significance between groups was determined using a pairwise t test with Welch's correction. * = p<0.05, **=p<0.01, *** =p<0.001, n=3.*

The effect of dexamethasone on glycolysis in TLR7 stimulated BMDM **(Fig. 61)** included a significant increase in glucose levels compared with media alone cells, and TLR7 stimulated cells treated with dexamethasone. Furthermore, dexamethasone alone greatly increased phosphoenolpyruvate compared with all other groups. Cells stimulated with imiquimod displayed greater levels of fructose 1,6-bisphosphate, an effect also noted in TL8-506 stimulated cells. TLR8 stimulation also increased glycerone phosphate, glyceraldehyde 3-phosphate, pyruvate, 3-phoshpoglycerate, 2-phosphoglycerate, and lactate. Dexamethasone alone also increased the levels of pyruvate, but to a lesser degree when compared with media alone cells **(Fig. 62).**

After glycolysis, the pyruvate generated in this pathway is converted to acetyl CoA and this begins the TCA cycle. Under TLR7 stimulation, NISV can significantly reduce citrate levels compared to TLR7 alone group **(Fig.63)**, whilst increasing cis-aconitate. The combination of NISV and TLR7 stimulation displayed a slight increase in succinate levels when compared with TLR alone. TLR7 stimulation significantly reduced fumarate and malate levels which is unaffected by the addition of NISV.

A reduction in fumarate is also noted in TLR8 stimulated cells **(Fig.64)**. A modest increase in alpha-ketoglutarate was observed after TLR8 stimulation, which was abrogated when treated with NISV. Combined stimulation with TLR8 and NISV increased phosphoenolpyruvate and cis-aconitate. No significant changes in citrate, malate, succinate, or oxaloacetate were observed when cells were stimulated with TLR8, NISV, or both.

Treatment of cells with dexamethasone decreased both alpha-ketoglutarate and fumarate levels even when cells were stimulated with imiquimod **(Fig.65)**. Addition of dexamethasone to TLR7 stimulated cells increased succinate levels compared withTLR7 treatment alone.

In a similar manner to TLR7 and dexamethasone groups, fumarate was decreased when dexamethasone, TL8-506, or both were given to cells **(Fig.69**). As in treatment with NISV, alpha-ketoglutarate levels were reduced in TLR8 stimulated cells when treated with dexamethasone. Combination of dexamethasone and TLR8 stimulation increased succinate levels greater than that of each treatment alone. A similar increase in malate and citrate was found in TLR8 stimulated cells treated with dexamethasone compared with dexamethasone alone, and TLR8 alone, respectively. Another effect of combined treatment with the TLR8 ligand and dexamethasone is the reduction in oxaloacetate compared with that of the media alone control, following the trend of gradual decrease after dexamethasone alone treatment, and then TLR8 alone stimulation.

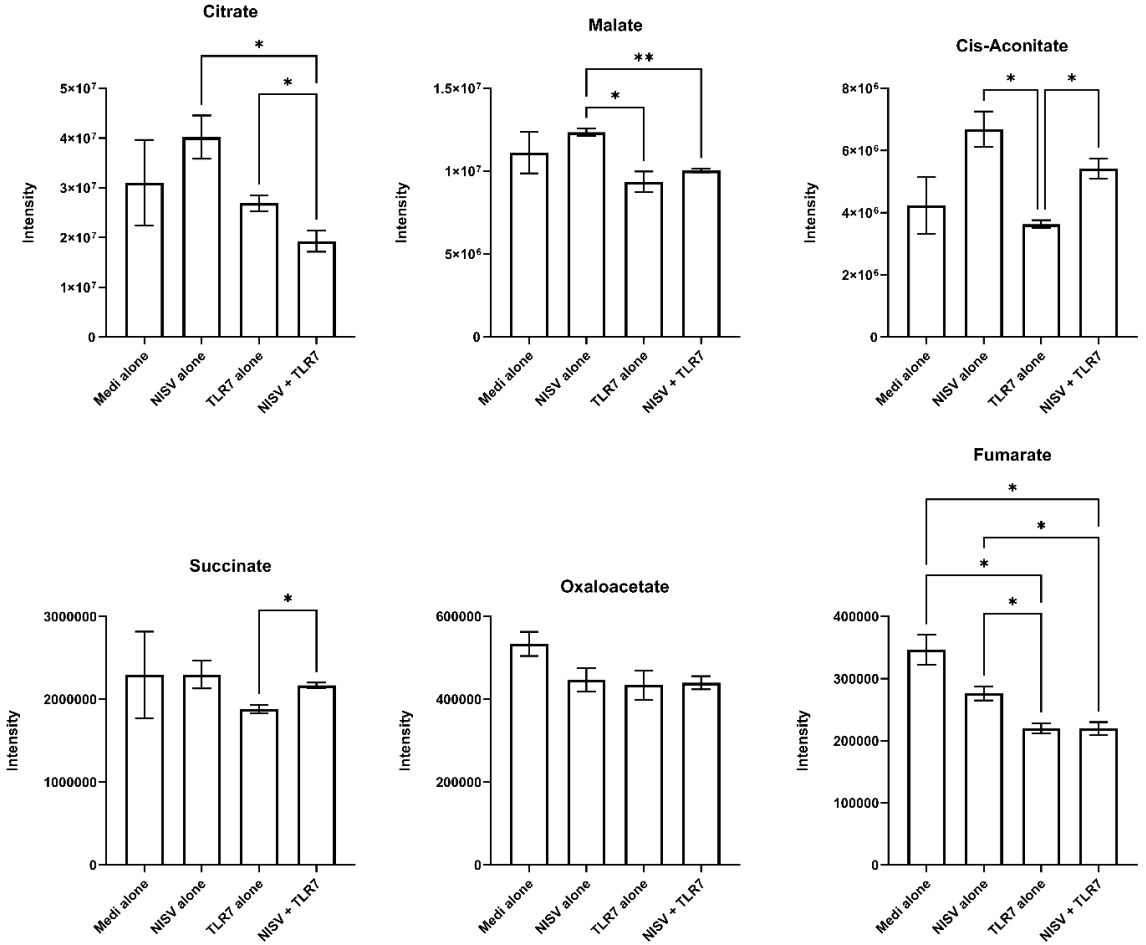

Figure 63: Detected metabolites of the TCA cycle from BMDM stimulated with the TLR7 agonist imiquimod and treated with NISV. *Metabolites from cells treated with either media alone, NISV alone, imiquimod (TLR7) alone, or NISV and imiquimod were extracted and peak intensities measured using LC-MS. Significance between groups was determined using a pairwise t test with Welch's Correction. * = p<0.05, **=p<0.01, n=3.*

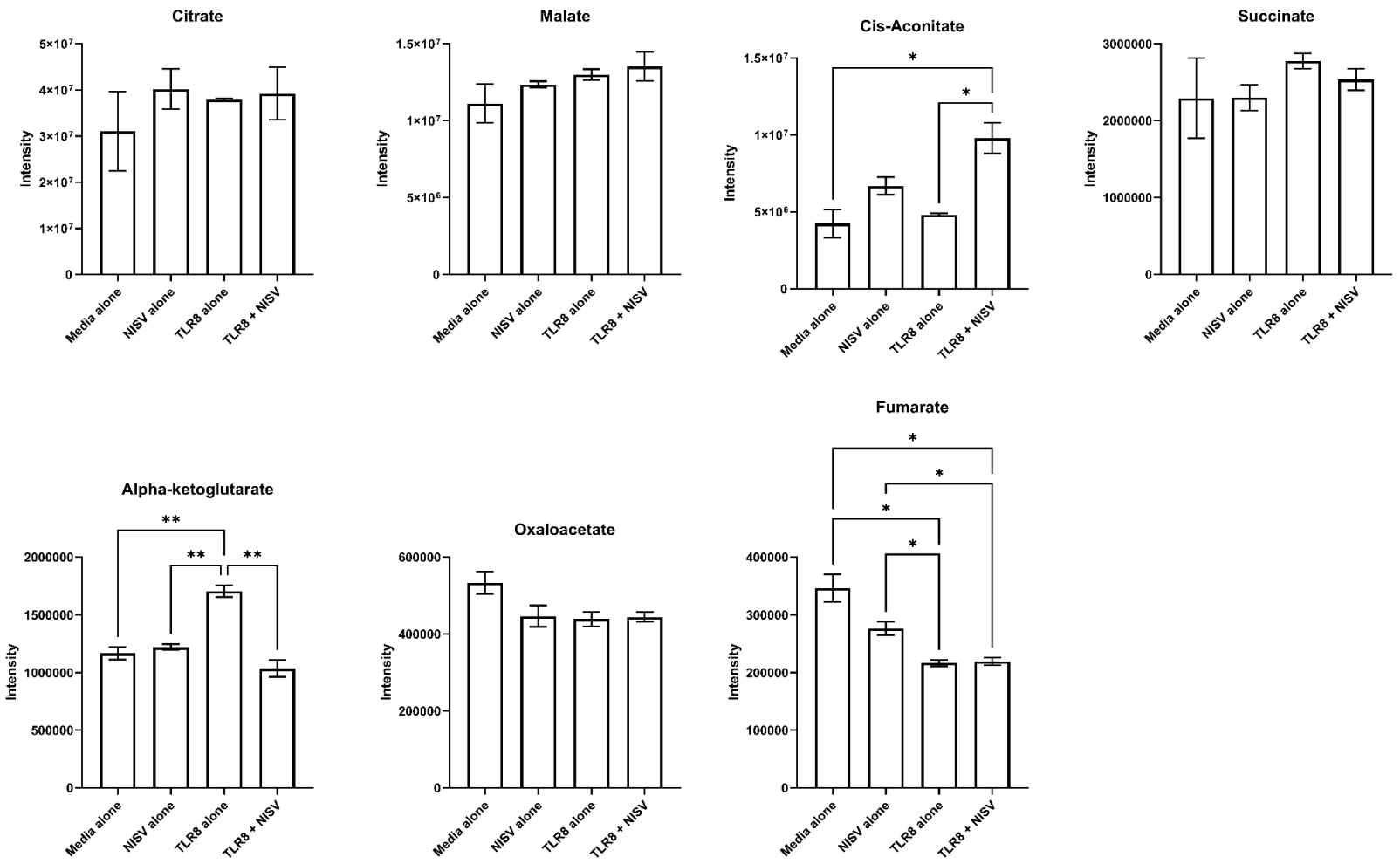

Figure 64: Detected metabolites of the TCA cycle from BMDM stimulated with the TLR8 agonist TL8-506 and treated with NISV. *Metabolites from cells treated with either media alone, NISV alone, TL8-506 (TLR8) alone, or NISV and TL8-506 were extracted and peak intensities measured using LC-MS. Significance between groups was determined using a pairwise t test with Welch's Correction. * = p<0.05, **=p<0.01, n=3.*

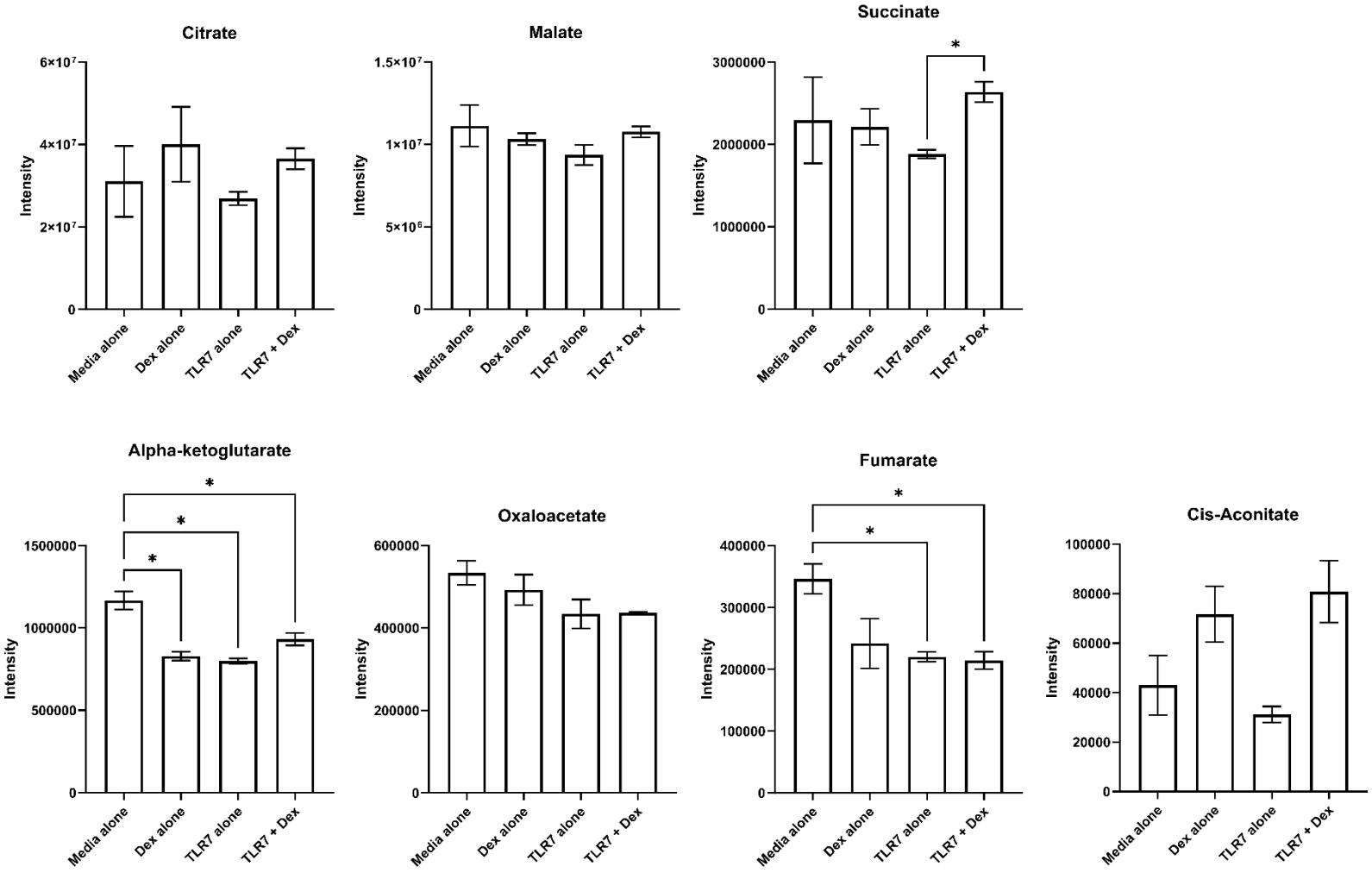

Figure 65: Detected metabolites of the TCA cycle from BMDM stimulated with the TLR7 agonist imiquimod and treated with dexamethasone. *Metabolites from cells treated with either media alone, dexamethasone alone, imiquimod (TLR7) alone, or dexamethasone and imiquimod were extracted and peak intensities measured using LC-MS. Significance between groups was determined using a pairwise t test with Welch's Correction. * = p<0.05, n=3.*

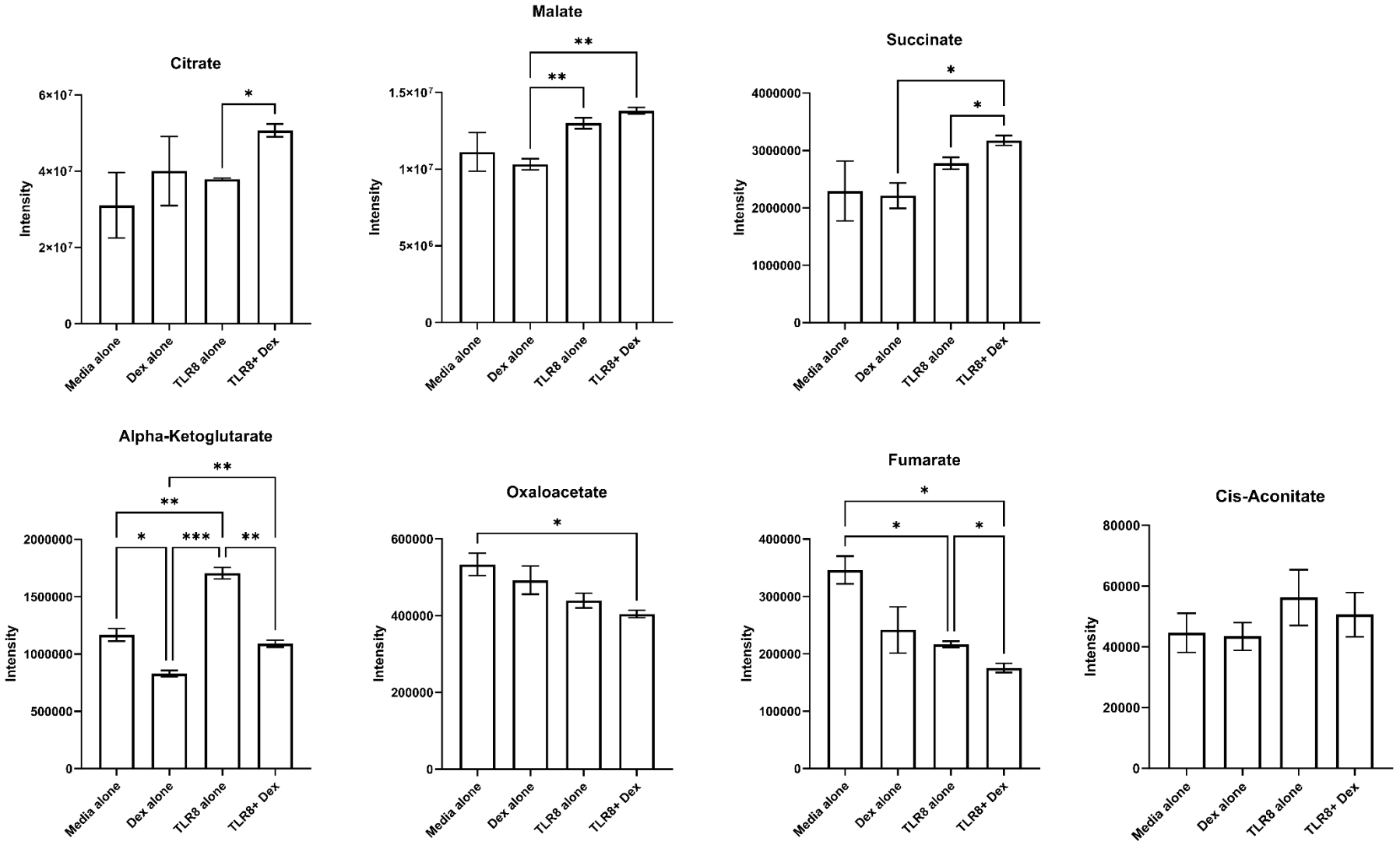

Figure 66: Detected metabolites of the TCA cycle from BMDM stimulated with the TLR8 agonist TI8-506 and treated with dexamethasone. *Metabolites from cells treated with either media alone, dexamethasone alone, TI8-506 (TLR8) alone, or dexamethasone and TI8-506 were extracted and peak intensities measured using LC-MS. Significance between groups was determined using a pairwise t test with Welch's Correction. * = p<0.05, n=3.*

5.5 Discussion

5.5.1 Limitations of untargeted metabolomics

Untargeted metabolomics can provide a broad overview of the compounds detected in a given sample but the term untargeted is somewhat of a misnomer. Whilst less focused than alternative methods that aim to detect specific compounds, selection of the column used in LC-MS, the library of authentic standards used, and the timepoints of extraction reduce the number of potentially detectable metabolites considerably, somewhat targetting the analysis. However, due to the large amount of data generated and therefore the likelihood of false positives/negatives, the results may lack sensitivity compared with a more traditionally targeted approach. Particularly with the data presented in this thesis, we display figures detailing the proportion of authentically identified metabolites which was a fraction of the total metabolites detected. Whilst the identified metabolites numbered between 70-120 providing a fairly large overview of metabolism, it would be desirable to further expand this coverage by providing a greater array of standards with which to match our chromatographic peaks.

Furthermore, as untargeted metabolomics relies upon statistical analysis in a case vs control setup, the number of samples should be increased to increase the power of the experiment. For example, an issue encountered during this experiment was the poor grouping of media alone cells. Whilst other groups were tightly clustered with only 3 replicates, unstimulated cells likely require more replicates to provide a more accurate mean. By adding a compound such as a TLR ligand or treatment, cells are essentially polarised into a unified response, reducing the variation. The lack of stimulation, paired with the likelihood of our unstimulated BMDM population being at various stages of the cell cycle increased the variation of our media alone cells. Whilst these limitations of the experiment are evident, untargeted metabolomics remains a powerful tool for biomarker discovery and generation of a hypothesis that can be explored further, using a more targeted approach with a greater number of replicates.

5.5.2 NISV effect on macrophage metabolism

Analysis indicates that whilst NISV and dexamethasone alone do cause perturbations in cellular metabolism, this effect is fairly minor when compared with more potent stimuli such as TLR ligation. When interpreting volcano plots, it was noted that both NISV and dexamethasone have a bias towards significant upregulation of the few metabolites they effect. In other groups, this bias is lessened, and a fairly equal balance of upregulation and downregulation of metabolites is observed. Furthermore, it was observed that TLR8 appears

to have a greater effect on metabolism than TLR7. Research conducted using TLR7 and TLR8 specific agonists similar to the compounds used in this thesis have identified differences in activation of various cells in humans. For example, it was demonstrated that TLR8 potently activates myeloid DCs, monocytes, and monocyte derived DCs, whereas TLR7 displayed a narrower spectrum of activation with only plasmacytoid DCs and to a lesser degree, monocytes activated *(Gorden, et al., 2005).* Therefore, if the BMDM culture also contains some DCs as suspected, then these findings would agree with the current literature.

To process the data, I opted to augment the standard high-dimensionality data reduction approach with PCA through the addition of OPLS-DA. Traditionally, PCA is an unsupervised approach and can be used to identify sample grouping by reducing a vast number of variables to two or more principal components that explain the majority of variance between each sample. As this approach does not consider sample groups, PCA allows visualisation of sample grouping as a form of QC, recognition of patterns within the data, and can display areas where replicates may deviate from their companions. On the other hand, OPLS-DA is a supervised method of multivariate analysis which considers the group labels provided to identify the key differences between the two groups. Therefore, OPLS-DA can falsely create divisions in the samples by forcing them into groups and thus should only be performed when clear divisions in samples are found using unsupervised PCA analysis *(Worley and Powers, 2016).* In this analysis, after overall PCA analysis to visualise sample grouping, individual comparisons were examined using PCA prior to OPLS-DA and found that due to the large spread of the media alone samples, it was not advisable to progress to OPLS-DA for the media vs NISV, dexamethasone, TLR7, or TLR8 groups. However, good group separation was observed in the experimental setups designed to compare the effect of NISV or dexamethasone on TLR7 or TLR8 stimulated BMDM and thus OPLS-DA was utilised.

From this data we noted some common areas most affected by NISV in both TLR7 and TLR8 stimulated BMDM. Once such area was phospholipid synthesis. A simplistic view may highlight increased phagocytosis and subsequent formation of endosomes as a key factor driving requirements for phospholipid production, and thus a decrease in fatty acid and phospholipid synthesis intermediates as they are consumed during phosphatidylcholine and phosphatidylethanolamine production

Increased phagocytosis of large particles (>500nm) is typically associated with increased energy demands and thus perturbations in the glycolysis and TCA cycle pathways would be expected to coincide with this increased phospholipid synthesis. From a focused view of glycolysis, it was noted that the major changes imparted by NISV on TLR7 stimulated

BMDM tend to return compounds upregulated by stimulation to levels comparable to unstimulated cells. A similar effect is also noted in TLR8 stimulated cells. Furthermore, whilst there are changes present in the TCA cycle it is difficult to determine whether these changes indicate an increased demand for energy generation. Thus, whether NISV affect phospholipid synthesis purely due to an increase in phagocytosis and particle uptake requires further investigation.

A consistent change affected by NISV in both TLR pathways investigated is a significant increase in cis-aconitate, alongside our OPLS-DA VIP identifying itaconate amongst the top most important metabolites driving variance. Cis-aconitate is a precursor to itaconate and is converted between the two by the enzyme cis-aconitate decarboxylase. Itaconate exerts anti-inflammatory actions primarily through interaction with the proteins KEAP1 and Nrf2 (refs). As a complex, KEAP1/Nrf2 is maintained in homeostatic conditions, with KEAP1 ubiquitinating Nrf2, marking it for degradation by the proteosome. Upon disruption of KEAP1 by ROS (or indeed itaconate), Nrf2 can accumulate and bind to the antioxidant response elements on DNA. Itaconate can also exert anti-inflammatory actions through inhibition of STING, decreasing transcription of interferon-related genes *(Mills, et al., 2018).* Interestingly, we noted that itaconate is upregulated when treating TLR7 stimulated BMDM with NISV but downregulated in the TLR8 stimulation scenario, which is further complicated by cis-aconitate being upregulated in both TLR stimulated groups. Whilst previous studies have demonstrated that TLR7 (much like TLR4) stimulation can induce itaconate accumulation, there is a gap in our understanding of this mechanism in TLR8 stimulated cells *(Olagnier, et al., 2018).* However, the data indicates that NISV appear to contribute to the TLR7 induced itaconate accumulation, which is in agreement with previous data from our laboratory using TLR4 stimulation *(Mcgahon, 2021).* A significant increase in succinate caused by NISV was demonstrated when treating TLR7 stimulated BMDM, another feature associated with the anti-inflammatory itaconate pathway, as itaconate inhibits succinate dehydrogenase through competitive binding to the enzyme's active site and thus succinate accumulates *(Lampropoulou, et al., 2016).* Further elucidation of the metabolic differences between TLR7 and TLR8 activation of BMDM is required using a more focused approach.

Also, of interest was the Warburg effect, as this is a common feature seen during viral infections and has also been well-studied in the field of oncology. Typical hallmarks of the Warburg effect include increased reliance on glycolysis (even under normoxic conditions), increased lactate production, and increased fatty acid synthesis. It should be noted that whilst binding of a ligand to TLR can elicit a response like that of the Warburg effect, this process does not fully emulate viral reprogramming of cellular metabolism. Furthermore, even amongst the ssRNA viruses, there will be diversity in their replication cycles and

therefore different metabolic requirement, causing variation in the Warburg effect. Nonetheless, it was the aim to examine the effect of NISV on this oxidative glycolysis in the context of both TLR7 and TLR8 stimulation. When comparing the effects of TLR7 alone, to that of NISV + TLR7, a slight decrease in lactate levels was observed with TLR7 stimulation alone. With the addition of NISV a slight increase in lactate levels was observed. However, in the case of TLR8 stimulation the opposite effect was observed, with a greater increase in lactate, which was decreased with NISV treatment. This pattern is also observed when treating stimulated cells with dexamethasone, indicating that TLR specific mechanisms may be influencing lactate levels more than the treatments. To contextualise the Warburg effect further, it is difficult to say that there is increased glucose uptake as the levels are unaltered across all groups. Similarly, it is difficult to draw conclusions on the state of fatty acid synthesis as the internal standards used to identify our metabolites were focused on energy metabolism, and thus many fatty acid compounds are annotated rather than matched to authentic standards. Tentatively, a decrease in (annotated) fatty acids upon either TLR7 or TLR8 stimulation was observed. Fatty acid levels were increased upon treatment of the cells with NISV, or dexamethasone. Further work including the use of a model virus such as the alphavirus Semliki Forest virus paired with a more robust, targeted, interrogation of lipids, proline, lactate, and glutamine could shed further light on NISV's contribution to Warbug-like metabolic effects.

6 Chapter 6

Transcriptomic analysis of NISV effect on TLR7 or TLR8 BMDM in comparison to dexamethasone

6.1 Abstract

Response to a given stimuli induces a change within cells that may manifest, for example, as a change in phenotype, function, or release of soluble mediators to initiate a wider reaction from the immune system. Whilst investigation of these changes can be achieved by measuring proteins, or morphological changes, the common denominator of gene expression is present as a central deterministic factor that controls these features. Modern high throughput RNA sequencing provides the ability to survey transcription of genes in response to experimental conditions ever more quickly and cheaply as technology progresses. Utilising this technique to perform transcriptomic analysis, the aim is to investigate gene transcription in response to TLR7 or TLR8 stimulation, alongside the effect of NISV or dexamethasone treatment alone or used in conjunction with TLR ligation. To this end, the intention is to illuminate the mechanism(s) of NISV activity and evaluate their potential as an adjunct treatment for ssRNA virus induced sepsis, such as that observed in severe COVID-19. Bone marrow derived macrophages were stimulated with the TLR7-specific agonist imiquimod, and TLR8-specific agonist TL8-506 and then the cells were treated with either NISV or dexamethasone at IC90 concentrations. 6hrs after treatment RNA was extracted and sequenced in 1x100bp single- end fragments to a depth of >10M reads using QuantSeq, a method of cDNA library preparation that combines polyA selection and sequencing whilst including unique molecular identifiers (UMIs) to remove PCR duplicates. Gene use normalised transcript counts were quantified to differentially compare gene expression as a whole, alongside focusing on endosomal TLR signalling, activation of NF-kB and induction of the NLRP3 inflammasome. The data indicates that NISV and dexamethasone alone can induce transcriptional changes in unstimulated macropahges but to a lesser extent than TLR stimulated macrophages. Upon treatment with NISV greater downregulation of IL cytokines and CXCL chemokines in both TLR7 and TLR8 stimulated BMDM were observed when compared with dexamethasone treatment. Furthermore, a greater effect of NISV on endosomal TLR pathways than dexamethasone was observed and it was further identified that whilst both compounds can downregulate NF-kB signalling, NISV also regulates activation of the NLRP3 inflammasome required for IL-1 cytokine cleavage and release.

6.2 Introduction

6.2.1 Transcriptomic analysis

The field of genomics has steadily advanced since the development of sanger sequencing in 1977 using chain termination methods *(Sanger, and Coulson, 1977).* Discoveries in this field have enabled milestone scientific achievements such as sequencing of the whole human genome *(Lander, et al, 2001)*, as well as providing whole reference genomes for research-relevant species such as *mus musculus (Waterston, et al.,2002),* and *drosphilia melanogaster (Adams, et al., 2000).* In this chapter, the advances made in sequencing, molecular biology, and genome annotation are utilised to investigate the effect of NISV and dexamethasone on BMDM using the TLR7 and TLR8 ligands imiquimod and TL8-506.

Whilst previous chapters have explored the production of cytokines as an indicator of cellular activity, examining gene expression can provide an overview of proteins actively being produced by a cell. The well-established central dogma of molecular biology proposed by Francis Crick in 1958 states that the general schema of gene expression relies upon DNA being transcribed into RNA, which can then be translated into amino acids, producing proteins in a non-reversible manner *(Crick, 1958)*. Currently, transcriptomic analysis allows researchers to delve into this realm of DNA and RNA to provide a snapshot of active RNA transcription at the timepoint examined. As the bridge between DNA and proteins, RNA such as mRNA is fleeting and degraded after use, being recycled to provide nucleotides for transcription of new mRNA *(Shyu, et al., 2008).* Thus, experiments designed to examine gene expression using transcripts must choose an RNA extraction timepoint upstream of protein production that coincides with transcriptional events of interest. Furthermore, some genes may be expressed shortly after stimuli whilst others are expressed later, further complicating selection of an appropriate timepoint to intercept transcripts of interest. Some studies have endeavoured to develop a method for the determination of when to extract RNA by frequently examining a small set of genes being expressed over time to provide an indicator of optimised RNA extraction timepoint *(Kleyman, et al., 2017).*

As it stands, the use of modern high-throughput sequencing-by-synthesis has enabled researchers to survey both the genome and transcriptome of organisms with high resolution quickly and relatively cheaply. Due to the ever-decreasing cost of RNA sequencing, some of the challenges such as deciding when to extract RNA can be overcome by including multiple extractions over a range of times post-stimulation and increased replicate number into the sample pool. Next-generation sequencing platforms like Illumina can facilitate larger

experiments using massively parallel sequencing and, depending on the research goals, transcripts can be sequenced to a depth of >10 million reads per sample. Furthermore, by barcoding RNA with a sample-specific identifier allows samples to be multiplexed and run on a single flow cell, reducing costs once more. De-multiplexing can then be performed prior to analysis to identify reads according to their sample of origin using this barcoding method *(Fadrosh, et al., 2014).* A brief explanation of the illumina sequencing-by-synthesis process if available in **figure 67**

Notably, for researchers interested in quantifying transcripts rather than exploring alternative splicing, polymorphisms, fusion genes, or polyadenylation sites, etc. the pipeline used to gather this information can be further streamlined using 3’ Digital Gene Expression (3’ DGE) sequencing.

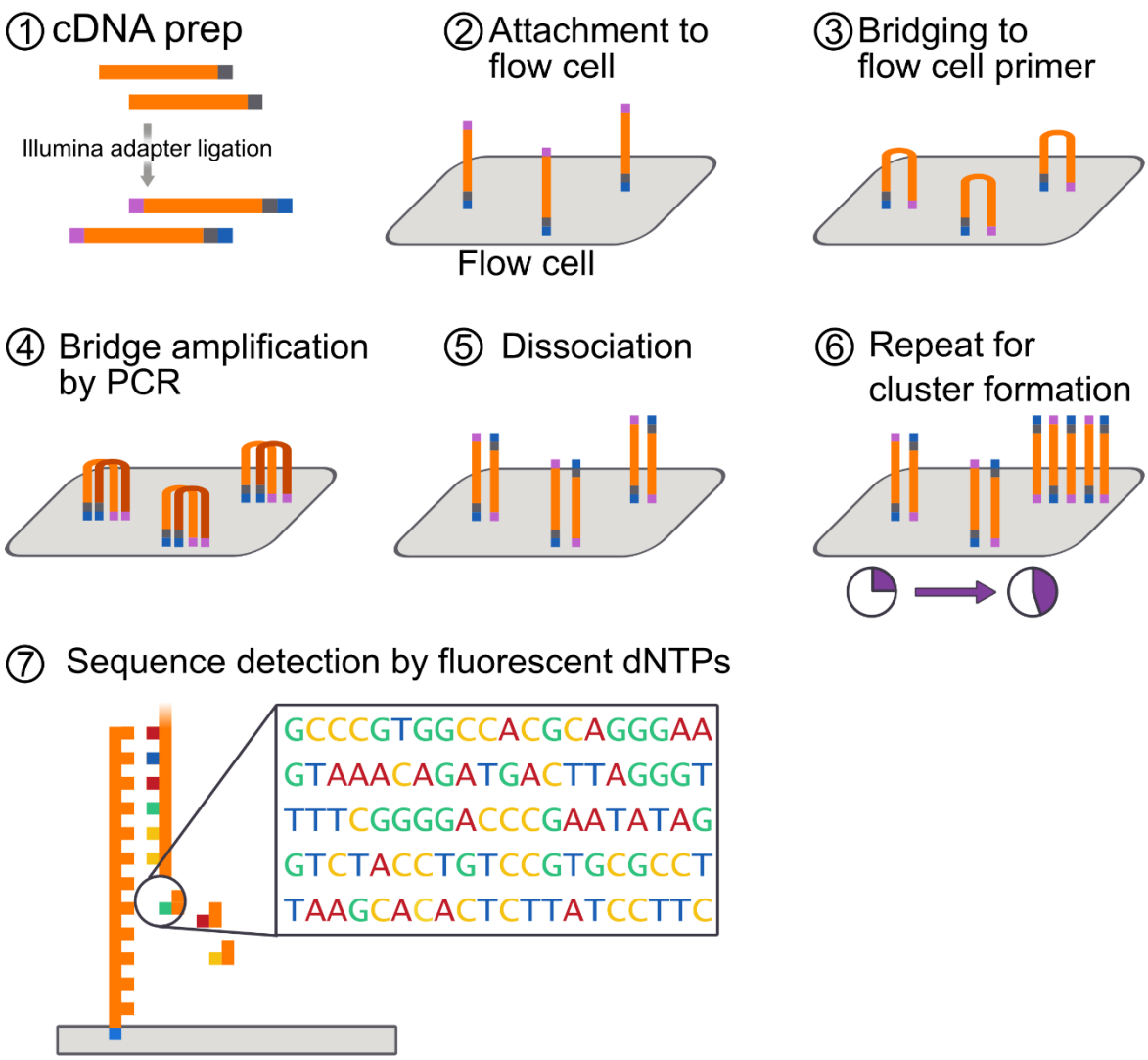

Figure 67: Principle of Illumina sequencing-by-synthesis. *After generation of cDNA libraries from transcripts, illumina adapter sequences are ligated to cDNA fragments at both ends. The adapter sequence on one end of the cDNA fragment binds to the complimentary oligo on the surface of the flow cell, which is then hybridized, and the original cDNA fragment dissociated. The new cDNA fragment will then form a bridge-like structure as both adapters bind to their complimentary oligos on the flow cell that includes a primer. This bridge is then amplified by PCR before on end dissociates and the process repeats anew, generating clusters of clonal sequences. During PCR, fluorescently tagged dNTPs are used, allowing the specific base sequence to be determined using a laser, sequencing the fragments. This sequence, known as a read, can then be mapped to a genome.*

6.2.2 3’ Digital Gene Expression

3’ DGE sequencing combines polyA selection and unique molecular identifiers (UMI) to provide accurate quantitative transcript counts that can be easily compared between samples **(Fig. 68).** In comparison to traditional mRNAseq techniques, 3’DGE builds upon principles common to both practices but omits steps that have become unnecessary to this technique, streamlining the process. After isolation of total RNA from a tissue sample and quality control checks, polyA selection occurs which utilises oligodeoxythymine (oligo(dT)) primers to bind to the 3’ polyadenylated tail of mature mRNA, which is then reverse transcribed to produce complimentary DNA (cDNA) libraries. This is distinct from polyA enrichment which may be performed on eukaryotic RNA samples in traditional mRNASeq. Steps such as polyA enrichment and ribosomal RNA depletion are not needed as the primers used for 3’ DGE only bind to polyA tails, thus replacing the need for enrichment of polyA mRNA, or depletion of rRNA as this will not be reverse transcribed due to lack of polyA tail and thus no primer binding.

The cDNA libraries generated from the original polyA mRNA can be thought of as the 1st strand synthesis product, which is then transcribed using random primers linked to a unique molecular identifier (UMI). This allows the 2nd strand to then be sequenced by synthesis using fluorescently tagged deoxynucleotide triphosphate (dNTPS). These reads can then be mapped onto a genome to provide identification and the UMI counted for direct quantification of transcript levels. 3’ DGE also benefits from reduced analysis time as there is no need to normalise data by transcript length as there is only one UMI read per transcript rather than multiple fragments per transcript that may introduce bias with long transcripts. This direct counting of UMI rather than fragments alongside shorter read length means that a lower depth of sequencing is required, as there is no requirement to sequence many fragments for whole transcript construction. Typical 3’DGE experiments only require 3-10 million reads, compared with around 30 million reads for whole transcript mRNASeq.

Studies comparing 3’ DGE and traditional mRNASeq have indicated that results are comparable when researchers are concerned with transcript quantification rather than qualitative exploration of transcriptome features. Studies comparing the library preparation method used in this thesis (Lexogen Quant-seq) to traditional mRNASeq concluded that there was no discernible advantage of one kit over the other for the application of gene expression profiling *(Ma, et al., 2019)*. Others have indicated that there is reported around a 15% loss of sensitivity in 3’ DGE compared to whole transcript mRNA but maintains good reproducibility and strong overlap in the detectable genes *(Xiong, et al., 2017).* Whilst these

observations are valid and could impact experimental outcomes, the reduced costs and processing time make this technology attractive for differential gene expression experiments which can then be followed up by more focused whole transcript mRNASeq to reinforce results.

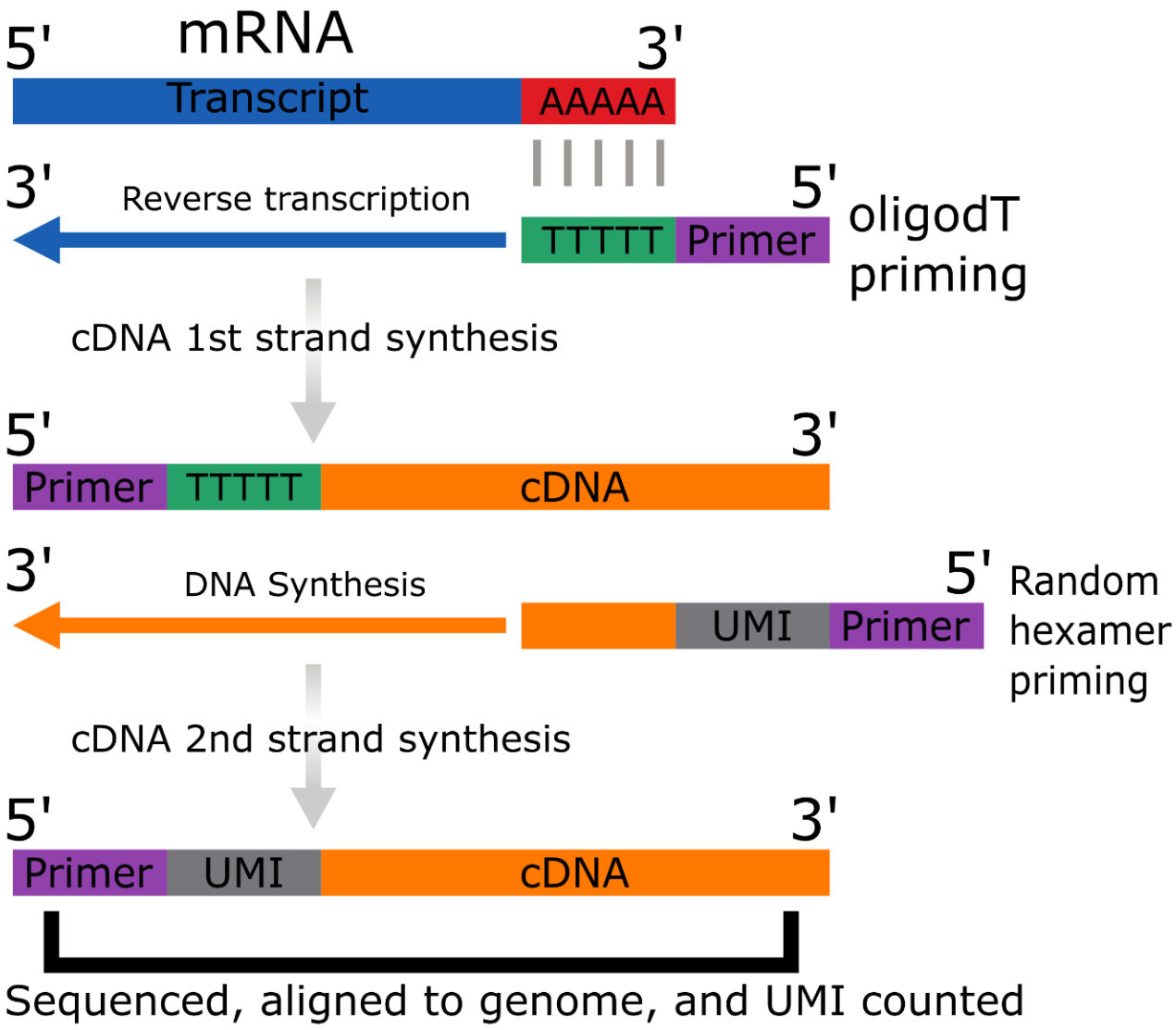

Figure 68: Simplified mechanism of library preparation and incorporation of UMI in 3' DGE sequencing. *OligodT primers bind to polyadenylated tails of mature mRNA transcripts and reverse transcriptase transcribes RNA into complimentary DNA (cDNA), generating the 1st strand cDNA. Random hexamer primers with linked UMI bind to 1st strand and begin synthesis of 2nd strand cDNA. This is then sequenced by synthesis using fluorescently tagged dNTPs and resulting sequence mapped to the genome for identification. UMI can then be counted to provide direct 1:1 quantification of transcript counts.*

6.2.3 TLR signalling and gene expression

A goal when undertaking this experiment was to de-tangle the intracellular signalling that occurs upon TLR ligation and elucidate any TLR specific action of NISV. As discussed in earlier chapters, key differences in adapter protein engaged upon TLR dimerization may influence the downstream transcriptional events. Thus, by surveying the gene expression, and the transcription factors responsible for our findings, we aim to provide insight into the mechanism by which NISV exert their immunomodulatory effect. Whilst this study focuses on TLR7 and TLR8 to contextualise the findings for a ssRNA viral infection response, previous work has examined the effect of NISV on TLR4 using a similar cell stimulation and subsequent transcriptomics method.

Some key findings from this work included NISV alone causing upregulation of chemokines, cell surface receptors, interleukin cytokines, and TNF superfamily cytokines. Alongside this there was positive regulation of the transcription factors NF-kB, the MyD88 adaptor protein, and NLRP3 inflammasome. However, when treating LPS stimulated BMDM, NISV were able to decrease the levels of chemokines of the CC, CXC, CX3C, and XC subfamilies when compared with the TLR4 stimulated control cells. A decrease in the level of inflammation associated genes encoding the cytokines IL-1α, IL-1β, IL-6, IL-10, and IL-12, as well as the TNF family of cytokines. To further contrast the effect of NISV alone, NISV elicited significant downregulation of NF-kB subunits, providing a potential mechanistic explanation of the immunomodulatory effects observed at both the transcription and protein level.

This chapter focuses on TLR7 and TLR8 as sources of cellular stimulation, which utilises the MyD88 adaptor protein exclusively, whereas TLR4 can signal through both MyD88 and TRIF. By investigating this TLR pathway, cytokine and chemokine production, alongside various transcriptions factors, we aim to further elucidate the mechanism of NISV immunomodulatory action. A particular area of interest to us is the differences between endosomal and surface TLR receptors, and the subsequent effects NISV may have on internal TLR. Furthermore, we focus on NF-kB and activation of the NLRP3 inflammasome to investigate effects on pro-inflammatory gene expression and release of leaderless cytokines (those that lack a signal peptide, such as IL-1α/β).

6.3 Aims and Hypothesis

This chapter aims to:

i. Utilise 3'DGE sequencing to evaluate the effect of NISV or dexamethasone on gene expression and examine the immunomodulatory abilities of each treatment using TLR7 or TLR8 stimulated BMDM. The overall holistic changes in gene expression will be investigated through quantification of transcripts and evaluation of the most significantly changed genes as a result of both treatment or stimulation alone, and in combination. To reinforce our earlier understanding of the effects of NISV and dexamethasone on cytokine production from stimulated cells, transcriptional changes in cytokine/chemokine gene expression were investigated.

ii. Compare the intracellular signalling cascade downstream of TLR7 or TLR8 activation and determine potential differences in gene expression induced by ligation of these receptors. Examining the differences in TLR7 and TLR8 induced gene expression may provide insight into the development of treatments that preferentially stimulate one receptor over the other and enhance the immune response to ssRNA viruses.

iii. Further contextualise the previously proposed action of NISV on NF-kB signalling as a demonstrated in the context of TLR4 stimulation and expand this investigation to include TLR7 and TLR8 stimulation. The aim is to relate any findings to the release of the leaderless IL-1 cytokines and activation of the NLRP3 inflammasome and caspase 1.

6.4 Results

6.4.1 RNA sequencing QC and overview

Prior to sequencing, and throughout the processing of samples, quality control (QC) measures were undertaken to ensure robust analysis. Chiefly, the integrity of RNA was evaluated after extraction using an Agilent Bioanalyzer. All samples displayed RIN >7 with many samples achieving high RIN of 9 or 10. QC steps were performed during sample processing by the sequencing facility, as well as during data analysis. These steps evaluated the raw reads before and after trimming, the alignment, and subsequent feature assignment. All QC results were satisfactory and differential gene expression analysis could proceed.

Before differential gene expression analysis, PCA was used to evaluate sample grouping **(Fig. 69).** Due to the large dataset, features with no detected counts across all samples were omitted, as this would not contribute to sample variance and reduce processing workload. Samples were grouped well with the greatest spread of samples occuring within the TLR7 alone group, although this was only a slight increase compared with other groups. Notably, the NISV alone and dexamethasone alone groups cluster closely, and are nearby to the media alone group.

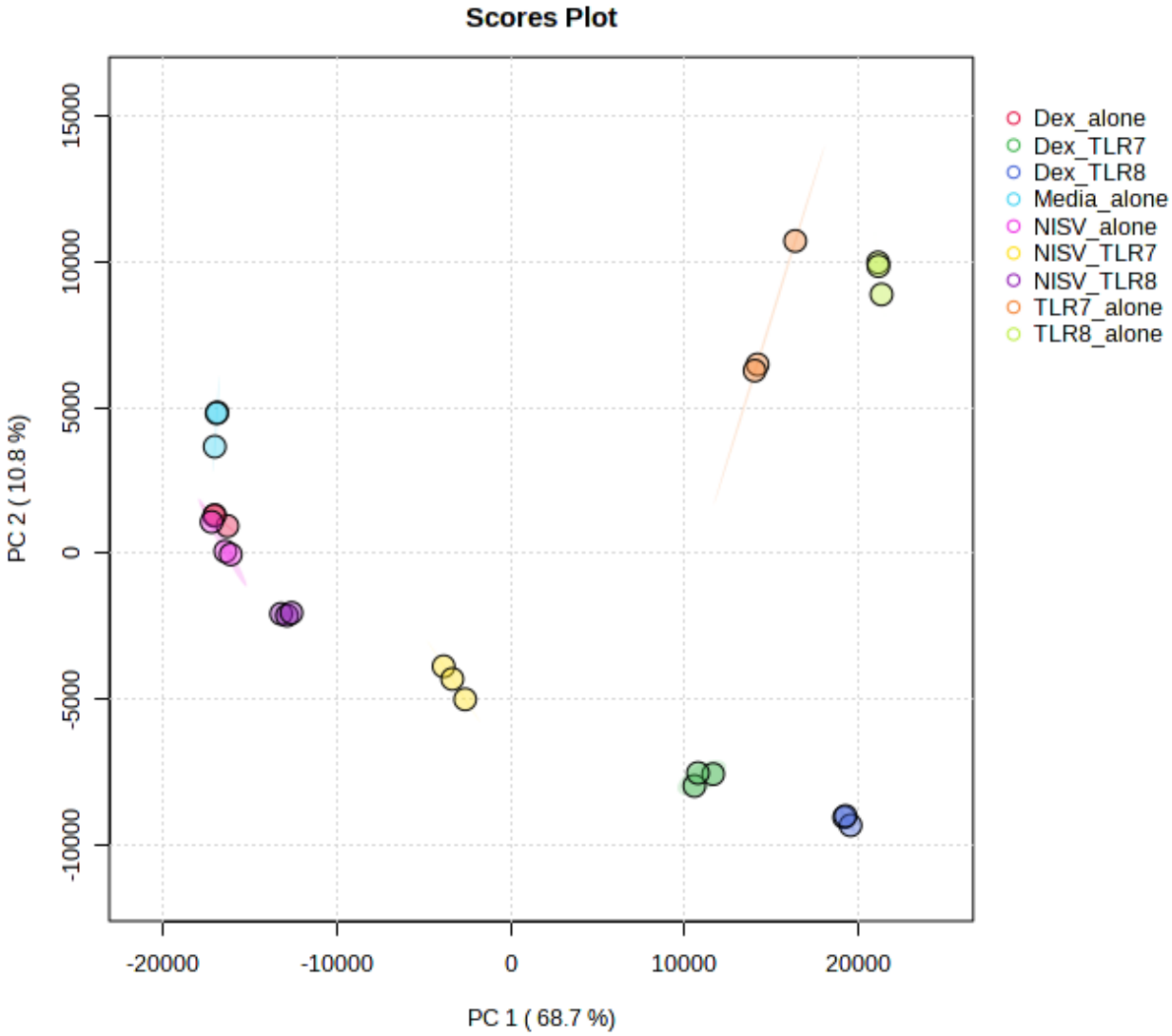

Figure 69: PCA plot comparing grouping of samples used in transcriptomic experiments. *BMDM were stimulated with either 1.6µg/ml of the TLR7 ligand imiquimod, 1.3µg/m TLR8 ligand TL8-506. Cells were also treated with either 1.2mM of NISV or 1.6µM of dexamethasone. Control cells were either unstimulated (media alone) or given a TLR ligand or treatment alone. After 6hrs RNA was extracted and sequenced. Transcripts were aligned to an annotated reference genome for* mus musculus *and features counted.*

After alignment and feature counting, transcripts were assigned to genes to provide an overview of the most significantly changing genes and the directionality of their modulation, volcano plots were produced comparing each experimental group to their appropriate control **(Fig 70 - 73).** Alongside this, the top 10 most significant genes were labelled for each comparison. Comparing the effect of NISV alone to dexamethasone alone, the volcano plot for NISV alone is much narrower, with dexamethasone displaying greater fold changes in significant genes. Alongside this, the most significantly changed genes in NISV display a more even balance of downregulation and upregulation, whereas there is a skew towards upregulation of significant genes in the dexamethasone alone group. This skew is also seen in the TLR7 and TLR8 alone groups which present similar overall shapes. The degree to which genes are changing is generally higher reaching log2FC changes of 5-10, compared with only reaching 4-5 in NISV or dexamethasone alone groups. Alongside this, there are a greater number of genes being significantly differentially expressed in TLR7 and TLR8 stimulated BMDM with values of >100 -log10 p-value, compared with most genes displaying a -log10 p-value of <50 in NISV or dexamethasone treated cells. When treating TLR7 or TLR8 stimulated cells with NISV the skew shifts towards a pattern of downregulation, indicating that NISV can modulate the transcriptional activity of stimulated cells whilst having a relatively small effect on unstimulated cells. Despite the broadly immunosuppressive actions of dexamethasone, the volcano plot reveals that it achieves this effect not through blanket downregulation of gene transcription. This balance of both upregulation and downregulation of genes is consistent with the current understanding of dexamethasone's mechanism of action. Both trans-activation and trans-repression can occur after dexamethasone binding to the GR, which could increase transcription of genes that provide and anti-inflammatory effect or decrease transcription of genes for pro-inflammatory processes or proteins.

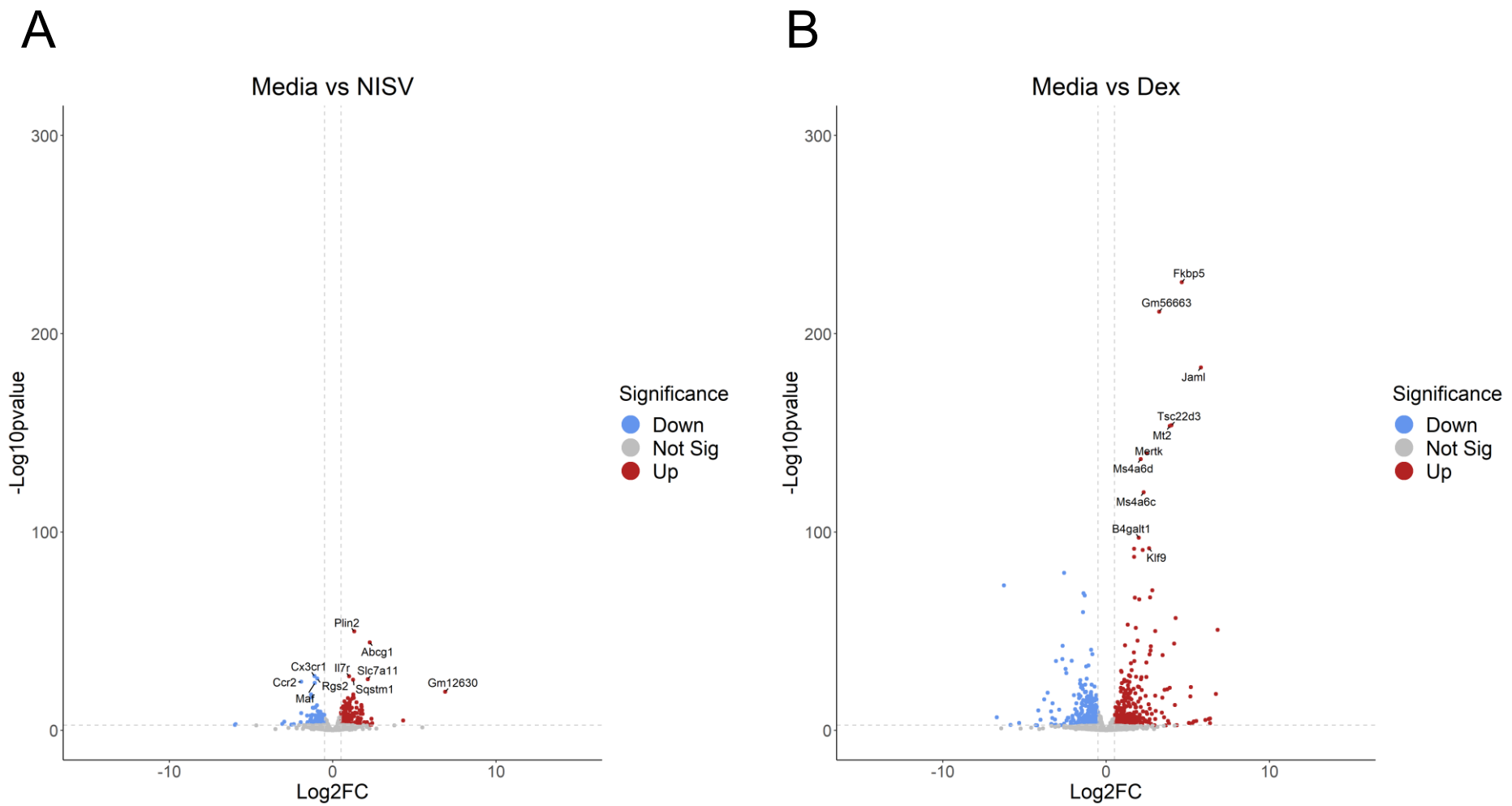

Figure 70: Volcano plots of differentially expressed genes in NISV or dexamethasone treated cells. *BMDM were treated with either media alone, NISV alone, or dexamethasone alone and total RNA extracted. After QuantSeq sequencing, alignment, and feature counting, gene counts were normalised, and differential gene expression analysis was performed using Deseq2. Log2 fold change values and adjusted p-values (FDR Benjamini-Hochberg) were calculated and plotted. Top 10 most significant genes are labelled. (A) Media alone vs NISV alone, (B) Media alone vs dexamethasone alone. Values in red = increased expression, blue = decreased expression, grey = not significant (p>0.05) Grey lines indicate bounds of p-value and fold change.*

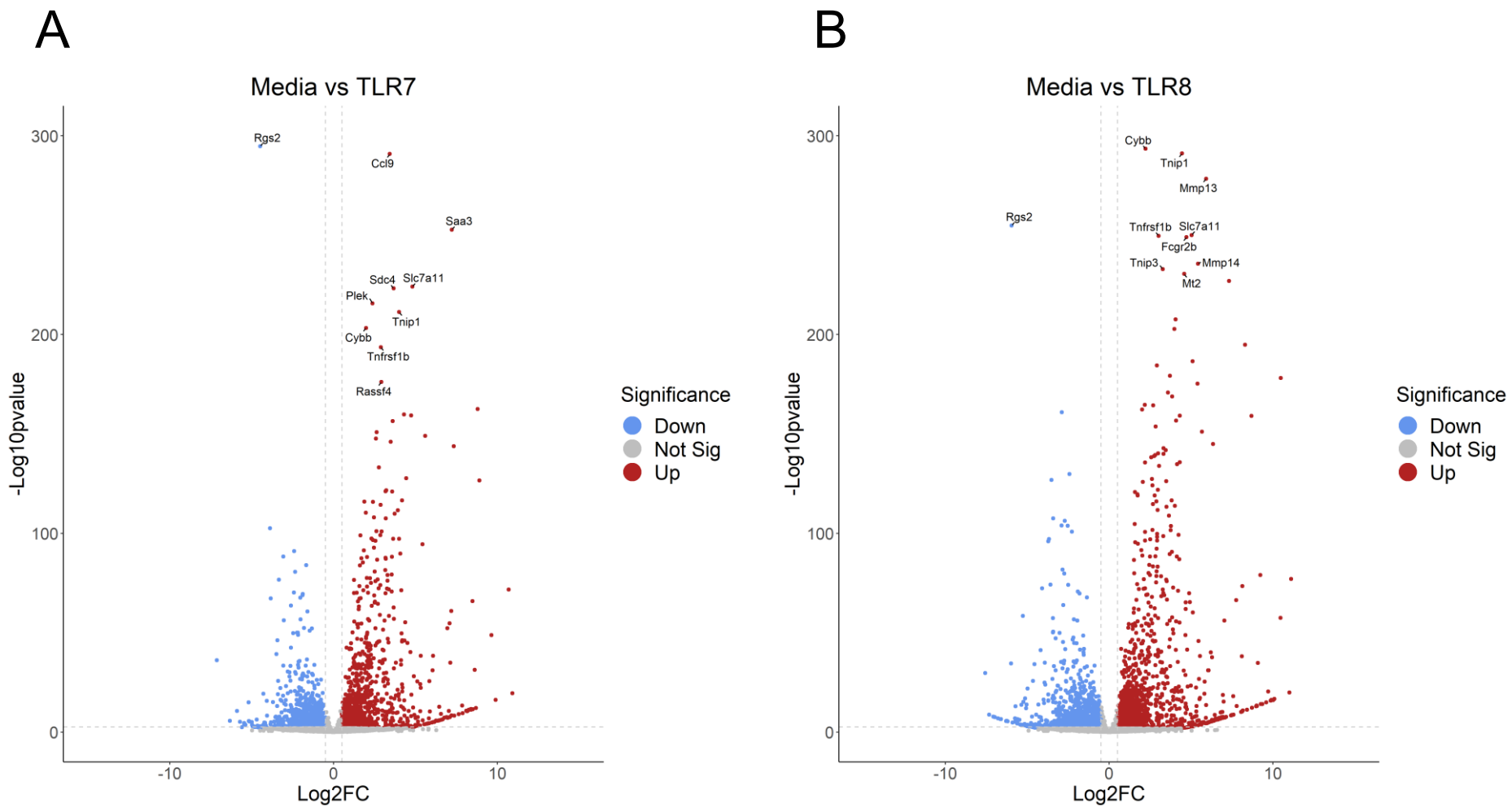

Figure 71: Volcano plots of differentially expressed genes in TLR7 or TLR8 stimulated cells. *BMDM were treated with either media alone, imiquimod (TLR7) alone, or TL8-506 (TLR8) alone and total RNA extracted. After QuantSeq sequencing, alignment, and feature counting, gene counts were normalised, and differential gene expression analysis was performed using Deseq2. Log2 fold change values and adjusted p-values (FDR Benjamini-Hochberg) were calculated and plotted. Top 10 most significant genes are labelled. (A) Media alone vs TLR7 alone, (B) Media alone vs TLR8 alone. Values in red = increased expression, blue = decreased expression, grey = not significant (p>0.05) Grey lines indicate bounds of p-value and fold change.*

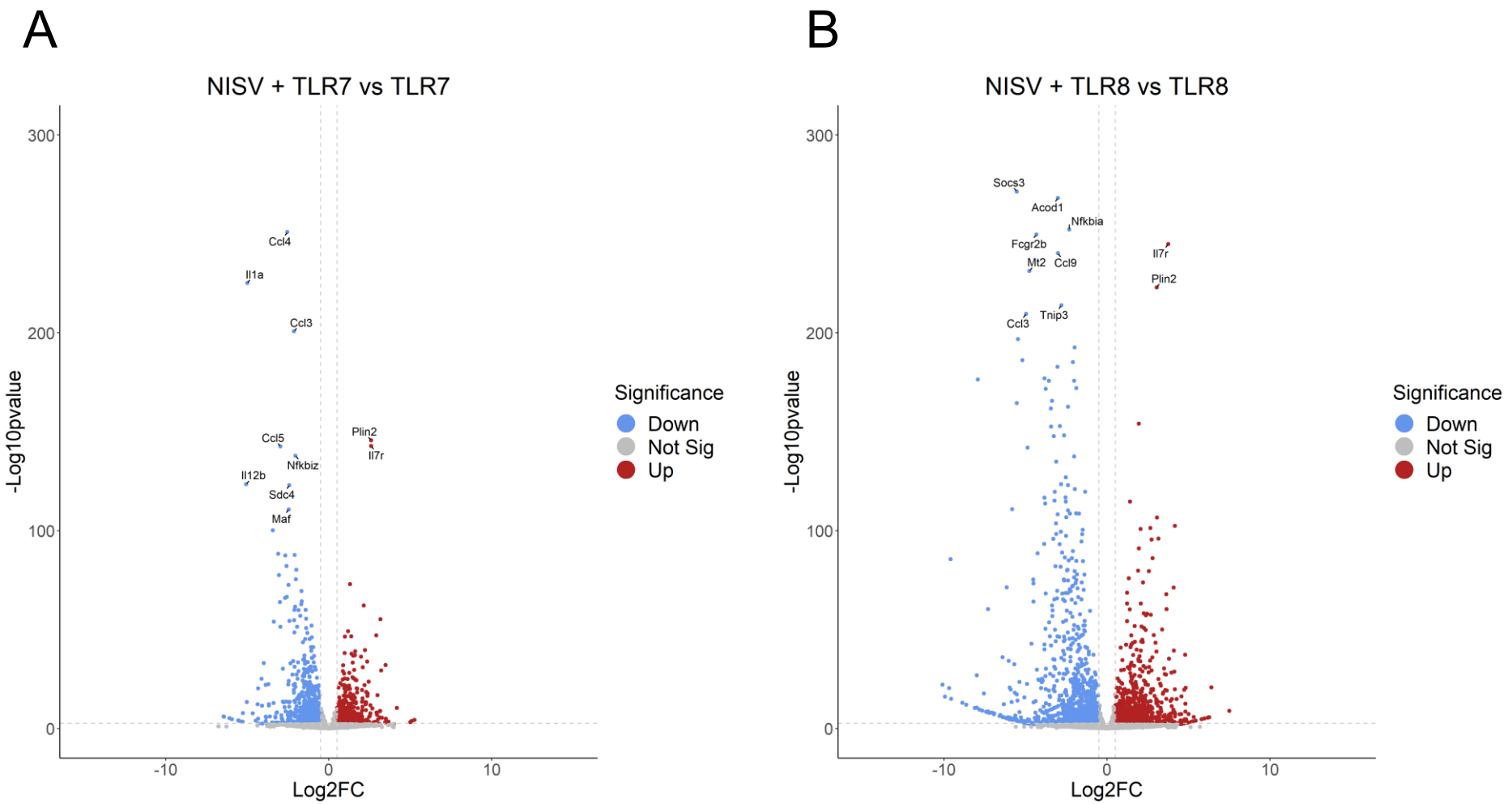

Figure 72: Volcano plots of differentially expressed genes TLR stimulated cells treated with NISV. *BMDM were stimulated with either imiquimod (TLR7) or TL8-506 (TLR8) and treated with NISV. Total RNA was extracted. After QuantSeq sequencing, alignment, and feature counting, gene counts were normalised, and differential gene expression analysis was performed using Deseq2. Log2 fold change values and adjusted p-values (FDR Benjamini-Hochberg) were calculated and plotted. Top 10 most significant genes are labelled. (A) NISV+TLR7 vs TLR7 alone, (B) NISV + TLR8 vs TLR8 alone. Values in red = increased expression, blue = decreased expression, grey = not significant (p>0.05) Grey lines indicate bounds of p-value and fold change.*

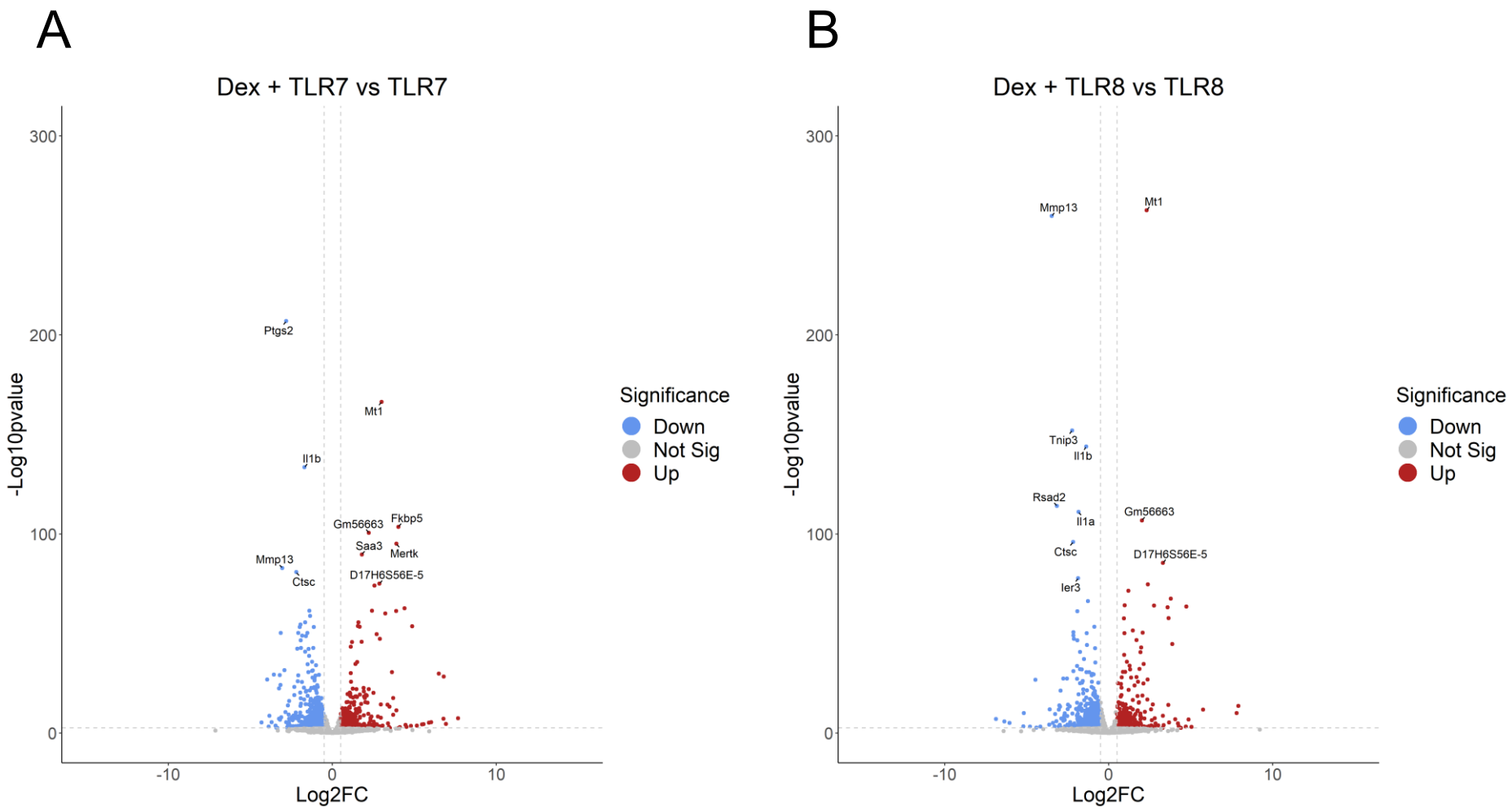

Figure 73: Volcano plots of differentially expressed genes TLR stimulated cells treated with dexamethasone. *BMDM were stimulated with either imiquimod (TLR7) or TL8-506 (TLR8) and treated with dexamethasone. Total RNA was extracted. After QuantSeq sequencing, alignment, and feature counting, gene counts were normalised, and differential gene expression analysis was performed using Deseq2. Log2 fold change values and adjusted p-values (FDR Benjamini-Hochberg) were calculated and plotted. Top 10 most significant genes are labelled. (A) dexamethasone +TLR7 vs TLR7 alone, (B) dexamethasone + TLR8 vs TLR8 alone. Values in red = increased expression, blue = decreased expression, grey = not significant (p>0.05) Grey lines indicate bounds of p-value and fold change.*

To provide a more in-depth overview of our data, heatmaps based on the normalised counts for each transcript were generated. Alongside examining the clustering of genes between the control vs case, we also determined the Log2 fold change (Log2FC) of each gene between the two experimental groups. We also display the average expression of each gene as an identifier of transcript abundance. To streamline this analysis, we chose to include only significant (adjusted p value <0.05) differentially expressed genes that displayed a Log2FCgreater than 0.5.

As seen indicated earlier in the volcano plots, the number of genes significantly changing in response to NISV or dexamethasone alone **(Fig. 74 -75)** with only 345 and 767 differentially expressed genes. This is contrast with the TLR7 and TLR8 stimulated groups **(Fig. 76 - 77)**, which displayed the highest amount of differentially expressed transcripts at 2645 and 3200 respectively. Another contrast between the treatment alone and stimulation alone groups is the average expression of genes, with the spread of gene expression appearing much wider in NISV and dexamethasone groups, spanning both upregulated and downregulated genes, compared with an abundance of highly upregulated transcripts in TLR7 and TLR8 stimulated BMDM. When observing the effect of NISV on both TLR7 and TLR8 **(Fig. 78 - 79)**, the balance of average expression returns to a more even spread, reinforcing the notion that the effect of NISV regulates gene transcription. This can also be seen with a decrease in the number of significant differentially expressed transcripts falling from 2645 to 1282 in NISV treated TLR7 stimulated BMDM, and 3200 to 2482 in NISV treated TLR8 stimulated BMDM.

When observing transcriptional changes imparted by dexamethasone treatment **(Fig. 80 - 81)**, this effect is even greater, with the abundance of upregulated transcripts returning to a state that resembles pre-stimulated BMDM. However, the number of significant differentially expressed genes falls considerably to 838 for dexamethasone treated TLR7 stimulated BMDM, and 709 for dexamethasone treated TLR8 stimulated BMDM.

Regardless of experimental comparison, we observed an abundance of transcripts that were changing slightly, i.e., low Log2FC values. This could be interpreted as “housekeeping” gene transcription and occurs irrespective of polarising stimuli.

During these experiments we opted to highlight the top 15 most significantly changing genes to explore the data in an untargeted manner.

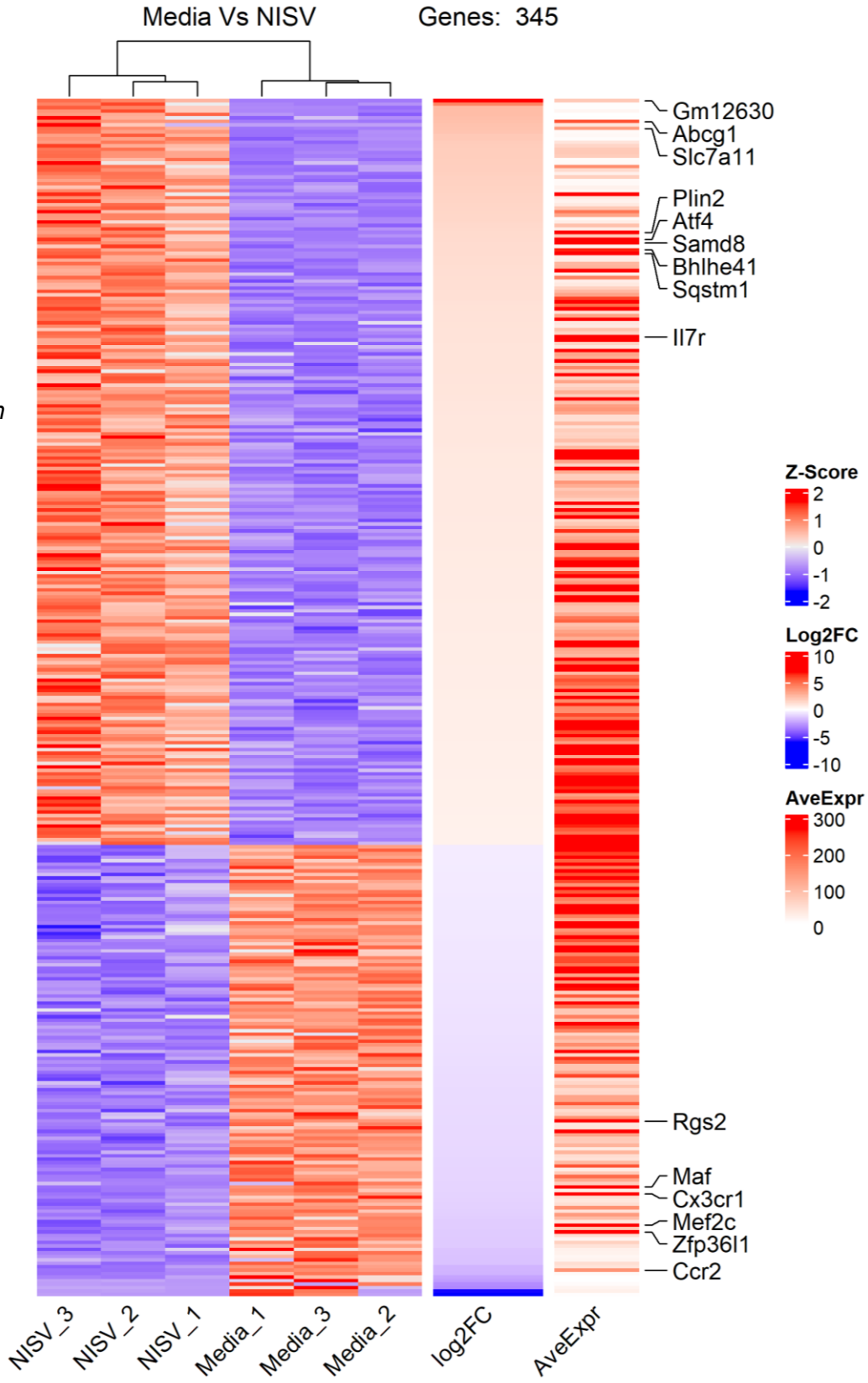

Figure 74: Heatmap comparing overall expression pattern of significant differentially expressed genes in NISV treated BMDM vs unstimulated BMDM. *Significant transcripts with fold change > 0.5 were selected and Euclidean distance clustering was performed on columns to assess replicate consistency. Log2FC was calculated for each transcript, alongside the average expression across all samples of each transcript as a measurement of transcript abundance. Top 15 most significant transcripts are labelled (p<0.05).*

Figure 75: Heatmap comparing overall expression pattern of significant differentially expressed genes in dexamethasone treated BMDM vs unstimulated BMDM. *Significant transcripts with fold change > 0.5 were selected and Euclidean distance clustering was performed on columns to assess replicate consistency. Log2FC was calculated for each transcript, alongside the average expression across all samples of each transcript as a measurement of transcript abundance. Top 15 most significant transcripts are labelled (p<0.05).*

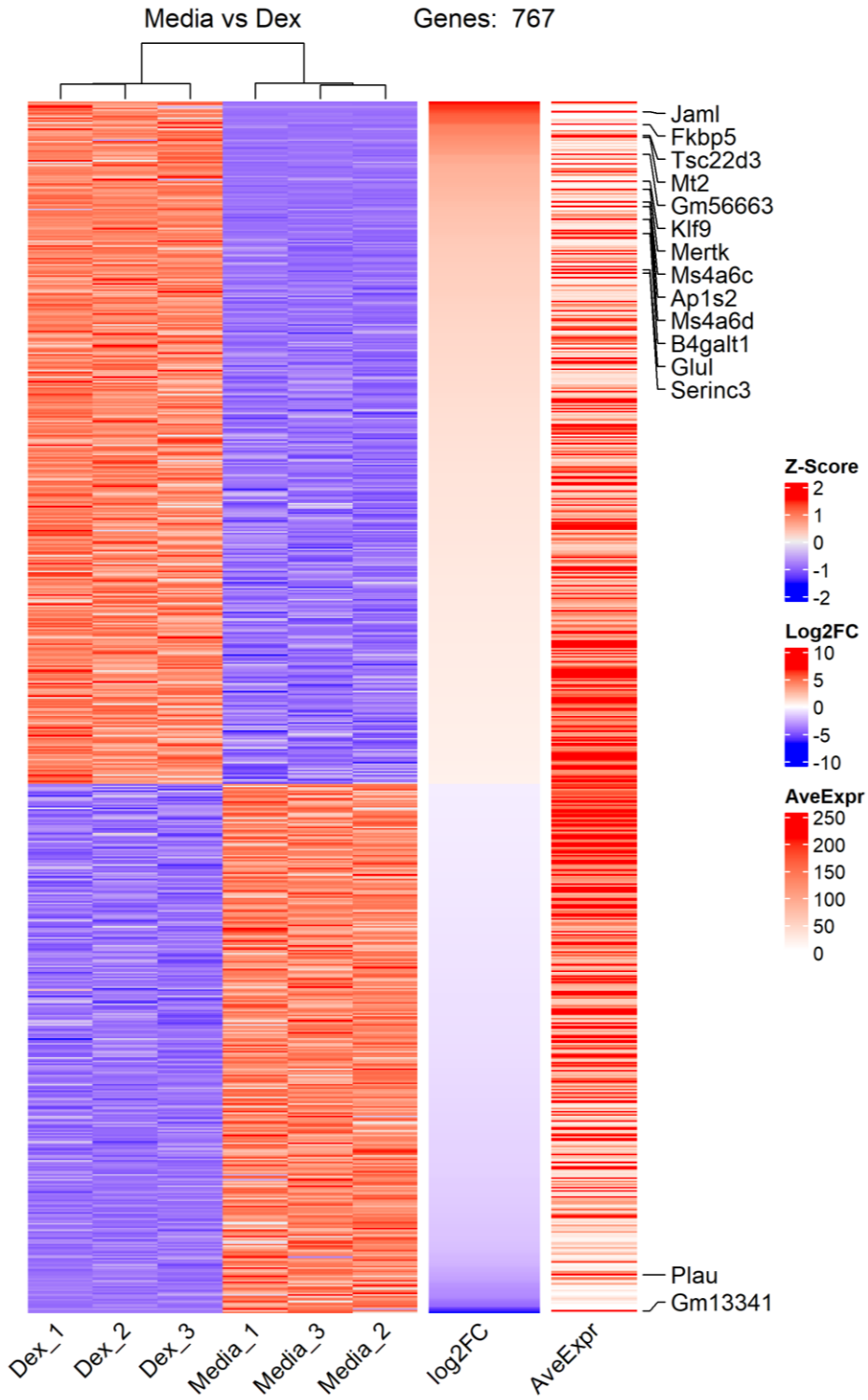

Figure 76: Heatmap comparing overall expression pattern of significant differentially expressed genes in TLR7 stimulated BMDM vs unstimulated BMDM. *Significant transcripts with fold change > 0.5 were selected and Euclidean distance clustering was performed on columns to assess replicate consistency. Log2FC was calculated for each transcript, alongside the average expression across all samples of each transcript as a measurement of transcript abundance. Top 15 most significant transcripts are labelled (p<0.05).*

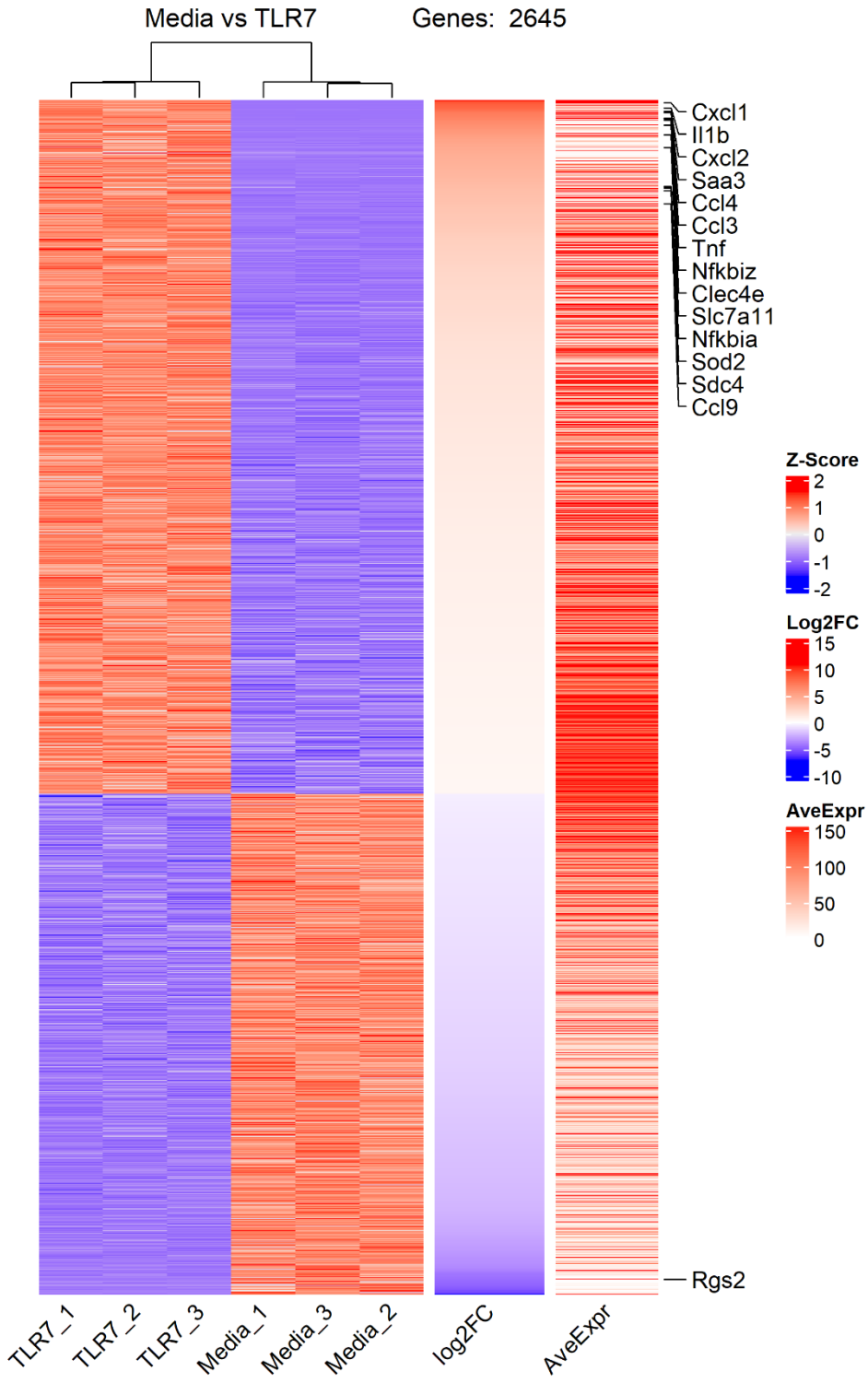

Figure 77: Heatmap comparing overall expression pattern of significant differentially expressed genes in TLR8 stimulated BMDM vs unstimulated BMDM. *Significant transcripts with fold change > 0.5 were selected and Euclidean distance clustering was performed on columns to assess replicate consistency. Log2FC was calculated for each transcript, alongside the average expression across all samples of each transcript as a measurement of transcript abundance. Top 15 most significant transcripts are labelled (p<0.05).*

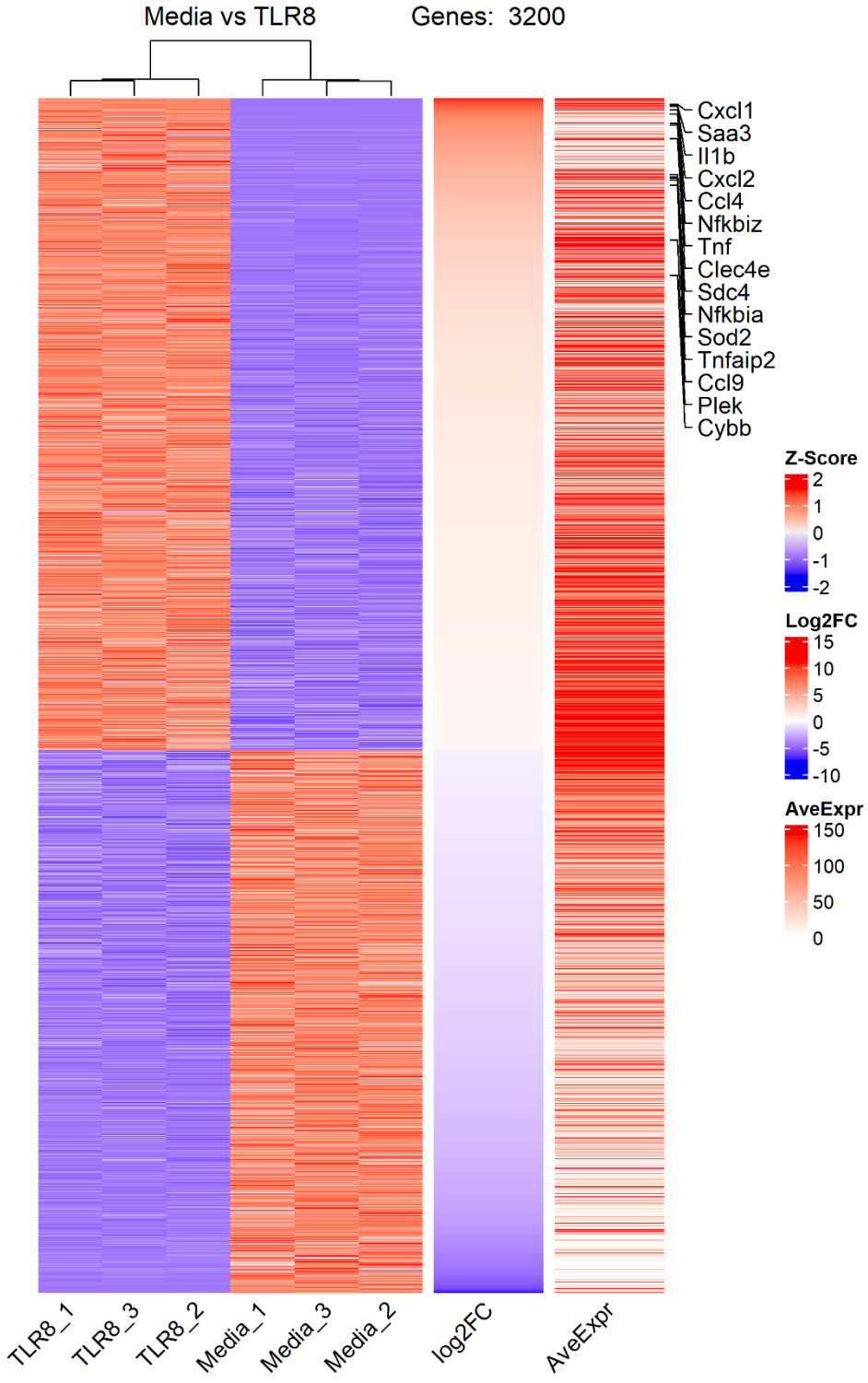

Figure 78: Heatmap comparing overall expression pattern of significant differentially expressed genes in TLR7 stimulated BMDM treated with NISV vs TLR7 stimulated BMDM alone. *Significant transcripts with fold change > 0.5 were selected and Euclidean distance clustering was performed on columns to assess replicate consistency. Log2FC was calculated for each transcript, alongside the average expression across all samples of each transcript as a measurement of transcript abundance. Top 15 most significant transcripts are labelled (p<0.05).*

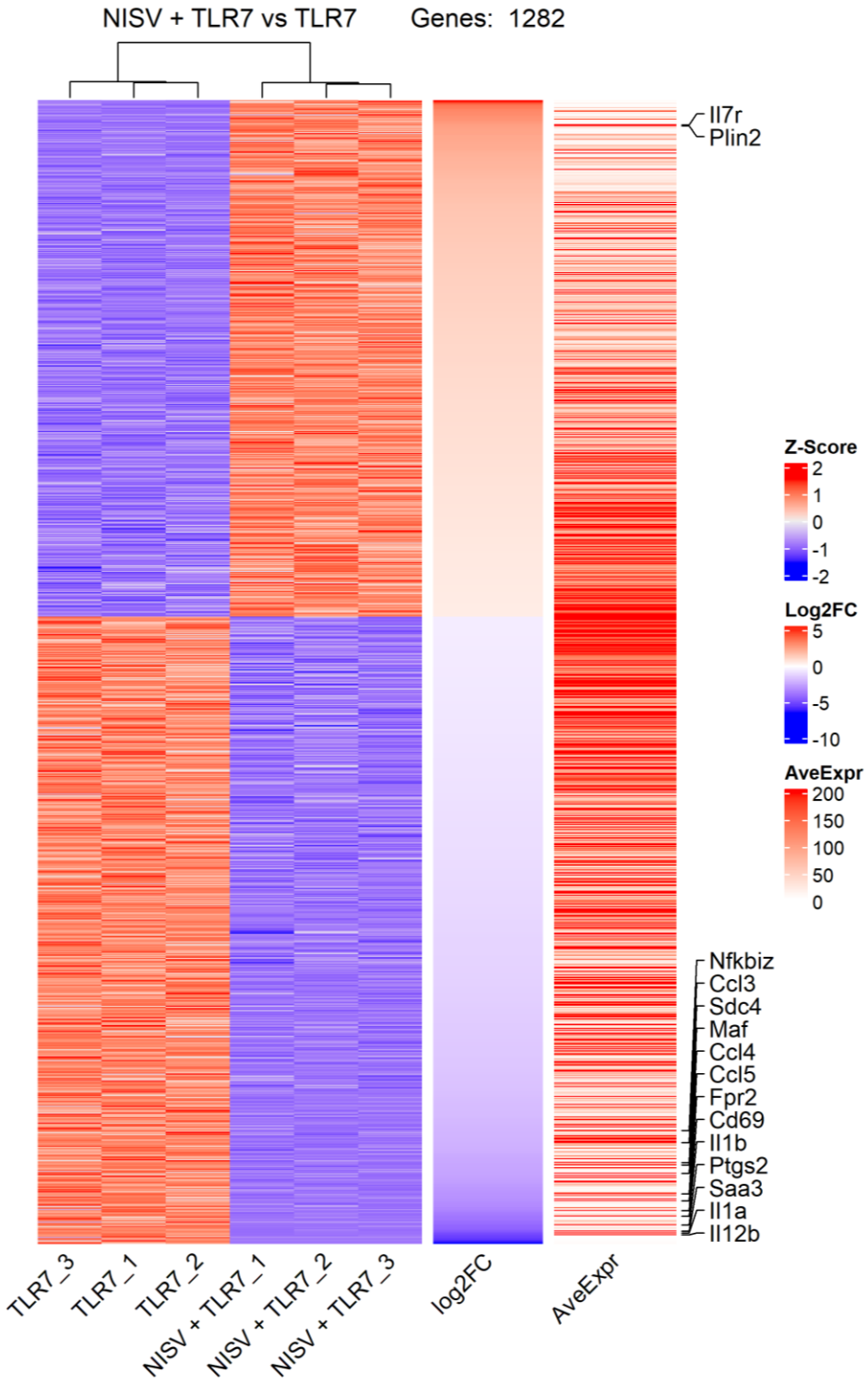

Figure 79: Heatmap comparing overall expression pattern of significant differentially expressed genes in TLR8 stimulated BMDM treated with NISV vs TLR8 stimulated BMDM alone.
Significant transcripts with fold change > 0.5 were selected and Euclidean distance clustering was performed on columns to assess replicate consistency. Log2FC was calculated for each transcript, alongside the average expression across all samples of each transcript as a measurement of transcript abundance. Top 15 most significant transcripts are labelled (p<0.05).

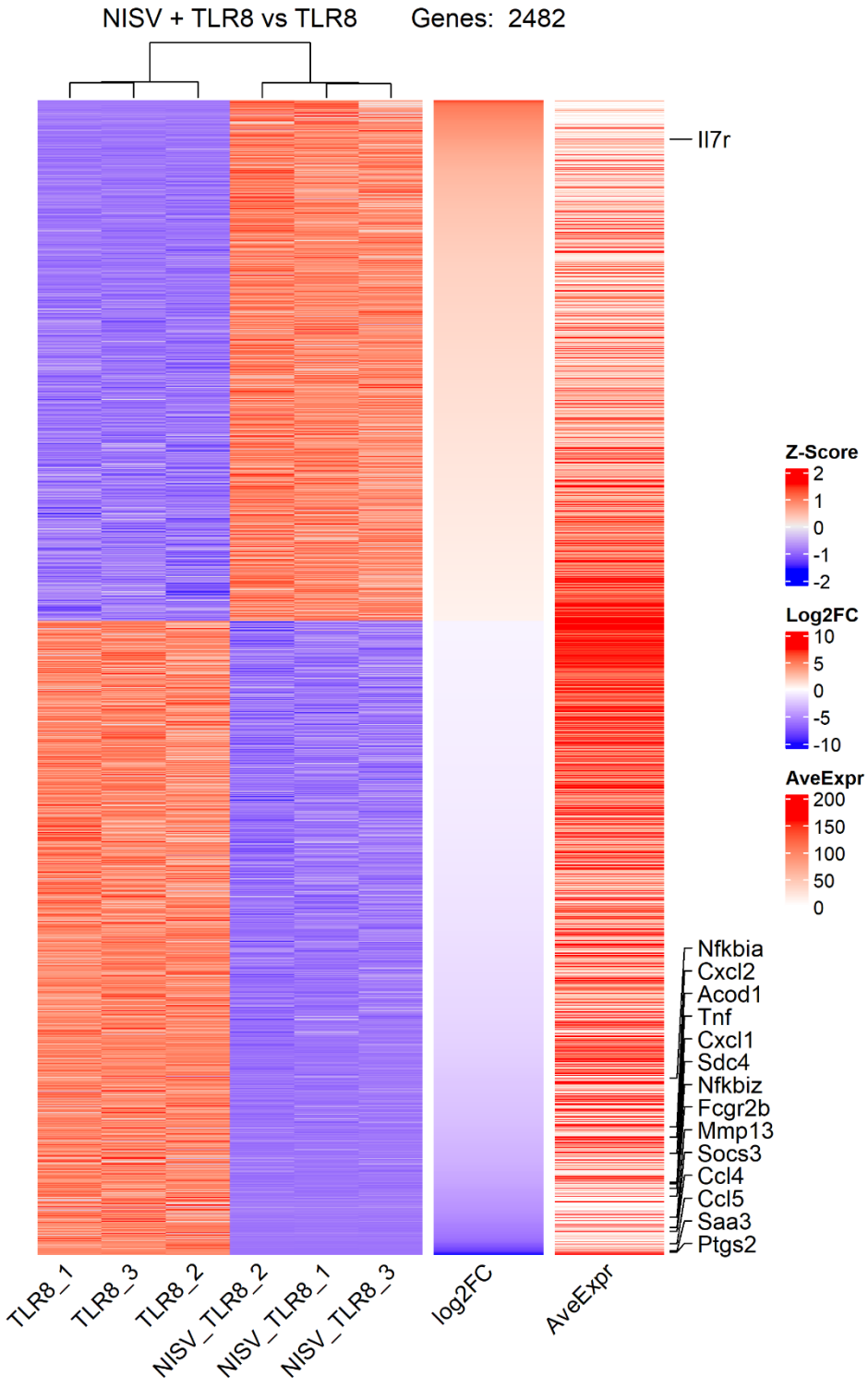

Figure 80: Heatmap comparing overall expression pattern of significant differentially expressed genes in TLR7 stimulated BMDM treated with dexamethasone vs TLR7 stimulated BMDM alone. *Significant transcripts with fold change > 0.5 were selected and Euclidean distance clustering was performed on columns to assess replicate consistency. Log2FC was calculated for each transcript, alongside the average expression across all samples of each transcript as a measurement of transcript abundance. Top 15 most significant transcripts are labelled (p<0.05).*

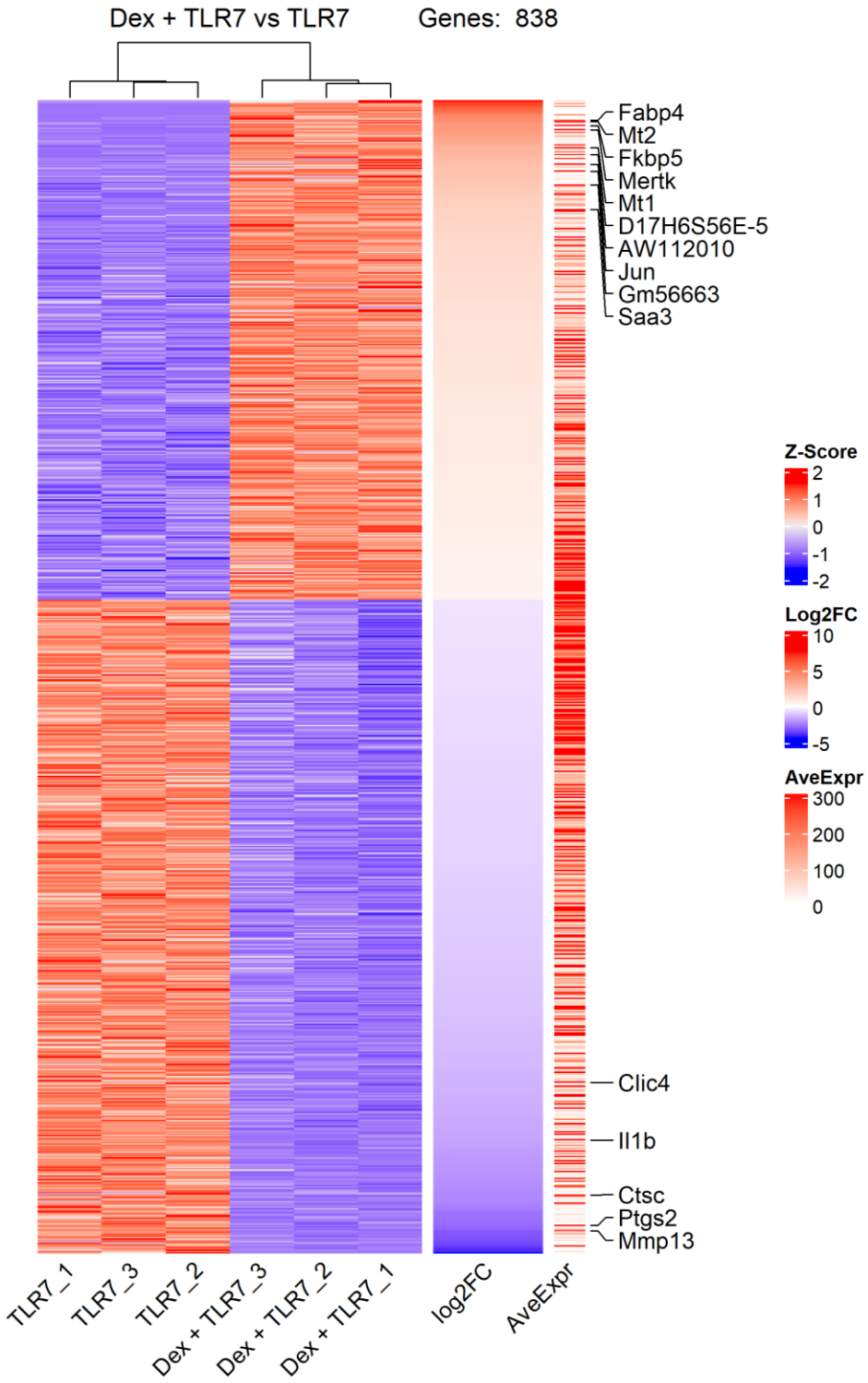

Figure 81: Heatmap comparing overall expression pattern of significant differentially expressed genes in TLR8 stimulated BMDM treated with dexamethasone vs TLR8 stimulated BMDM alone. *Significant transcripts with fold change > 0.5 were selected and Euclidean distance clustering was performed on columns to assess replicate consistency. Log2FC was calculated for each transcript, alongside the average expression across all samples of each transcript as a measurement of transcript abundance. Top 15 most significant transcripts are labelled (p<0.05).*

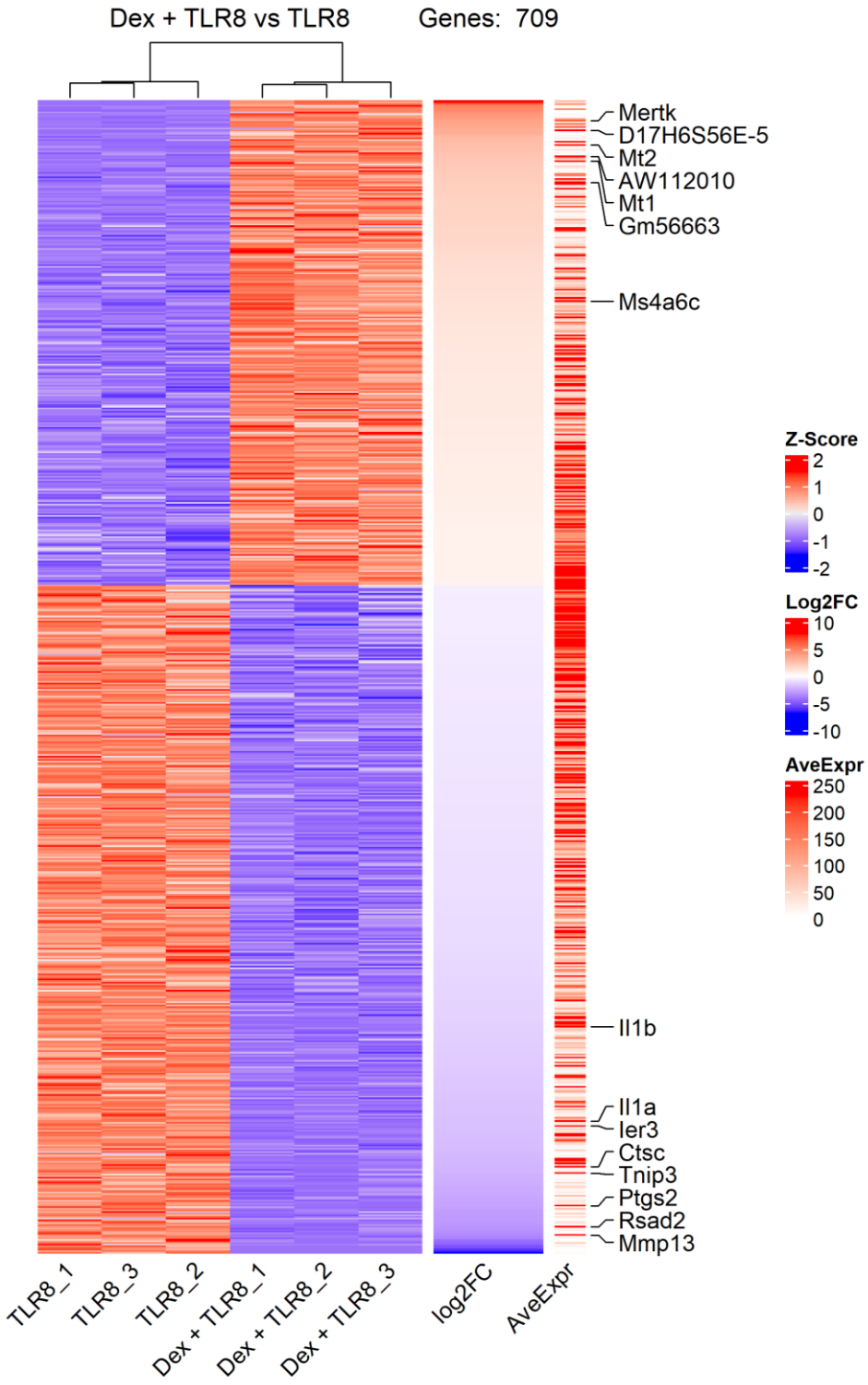

From analysis of the 15 most significant genes, it was noted that genes were changed in multiple groups. Two such genes were Plin2 and Il7r, which was found to be upregulated in all groups that contained NISV (NISV alone, NISV + TLR7, NISV + TLR8). Plin2 encodes the protein perilipin 2 which is part of the cytoplasmic lipid binding family of proteins and is involved in the formation of lipid droplets by forming part of their structural coat. An increase in Plin2 transcripts could indicate increased lipid droplet formation and upregulation of lipid metabolism. Gene expression is also increased for Il7r, which encodes the IL-7 receptor. Whilst IL-7 is associated with development lymphoid lineage cells (particularly B and T cells), IL-7R expression on macrophages is associated with differentiation of monocytes into tissue resident macrophages and can be indicative of an M1 phenotype.

Other effects of NISV includes mimicking the effects of TLR7 and TLR8 stimulation, with both NISV and TLR stimulation upregulating Slc7a11 transcripts. This gene encodes a protein that acts as a subunit in an antiporter which transports cysteine into cells and exports glutamate and can be regulated by transcription factors such as NRF2, KEAP1, and STAT3/5. Rgs2 also appears in the most significantly regulated transcripts for NISV and both TLR7 and TLR8, although it is increased in NISV alone treated samples, but downregulated in TLR7 and TLR8 stimulated cells.

Alongside the above effects, common transcripts in our 10 most significantly expressed genes for TLR7 and TLR8 stimulated BMDM include the regulator of NF-kB, Tnip1, and the gene Cybb, which is involved in the NADPH oxidase complex. As for dexamethasone specific effects, unsurprisingly we see positive effects on Fkbp5 which encodes the immunophilin FKBP5. This protein forms part of the chaperone complex (alongside HSP90) that sequesters the GR receptor in the cytoplasm when no ligand is bound. Upon binding, FKBP5 dissociates and allows translocation of the GR-ligand complex to the nucleus to regulate transcription of various genes. Upon binding to the GRE element on the DNA, Fkbp5 gene is expressed to replace the dissociated FKBP5. Dexamethasone also induces transcriptional upregulation of Mertk, which could indicate increased expression of MERTK on the surface of macrophages, a phenotype associated with M2 macrophages.

6.4.2 Gene ontology analysis identifies lysosomes, antioxidant production, and protein binding as targets of NISV

To provide an overview of the general effects of each treatment or TLR ligand, gene ontology (GO) analysis was utilised. For each gene detected in our experiment, a single or multiple GO terms may be associated, identifying the pathways, functions, disease states, or function in the organism that the gene belongs to. A single gene may belong to multiple GO categories. This provides a broad overview of the particular areas in which genes are differentially expressed, and thus can direct further investigation by providing a jumping-off point for downstream analysis. Using the tool Goseq, I chose to include the GO categories of molecular function, and cellular component, whilst omitting the biological process category. In practice, whilst biological processes can provide valuable information, the annotations from this category would override the annotations for the others resulting in less specific information. For example, the molecular function category may reveal that genes relating to protein binding, or signalling receptor binding are differentially expressed, whereas inclusion of the biological process category would override this by broadly grouping genes as “immune response” or “response to stimuli”, reducing the specificity of GO analysis. Furthermore, whilst the list of categories highlights the most over-represented GO categories (either from significant downregulation or upregulation), other GO categories may also be over-represented but to a lesser degree and thus not present on the GO plot.

With this in mind, GO analysis comparisons were performed on the groups displayed in the volcano plots, i.e., Media alone vs NISV alone, NISV+ TLR7 vs TLR7 alone, etc, yielding 8 comparisons **(App.3-12).** GO analysis provided the top 10 over-represented categories for each comparison. Surveying the data overall, there are GO categories that are common to all/many of the groups, as well as a degree of category redundancy. For example, when examining cellular component GO categories, plasma membrane, cell periphery, cell surface, membrane, intrinsic components of membrane, extracellular space, extracellular region, and intrinsic components of plasma membrane are present in all groups or all but one or two groups. Thus, the categories with few occurrences in our comparison groups may indicate the defining features. Particularly in the media alone vs NISV alone group, both lytic vacuole and vacuole categories are present whilst absent from other groups, indicating that a key interaction between NISV and cells could involve lysosomes. Whilst the categories included in the cellular component GO analysis fail to reveal a great deal of information, we also investigated the molecular function GO categories.

As before, there were a number of categories that were redundant in this analysis as they were near-constant between groups. This included the categories of protein binding, signalling receptor activity, molecular transducer activity, signalling receptor binding,

signalling receptor regulator activity, and receptor ligand activity. An observation emerging from this analysis, included the over-representation of cell adhesion molecule binding and integrin binding in both the media alone vs NISV alone and media alone vs dexamethasone alone groups. Another notable feature of NISV alone treatment is the over-representation of genes involved in proteoglycan binding, protein heterodimerisation activity, and antioxidant activity. The inclusion of these categories is likely due to the absence of TLR stimulation, which may be masking these effects in other groups, instead displaying the obvious interactions with receptors and ligands, or signalling receptors. Unsurprisingly, cytokine activity was present in all groups that included a TLR ligand, although over-representation of cytokine receptor binding genes was limited to both dexamethasone + TLR stimulation groups, and TLR8 stimulation alone group.

6.4.3 Investigating pathways

After a broad overview of the data, I aimed to investigate particular pathways of potential relevance. To decrease processing time, I chose pathways using the Kyoto Encylopedia of Genes and Genomes (KEGG), an extensive annotated repository of pathways that cover the breadth of biological processes in an organism alongside pathways specific to certain immune response or disease states. These pathways and their respective KEGG identifier are available in **Table 6.** To achieve this, I utilised the output of deseq2 resulting from the differential gene expression analysis and the programme Pathview available through The Galaxy Project. This workflow also enables the inclusion of a compound data file, allowing integration of metabolites with genes for pathways identification. To this end, metabolites that were both identified and significantly changed in the comparison groups were included. Whilst in some cases this included no metabolites, or only a few, some groups consisted of >50 significant metabolites. Furthermore, as this analysis probed 18 KEGG pathways, to avoid repetition and redundancy the following results include only segments of those pathways that inspire robust conclusions. When referencing a particular KEGG pathway, the corresponding whole pathway map for each group comparison is available in **appendices 13-28**.

Table 6: Pathways investigated after differential gene expression analysis and their respective KEGG identifiers.

Pathway name	KEGG identifier
Endocytosis	04144
Phagosome	04145
Lysosome	04142
Cell cycle	04110
Apoptosis	04210
MAPK	04010
JAK/STAT	04630
NF-kB	04064
TNF signalling	04668
Cytokine-cytokine receptor interaction	04060
Viral protein interaction with cytokine and cytokine receptor	04061
Cell adhesion molecules	04514
Toll-like receptor signalling	04620
NOD-like receptor signalling	04621
RIG-I signalling pathway	04633
Antigen processing and presentation	04612
Chemokine signalling pathway	04062
COVID-19	05171
Systemic Lupus Erythematosus	05322

As previously demonstrated using ELISAs and cytometric bead arrays, NISV and dexamethasone are effective modulators of cytokine production in TLR stimulated cells. To investigate these effects at the transcriptional level, I examined the cytokine-cytokine receptor pathway which I present as a summary heatmap **(Fig 82).** First, examining the effect of NISV **(App. 13)** or dexamethasone **(App. 14)** on unstimulated cells, I observed that there were few significant changes with only IL1B displaying a decrease, alongside chemokine receptors such as CCR5, CCR2, and CX3CR1. However, the expression of CXC family chemokines (CXCL1, CXCL2, CXCL3) was significantly increased, alongside genes encoding cytokine receptors IL7R, IL11RA, IL1RN, and TNFR2. In comparison, the effect of dexamethasone on unstimulated BMDM was more pronounced, with similar downregulation of chemokine receptor transcripts (CCR2, CCR3, CCR5), but now accompanied by significant decrease in the gene transcription for the chemokines themselves (CCL3L1, CCL4, CCL4L1, CCL4L2, CCL3 etc.). Notably a contrast between the NISV alone and dexamethasone alone is the increase in transcripts for IL6/12 family cytokine receptors IL6R (and the signal transducer IL6ST) and LIFR (CD118). Transcripts for both TGFB3 and its receptor TGFBR1 are also increased in the dexamethasone treated samples.

To provide context for the potential immunomodulatory effects of NISV I also examined the transcriptional effects of TLR7 **(App. 15)** and TLR8 **(App. 16)** ligation alone. Unsurprisingly, upregulation of many of the chemokines mentioned previously was present in both TLR7 and TLR8 stimulated cells but expanded to include many of the CC family (CCL3L1, CCL4, CCL4L1, CCL4L2, CCL5, CCL3, CCL9, CCL7, CCL2, CCL12) and CXC family chemokines (CXCL1, CXCL5, CXCL6, CXCL2, CXCL3, CXCL4, CXCL4L1, CXCL10, CXCL11, CXCL16). Also expectedly, IL-6/IL-12 family cytokine transcripts were upregulated including IL6, IL12, IL23A, IL27, and IL35. Despite relatively high similarity between both TLR stimulation groups, differences were observed such as increased IL19 and IL18 expression in TLR8 stimulated cells but not in TLR7 stimulated cells. TLR8-specific transcriptional upregulation also includes the prolactin CSF3 and OSM, a regulator of IL-6 and GM-CSF.

Figure 82: Change in cytokine and chemokine gene expression in TLR7 and TLR8 stimulated BMDM treated with NISV or dexamethasone. *Total RNA was extracted at 6hrs from BMDM, and cDNA libraries were prepared using QuantSeq kit. After cDNA sequencing, differential gene expression analysis was performed on the resulting transcripts and Log2FC was calculated. Shown are significant differentially expressed cytokine/chemokine transcripts for each group where at least 1 transcript is present in the overall analysis. Values in red indicate an increase in transcription vs control, blue values indicate a decrease in transcription vs control, and grey values indicate not significant/undetected.*

NISV, dexamethasone, TLR7, and TLR8 alone samples were compared to unstimulated BMDM given media alone. NISV + TLR ligand samples were compared to BMDM stimulated with TLR ligand alone, and likewise for dexamethasone + TLR ligand groups.

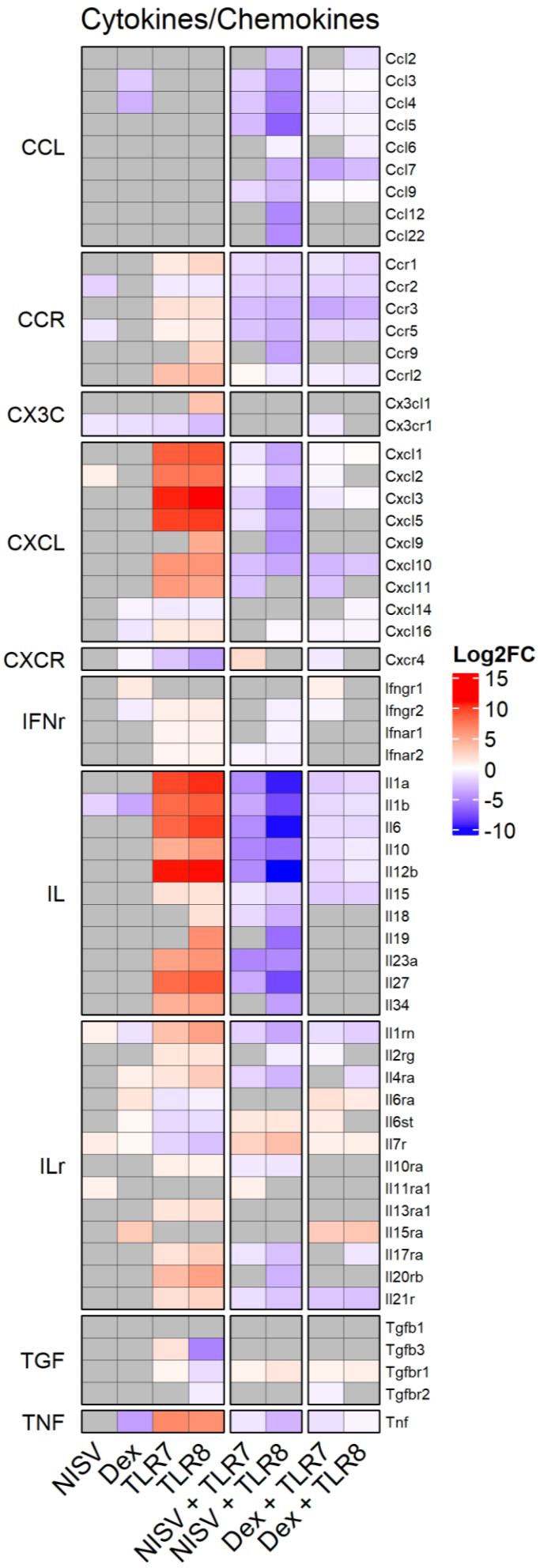

Following this, I investigated the effects of NISV on TLR7 **(App. 17)** and TLR8 **(App. 18)** stimulated gene transcription. In both groups significant downregulation of transcripts for chemokines in the CC and CXC subfamily was observed. This contrasts with the effect of NISV alone in which upregulation of CXCL1, CXCL2 and CXCL3 was noted. Another feature of NISV effect that was noted was the downregulation of the IL-6/IL-12 family genes, observing a decrease in IL6, IL12, IL23A, IL27, IL35, and CLCF1 gene expression. A decrease in gene transcription of these cytokines is accompanied by an increase in expression of IL6ST, the gene that encodes gp130. Both experimental groups also display a decrease in IL10 gene expression

Notably, whilst the overall pattern of gene regulation conferred by NISV is maintained between both TLR stimulation scenarios, a greater number of genes found in the cytokine-cytokine receptor pathway are significantly affected in the TLR8 stimulated group. Particularly more genes of the CC subfamily of chemokines are downregulated than in the NISV+TLR7 group, along with downregulation of interferon receptors IFNAR1 and IFNGR2. Alongside this, various genes in the TGF family are affected by NISV in TLR8 stimulated cells but not TLR7 stimulated cells such as ACVRL1 and ACVR1B which act as receptors for TGF-β, and GDFs.

The effect of dexamethasone was also observed on gene expression in TLR7 **(App. 19)** or TLR8 **(App. 20)** stimulated cells. Similar to the effect of NISV, in both dexamethasone treated groups a decrease in transcripts for CC and CXC subfamily chemokines was observed. Both groups displayed decreased transcripts for IL1A, IL1B and IL1RN, alongside downregulation of TNF and CD40. A clear difference in the effect of dexamethasone between the two TLR stimulation scenarios was modulation of gene expression relating to cytokine receptors. For example, in TLR7 stimulated cells, dexamethasone caused upregulation of IL6ST, IL6R, and LIFR, whereas only IL6R was increased in the TLR8 stimulated group. Alongside this was a downregulation in IL2RG, IL17RA, TGFBR2, and IFNGR2, with upregulation of IFNGR1 when dexamethasone was used to treat TLR7 stimulated BMDM but not in TLR8 stimulated BMDM.

After surveying cytokines and cytokine receptors, we investigated the TLR signalling pathways to further determine the TLR or NISV/dexamethasone specific effects, as well as confirm previous data from our laboratory generated using TLR4 stimulation and NISV.

6.4.3.1 NISV downregulate MyD88, dexamethasone increases TLR7 expression

To determine the changes in TLR signalling imparted by the various treatments, TLR stimulation, and a combination of both, I chose to broadly examine the TLR pathway annotated in KEGG. I also opted to place emphasis on the endosomal TLR pathway as this pertains to TLR7 and TLR8. As such, to provide a clear view of this pathway a focused simplified view of endosomal TLR signalling is presented, with larger comprehensive maps available in **appendices 21 -28**

NISV alone had little effect on the overall TLR signalling cascade **(App. 21)** Despite this, the few significant changes in gene expression tended towards an anti-inflammatory effect with upregulation in the transcripts of genes encoding the inhibitory molecules TOLLIP (Toll interacting protein) and IKKy (inhibitor of nuclear factor kappa-B kinase subunit gamma). Alongside this, transcripts for CD14, AP-1, and IL-1B were decreased vs the media alone control group. Examination of the effect of dexamethasone alone revealed a greater number of significant changes than in the NISV group.

The overall effect of dexamethasone **(App. 22)** alone resulted in a mixed effect, with both anti-inflammatory aspects and pro-inflammatory aspects. Significant downregulation of the transcription factor AP-1, and subsequently a decrease in transcripts for TNFα, MIP-1α (CCL3) and MIP-1β (CCL4), indicate a reduced ability to induce chemotaxis and recruitment of other monocytic cells or T-cells, alongside increased PI3K expression which contributes to controlling the inflammatory response in macrophages. Outside of this, pro-inflammatory factors such as upregulation of CD14 which aids TLR4 in the recognition of LPS, TBK1 which induces IRF3 to promote transcription of anti-viral genes like that of the type I interferons. Interestingly, dexamethasone alone increased transcripts for TLR7/8.

As one would expect, in contrast to the few perturbations in TLR signalling found in NISV and dexamethasone alone treated samples, TLR7 **(App. 23)** and TLR8 **(App. 24)** ligation induce significantly increased expression of many genes in this pathway, resulting in a pro-inflammatory effect. Interestingly, despite using the MyD88 signalling adaptor, TLR7 and TLR8 ligation induces increased expression of both TRIF and TRAF3, although expression of the associated downstream genes such as IRF3 and IRF7 are not significantly changed. Significantly increased expression of NF-kB and the subsequent pro-inflammatory cytokines is present, coinciding with increased expression of IKK genes that degrade IkB, allowing NF-kB to translocate to the nucleus and bind DNA response elements. An increase in the expression of IkB was also observed, which could be due to a feedback mechanism induced to replace molecules degraded by IKK enzymes.

To elucidate any differences in the effects of our treatments, I compared treatment of TLR7 stimulated BMDM with NISV **(App. 25)** to treatment with dexamethasone **(App. 27) (Fig. 83).** Whilst a common feature of both treatments include downregulation of MyD88, there are differences in the effect of NISV and dexamethasone. Notably, NISV can significantly downregulate transcripts of TLR7 and TLR8, as well as TRAF3 and Ikkε, whereas this effect is absent in the dexamethasone + TLR7 group. In contrast, an increase in TLR 7 transcripts induced both by dexamethasone alone, and dexamethasone + TLR7 was observed. Interestingly, whilst TRAF3 is downregulated by NISV, no changes in IRF3 or IRF7 was observed, whereas the opposite is true of dexamethasone: no effect on TRIF, TRAF, or IKKε/TBK1 complex, but a decrease in IRF7 transcripts. Whilst it is possible that downregulation of IRF7 is caused by dexamethasone's effect on MyD88, (stronger) downregulation of MyD88 in the NISV + TLR7 group was also observed.

Extending this analysis to TLR8 stimulated BMDM **(Fig. 84),** some differences when compared with the TLR7 stimulated groups were noted. NISV **(App. 26)** do not downregulate TLR7 or TLR8 expression or decrease transcripts of TRAF3. However, NISV's effect on MyD88 and Ikkε is maintained. Interestingly, there is a downregulation of IRF7 and IRF3 despite no significant change in TRAF3 expression, and this contrasts with IRF5 which displays increased expression in the NISV + TLR8 group when compared with the TLR8 alone group. Comparing these results to TLR8 stimulated BMDM treated with dexamethasone **(App. 28)**, we note that dexamethasone can also significantly downregulate IRF7. Otherwise, there are no significant changes to this pathway imparted by a combination of TLR8 stimulation and dexamethasone, outside of the upregulation of TLR7 which was also observed in the dexamethasone + TLR7 group.

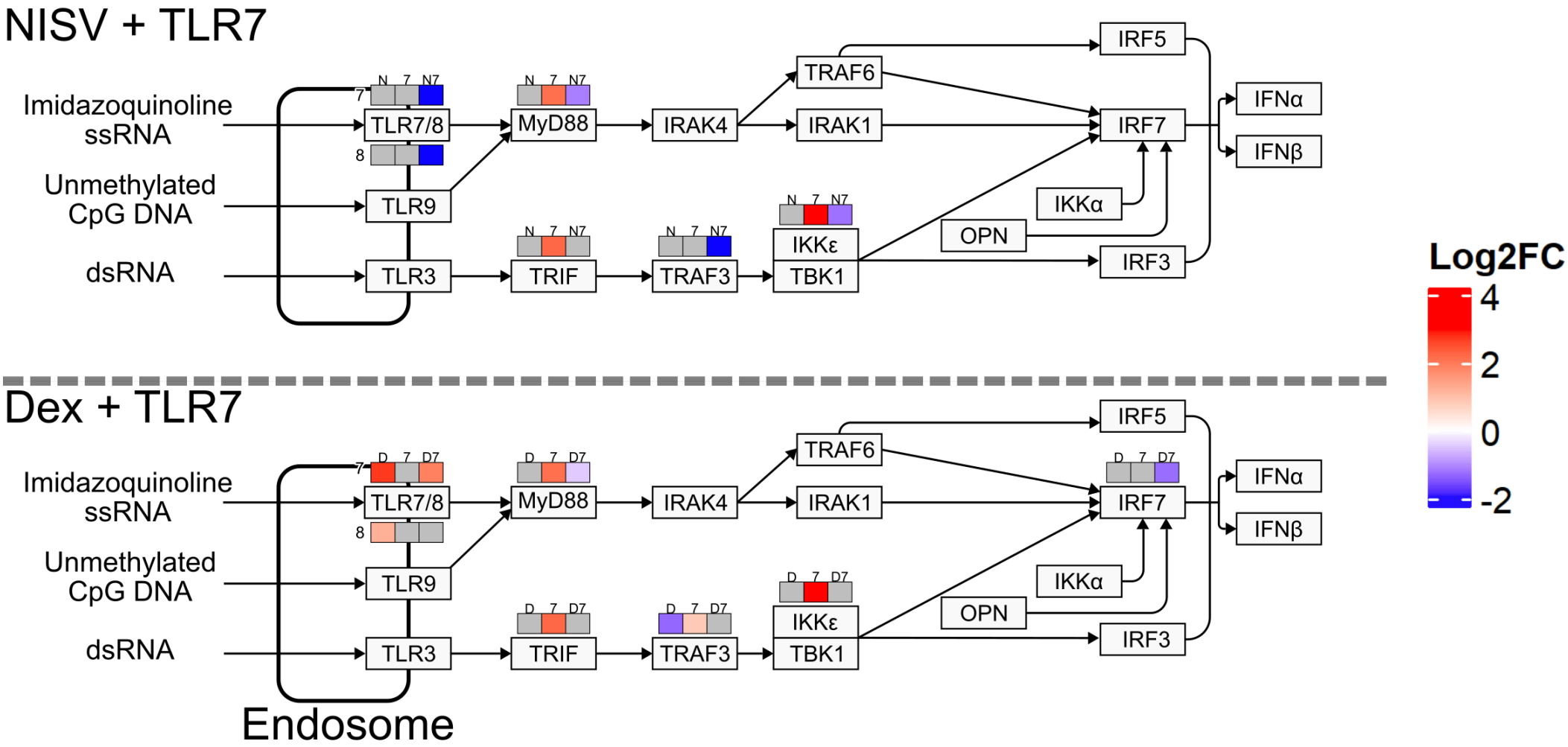

Figure 83: Significant changes in expression of genes involved in endosomal TLR signalling in TLR7 stimulated BMDM. *Differential gene expression analysis was performed on BMDM stimulated with TLR7 and treated with either NISV or dexamethasone. Log2FC was calculated for each group as follows: NISV (N), dexamethasone (D), and TLR7 (7) groups were compared with unstimulated BMDM given media alone, NISV + TLR7 (N7), and dexamethasone + TLR7 (D7) groups were compared with TLR7 stimulated BMDM with no treatment. Values in red indicate an increase in transcripts vs control, values in blue indicate a decrease in transcripts vs control, and grey values indicate missing /not significant values. Significance determined as $p < 0.05$ using Benjamini-Hochberg FDR adjusted p values.*

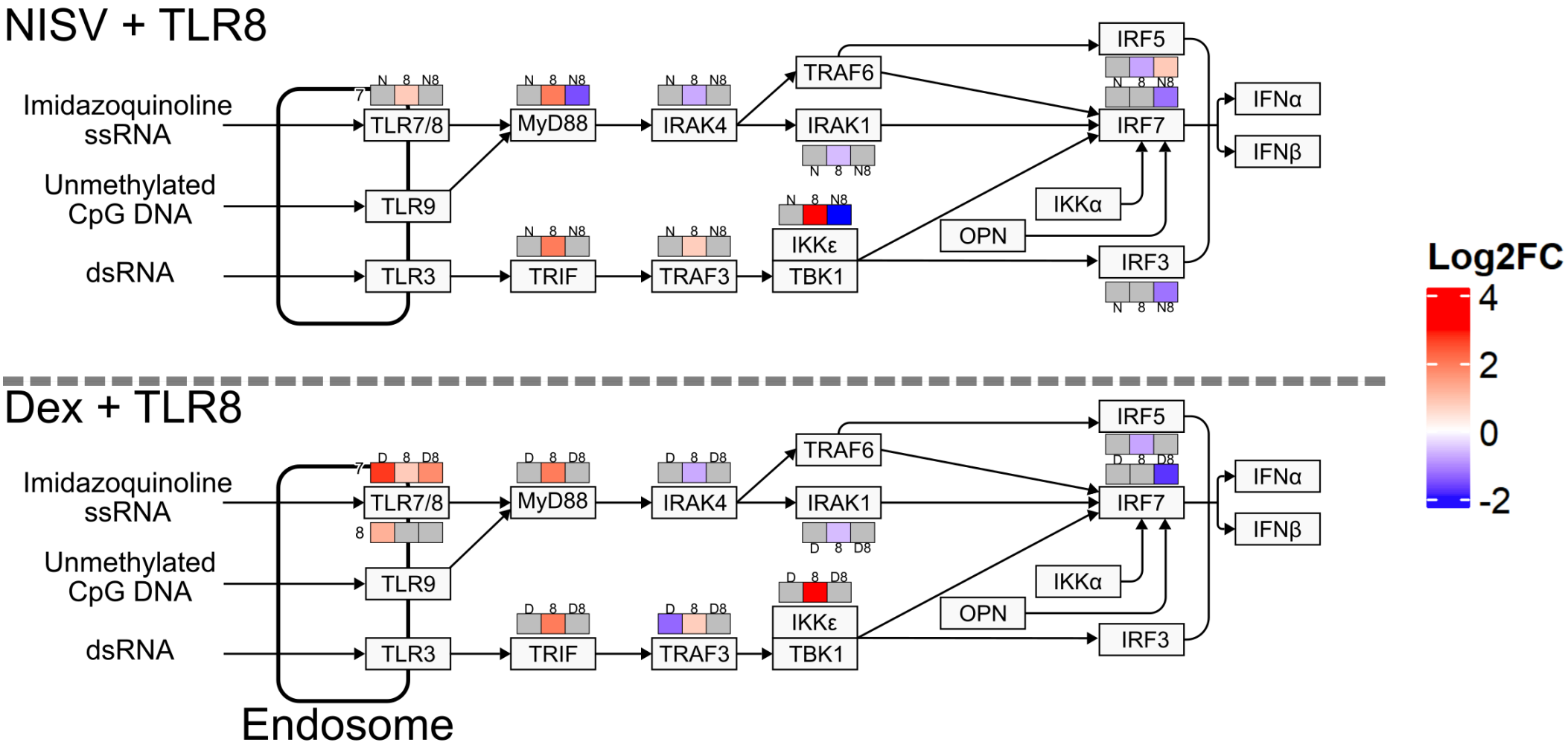

Figure 84: Significant changes in expression of genes involved in endosomal TLR signalling in TLR8 stimulated BMDM. *Differential gene expression analysis was performed on BMDM stimulated with TLR8 and treated with either NISV or dexamethasone. Log2FC was calculated for each group as follows: NISV (N), dexamethasone (D), and TLR8 (8) groups were compared with unstimulated BMDM given media alone, NISV + TLR8 (N8), and dexamethasone + TLR8 (D8) groups were compared with TLR8 stimulated BMDM with no treatment. Values in red indicate an increase in transcripts vs control, values in blue indicate a decrease in transcripts vs control, and grey values indicate missing /not significant values. Significance determined as $p < 0.05$ using Benjamini-Hochberg FDR adjusted p values.*

Whilst this analysis primarily investigates the endosomal TLR pathways, which utilise IRFs as their transcription factor, the aim was also to investigate NF-kB and IL-1 release. Previously, the ability of NISV to downregulate many cytokines has been identified, whilst a consistent feature of our cytometric bead array analysis was increased IL-1a and IL-1b in the supernatant of our TLR stimulated BMDM. Furthermore, previous work in our laboratory has identified NISV as potential modulators of NF-kB using similar methods and TLR4 stimulation, and thus, I aimed to compare my findings with these data.

6.4.3.2 NISV effect NF-kB through IKKε and modulate IL-1 transcription through the NLRP3 inflammasome

To present this data I opted to include the canonical pathway of NF-kB activation, as well as activation of the NLRP3 inflammasome and IL-1 release. I also chose to include the JAK/STAT pathway activated after IFNAR ligation as this contributes to the production of caspase 11 for the cleavage of gasdermin D.

The effect of NISV alone **(Fig. 85 - 86)** displays very few significant perturbations in the canonical pathway of NF-kB activation, with only upregulation of NEMO (Inhibitor of Nuclear Factor Kappa B Kinase Regulatory Subunit Gamma) detected. A similar trend was observed for unstimulated BMDM treated with dexamethasone alone, as only upregulation of IkBα, and the p65 subunit of NF-kB was recorded. When measuring transcript levels of TLR7 stimulated BMDM **(Fig. 85),** as expected, a significant increases in transcript levels of IFNAR1, IFNAR2, NEMO, STAT1, STAT2, IkBα, and both the p50 and p65 subunits of NF-kB was observed. Furthermore, a subsequent increase in NLRP3 and caspase 1 expression was also observed Whilst I accurately present NF-kB as an inducer of NLRP3 expression, it should be noted that NLRP3 and other inflammasomes can also activate NF-kB themselves. Alongside this activation of the inflammasome, there is an upregulation in both IL1A and IL1B expression. The above effects were also noted after TLR8 stimulation **(Fig. 86)** with the inclusion of increased JAK1, and the canonical IKK complex expression.

In contrast to the clear activation of this pathway by TLR stimulation, a significant decrease in many of the transcripts when NISV treatment is applied to the stimulated cells was also observed, such as: IFNAR2, STAT1, STAT2, IKKβ IkBα, both NF-kB subunits p50 and p65, NLRP3, ASC, and caspase 1. A decrease in expression for IL-1α and IL-1β was also observed. This implies that NISV can inhibit the production of the leaderless cytokines at the transcriptional level, much like those cytokines that include a signal peptide. A transcript that deviates from the overall downregulation imparted by NISV is NEMO. With upregulation of NEMO, the IKK complex cannot degrade IkBα and thus NF-kB remains inhibited, unable to translocate to the nucleus and bind target response elements to initiate transcription.

Dexamethasone treatment also displays some significant downregulation of this pathway, namely: STAT1, STAT2, IkBα, p50, and p65. Alongside this upregulation of NEMO as seen in the NISV treated samples was also observed. Whilst dexamethasone treatment does cause broad decreases in cytokine production, the transcriptional effects of NISV may be somewhat stronger, and may target multiple transcription factors.

Whilst outside the scope of this thesis, investigation of other transcription factors, alternative pathways of NF-kB, and inflammasome activation may yield interesting results that could assist in elucidation of the precise mechanism of NISV action.

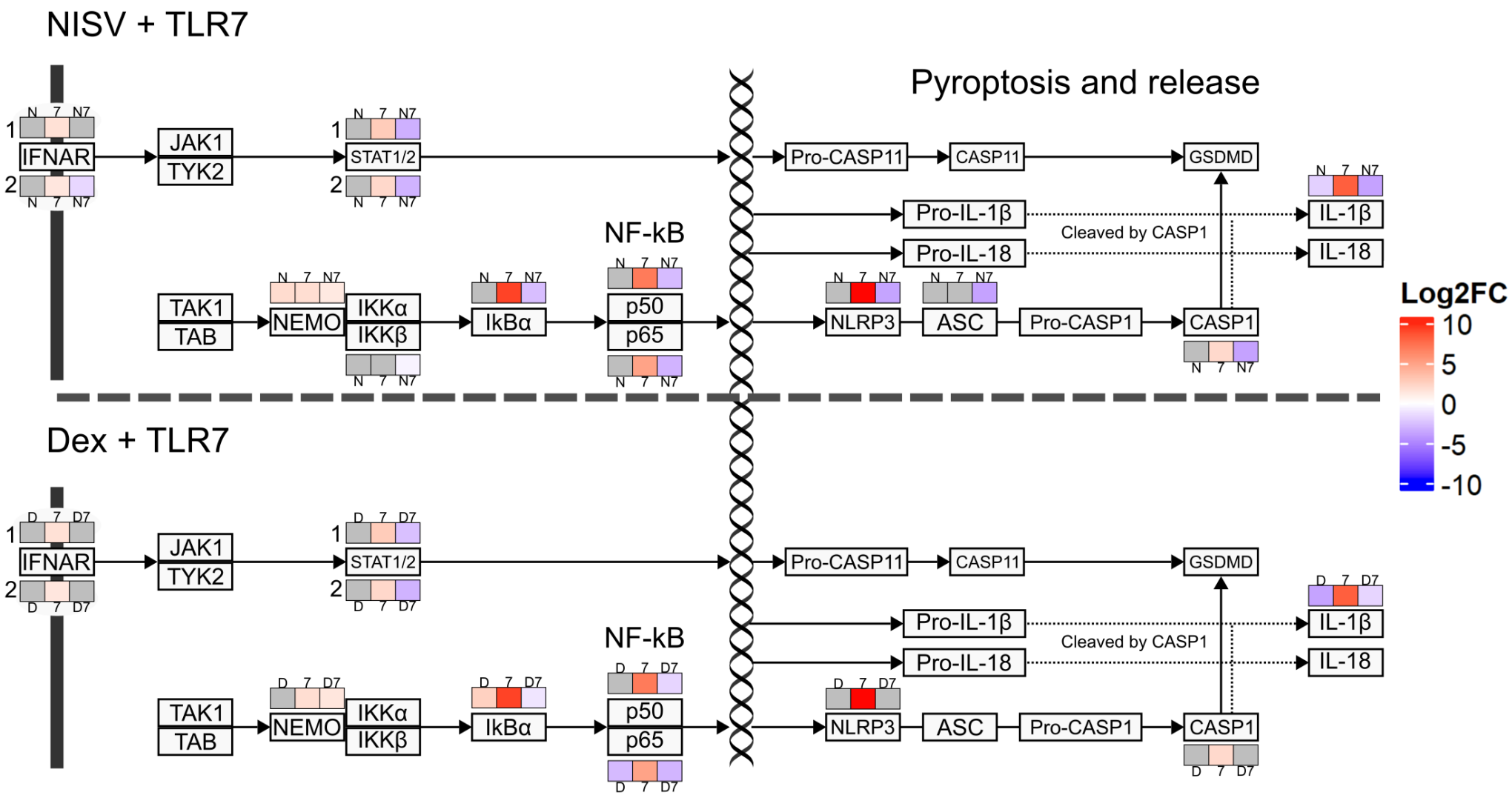

Figure 85: Significant changes in expression of genes involved in NF-kB signalling and IL-1 release in TLR7 stimulated BMDM.

Differential gene expression analysis was performed on BMDM stimulated with TLR7 and treated with either NISV or dexamethasone. Log2FC was calculated for each group as follows: NISV (N), dexamethasone (D), and TLR7 (7) groups were compared with unstimulated BMDM given media alone, NISV + TLR7 (N7), and dexamethasone + TLR7 (D7) groups were compared with TLR7 stimulated BMDM with no treatment. Values in red indicate an increase in transcripts vs control, values in blue indicate a decrease in transcripts vs control, and grey values indicate missing /not significant values. Significance determined as $p < 0.05$ using Benjamini-Hochberg FDR adjusted p values.

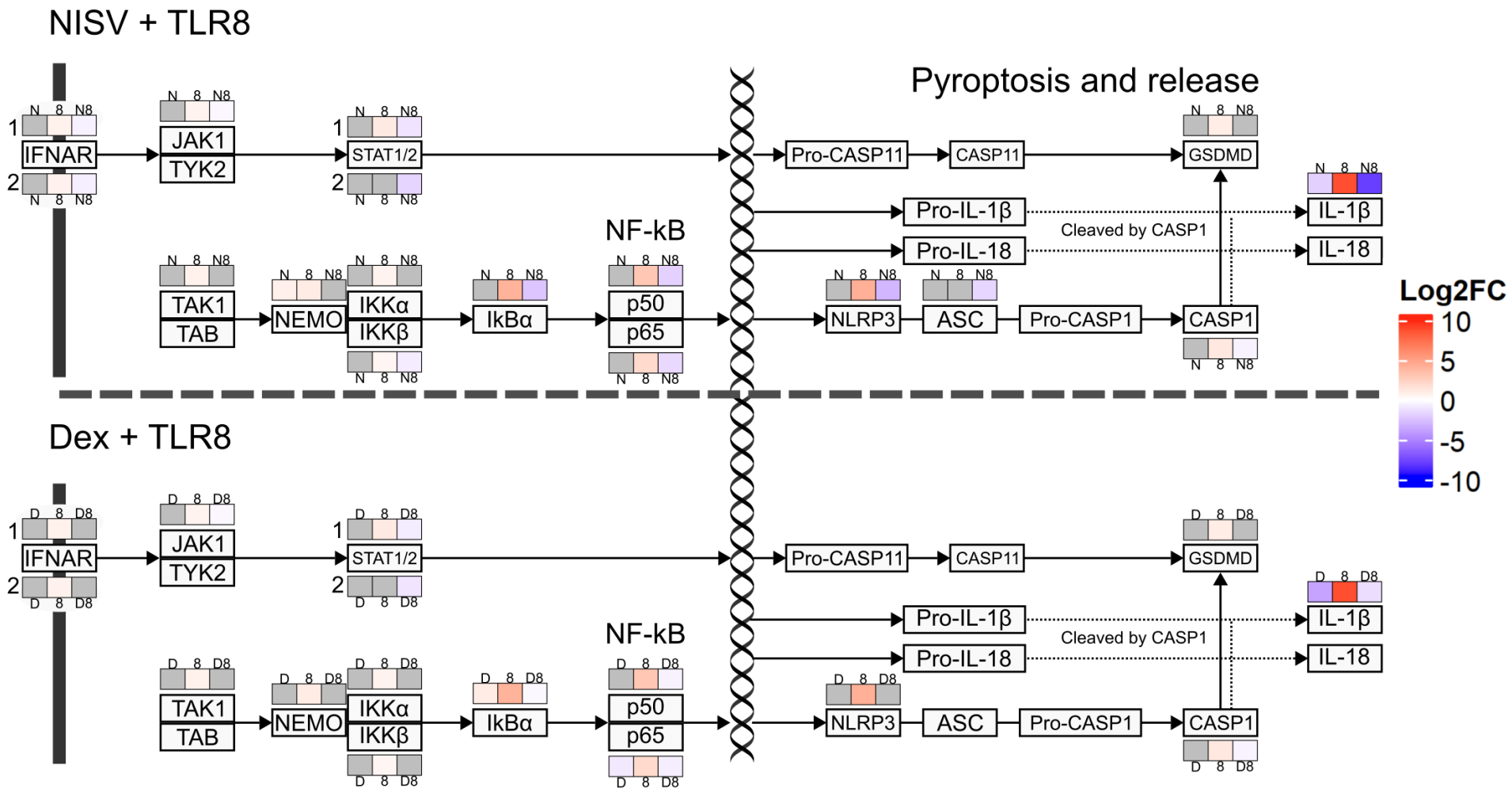

Figure 86: Significant changes in expression of genes involved in NF-kB signalling and IL-1 release in TLR8 stimulated BMDM.

Differential gene expression analysis was performed on BMDM stimulated with TLR8 and treated with either NISV or dexamethasone. Log2FC was calculated for each group as follows: NISV (N), dexamethasone (D), and TLR8 (8) groups were compared with unstimulated BMDM given media alone, NISV + TLR8 (N8), and dexamethasone + TLR8 (D8) groups were compared with TLR8 stimulated BMDM with no treatment. Values in red indicate an increase in transcripts vs control, values in blue indicate a decrease in transcripts vs control, and grey values indicate missing /not significant values. Significance determined as $p < 0.05$ using Benjamini-Hochberg FDR adjusted p values.

6.5 Discussion

As with all “omics” data, analysis can be a challenge due to the large datasets, and thus, computational power required to perform data manipulation and statistical analysis. To overcome these problems, a number of cloud-based services are available that incorporate well known software packages that have been developed in the R environment, or python, etc. One such service used in this thesis is the galaxy project, a web-based platform that aims to increase reproducibility in bioinformatics by providing a platform for processing data, generating workflows, and sharing analysis pipelines with the broader bioscience community. Benefits of this methodology include centrally maintained and updated tools, extensive guides and recommendations, and a wide variety of processing options. Thus, it should be noted that the analysis presented in this thesis represents a fraction of the possible routes that could be used to investigate transcriptional changes within this dataset. I hope to continually refine my analysis and dive deeper into the data to provide insight into multiple areas of NISV and dexamethasone interaction with TLR receptor stimulation. Best practices and optimal workflows will undoubtedly change this dataset continues to be examined.

Whilst PCA as a QC method has been used to visualise sample grouping and examine accuracy of replicates, PCA can also indicate the broad effects observed in each experimental group. For example, I observed that outside of close replicate grouping, media alone, dexamethasone alone, and NISV alone groups are found in close proximity, with TLR8 and TLR7 alone stimulated cells are separated from these treatments and controls. We also noted that NISV treatment of TLR7 and TLR8 stimulated cells localises closer to the media, NISV, and dexamethasone alone samples. This observation broadly displays that NISV can return cell activity to that which is comparable to unstimulated cells whilst also having a relatively small effect when given alone.

Dexamethasone treatment of TLR7 and TLR8 stimulated cells displays sample localisation that is separate from the other groups and is quite distinct from both the TLR stimulated alone samples, and the treatment alone samples. In all groups, however, there is significant separation between those samples that received TLR7 and TLR8 stimulation, even when given the same treatment, reinforcing the idea that TLR7 and TLR8 have non-redundant and distinct downstream effects. Studies have demonstrated this idea in human PBMCs and have indicated that whilst TLR7 has been studied to a greater degree, TLR8 displays increased activation of the NF-kB pathway and thus pro-inflammatory cytokine signalling (ref). TLR7 has been more closely associated with production of type I interferons. It should

be noted however, that TLR7 and TLR8 expression levels and the downstream signalling effects of these TLR can vary by cell type, so expanding study of these receptors to T and B cells rather than just monocytes/macrophages may yield greater insight *(Bender, et al., 2020).*

The previous idea that NISV and dexamethasone alone have relatively minor effects on unstimulated cells is further reinforced by our volcano plots and heatmaps. Clearly, the number of genes significantly changing after treatment is low when compared to the TLR7 and TLR8 stimulated samples. Another notable observation in the data is that the most abundant transcripts tend towards those that display low log2FC values. One hypothesis is that these are the genes subject to greater turnover and may be involved in typical cell functioning and homeostasis. Likely these abundant transcripts are rate-limited by protein or mRNA decay, with high turnover proteins driving demand for gene expression to maintain homeostatic levels.

Outside of the holistic view of overall gene expression, I aimed to direct my analysis using tools such as gene ontology. Whilst this methodology can be applied to highlight the broad areas where transcripts are differentially expressed, the specificity of gene ontology can be hindered by the category redundancy. As mentioned previously, GO categories that may provide useful insight can often be masked by broad categories such as "immune response" as many genes will map to this category despite having more specific designations. Nonetheless, a targeted approach could be developed, by excluding categories, or by utilising tools such as GOrilla which provides a branching/nested “Ancestor" tree of categories. Due to the size of the dataset generated in this thesis, I aim to further explore this data using these alternate methodologies and filter down to more specific mechanisms in future.

Despite these clear drawbacks, the analysis did yield some interesting results, such as the interaction of NISV with lysosomes/lytic vacuole, alongside proteoglycan binding, protein heterodimerisation, and antioxidant activity. Examining these categories together, NISV effect on lysosomes and their antioxidant activity may reveal that NISV could be reducing oxidative stress and thus preserving lysosomes which can be damaged by free radicals (as can other membranes). Outside of their function in degradation of macromolecules, studies have revealed that lysosomes are involved in a range of processes critical to cell homeostasis including nutrient sensing, metabolite shuttling, maintaining ionic balance, and signalling between organelles *(Trivedi, et al., 2020).* Thus, the potential effect of NISV protecting lysosomes from degradation may be beneficial in a number of malignancies that

arise to due lysosomal dysfunction such as Niemann-Pick disease, and Gaucher disease *(Sun, 2018).*

Whilst GO terms associated with cell adhesion molecules were highlighted in both NISV and dexamethasone alone samples, it has been noted previously that dexamethasone can have inhibitory actions on cell adhesion molecules such as ICAM-1, LFA-1, and CD2 *(Goulding, et al., 1999; Wheller, and Perretti, 1997).*

After GO analysis, I opted to interrogate a variety of pathways available on KEGG using a custom workflow in Galaxy. Many of the pathways chosen for this analysis displayed a degree of redundancy in terms of individual genes, as there was overlap between the KEGG pathway annotations. For example, transcripts signalling pathway intermediates such as TRAF6 may be shared between multiple pathways *(Gohda, et al., 2004).* One benefit of this method was the ability to expand this analysis of KEGG pathways to as many or as little as we choose by simply editing the KEGG identifiers supplied to our workflow, and this can be utilised downstream to interrogate a broad array of processes or even disease states. Due to this, I opted to focus analysis on a few pathways for display, which included an examination of the cytokine and chemokine milieu that was affected.

Displaying only the significantly changed mediators, it was noted that whilst able to modulate CCL chemokines in TLR stimulated BMDM, NISV and dexamethasone alone did not induce significant alterations in these proteins. Interestingly, TLR7 nor TLR8 stimulation induced significant increases in CCL chemokine production, but combined TLR and treatment displayed a decrease in CCL expression. Elucidation of the mechanism of this effect of combined therapy and stimulation may be difficult as CCL chemokines are regulated at the transcriptional level by a variety of transcription factors such as NF-kB, AP-1, IRF1, IRF3, and IRF7.

In contrast, TLR7 and TLR8 stimulation did increase expression of the CCL chemokine receptors, the CCRs, whereas NISV and dexamethasone alone did not. As the effect of both treatments on stimulated cells resulted in very similar downregulation of these CCR, it is possible that a common mechanism is being exploited by these therapies.

It was also noted that NISV appeared to downregulate TLR induced transcription of IL cytokines more effectively than dexamethasone. Whilst both could inhibit expression of IL-1α, IL-1β, IL-6, IL-10, IL-12, and IL-15, NISV could decrease transcripts of IL-18, IL-19, IL-23, IL-27 and IL-34. These NISV-affected cytokines are involved in the polarisation and promotion of T cells and macrophages, with a generally mixed effect on inflammation. Decreased IL-18 production can reduce the production of IFNy and therefore reduce the Th1 response and cytotoxic CD8+ T cell activation (ref). Typically, this effect was achieved in

conjunction with IL-12, with the expression of the P40 subunit being downregulated by NISV *(Ihim, et al., 2022).* Alongside this there is a decrease in IL-23 which induces pro-inflammatory Th17 differentiation and activates macrophages *(Korta, et al., 2023).* Notably, the transcripts for genes encoding both subunits of IL-23 are downregulated, effectively abrogating production of the bioactive cytokine. On the other hand, some downregulation of transcripts for IL-27 is observed, which can inhibit the Th17 response *(liu, and Rohowsky-Kochan, 2011).* Other pro-inflammatory effects include downregulation of IL-19, a member of the IL-10 superfamily that promotes the Th2 response and polarisation of macropahges towards an M2 phenotype *(Horiuchi, et al., 2021).* Finally, IL-34 can bind to the CSF-1 receptor, which promotes expansion and survival of mononuclear phagocytes, and thus lower expression of this cytokine may inhibit macrophage differentiation *(Lelios, et al. 2020).* Ultimately, the effect of NISV is TLR dependent, and thus NISV can elicit pro-inflammatory responses with TLR7 and TLR8 stimulation, whereas NISV display anti-inflammatory properties in TLR3 and TLR4 stimulation scenarios. Thus, it is clear NISV are immunomodulatory, rather than solely anti-inflammatory.

When examining the endosomal TLR signalling pathways we noted that in both TLR7 and TLR8 stimulation scenarios, MyD88 transcripts were decreased, as were transcripts for Ikkε. Whilst dexamethasone could also decrease MyD88 transcripts in TLR7 stimulated BMDM, the decrease in gene expression was much weaker than in NISV treated cultures. Previous work in our laboratory using TLR4 stimulation is in good agreement with this data, also displaying the downregulation of MyD88 *(McGahon, 2021).* Clearly, downregulation of the adaptor protein that links the TIR domain of the TLR to the IRAK complex serves to inhibit the downstream cascade of the TLR signalling pathway by effectively catching the signal early. Alongside this, the decrease in transcripts for the non-canonical Ikkε reduces the degradation of IkBα, sequestering NF-kB in the cytoplasm. Decreased transcription of IkBα, is observed which may be explained as lower IkBα turnover as it is no longer being degraded. However, experiments targetting this process closely may be needed to elucidate the transcriptional regulation and interaction of these proteins.

It was also demonstrated here that whilst in previous experiments an increase in IL-1α and IL-1β in the supernatant of cells stimulated with various TLR and treated with NISV had been observed, transcripts for both of these cytokines are decreased by NISV in TLR7 and 8 treated cultures. As mentioned previously, these leaderless cytokines are processed differently from the typical route of cytokine transcription and secretion, instead being stored as a pro-protein which is then cleaved as needed. Instead of exocytosis via the typical Golgi-ER route, they instead exit through pores generated by gasdermin D during a form of cell death known as pyroptosis. The data indicates that it is likely that IL-1 cytokines detected in

our supernatant are likely the stored proteins, and longitudinal study of cells treated with NISV and the supernatant removed and replaced with fresh media would contain no IL-1α or IL-1β as they are transcriptionally downregulated by decreased NF-kB activity. Alongside this hypothesis, it is likely that this downregulation of NF-kB contributes to a decrease in the NLRP3 subunit of the non-canonical inflammasome required to cleave IL-1β. Furthermore, despite downregulation of STAT1/2 there is no effect on caspase 11 transcripts, or that of gasdermin D, reinforcing the NF-kB hypothesis.

Interestingly, dexamethasone treatment appeared to have a fairly minor effect on endosomal TLR signalling but did display consistent upregulation of TLR7 expression. This effect was observed both with dexamethasone alone and in conjunction with either TLR7 or TLR8 stimulation. Studies have indicated that in patients with systemic lupus erythramatosus, chronic activation of TLR7 by self-antigens (endogenous RNA) decreases glucocorticoid efficacy. As this resistance seems to be independent of GR and NF-kB mRNA levels, our data indicates that this effect may in part be due to exacerbated expression of TLR7 by glucocorticoids such as dexamethasone *(Melo, et al., 2013; Guiducci, et al., 2010).*

Another effect of dexamethasone consistent across both TLR stimulation scenarios was the downregulation of IRF7. As both the IKKε/TBK1 complex downstream of TRIF, and IRAK1/TRAF6 pathway is unaffected by dexamethasone treatment, it is difficult to elucidate how dexamethasone is directly affecting IRF7. Studies utilising data gathered from Covid-19 patients treated with dexamethasone corroborate this finding, also noting negative effects on IRF7 and the subsequent decrease in ISG transcription followed by decreased interferon production *(Engel, et al., 2023).* Disruption of cytokine production by dexamethasone's effects on NF-kB or through binding the GRE on DNA may induce a break in the autocrine signalling needed for IRF7 activation, although further study is needed to investigate this avenue. It should be noted that IRF7 is constitutively expressed in BMDM, but not in other bone marrow derived APC such as dendritic cells. Studies have demonstrated that basal interferon signalling through IFNAR and STAT1 signalling is required for expression of IRF7, indicating that dexamethasone may utilise this mechanism *(Sin et al., 2020).* The data does not display an effect on IFNAR1 or IFNAR2 by dexamethasone, although a decreased STAT1 in the dexamethasone and TLR7 stimulated group is observed.

7 Conclusions and future work

Whilst the data presented in this thesis builds upon a strong foundation of NISV as an anti-inflammatory, I believe that NISV can fill multiple scientific niches that some conventional immunosuppressing drugs such as dexamethasone may not.

Chiefly it has been demonstrated that whilst previously, modulation of pro-inflammatory cytokines by NISV has been studied using other TLR, our approach in focusing on the viral-sensing endosomal TLR7 and TLR8 receptors helps to further qualify the multi-faceted activity of these vesicles. By replicating previous data using NISV, LPS and Poly(I:C) to stimulate TLR4 and TLR3 and comparing this to TLR7 and TLR8 stimulated macrophages, I highlight that NISV have differential effects on cytokine production dependent on the TLR stimulation being used, but broadly downregulate many pro-inflammatory genes at the transcriptional level. Furthermore, I have demonstrated that the overall effect of NISV is not size dependent but may increase potency of the treatment through increased NISV uptake. Future experiments utilising confocal microscopy and fluorescently tagged vesicles may shed light on the uptake of NISV into macrophages. Alongside this, mixed cultures may be used to determine if there is preferentially uptake of NISV by various cell types. This may be achieved with flow cytometry and confirmed with confocal microscopy. To further characterise NISV uptake, fluorescent NISV paired with IVIS imaging may reveal tissues where NISV accumulate *in vivo*, which may be confirmed with histological methods. This route of investigation may also shed light on the increased IL-1 release observed in our data: potential size-dependent disruption of the plasma membrane by NISV may be attributed to increased release of these pre-stored alarmin cytokines, something which could simultaneously be investigated using the above methods.

In our comparison to dexamethasone, we noted that IL-12 was resistant to modulation at concentrations previously effective with other cytokines. As glucocorticoid resistance is relevant to a number of malignancies, it would be of interest to utilise a combined therapy of NISV and dexamethasone to determine any potential benefit. As dexamethasone shares a similar steroid structure to that of cholesterol, NISV could be made that incorporate dexamethasone into the membrane, which could be compared with a mix of free dexamethasone and NISV, dexamethasone entrapped within NISV and dexamethasone/NISV alone.

A challenge encountered during our metabolomic analysis was the large spread of our media alone control samples. A simple improvement to our methodology would be to increase the

number of replicates to between 5-10 for each group. As the metabolomic data leaves questions concerning the Warburg effect, we may utilise a targeted approach by peak matching to a selection of custom compounds selected by our lab. Furthermore, as it appears that NISV have a significant effect on lipid metabolism, future studies could incorporate lipidomics into the analysis.

As mentioned, the transcriptomic data presented in this thesis represents a small area of the total dataset, which I aim to continue to analyse. Focusing on other transcription factors such as AP-1 may yield greater insight into the mechanism of action of NISV. It was noted that NISV appear to downregulate cytokine production at the transcriptional level in TLR7 and TLR8 stimulated BMDM, although this is not reflected in our cytokine assays when compared with TLR3 and TLR4 stimulate BMDM. A key difference in these TLR pathways is the use of TRIF as an adaptor protein. As demonstrated, NISV downregulate transcripts for MyD88, which is exclusively used by TLR7 and TLR8, with TLR4 using both MyD88 and TRIF, TLR3 using TRIF alone. Therefore, NISV may influence cytokine production through a mechanism unrelated to MyD88. Inclusion of another MyD88 dependent TLR such as TLR2 or TLR9 may help to further highlight differences in NISV effect independent of this adaptor protein. Outside of effects on MyD88, it has been demonstrated that NISV affect NF-kB through weak downregulation of the canonical IKK complex and strong downregulation of the non-canonical IKKε complex, thus reducing the degradation of the inhibitor of NF-kB, IkBα. In comparison to dexamethasone, it is noted that whilst NF-kB is affected by the corticosteroid drug, there is no significant interaction of dexamethasone with IKKε. Alongside this dexamethasone has no effect on activation of the non-canonical NLRP3 inflammasome, whereas NISV does, highlighting the multi-modal effect of NISV downregulation.

Ultimately, this thesis relies on *in vitro* data using TLR agonists to examine the potential benefits of NISV as a treatment for viral sepsis. Further *in vitro* investigations using an ssRNA virus like the well-studied Semliki Forest virus may yield greater insight into the dynamics of a viral infection and how NISV may interact with this, particularly the metabolic restructuring imposed by viral replication. Comparison to dexamethasone could be further investigated using *in vivo* studies, as physiological side effects of chronic steroid use are an important factor in the treatment of many inflammatory diseases for which they are prescribed. From the preliminary data generated here, NISV's modest effect on cellular metabolism may indicate fewer side effects than that of dexamethasone.

Clearly, I have demonstrated that NISV alone can have potent effects *in vitro* not only when supplied to resting macrophages but also as an immunomodulatory treatment for TLR7 and TLR8 stimulated cells. Further studies, importantly in vivo to determine the effects of NISV

on transcription and metabolism of inflammatory mediators induced with different infections and inflammatory stimuli are required.

8 References

1. Abidi, E. et al. (2022) 'Tocilizumab and COVID-19: Timing of Administration and Efficacy'. Frontiers in Pharmacology, 13.

2. Abugroun, A. et al. (2021) 'Impact of Malnutrition on Hospitalization Outcomes for Older Adults Admitted for Sepsis'. The American Journal of Medicine, 134 (2), pp. 221-226.

3. Abumayyaleh, M. et al. (2021) 'Sepsis of Patients Infected by SARS-CoV-2: Real-World Experience From the International HOPE-COVID-19-Registry and Validation of HOPE Sepsis Score'. Frontiers in Medicine (Lausanne), 8, 728102.

4. Adams, M.D. et al. (2000) 'The genome sequence of Drosophila melanogaster'. Science, 287 (5461), pp. 2185-2195.

5. Aderem, A.A. and Underhill, D.M. (1999) 'MECHANISMS OF PHAGOCYTOSIS IN MACROPHAGES'. Annual Review of Immunology, 17 (1), pp. 593-623.

6. Afonina, I.S. et al. (2015) 'Proteolytic Processing of Interleukin-1 Family Cytokines: Variations on a Common Theme'. Immunity, 42 (6), pp. 991-1004.

7. Akbarzadeh, A. et al. (2013) 'Liposome: classification, preparation, and applications'. Nanoscale Research Letters, 8 (1), 102.

8. Akira, S., Uematsu, S. and Takeuchi, O. (2006) 'Pathogen Recognition and Innate Immunity'. Cell, 124 (4), pp. 783-801.

9. Albanesi, C., Cavani, A. and Girolomoni, G. (1998) 'Interferon-gamma-stimulated human keratinocytes express the genes necessary for the production of peptide-loaded MHC class II molecules'. Journal of Investigative Dermatology, 110 (2), pp. 138-142.

10. Alcami, A. and Koszinowski, U.H. (2000) 'Viral mechanisms of immune evasion'. Immunology Today, 21 (9), pp. 447-455.

11. Andar, A.U. et al. (2014) 'Microfluidic Preparation of Liposomes to Determine Particle Size Influence on Cellular Uptake Mechanisms'. Pharmaceutical Research, 31 (2), pp. 401-413.

12. Arango Duque, G. and Descoteaux, A. (2014) 'Macrophage cytokines: involvement in immunity and infectious diseases'. Frontiers in Immunology, 5, 491.

13. Arnold, P.K. and Finley, L.W.S. (2023) 'Regulation and function of the mammalian tricarboxylic acid cycle'. Journal of Biological Chemistry, 299 (2), p. 102838.

14. Ashraf, U.M. et al. (2021) 'SARS-CoV-2, ACE2 expression, and systemic organ invasion'. Physiological Genomics, 53 (2), pp. 51-60.

15. Aston, W.J. et al. (2019) 'Dexamethasone differentially depletes tumour and peripheral blood lymphocytes and can impact the efficacy of chemotherapy/checkpoint blockade combination treatment'. Oncoimmunology, 8 (11), p. e1641390.

16. Attia, I.A. et al. (2007) 'Influence of a niosomal formulation on the oral bioavailability of acyclovir in rabbits'. AAPS PharmSciTech, 8 (4), pp. 206-212.

17. Baillie, A.J. et al. (1985) 'The preparation and properties of niosomes--non-ionic surfactant vesicles'. Journal of Pharmacy and Pharmacology, 37 (12), pp. 863-868.

18. Baltimore, D. (1971) 'Expression of animal virus genomes'. Bacteriological Reviews, 35 (3), pp. 235-241.

19. Bangham, A.D., Standish, M.M. and Watkins, J.C. (1965) 'Diffusion of univalent ions across the lamellae of swollen phospholipids'. Journal of Molecular Biology, 13 (1), pp. 238-252.

20. Baranov, M.V. et al. (2021) 'Modulation of Immune Responses by Particle Size and Shape'. Frontiers in Immunology, 11.

21. Barreiro, L.B. et al. (2009) 'Evolutionary dynamics of human Toll-like receptors and their different contributions to host defense'. PLoS Genetics, 5 (7), p. e1000562.

22. Barton, G.M. and Kagan, J.C. (2009) 'A cell biological view of Toll-like receptor function: regulation through compartmentalization'. Nature Reviews Immunology, 9 (8), pp. 535-542.

23. Batah, S.S. and Fabro, A.T. (2021) 'Pulmonary pathology of ARDS in COVID-19: A pathological review for clinicians'. Respiratory Medicine, 176, 106239.

24. Batzri, S. and Korn, E.D. (1973) 'Single bilayer liposomes prepared without sonication'. Biochimica et Biophysica Acta (BBA) - Biomembranes, 298 (4), pp. 1015-1019.

25. Bekhbat, M., Rowson, S.A. and Neigh, G.N. (2017) 'Checks and balances: The glucocorticoid receptor and NFκB in good times and bad'. Frontiers Neuroendocrinology, 46, pp. 15-31.

26. Bender, A.T. et al. (2020) 'TLR7 and TLR8 Differentially Activate the IRF and NF-κB Pathways in Specific Cell Types to Promote Inflammation'. ImmunoHorizons, 4 (2), pp. 93-107.

27. Bojkova, D. et al. (2021) 'Targeting the Pentose Phosphate Pathway for SARS-CoV-2 Therapy'. Metabolites, 11 (10), 669.

28. Bovijn, C. et al. (2012) 'Identification of interaction sites for dimerization and adapter recruitment in Toll/interleukin-1 receptor (TIR) domain of Toll-like receptor 4'. Journal of Biological Chemistry, 287 (6), pp. 4088-4098.

29. Brewer, J.M. and Alexander, J. (1992) 'The adjuvant activity of non-ionic surfactant vesicles (niosomes) on the BALB/c humoral response to bovine serum albumin'. Immunology, 75 (4), pp. 570-575.

30. Brewer, J.M. and Alexander, J. (1994) 'Studies on the adjuvant activity of non-ionic surfactant vesicles: adjuvant-driven IgG2a production independent of MHC control'. Vaccine, 12 (7), pp. 613-619.

31. Brewer, J.M. et al. (2004) 'Vesicle Size Influences the Trafficking, Processing, and Presentation of Antigens in Lipid Vesicles'. The Journal of Immunology, 173 (10), pp. 6143-6150.

32. Burns, J.S. and Manda, G. (2017) 'Metabolic Pathways of the Warburg Effect in Health and Disease: Perspectives of Choice, Chain or Chance'. International Journal of Molecular Sciences, 18 (12), 2755

33. Canna, S.W. and Behrens, E.M. (2012) 'Making sense of the cytokine storm: a conceptual framework for understanding, diagnosing, and treating hemophagocytic syndromes'. Pediatric Clinics of North America, 59 (2), pp. 329-344.

34. Cannon, G.J. and Swanson, J.A. (1992) 'The macrophage capacity for phagocytosis'. Journal of Cell Science, 101 (4), pp. 907-913.

35. Canton, J. (2018) 'Macropinocytosis: New Insights Into Its Underappreciated Role in Innate Immune Cell Surveillance'. Frontiers in Immunology, 9, 2286.

36. Canton, M. et al. (2021) 'Reactive Oxygen Species in Macrophages: Sources and Targets'. Frontiers in Immunology, 12, 734229.

37. Carlson, C.J. et al. (2022) 'Climate change increases cross-species viral transmission risk'. Nature, 607 (7919), pp. 555-562.

38. Carroll, D. et al. (2018) 'The Global Virome Project'. Science, 359 (6378), pp. 872-874.

39. Carugo, D. et al. (2016) 'Liposome production by microfluidics: potential and limiting factors'. Scientific Reports, 6, 25876.

40. Casella, G. et al. (2016) 'IL4 induces IL6-producing M2 macrophages associated to inhibition of neuroinflammation in vitro and in vivo'. Journal of Neuroinflammation, 13 (1). 139.

41. Chandel, N.S. (2021) 'Lipid Metabolism'. Cold Spring Harbor Perspectives in Biology, 13 (9), a040576.

42. Chang, C.H. et al. (2013) 'Circulating interleukin-6 level is a prognostic marker for survival in advanced nonsmall cell lung cancer patients treated with chemotherapy'. International Journal of Cancer, 132 (9), pp. 1977-1985.

43. Chen, I.-C. et al. (2011) 'Rapid Range Shifts of Species Associated with High Levels of Climate Warming'. Science, 333 (6045), pp. 1024-1026.

44. Chen, L. et al. (2019) 'NADPH production by the oxidative pentose-phosphate pathway supports folate metabolism'. Nature Metabolism, 1 (3), pp. 404-415.

45. Chen, L.Y.C. et al. (2020) 'Confronting the controversy: interleukin-6 and the COVID-19 cytokine storm syndrome'. European Respiratory Journal, 56 (4), 2003006.

46. Chen, P. et al. (2023) 'Metabolic alterations upon SARS-CoV-2 infection and potential therapeutic targets against coronavirus infection'. Signal Transduction and Targeted Therapy, 8 (1), 237.

47. Cheng, S.-C., Joosten, L.A.B. and Netea, M.G. (2014) 'The interplay between central metabolism and innate immune responses'. Cytokine & Growth Factor Reviews, 25 (6), pp. 707-713.

48. Choi, S.H., Aid, S. and Bosetti, F. (2009) 'The distinct roles of cyclooxygenase-1 and -2 in neuroinflammation: implications for translational research'. Trends in Pharmacological Sciences, 30 (4), pp. 174-181.

49. Christian Isalomboto, N. et al. (2019) 'General Perception of Liposomes: Formation, Manufacturing and Applications'. In: Angel, C. (ed.) Liposomes. Rijeka: IntechOpen, Ch. 3.

50. Chu, J. et al. (2021) 'Pharmacological inhibition of fatty acid synthesis blocks SARS-CoV-2 replication'. Nature Metabolism, 3 (11), pp. 1466-1475.

51. Conacher, M., Alexander, J. and Brewer, J.M. (2001) 'Oral immunisation with peptide and protein antigens by formulation in lipid vesicles incorporating bile salts (bilosomes)'. Vaccine, 19 (20), pp. 2965-2974.

52. Coomes, E.A. and Haghbayan, H. (2020) 'Interleukin-6 in Covid-19: A systematic review and meta-analysis'. Reviews in Medical Virology, 30 (6), pp. 1-9.

53. Costela-Ruiz, V.J. et al. (2020) 'SARS-CoV-2 infection: The role of cytokines in COVID-19 disease'. Cytokine & Growth Factor Reviews, 54, pp. 62-75.

54. Crick, F.H. (1958) 'On protein synthesis'. Symp Soc Exp Biol, 12, pp.138-163.

55. Cunha, B.A. (2004) 'The cause of the plague of Athens: plague, typhoid, typhus, smallpox, or measles?'. Infectious Disease Clinics of North America, 18 (1), pp. 29-43.

56. Danaei, M. et al. (2018) 'Impact of Particle Size and Polydispersity Index on the Clinical Applications of Lipidic Nanocarrier Systems'. Pharmaceutics, 10 (2), 57.

57. de Araújo, G.C., Pardini, A. and Lima, C. (2023) 'The impact of comorbidities and COVID-19 on the evolution of community onset sepsis'. Scientific Reports, 13 (1), 10589.

58. De Bosscher, K., Vanden Berghe, W. and Haegeman, G. (2003) 'The Interplay between the Glucocorticoid Receptor and Nuclear Factor-κB or Activator Protein-1: Molecular Mechanisms for Gene Repression'. Endocrine Reviews, 24 (4), pp. 488-522.

59. Declercq, J., De Leeuw, E. and Lambrecht, B.N. (2022) 'Inflammasomes and IL-1 family cytokines in SARS-CoV-2 infection: from prognostic marker to therapeutic agent'. Cytokine, 157, 155934.

60. de Jong, M.D. et al. (2006) 'Fatal outcome of human influenza A (H5N1) is associated with high viral load and hypercytokinemia'. Nature Medicine, 12 (10), pp. 1203-1207.

61. D'Elia, R.V. et al. (2013) 'Targeting the “Cytokine Storm” for Therapeutic Benefit'. Clinical and Vaccine Immunology, 20 (3), pp. 319-327.

62. D'Elia, R.V. et al. (2019) 'Exploitation of the bilosome platform technology to formulate antibiotics and enhance efficacy of melioidosis treatments'. Journal of Controlled Release, 298, pp. 202-212.

63. Deretic, V., Saitoh, T. and Akira, S. (2013) 'Autophagy in infection, inflammation and immunity'. Nature Reviews Immunology, 13 (10), pp. 722-737.

64. Desquiret, V. et al. (2008) 'Mitochondrial effects of dexamethasone imply both membrane and cytosolic-initiated pathways in HepG2 cells'. The International Journal of Biochemistry & Cell Biology, 40 (8), pp. 1629-1641.

65. Devant, P. and Kagan, J.C. (2023) 'Molecular mechanisms of gasdermin D pore-forming activity'. Nature Immunology, 24 (7), pp. 1064-1075.

66. Dienz, O. and Rincon, M. (2009) 'The effects of IL-6 on CD4 T cell responses'. Clinical Immunology, 130 (1), pp. 27-33.

67. Doshi, R.H. et al. (2020) 'Monkeypox Rash Severity and Animal Exposures in the Democratic Republic of the Congo'. Ecohealth, 17 (1), pp. 64-73.

68. Dunkelberger, J.R. and Song, W.-C. (2010) 'Complement and its role in innate and adaptive immune responses'. Cell Research, 20 (1), pp. 34-50.

69. Eichhorn, T. et al. (2023) 'Infection with SARS-CoV-2 Is Associated with Elevated Levels of IP-10, MCP-1, and IL-13 in Sepsis Patients'. Diagnostics, 13 (6), 1069.

70. Elkhalifa, A.M.E. et al. (2023) 'Insight into Oncogenic Viral Pathways as Drivers of Viral Cancers: Implication for Effective Therapy'. Current Oncology, 30 (2), pp. 1924-1944.

71. Engel, J.J. et al. (2023) 'Dexamethasone attenuates interferon-related cytokine hyperresponsiveness in COVID-19 patients'. Frontiers in Immunology, 14, 1233318.

72. Epelman, S., Lavine, K.J. and Randolph, G.J. (2014) 'Origin and functions of tissue macrophages'. Immunity, 41 (1), pp. 21-35.

73. Epstein-Barash, H. et al. (2010) 'Physicochemical parameters affecting liposomal bisphosphonates bioactivity for restenosis therapy: Internalization, cell inhibition, activation of cytokines and complement, and mechanism of cell death'. Journal of Controlled Release, 146 (2), pp. 182-195.

74. Ezenwa, V.O. et al. (2006) 'Avian diversity and West Nile virus: testing associations between biodiversity and infectious disease risk'. Proceedings of the Royal Society B: Biological Sciences, 273 (1582), pp. 109-117.

75. Fadrosh, D.W. et al. (2014) 'An improved dual-indexing approach for multiplexed 16S rRNA gene sequencing on the Illumina MiSeq platform'. Microbiome, 2 (1), 6.

76. Fappi, A. et al. (2019) 'Skeletal Muscle Response to Deflazacort, Dexamethasone and Methylprednisolone'. Cells, 8 (5), 406.

77. Farhat, K. et al. (2008) 'Heterodimerization of TLR2 with TLR1 or TLR6 expands the ligand spectrum but does not lead to differential signaling'. Journal of Leukocyte Biology, 83 (3), pp. 692-701.

78. Ferrara, J.L., Abhyankar, S. and Gilliland, D.G. (1993) 'Cytokine storm of graft-versus-host disease: a critical effector role for interleukin-1'. Transplant Proceedings, 25 (1 Pt 2), pp. 1216-1217.

79. Flannagan, R.S., Jaumouillé, V. and Grinstein, S. (2012) 'The cell biology of phagocytosis'. Annual Review of Pathology, 7, pp. 61-98.

80. Franchi, L. et al. (2009) 'Function of Nod-like receptors in microbial recognition and host defense'. Immunological Reviews, 227 (1), pp. 106-128.

81. Frimpong, A. et al. (2022) 'Cytokines as Potential Biomarkers for Differential Diagnosis of Sepsis and Other Non-Septic Disease Conditions'. Frontiers in Cellular and Infection Microbiology, 12, 901433.

82. Fukuzumi, M. et al. (1996) 'Endotoxin-induced enhancement of glucose influx into murine peritoneal macrophages via GLUT1'. Infection and Immunity, 64 (1), pp. 108-112.

83. Gabay, C. (2006) 'Interleukin-6 and chronic inflammation'. Arthritis Research and Therapy, 8 (Suppl 2), S3.

84. Gabizon, A. et al. (1989) 'Systemic administration of doxorubicin-containing liposomes in cancer patients: a phase I study'. European Journal of Cancer and Clinical Oncology, 25 (12), pp. 1795-1803.

85. Gaudino, S.J. and Kumar, P. (2019) 'Cross-Talk Between Antigen Presenting Cells and T Cells Impacts Intestinal Homeostasis, Bacterial Infections, and Tumorigenesis'. Frontiers in Immunology, 10.

86. Gdowski, A. et al. (2018) 'Optimization and scale up of microfluidic nanolipomer production method for preclinical and potential clinical trials'. Journal of Nanobiotechnology, 16 (1), 12.

87. Gianchecchi, E. et al. (2022) 'Yellow Fever: Origin, Epidemiology, Preventive Strategies and Future Prospects'. Vaccines, 10 (3), 372.

88. Gibbs, W. (1873) 'A Method of Geometrical Representation of the Thermodynamic Properties of Substances by Means of Surfaces'. Transactions of the Conneticut Academy, 2, pp. 382-404.

89. Gibson, P.G., Qin, L. and Puah, S.H. (2020) COVID -19 acute respiratory distress syndrome (ARDS): clinical features and differences from typical pre-COVID-19 ARDS'. Medical Journal of Australia, 213 (2), 54.

90. Girdhar, K. et al. (2021) 'Viruses and Metabolism: The Effects of Viral Infections and Viral Insulins on Host Metabolism'. Annu Review of Virology, 8 (1), pp. 373-391.

91. Gohda, J., Matsumura, T. and Inoue, J.-i. (2004) 'Cutting Edge: TNFR-Associated Factor (TRAF) 6 Is Essential for MyD88-Dependent Pathway but Not Toll/IL-1 Receptor Domain-Containing Adaptor-Inducing IFN-β (TRIF)-Dependent Pathway in TLR Signaling1'. The Journal of Immunology, 173 (5), pp. 2913-2917.

92. Goluszko, P. and Nowicki, B. (2005) 'Membrane Cholesterol: a Crucial Molecule Affecting Interactions of Microbial Pathogens with Mammalian Cells'. Infection and Immunity, 73 (12), pp. 7791-7796.

93. Gorden, K.B. et al. (2005) 'Synthetic TLR Agonists Reveal Functional Differences between Human TLR7 and TLR8'. The Journal of Immunology, 174 (3), pp. 1259-1268.

94. Gouel-Chéron, A. et al. (2012) 'Early interleukin-6 and slope of monocyte human leukocyte antigen-DR: a powerful association to predict the development of sepsis after major trauma'. PLoS One, 7 (3), e33095.

95. Goulding, N.J. et al. (1999) 'The inhibitory effect of dexamethasone on lymphocyte adhesion molecule expression and intercellular aggregation is not mediated by lipocortin 1'. Clinical and Experimental Immunology, 118 (3), pp. 376-383.

96. Grant, R.L. et al. (1992) 'Evaluation of surfactant cytotoxicity potential by primary cultures of ocular tissues: I. Characterization of rabbit corneal epithelial cells and initial injury and delayed toxicity studies'. Toxicology, 76 (2), pp. 153-176.

97. Guo, Y., Cao, W. and Zhu, Y. (2019) 'Immunoregulatory Functions of the IL-12 Family of Cytokines in Antiviral Systems'. Viruses, 11 (9), 772.

98. Guo, Y. et al. (2022) 'Targeting TNF-α for COVID-19: Recent Advanced and Controversies'. Frontiers in Public Health, 10, 833967.

99. Handjani R.M., et al. (1989). 'Cosmetic and pharmaceutical compositions containing niosomes and a water-soluble polyamide, and a process for preparing these compositions'. US4830857A Available online: https://patents.google.com/patent/US4830857A/en#patentCitations (last cited: 11/05/23)

100. Hard, G.C. (1970) 'Some biochemical aspects of the immune macrophage'. British Journal of Experimental Pathology, 51 (1), pp. 97-105.

101. Hasan, M.Z. et al. (2021) 'SARS-CoV-2 infection initiates interleukin-17-enriched transcriptional response in different cells from multiple organs'. Scientific Reports, 11 (1), 16814.

102. Havasi, A. et al. (2022) 'Influenza A, Influenza B, and SARS-CoV-2 Similarities and Differences – A Focus on Diagnosis'. Frontiers in Microbiology, 13, 908525.

103. Haythorne, E. et al. (2019) 'Diabetes causes marked inhibition of mitochondrial metabolism in pancreatic β-cells'. Nature Communications, 10 (1), 2474.

104. Heaton, N.S. et al. (2010) 'Dengue virus nonstructural protein 3 redistributes fatty acid synthase to sites of viral replication and increases cellular fatty acid synthesis'. Proceedings of the National Academy of Sciences, 107 (40), pp. 17345-17350.

105. Heaton, N.S. and Randall, G. (2011) 'Multifaceted roles for lipids in viral infection'. Trends in Microbiology, 19 (7), pp. 368-375.

106. Hemmi, H. et al. (2002) 'Small anti-viral compounds activate immune cells via the TLR7 MyD88-dependent signaling pathway'. Nature Immunology, 3 (2), pp. 196-200.

107. Hensler, T. et al. (1998) 'Increased Susceptibility to Postoperative Sepsis in Patients with Impaired Monocyte IL-12 Production1'. The Journal of Immunology, 161 (5), pp. 2655-2659.

108. Herb, M. and Schramm, M. (2021) 'Functions of ROS in Macrophages and Antimicrobial Immunity'. Antioxidants, 10 (2), 313.

109. Heubner, L. et al. (2022) 'Characteristics and outcomes of sepsis patients with and without COVID-19'. Journal of Infection and Public Health, 15 (6), pp. 670-676.

110. Hibi, M. et al. (1990) 'Molecular cloning and expression of an IL-6 signal transducer, gp130'. Cell, 63 (6), pp. 1149-1157.

111. Hildebrand, F., Pape, H.C. and Krettek, C. (2005) '[The importance of cytokines in the posttraumatic inflammatory reaction]'. Unfallchirurg, 108 (10), pp. 793-794.

112. Hirano, T. et al. (1986) 'Complementary DNA for a novel human interleukin (BSF-2) that induces B lymphocytes to produce immunoglobulin'. Nature, 324 (6092), pp. 73-76.

113. Hoffmann, M. et al. (2020) 'SARS-CoV-2 Cell Entry Depends on ACE2 and TMPRSS2 and Is Blocked by a Clinically Proven Protease Inhibitor'. Cell, 181 (2), pp. 271-280.

114. Horiuchi, H. et al. (2021) 'Interleukin-19 Abrogates Experimental Autoimmune Encephalomyelitis by Attenuating Antigen-Presenting Cell Activation'. Frontiers in Immunology, 12, 615898.

115. Hu, X. et al. (2021) 'The JAK/STAT signaling pathway: from bench to clinic'. Signal Transduction and Targeted Therapy, 6 (1), 402.

116. Huang, I. and Pranata, R. (2020) 'Lymphopenia in severe coronavirus disease-2019 (COVID-19): systematic review and meta-analysis'. Journal of Intensive Care, 8 (1), 36.

117. Ihim, S.A. et al. (2022) 'Interleukin-18 cytokine in immunity, inflammation, and autoimmunity: Biological role in induction, regulation, and treatment'. Frontiers in Immunology, 13, 919973.

118. Inácio Â, S. et al. (2011) 'In vitro surfactant structure-toxicity relationships: implications for surfactant use in sexually transmitted infection prophylaxis and contraception'. PLoS One, 6 (5), e19850.

119. IPCC (2022). 'Climate Change 2022: Impacts, Adapatation, and Vulnerability'. Cambridge University Press

120. Irani, S. (2022) 'Immune Responses in SARS-CoV-2, SARS-CoV, and MERS-CoV Infections: A Comparative Review'. International Journal of Preventative Medicine, 13, 45.

121. Jackson, C.B. et al. (2022) 'Mechanisms of SARS-CoV-2 entry into cells'. Nature Reviews Molecular Cell Biology, 23 (1), pp. 3-20.

122. Jadon, P.S. et al. (2009) 'Enhanced Oral Bioavailability of Griseofulvin via Niosomes'. AAPS PharmSciTech, 10 (4), pp. 1186-1192.

123. Jalah, R. et al. (2013) 'The p40 subunit of interleukin (IL)-12 promotes stabilization and export of the p35 subunit: implications for improved IL-12 cytokine production'. Journal of Biological Chemistry, 288 (9), pp. 6763-6776.

124. Jana, M. et al. (2009) 'IL-12 p40 homodimer, the so-called biologically inactive molecule, induces nitric oxide synthase in microglia via IL-12R beta 1'. Glia, 57 (14), pp. 1553-1565.

125. Jaumouillé, V. and Waterman, C.M. (2020) 'Physical Constraints and Forces Involved in Phagocytosis'. Frontiers in Immunology, 11, 3389.

126. Janeway, C.A. and Medzhitov, R. (2002) 'Innate Immune Recognition'. Annual Review of Immunology, 20 (1), pp. 197-216.

127. Jenks, J.A., Goodwin, M.L. and Permar, S.R. (2019) 'The Roles of Host and Viral Antibody Fc Receptors in Herpes Simplex Virus (HSV) and Human Cytomegalovirus (HCMV) Infections and Immunity'. Frontiers in Immunology, 10, 2110.

128. Jevnikar, Z. et al. (2019) 'Epithelial IL-6 trans-signaling defines a new asthma phenotype with increased airway inflammation'. Journal of Allergy and Clinical Immunology, 143 (2), pp. 577-590.

129. Jin, M.S. and Lee, J.-O. (2008) 'Structures of the toll-like receptor family and its ligand complexes'. Immunity, 29 (2), pp. 182-191.

130. Joffre, O.P. et al. (2012) 'Cross-presentation by dendritic cells'. Nature Reviews Immunology, 12 (8), pp. 557-569.

131. Johnston, S.T., Faria, M. and Crampin, E.J. (2018) 'An analytical approach for quantifying the influence of nanoparticle polydispersity on cellular delivered dose'. Journal of The Royal Society Interface, 15 (144), 20180364.

132. Jones, B.A. et al. (2013) 'Zoonosis emergence linked to agricultural intensification and environmental change'. Proceedings of the National Academy of Sciences, 110 (21), pp. 8399-8404.

133. Jones, J.E., Le Sage, V. and Lakdawala, S.S. (2021) 'Viral and host heterogeneity and their effects on the viral life cycle'. Nature Reviews Microbiology, 19 (4), pp. 272-282.

134. Jones, K.E. et al. (2008) 'Global trends in emerging infectious diseases'. Nature, 451 (7181), pp. 990-993.

135. Junyaprasert, V.B., Teeranachaideekul, V. and Supaperm, T. (2008) 'Effect of Charged and Non-ionic Membrane Additives on Physicochemical Properties and Stability of Niosomes'. AAPS PharmSciTech, 9 (3), pp. 851-859.

136. Kaksonen, M. and Roux, A. (2018) 'Mechanisms of clathrin-mediated endocytosis'. Nature Reviews Molecular Cell Biology, 19 (5), pp. 313-326.

137. Kang, S. and Tang, H. (2020) 'HIV-1 Infection and Glucose Metabolism Reprogramming of T Cells: Another Approach Toward Functional Cure and Reservoir Eradication'. Frontiers in Immunology, 11, 572677.

138. Kang, S. and Kishimoto, T. (2021) 'Interplay between interleukin-6 signaling and the vascular endothelium in cytokine storms'. Experimental & Molecular Medicine, 53 (7), pp. 1116-1123.

139. Kang, W. et al. (2021) 'Emerging Role of TCA Cycle-Related Enzymes in Human Diseases'. International Journal of Molecular Sciences, 22 (23), 13507.

140. Karst, S.M. and Tibbetts, S.A. (2016) 'Recent advances in understanding norovirus pathogenesis'. Journal of Medical Virology, 88 (11), pp. 1837-1843.

141. Kawai, T. and Akira, S. (2006) 'Innate immune recognition of viral infection'. Nature Immunology, 7 (2), pp. 131-137.

142. Kawai, T. and Akira, S. (2007) 'Signaling to NF-kappaB by Toll-like receptors'. Trends in Molecular Medicine, 13 (11), pp. 460-469.

143. Kayagaki, N. et al. (2015) 'Caspase-11 cleaves gasdermin D for non-canonical inflammasome signalling'. Nature, 526 (7575), pp. 666-671.

144. Kazi, K.M. et al. (2010) 'Niosome: A future of targeted drug delivery systems'. Journal of Advanced Pharmaceutical Technology & Research, 1 (4), pp. 374-380.

145. Kilbourne, E.D. (2006) 'Influenza Pandemics of the 20th Century'. Emerging Infectious Diseases, 12 (1), pp. 9-14.

146. Kim, S., et al. (2023). PubChem 2023 update. Nucleic Acids Research., 51(D1), D1373–D1380. https://doi.org/10.1093/nar/gkac956

147. Kimura, A. and Kishimoto, T. (2010) 'IL-6: Regulator of Treg/Th17 balance'. European Journal of Immunology, 40 (7), pp. 1830-1835.

148. King, E.M. et al. (2013) 'Glucocorticoid repression of inflammatory gene expression shows differential responsiveness by transactivation- and transrepression-dependent mechanisms'. PLoS One, 8 (1), e53936.

149. Kishimoto, T., Akira, S. and Taga, T. (1992) 'Interleukin-6 and its receptor: a paradigm for cytokines'. Science, 258 (5082), pp. 593-597.

150. Kishimoto, T. (2010) 'IL-6: from its discovery to clinical applications'. International Immunology, 22 (5), pp. 347-352.

151. Klos, A. et al. (2009) 'The role of the anaphylatoxins in health and disease'. Molecular Immunology, 46 (14), pp. 2753-2766.

152. Kolev, M. and Kemper, C. (2017) 'Keeping It All Going—Complement Meets Metabolism'. Frontiers in Immunology, 8, 1.

153. Koonin, E.V., Krupovic, M. and Agol, V.I. (2021) 'The Baltimore Classification of Viruses 50 Years Later: How Does It Stand in the Light of Virus Evolution?'. Microbiology and Molecular Biology Reviews, 85 (3), 1128.

154. Korta, A., Kula, J. and Gomułka, K. (2023) 'The Role of IL-23 in the Pathogenesis and Therapy of Inflammatory Bowel Disease'. International Journal of Molecular Sciences, 24 (12), 10172.

155. Krebs, H.A. and Johnson, W.A. (1937) 'Metabolism of ketonic acids in animal tissues'. Biochemical Journal, 31 (4), pp. 645-660.

156. Kumari, N. et al. (2016) 'Role of interleukin-6 in cancer progression and therapeutic resistance'. Tumour Biology, 37 (9), pp. 11553-11572.

157. Kutscher, H.L. et al. (2010) 'Threshold size for optimal passive pulmonary targeting and retention of rigid microparticles in rats'. Journal of Controlled Release, 143 (1), pp. 31-37.

158. Land, W.G. (2021) 'Role of DAMPs in respiratory virus-induced acute respiratory distress syndrome—with a preliminary reference to SARS-CoV-2 pneumonia'. Genes & Immunity, 22 (3), pp. 141-160.

159. Lander, E.S. et al. (2001) 'Initial sequencing and analysis of the human genome'. Nature, 409 (6822), pp. 860-921.

160. Lang, F.M. et al. (2020) 'GM-CSF-based treatments in COVID-19: reconciling opposing therapeutic approaches'. Nature Reviews Immunology, 20 (8), pp. 507-514.

161. Lazarevic, V., Glimcher, L.H. and Lord, G.M. (2013) 'T-bet: a bridge between innate and adaptive immunity'. Nature Reviews Immunology, 13 (11), pp. 777-789.

162. Leal Filho, W. et al. (2022) 'Climate Change and Zoonoses: A Review of Concepts, Definitions, and Bibliometrics'. International Journal of Environmental Research and Public Health, 19 (2), 893.

163. Lelios, I. et al. (2020) 'Emerging roles of IL-34 in health and disease'. Journal of Experimental Medicine, 217 (3), e20190290.

164. Lendeckel, U., Venz, S. and Wolke, C. (2022) 'Macrophages: shapes and functions'. ChemTexts, 8 (2), 12.

165. Lewis, J.M., Feasey, N.A. and Rylance, J. (2019) 'Aetiology and outcomes of sepsis in adults in sub-Saharan Africa: a systematic review and meta-analysis'. Critical Care, 23 (1), 212.

166. Lewis, S.L. and Maslin, M.A. (2015) 'Defining the Anthropocene'. Nature, 519 (7542), pp. 171-180.

167. Li, H. et al. (2020) 'SARS-CoV-2 and viral sepsis: observations and hypotheses'. The Lancet, 395 (10235), pp. 1517-1520.

168. Lind, N.A. et al. (2022) 'Regulation of the nucleic acid-sensing Toll-like receptors'. Nature Reviews Immunology, 22 (4), pp. 224-235.

169. Lindahl, J.F. and Grace, D. (2015) 'The consequences of human actions on risks for infectious diseases: a review'. Infection Ecology & Epidemiology, 5 (1), 30048.

170. Liu, J. et al. (2013) 'PEGylation and zwitterionization: pros and cons in the renal clearance and tumor targeting of near-IR-emitting gold nanoparticles'. Angewandte Chemie International Edition, 52 (48), pp. 12572-12576.

171. Liu, J. et al. (2020) 'Longitudinal characteristics of lymphocyte responses and cytokine profiles in the peripheral blood of SARS-CoV-2 infected patients'. EBioMedicine, 55, 102763.

172. Liu, T. et al. (2017) 'NF-κB signaling in inflammation'. Signal Transduction and Targeted Therapy, 2 (1), 17023.

173. Lopez-Berestein, G. et al. (1985) 'Liposomal Amphotericin B for the Treatment of Systemic Fungal Infections in Patients with Cancer: A Preliminary Study'. The Journal of Infectious Diseases, 151 (4), pp. 704-710.

174. Lopez-Castejon, G. and Brough, D. (2011) 'Understanding the mechanism of IL-1β secretion'. Cytokine & Growth Factor Reviews, 22 (4), pp. 189-195.

175. Lu, H. et al. (2012) 'VTX-2337 is a novel TLR8 agonist that activates NK cells and augments ADCC'. Clinical Cancer Research, 18 (2), pp. 499-509.

176. Lu, L. et al. (2021) 'A Potential Role of Interleukin 10 in COVID-19 Pathogenesis'. Trends in Immunology, 42 (1), pp. 3-5.

177. Lu, Z. et al. (2010) 'Effect of particle shape on phagocytosis of CdTe quantum dot–cystine composites'. RCS Medicinal Chemistry, 1 (1), 84.

178. Luan, G. et al. (2019) 'Dexamethasone-Induced Mitochondrial Dysfunction and Insulin Resistance-Study in 3T3-L1 Adipocytes and Mitochondria Isolated from Mouse Liver'. Molecules, 24 (10), 1982.

179. Ma, F. et al. (2019) 'A comparison between whole transcript and 3’ RNA sequencing methods using Kapa and Lexogen library preparation methods'. BMC Genomics, 20 (1), 9.

180. Ma, X. et al. (2015) 'Regulation of IL-10 and IL-12 production and function in macrophages and dendritic cells'. F1000Research, 4, F1000 Faculty Rev-1465.

181. MacDonald, R.C. et al. (1991) 'Small-volume extrusion apparatus for preparation of large, unilamellar vesicles'. Biochimica et Biophysica Acta (BBA) - Biomembranes, 1061 (2), pp. 297-303.

182. Maeda, K. et al. (2010) 'IL-6 increases B-cell IgG production in a feed-forward proinflammatory mechanism to skew hematopoiesis and elevate myeloid production'. Blood, 115 (23), pp. 4699-4706.

183. Malik, A. and Kanneganti, T.D. (2018) 'Function and regulation of IL-1α in inflammatory diseases and cancer'. Immunological Reviews, 281 (1), pp. 124-137.

184. Marani, M. et al. (2021) 'Intensity and frequency of extreme novel epidemics'. Proceedings of the National Academy of Sciences, 118 (35), e2105482118.

185. Matsushima, N. et al. (2007) 'Comparative sequence analysis of leucine-rich repeats (LRRs) within vertebrate toll-like receptors'. BMC Genomics, 8, 124.

186. Mawazi, S.M. et al. (2022) 'Regen-Cov and Covid-19, Update on the Drug Profile and Fda Status: A Mini-Review and Bibliometric Study'. Journal of Public Health Research, 10 (2 Suppl).

187. McAlvin, J.B. et al. (2014) 'Multivesicular liposomal bupivacaine at the sciatic nerve'. Biomaterials, 35 (15), pp. 4557-4564.

188. McGahon, J. (2021) Investigating the anti-inflammatory effects of non-ionic surfactant vesicles. http://purl.org/coar/resource_type/c_db06.

189. Medzhitov, R. and Janeway, C. (2000) 'Innate Immunity'. New England Journal of Medicine, 343 (5), pp. 338-344.

190. Meure, L.A., Foster, N.R. and Dehghani, F. (2008) 'Conventional and Dense Gas Techniques for the Production of Liposomes: A Review'. AAPS PharmSciTech, 9 (3), pp. 798-809.

191. Mehta, Y. et al. (2022) 'Sepsis Management in Southeast Asia: A Review and Clinical Experience'. Journal of Clinical Medicine, 11 (13), 3635.

192. Melchjorsen, J., Sørensen, L.N. and Paludan, S.R. (2003) 'Expression and function of chemokines during viral infections: from molecular mechanisms to in vivo function'. Journal of Leukocyte Biology, 74 (3), pp. 331-343.

193. Melo, A.K. et al. (2013) 'Persistent glucocorticoid resistance in systemic lupus erythematosus patients during clinical remission'. Genetics and Molecular Research, 12 (2), pp. 2010-2019.

194. Mifsud, E.J., Kuba, M. and Barr, I.G. (2021) 'Innate Immune Responses to Influenza Virus Infections in the Upper Respiratory Tract'. Viruses, 13 (10), 2090.

195. Moghimi, S.M., Hunter, A.C. and Andresen, T.L. (2012) 'Factors Controlling Nanoparticle Pharmacokinetics: An Integrated Analysis and Perspective'. Annual Review of Pharmacology and Toxicology, 52 (1), pp. 481-503.

196. Mohamedi, S.A. et al. (2000) 'Antibody responses, cytokine levels and protection of mice immunised with HSV-2 antigens formulated into NISV or ISCOM delivery systems'. Vaccine, 18 (20), pp. 2083-2094.

197. Moir, S., Chun, T.-W. and Fauci, A.S. (2011) 'Pathogenic Mechanisms of HIV Disease'. Annual Review of Pathology: Mechanisms of Disease, 6 (1), pp. 223-248.

198. Mokart, D. et al. (2002) 'Early postoperative compensatory anti-inflammatory response syndrome is associated with septic complications after major surgical trauma in patients with cancer'. British Journal of Surgery, 89 (11), pp. 1450-1456.

199. Moll-Bernardes, R. et al. (2021) 'IL-10 and IL-12 (P70) Levels Predict the Risk of Covid-19 Progression in Hypertensive Patients: Insights From the BRACE-CORONA Trial'. Frontiers in Cardiovascular Medicine, 8, 702507.

200. Moore, P.S. and Chang, Y. (2010) 'Why do viruses cause cancer? Highlights of the first century of human tumour virology'. Nature Reviews Cancer, 10 (12), pp. 878-889.

201. Morens, D.M., North, M. and Taubenberger, J.K. (2010) 'Eyewitness accounts of the 1510 influenza pandemic in Europe'. The Lancet, 376 (9756), pp. 1894-1895.

202. Mullen, P.J. et al. (2021) 'SARS-CoV-2 infection rewires host cell metabolism and is potentially susceptible to mTORC1 inhibition'. Nature Communications, 12 (1), 1876.

203. Muntjewerff, E.M., Meesters, L.D. and van den Bogaart, G. (2020) 'Antigen Cross-Presentation by Macrophages'. Frontiers in Immunology, 11, 1276.

204. Nathan, C.F. and Hibbs, J.B. (1991) 'Role of nitric oxide synthesis in macrophage antimicrobial activity'. Current Opinion in Immunology, 3 (1), pp. 65-70.

205. National Institutes of Health. (2023) 'COVID-19 Treatment Guidelines Panel.' Coronavirus Disease 2019 (COVID-19) Treatment Guidelines. Available at https://www.covid19treatmentguidelines.nih.gov/. Accessed September 2023.

206. Nava, G.M. and Madrigal Perez, L.A. (2022) 'Metabolic profile of the Warburg effect as a tool for molecular prognosis and diagnosis of cancer'. Expert Reviews of Molecular Diagnosis, 22 (4), pp. 439-447.

207. Nedeva, C., Menassa, J. and Puthalakath, H. (2019) 'Sepsis: Inflammation Is a Necessary Evil'. Frontiers in Cell & Developmental Biology, 7, 108.

208. Nemmar, A. et al. (2002) 'Ultrafine Particles Affect Experimental Thrombosis in an In Vivo Hamster Model'. American Journal of Respiratory and Critical Care Medicine, 166 (7), pp. 998-1004.

209. Nikitina, E. et al. (2018) 'Monocytes and Macrophages as Viral Targets and Reservoirs'. International Journal of Molecular Science, 19 (9), 2821.

210. Obeid, M.A. et al. (2017) 'Formulation of Nonionic Surfactant Vesicles (NISV) Prepared by Microfluidics for Therapeutic Delivery of siRNA into Cancer Cells'. Mol Pharmaceutics, 14 (7), pp. 2450-2458.

211. Olson, P.E. (1996) 'The Thucydides Syndrome: Ebola Déjà Vu? (or Ebola Reemergent?)'. Emerging Infectious Diseases, 2 (2), pp. 155-156.

212. Olzmann, J.A. and Carvalho, P. (2019) 'Dynamics and functions of lipid droplets'. Nature Reviews Molecular Cell Biology, 20 (3), pp. 137-155.

213. Ó Maoldomhnaigh, C. et al. (2021) 'The Warburg Effect Occurs Rapidly in Stimulated Human Adult but Not Umbilical Cord Blood Derived Macrophages'. Frontiers in Immunology, 12, 657261.

214. O'Neill, L.A.J. and Bowie, A.G. (2007) 'The family of five: TIR-domain-containing adaptors in Toll-like receptor signalling'. Nature Reviews Immunology, 7 (5), pp. 353-364.

215. O'Neill, L.A.J. and Pearce, E.J. (2016) 'Immunometabolism governs dendritic cell and macrophage function'. Journal of Experimental Medicine, 213 (1), pp. 15-23.

216. Oren, R. et al. (1963) 'Metabolic patterns in three types of phagocytizing cells'. Journal of Cell Biology, 17 (3), pp. 487-501.

217. Patil, N. et al. (2022) 'Monitoring and modelling the dynamics of the cellular glycolysis pathway: A review and future perspectives'. Molecular Metabolism, 66, 101635.

218. Patravale, V.B., Date, A.A. and Kulkarni, R.M. (2010) 'Nanosuspensions: a promising drug delivery strategy'. Journal of Pharmacy and Pharmacology, 56 (7), pp. 827-840.

219. Paul, D. et al. (2013) 'Phagocytosis Dynamics Depends on Target Shape'. Biophysical Journal, 105 (5), pp. 1143-1150.

220. Pandolfi, F. et al. (2020) 'Interleukin-6 in Rheumatoid Arthritis'. International Journal of Molecular Sciences, 21 (15), 5238.

221. Perrie, Y. et al. (2004) 'Surfactant vesicle-mediated delivery of DNA vaccines via the subcutaneous route'. International Journal of Pharmaceutics, 284 (1), pp. 31-41.

222. Peterson, T.R. et al. (2011) 'mTOR complex 1 regulates lipin 1 localization to control the SREBP pathway'. Cell, 146 (3), pp. 408-420.

223. Phillips, D. et al. (2009) 'Succinyl-CoA synthetase is a phosphate target for the activation of mitochondrial metabolism'. Biochemistry, 48 (30), pp. 7140-7149.

224. Pierrakos, C. and Vincent, J.L. (2010) 'Sepsis biomarkers: a review'. Critical Care, 14 (1), R15.

225. Platanias, L.C. (2005) 'Mechanisms of type-I- and type-II-interferon-mediated signalling'. Nature Reviews Immunology, 5 (5), pp. 375-386.

226. Prentki, M. et al. (2013) 'Metabolic Signaling in Fuel-Induced Insulin Secretion'. Cell Metabolism, 18 (2), pp. 162-185.

227. Quartuccio, L. et al. (2021) 'Interleukin 6, soluble interleukin 2 receptor alpha (CD25), monocyte colony-stimulating factor, and hepatocyte growth factor linked with systemic hyperinflammation, innate immunity hyperactivation, and organ damage in COVID-19 pneumonia'. Cytokine, 140, 155438.

228. Ragab, D. et al. (2020) 'The COVID-19 Cytokine Storm; What We Know So Far'. Frontiers in Immunology, 11, 1446.

229. Rampersad, S. and Tennant, P. (2018) 'Replication and Expression Strategies of Viruses'. Viruses, 55-82.

230. Rath, M. et al. (2014) 'Metabolism via Arginase or Nitric Oxide Synthase: Two Competing Arginine Pathways in Macrophages'. Frontiers in Immunology, 5, 532.

231. RECOVERY. (2021) 'Dexamethasone in Hospitalized Patients with Covid-19'. New England Journal of Medicine, 384 (8), pp. 693-704.

232. Reeh, H. et al. (2019) 'Response to IL-6 trans- and IL-6 classic signalling is determined by the ratio of the IL-6 receptor α to gp130 expression: fusing experimental insights and dynamic modelling'. Cell Communication and Signaling, 17 (1), 46.

233. REMAP-CAP. 'Interleukin-6 Receptor Antagonists in Critically Ill Patients with Covid-19'. (2021) New England Journal of Medicine, 384 (16), pp. 1491-1502.

234. Ritter, L.A. et al. (2021) 'The Impact of Corticosteroids on Secondary Infection and Mortality in Critically Ill COVID-19 Patients'. Journal of Intensive Care Medicine, 36 (10), pp. 1201-1208.

235. Roberts, C.W., Brewer, J.M. and Alexander, J. (1994) 'Congenital toxoplasmosis in the Balb/c mouse: prevention of vertical disease transmission and fetal death by vaccination'. Vaccine, 12 (15), pp. 1389-1394.

236. Rodríguez-Prados, J.-C. et al. (2010) 'Substrate Fate in Activated Macrophages: A Comparison between Innate, Classic, and Alternative Activation'. The Journal of Immunology, 185 (1), pp. 605-614.

237. Rosales, C. (2018) 'Neutrophil: A Cell with Many Roles in Inflammation or Several Cell Types?'. Frontiers in Physiology, 9, 113.

238. Rose-John, S. (2012) 'IL-6 trans-signaling via the soluble IL-6 receptor: importance for the pro-inflammatory activities of IL-6'. International Journal of Biological Sciences, 8 (9), pp. 1237-1247.

239. Rose-John, S. (2017) 'The Soluble Interleukin 6 Receptor: Advanced Therapeutic Options in Inflammation'. Clinical Pharmacology & Therapeutics, 102 (4), pp. 591-598.

240. Rose-John, S. (2018) 'Interleukin-6 Family Cytokines'. Cold Spring Harbor Perspectives in Biology, 10 (2), a028415

241. Rose-John, S. et al. (2023) 'Targeting IL-6 trans-signalling: past, present and future prospects'. Nature Reviews Immunology, 23, pp. 666-681.

242. Roser, M. et al (2013) "World Population Growth". Published online at OurWorldInData.org. Retrieved from: 'https://ourworldindata.org/world-population-growth' [Online Resource]

243. Rossi, F. and Zatti, M. (1964) 'CHANGES IN THE METABOLIC PATTERN OF POLYMORPHO-NUCLEAR LEUCOCYTES DURING PHAGOCYTOSIS'. British Journal of Experimental Pathology, 45 (5), pp. 548-559.

244. Rouse, B.T. and Horohov, D.W. (1986) 'Immunosuppression in viral infections'. Reviews of Infectious Diseases, 8 (6), pp. 850-873.

245. Roychoudhury, S. et al. (2020) 'Viral Pandemics of the Last Four Decades: Pathophysiology, Health Impacts and Perspectives'. International Journal of Environmental Research and Public Health, 17 (24), 9411.

246. Rubin, E.J., Longo, D.L. and Baden, L.R. (2021) 'Interleukin-6 Receptor Inhibition in Covid-19 — Cooling the Inflammatory Soup'. New England Journal of Medicine, 384 (16), pp. 1564-1565.

247. Rubio-Casillas, A., Redwan, E.M. and Uversky, V.N. (2022) 'SARS-CoV-2: A Master of Immune Evasion'. Biomedicines, 10 (6), 1339.

248. Rudd, K.E. et al. (2018) 'The global burden of sepsis: barriers and potential solutions'. Critical Care, 22 (1), 232.

249. Rudd, K.E. et al. (2020) 'Global, regional, and national sepsis incidence and mortality, 1990–2017: analysis for the Global Burden of Disease Study'. The Lancet, 395 (10219), pp. 200-211.

250. Rutter, H. et al. (2021) 'Visualising SARS-CoV-2 transmission routes and mitigations'. British Medical Journal, e065312.

251. Ryan, G.B. and Majno, G. (1977) 'Acute inflammation. A review'. American Journal of Pathology, 86 (1), pp. 183-276.

252. Sameer, A.S. and Nissar, S. (2021) 'Toll-Like Receptors (TLRs): Structure, Functions, Signaling, and Role of Their Polymorphisms in Colorectal Cancer Susceptibility'. BioMed Research International, 2021, 1157023.

253. Sanchez, E.L. and Lagunoff, M. (2015) 'Viral activation of cellular metabolism'. Virology, 479-480, pp. 609-618.

254. Sanger, F., Nicklen, S., and Coulson, A.R. (1977) 'DNA sequencing with chain-terminating inhibitors'. Proceedings of the National Academy of Sciences, 74 (12), pp. 5463-5467.

255. Santa Cruz, A. et al. (2021) 'Interleukin-6 Is a Biomarker for the Development of Fatal Severe Acute Respiratory Syndrome Coronavirus 2 Pneumonia'. Frontiers in Immunology, 12, 613422.

256. Santos e Silva, J.C. et al. (2021) 'Gene signatures of autopsy lungs from obese patients with COVID-19'. Clinical Nutrition ESPEN, 44, pp. 475-478.

257. Satarker, S. and Nampoothiri, M. (2020) 'Structural Proteins in Severe Acute Respiratory Syndrome Coronavirus-2'. Archives of Medical Research, 51 (6), pp. 482-491.

258. Savla, S.R., Prabhavalkar, K.S. and Bhatt, L.K. (2021) 'Cytokine storm associated coagulation complications in COVID-19 patients: Pathogenesis and Management'. Expert Review of Anti-Infective Therapy, 19 (11), pp. 1397-1413.

259. Schiliro, C. and Firestein, B.L. (2021) 'Mechanisms of Metabolic Reprogramming in Cancer Cells Supporting Enhanced Growth and Proliferation'. Cells, 10 (5), 1056.

260. Schmidt-Arras, D. and Rose-John, S. (2016) 'IL-6 pathway in the liver: From physiopathology to therapy'. Journal of Hepatology, 64 (6), pp. 1403-1415.

261. Schreiber, S. et al. (2021) 'Therapeutic Interleukin-6 Trans-signaling Inhibition by Olamkicept (sgp130Fc) in Patients With Active Inflammatory Bowel Disease'. Gastroenterology, 160 (7), pp. 2354-2366.

262. Sefik, E. et al. (2022) 'Inflammasome activation in infected macrophages drives COVID-19 pathology'. Nature, 606 (7914), pp. 585-593.

263. Shappell, C.N. et al. (2022) 'Prevalence, Clinical Characteristics, and Outcomes of Sepsis Caused by Severe Acute Respiratory Syndrome Coronavirus 2 Versus Other Pathogens in Hospitalized Patients With COVID-19'. Critical Care, 4 (5), e0703.

264. Sharma, V. et al. (2018) 'Selective Autophagy and Xenophagy in Infection and Disease'. Frontiers in Cell & Developmental Biology, 6, 147.

265. Sherry, L.V.-H. et al. (1998) 'Application and Evaluation of the Alamarblue Assay for Cell Growth and Survival of Fibroblasts'. In Vitro Cellular & Developmental Biology. Animal, 34 (3), pp. 239-246.

266. Shyu, A.B., Wilkinson, M.F. and van Hoof, A. (2008) 'Messenger RNA regulation: to translate or to degrade'. The EMBO Journal, 27 (3), pp. 471-481.

267. Simmons, J. and Pittet, J.F. (2015) 'The coagulopathy of acute sepsis'. Current Opinion in Anaesthesiology, 28 (2), pp. 227-236.

268. Sin, W.-X. et al. (2020) 'IRF-7 Mediates Type I IFN Responses in Endotoxin-Challenged Mice'. Frontiers in Immunology, 11, 640.

269. Singer, M. et al. (2016) 'The Third International Consensus Definitions for Sepsis and Septic Shock (Sepsis-3)'. Journal of the American Medical Association, 315 (8), pp. 801-810.

270. Sinha, A. et al. (2021) 'Virus-Encoded Complement Regulators: Current Status'. Viruses, 13 (2), 208.

271. Sitia, R. and Rubartelli, A. (2020) 'Evolution, role in inflammation, and redox control of leaderless secretory proteins'. Journal of Biological Chemistry, 295 (22), pp. 7799-7811.

272. Sofou, S. et al. (2010) 'Large anti-HER2/neu liposomes for potential targeted intraperitoneal therapy of micrometastatic cancer'. Journal of Liposome Research, 20 (4), pp. 330-340.

273. Somers, W., Stahl, M. and Seehra, J.S. (1997) '1.9 A crystal structure of interleukin 6: implications for a novel mode of receptor dimerization and signaling'. The EMBO Journal, 16 (5), pp. 989-997.

274. Spernovasilis, N. et al. (2021) 'Epidemics and pandemics: Is human overpopulation the elephant in the room?'. Ethics, Medicine, and Public Health, 19, 100728.

275. Stincone, A. et al. (2015) 'The return of metabolism: biochemistry and physiology of the pentose phosphate pathway'. Biological Reviews, 90 (3), pp. 927-963.

276. Sumbria, D. et al. (2020) 'Virus Infections and Host Metabolism-Can We Manage the Interactions?'. Frontiers in Immunology, 11, 594963.

277. Sun, A. (2018) 'Lysosomal storage disease overview'. Annals of Translational Medicine, 6 (24), 476.

278. Sych, T., Mély, Y. and Römer, W. (2018) 'Lipid self-assembly and lectin-induced reorganization of the plasma membrane'. Philosophical Transactions of the Royal Society of Lond B Biological Sciences, 373 (1747), 20170117

279. Taga, T. et al. (1989) 'Interleukin-6 triggers the association of its receptor with a possible signal transducer, gp130'. Cell, 58 (3), pp. 573-581.

280. Tan, Y. et al. (2022) 'Suppression of the caspase-1/GSDMD-mediated pyroptotic signaling pathway through dexamethasone alleviates corneal alkali injuries'. Experimental Eye Research, 214, 108858.

281. Tavakolpour, S. et al. (2020) 'Lymphopenia during the COVID-19 infection: What it shows and what can be learned'. Immunology Letters, 225, pp. 31-32.

282. Taylor, P.R. et al. (2005) 'Macrophage receptors and immune recognition'. Annual Review of Immunology, 23, pp. 901-944.

283. Thèves, C., Crubézy, E. and Biagini, P. (2016) 'History of Smallpox and Its Spread in Human Populations'. Microbiology Spectrum, 4 (10), 1128.

284. The Galaxy Community. (2022) ‘The Galaxy platform for accessible, reproducible and collaborative biomedical analyses: 2022 update’. Nucleic Acids Research, gkac247doi:10.1093/nar/gkac247

285. Thompson, M.R. et al. (2011) 'Pattern Recognition Receptors and the Innate Immune Response to Viral Infection'. Viruses, 3 (6), pp. 920-940.

286. Thorens, B. and Mueckler, M. (2010) 'Glucose transporters in the 21st Century'. American Journal of Physiology-Endocrinology and Metabolism, 298 (2), pp. E141-145.

287. Thucydides, 431 BCE, *The History of the Peloponnesian War*, Book 2, Chapter VII., trans. Crawley R. Project Gutenberg, University of North Carolina, USA.

288. Tjan, L.H. et al. (2021) 'Early Differences in Cytokine Production by Severity of Coronavirus Disease 2019'. The Journal of Infectious Diseases, 223 (7), pp. 1145-1149.

289. Todorović-Raković, N. and Whitfield, J.R. (2021) 'Between immunomodulation and immunotolerance: The role of IFNγ in SARS-CoV-2 disease'. Cytokine, 146, 155637.

290. Trac, N. and Chung, E.J. (2021) 'Overcoming physiological barriers by nanoparticles for intravenous drug delivery to the lymph nodes'. Experimental Biology & Medicine, 246 (22), pp. 2358-2371.

291. Trinchieri, G. (1998) 'Proinflammatory and Immunoregulatory Functions of Interleukin-12'. International Reviews of Immunology, 16 (3-4), pp. 365-396.

292. Trivedi, P.C., Bartlett, J.J. and Pulinilkunnil, T. (2020) 'Lysosomal Biology and Function: Modern View of Cellular Debris Bin'. Cells, 9 (5), 1131.

293. Usui, T. et al. (2006) 'T-bet regulates Th1 responses through essential effects on GATA-3 function rather than on IFNG gene acetylation and transcription'. Journal of Experimental Medicine, 203 (3), pp. 755-766.

294. Vander Heiden, M.G., Cantley, L.C. and Thompson, C.B. (2009) 'Understanding the Warburg effect: the metabolic requirements of cell proliferation'. Science, 324 (5930), pp. 1029-1033.

295. Vargas-Rodriguez, J.R. et al. (2022) 'Sustained Hyperglycemia and Its Relationship with the Outcome of Hospitalized Patients with Severe COVID-19: Potential Role of ACE2 Upregulation'. Journal of Personalized Medicine, 12 (5), 805.

296. Vaz de Paula, C.B. et al. (2020) 'IL-4/IL-13 remodeling pathway of COVID-19 lung injury'. Scientific Reports, 10 (1), 18689.

297. Vignali, D.A.A. and Kuchroo, V.K. (2012) 'IL-12 family cytokines: immunological playmakers'. Nature Immunology, 13 (8), pp. 722-728.

298. Vivas, M.C. et al. (2021) 'Plasma interleukin-6 levels correlate with survival in patients with bacterial sepsis and septic shock'. Interventional Medicine and Applied Science, 11 (4), pp. 224-230.

299. V'Kovski, P. et al. (2021) 'Coronavirus biology and replication: implications for SARS-CoV-2'. Nature Reviews Microbiology, 19 (3), pp. 155-170.

300. Vora, B., Khopade, A.J. and Jain, N.K. (1998) 'Proniosome based transdermal delivery of levonorgestrel for effective contraception'. Journal of Controlled Release, 54 (2), pp. 149-165.

301. Wakil, S.J., Stoops, J.K. and Joshi, V.C. (1983) 'FATTY ACID SYNTHESIS AND ITS REGULATION'. Annual Review of Biochemistry, 52 (1), pp. 537-579.

302. Wang, G.-L. et al. (2021) 'Serum IP-10 and IL-7 levels are associated with disease severity of coronavirus disease 2019'. Cytokine, 142, 155500.

303. Wang, S. et al. (2020) 'Cholesterol 25-Hydroxylase inhibits SARS-CoV-2 and other coronaviruses by depleting membrane cholesterol'. The EMBO Journal, 39 (21), e106057.

304. Wang, X. et al. (2022) 'The role of IL-6 in coronavirus, especially in COVID-19'. Frontiers in Pharmacology, 13, 1033674.

305. Wang, Z. and Wang, Z. (2023) 'The role of macrophages polarization in sepsis-induced acute lung injury'. Frontiers in Immunology, 14, 1209438.

306. World Health Organization. (2020) WHO COVID-19 Dashboard. Available online: https://covid19.who.int/ (last cited: May 2023)

307. Warburg, O., Wind, F. and Negelein, E. (1927) 'THE METABOLISM OF TUMORS IN THE BODY'. Journal of General Physiology, 8 (6), pp. 519-530.

308. Waterston, R.H. et al. (2002) 'Initial sequencing and comparative analysis of the mouse genome'. Nature, 420 (6915), pp. 520-562.

309. Weis, W.I., Taylor, M.E. and Drickamer, K. (1998) 'The C-type lectin superfamily in the immune system'. Immunological Reviews, 163, pp. 19-34.

310. Wheller, S.K. and Perretti, M. (1997) 'Dexamethasone inhibits cytokine-induced intercellular adhesion molecule-1 up-regulation on endothelial cell lines'. European Journal of Pharmacology, 331 (1), pp. 65-71.

311. World Health Organization. (2022) WHO R&D Blueprint for Epidemics. Available online: https://www.who.int/teams/blueprint/who-r-and-d-blueprint-for-epidemics (last cited May 2023)

312. Woods, S. et al. (2020) 'Glucosamine-NISV delivers antibody across the blood-brain barrier: Optimization for treatment of encephalitic viruses'. Journal of Controlled Release, 324, pp. 644-656.

313. Wong, M.W. et al. (2009) 'The effect of glucocorticoids on tendon cell viability in human tendon explants'. Acta Orthopaedica, 80 (3), pp. 363-367.

314. Worley, B. and Powers, R. (2016) 'PCA as a practical indicator of OPLS-DA model reliability'. Current Metabolomics, 4 (2), pp. 97-103.

315. Wynn, T.A. and Vannella, K.M. (2016) 'Macrophages in Tissue Repair, Regeneration, and Fibrosis'. Immunity, 44 (3), pp. 450-462.

316. Xiang, Q. et al. (2021) 'SARS-CoV-2 Induces Lymphocytopenia by Promoting Inflammation and Decimates Secondary Lymphoid Organs'. Frontiers in Immunology, 12, 661052.

317. Xiong, Y. et al. (2017) 'A Comparison of mRNA Sequencing with Random Primed and 3'-Directed Libraries'. Scientific Reports, 7 (1), 14626.

318. Xu, L. et al. (2022) 'Lipid Nanoparticles for Drug Delivery'. Advanced NanoBiomed Research, 2 (2), 2100109.

319. Yeramian, A. et al. (2006) 'Macrophages require distinct arginine catabolism and transport systems for proliferation and for activation'. European Journal of Immunology, 36 (6), pp. 1516-1526.

320. Youssef, J., Novosad, S.A. and Winthrop, K.L. (2016) 'Infection Risk and Safety of Corticosteroid Use'. Rheumatic Disease Clinics of North America, 42 (1), pp. 157-176.

321. Yu, Y., Maguire, T.G. and Alwine, J.C. (2011) 'Human Cytomegalovirus Activates Glucose Transporter 4 Expression To Increase Glucose Uptake during Infection'. Journal of Virology, 85 (4), pp. 1573-1580.

322. Yuan, S. et al. (2021) 'SARS-CoV-2 exploits host DGAT and ADRP for efficient replication'. Cell Discovery, 7 (1), 100.

323. Zafer, M.M., El-Mahallawy, H.A. and Ashour, H.M. (2021) 'Severe COVID-19 and Sepsis: Immune Pathogenesis and Laboratory Markers'. Microorganisms, 9 (1), 159.

324. Zhang, J.M. and An, J. (2007) 'Cytokines, inflammation, and pain'. International Anesthesiology Clinics , 45 (2), pp. 27-37.

325. Zhang, Y.N. et al. (2016) 'Nanoparticle-liver interactions: Cellular uptake and hepatobiliary elimination'. Journal of Controlled Release, 240, pp. 332-348.

326. Zhang, Z. et al. (2019) 'Host Lipids in Positive-Strand RNA Virus Genome Replication'. Frontiers in Microbiology, 10, 286.

327. Zhao, M. (2020) 'Cytokine storm and immunomodulatory therapy in COVID-19: Role of chloroquine and anti-IL-6 monoclonal antibodies'. International Journal of Antimicrobial Agents, 55 (6), 105982.

328. Zhao, Q. et al. (2022) 'Metabolic modeling of single bronchoalveolar macrophages reveals regulators of hyperinflammation in COVID-19'. iScience, 25 (11), 105319.

329. Zhao, R.Z. et al. (2019) 'Mitochondrial electron transport chain, ROS generation and uncoupling (Review)'. International Journal of Molecular Medicine, 44 (1), pp. 3-15.

330. Zheng, H. et al. (2016) 'Regulation of Interleukin-12 Production in Antigen-Presenting Cells'. Advances in Experimental and Medical Biology, pp. 117-138.

331. Zhu, X. et al. (2020) 'Stimulating pyruvate dehydrogenase complex reduces itaconate levels and enhances TCA cycle anabolic bioenergetics in acutely inflamed monocytes'. Journal of Leukocyte Biology, 107 (3), pp. 467-484.

332. Zizzo, G. et al. (2022) 'Immunotherapy of COVID-19: Inside and Beyond IL-6 Signalling'. Frontiers in Immunology, 13, 795315.

333. zur Hausen, H. and de Villiers, E.M. (2014) 'Cancer "causation" by infections--individual contributions and synergistic networks'. Seminars in Oncology, 41 (6), pp. 860-875.

9 Appendix

A

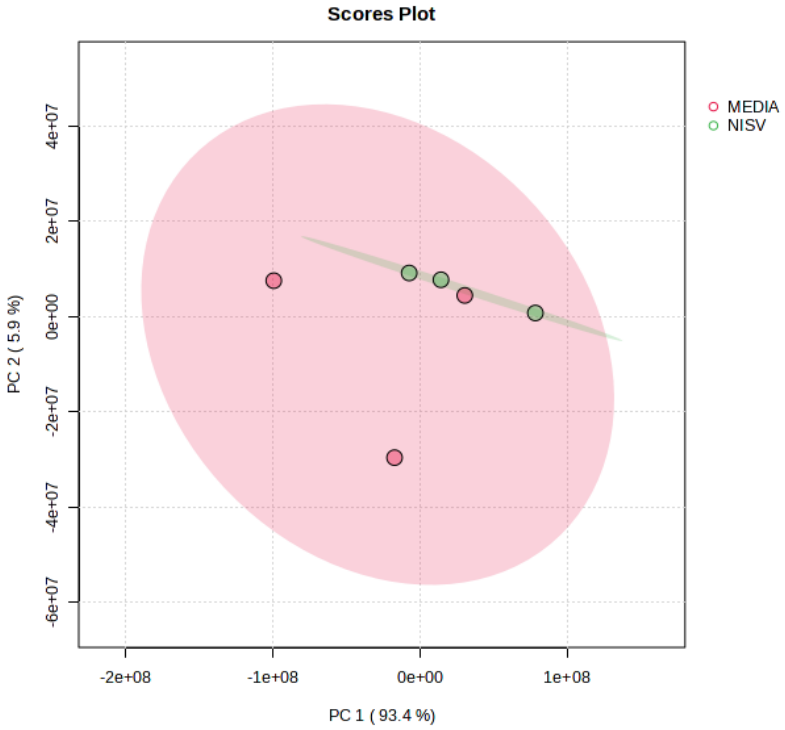

B

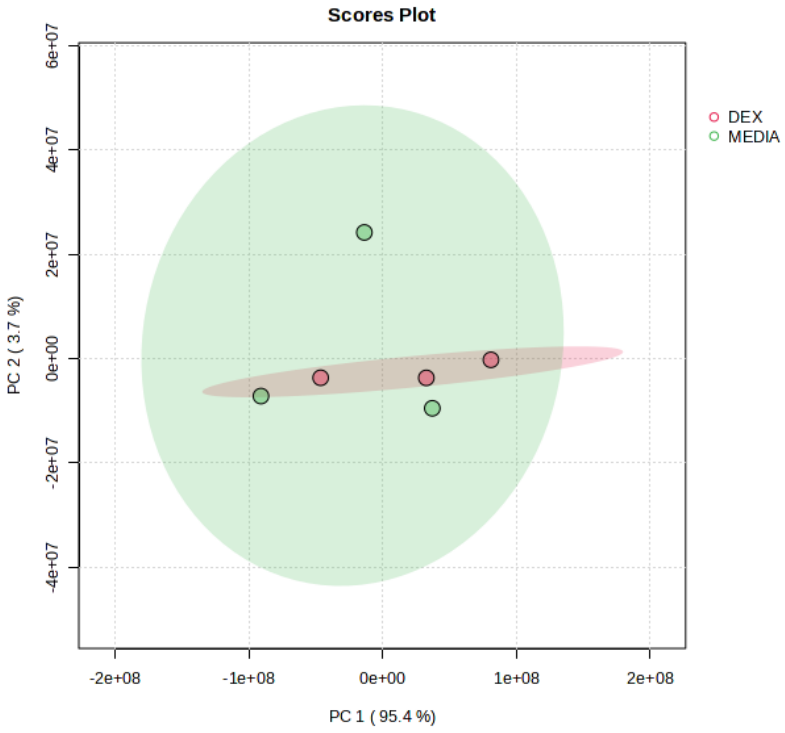

Appendix 1: **PCA plots of metabolites extracted from unstimulated BMDM treated with either NISV or dexamethasone.** *BMDM were treated with either 1.2mM of NISV or 1.6μM dexamethasone and metabolite extraction performed 24hrs post treatment. Samples were analysed using LC-MS with peaks matched to authentic internal standards for identification or annotated using online databases. PCA analysis was then performed to determine sample grouping and appropriateness of further OPLS-DA analysis. (A) NISV vs media, (B) dexamethasone vs media.*

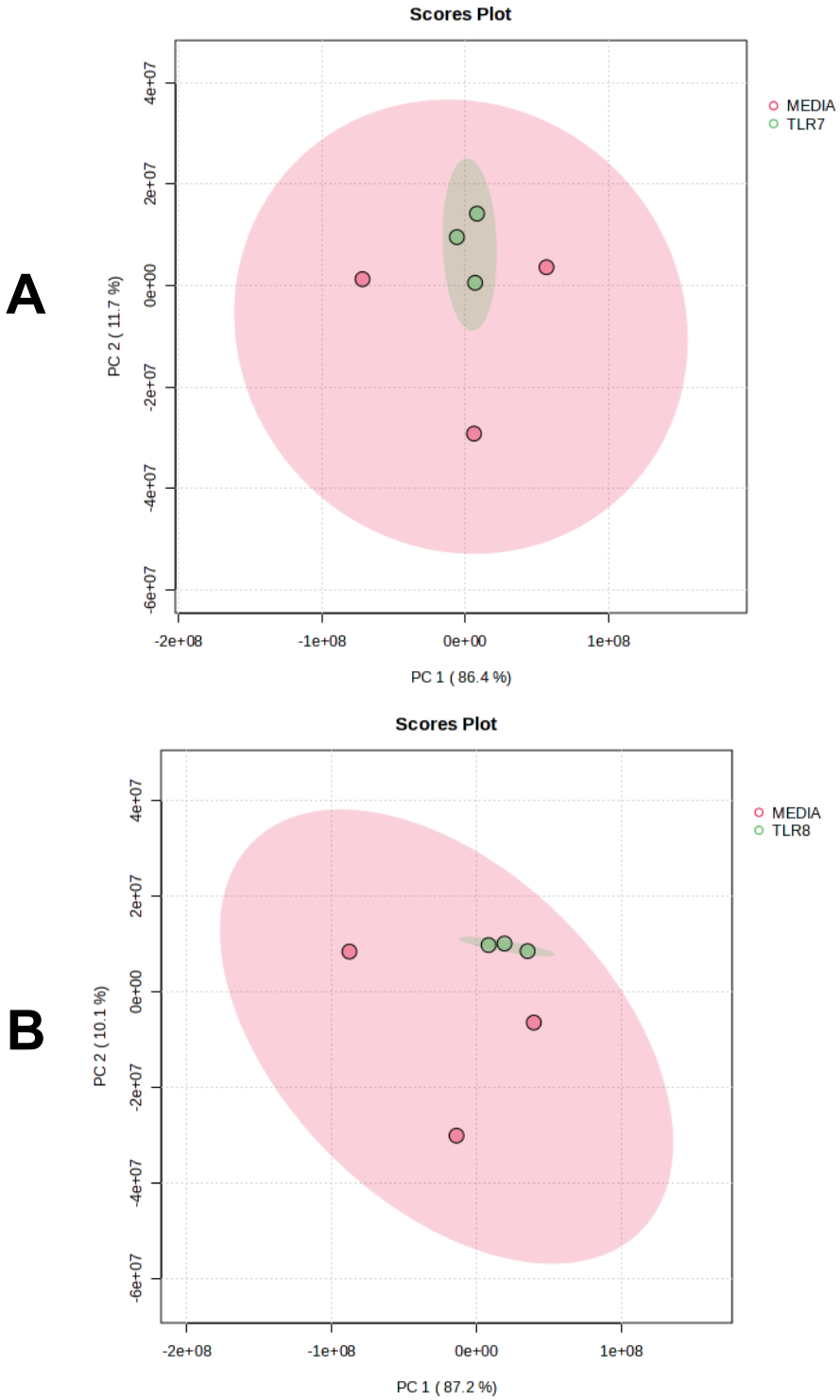

Appendix 2: **PCA plots of metabolites extracted from TLR7 or TLR8 stimulated BMDM.** *Cells were stimulated with either 1.6µg/ml of the TLR7 ligand imiquimod or 1.3µg/ml of the TLR8 ligand TL8-506 and metabolite extraction performed 24hrs post treatment. Samples were analysed using LC-MS with peaks matched to authentic internal standards for identification or annotated using online databases. PCA analysis was then performed to determine sample grouping and appropriateness of further OPLS-DA analysis. (A) TLR7 vs media, (B) TLR8 vs media.*

A

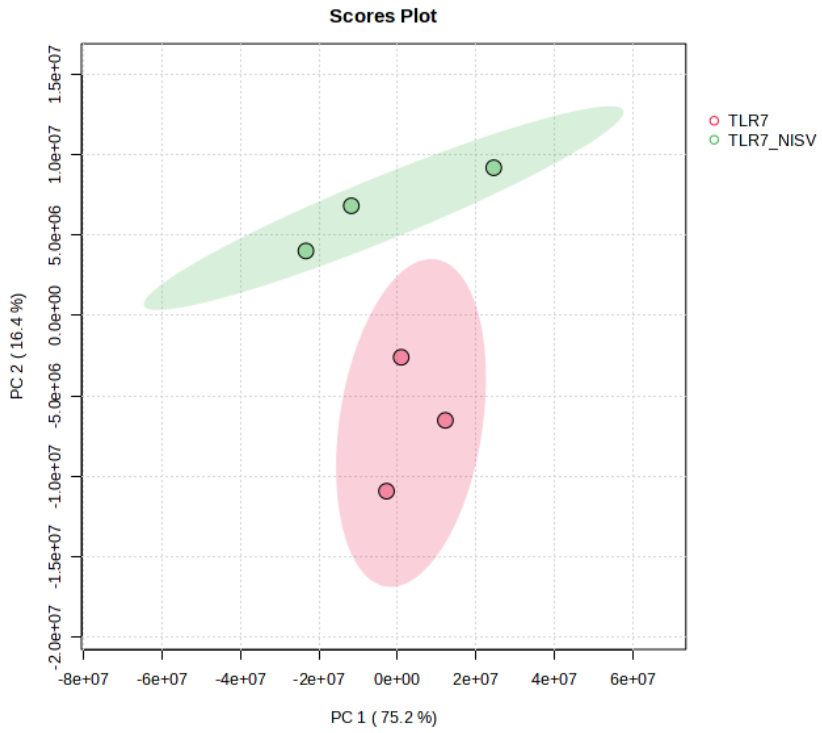

B

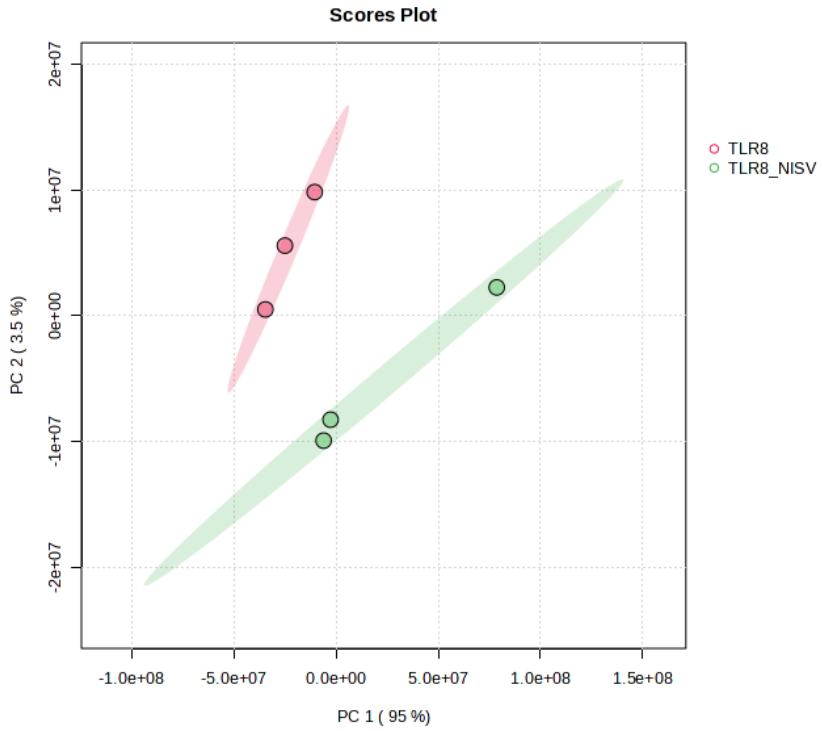

Appendix 3: **PCA plots of metabolites extracted from TLR7 or TLR8 stimulated BMDM treated with NISV** *Cells were stimulated with either 1.6µg/ml of the TLR7 ligand imiquimod or 1.3µg/ml of the TLR8 ligand TL8-506 and treated with 1.2mM of NISV. Metabolite extraction performed 24hrs post treatment. Samples were analysed using LC-MS with peaks matched to authentic internal standards for identification or annotated using online databases. PCA analysis was then performed to determine sample grouping and appropriateness of further OPLS-DA analysis. (A) NISV + TLR7 vs TLR7 alone, (B) NISV + TLR8 vs TLR8 alone.*

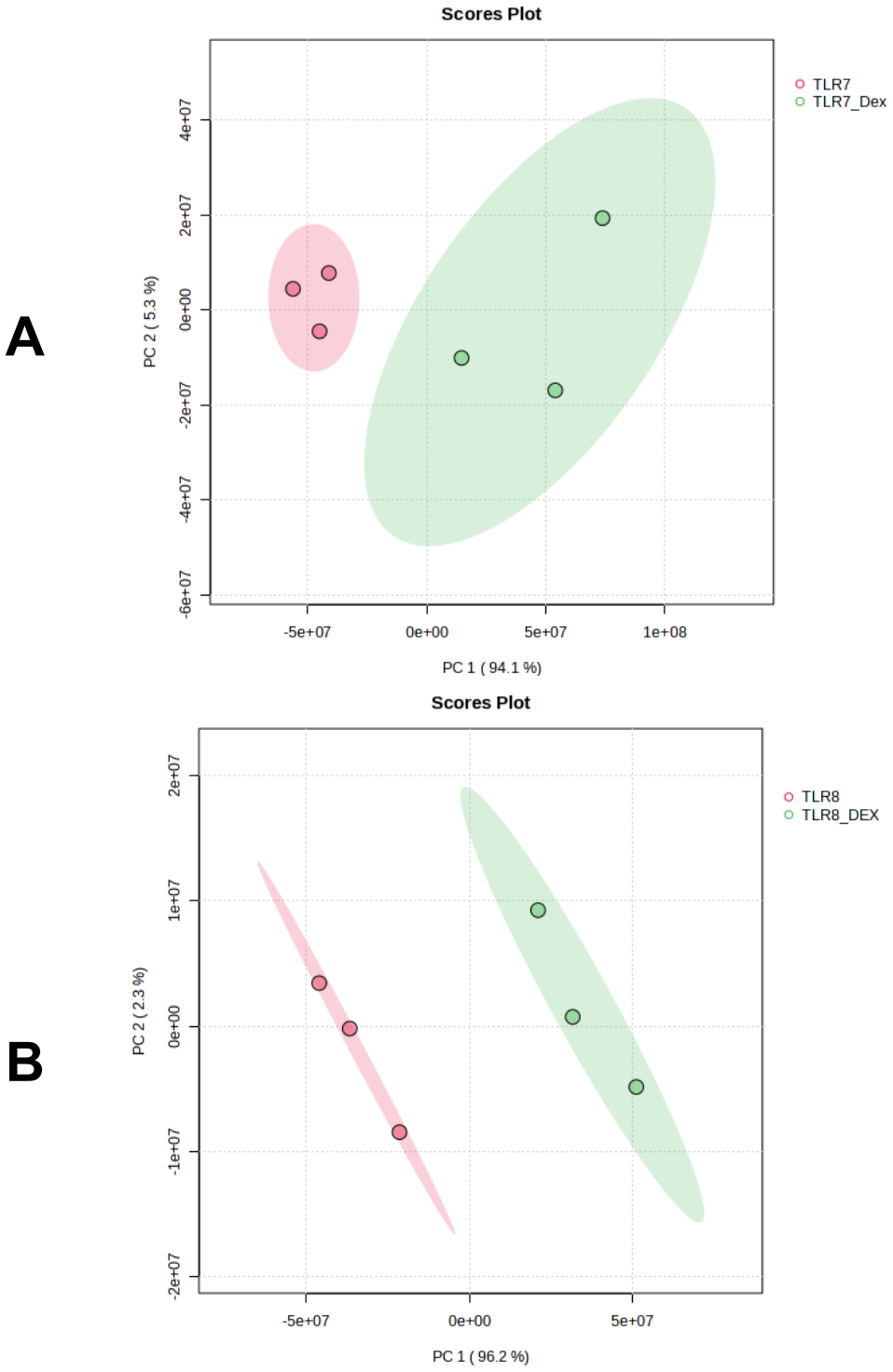

Appendix 4: **PCA plots of metabolites extracted from TLR7 or TLR8 stimulated BMDM treated with dexamethasone.** *Cells were stimulated with either 1.3µg/ml of the TLR7 ligand imiquimod or 1.3µg/ml of the TLR8 ligand TL8-506 and treated with 1.6µM of dexamethasone. Metabolite extraction performed 24hrs post treatment. Samples were analysed using LC-MS with peaks matched to authentic internal standards for identification or annotated using online databases. PCA analysis was then performed to determine sample grouping and appropriateness of further OPLS-DA analysis. (A) dexamethasone + TLR7 vs TLR7 alone, (B) dexamethasone + TLR8 vs TLR8 alone*

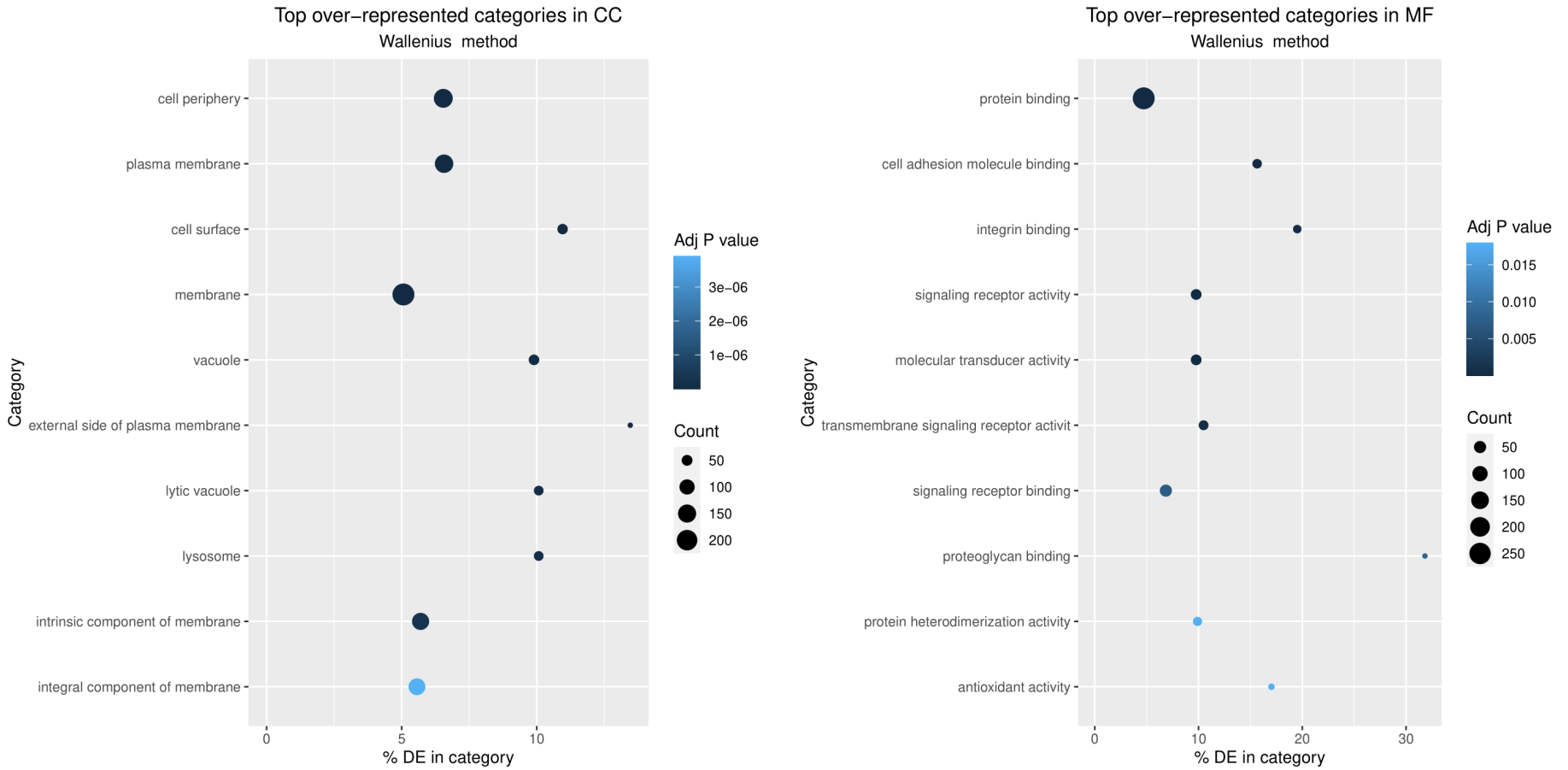

Appendix 5: gene ontology analysis of differentially expressed genes after NISV treatment. *Normalised gene counts were compared between unstimulated BMDM and those treated with NISV alone. Genes were annotated with their respective GO terms from mm10* mus musculus *genome assembly. 10 GO categories with the greatest number of significant differentially expressed genes were identified, organised by the categories of cellular component (CC), or molecular function (MF). Darkness of dot indicates greater statistical significance determined using FDR Benjamini-Hochberg method, whereas size indicates number of genes belonging to each GO annotation.*

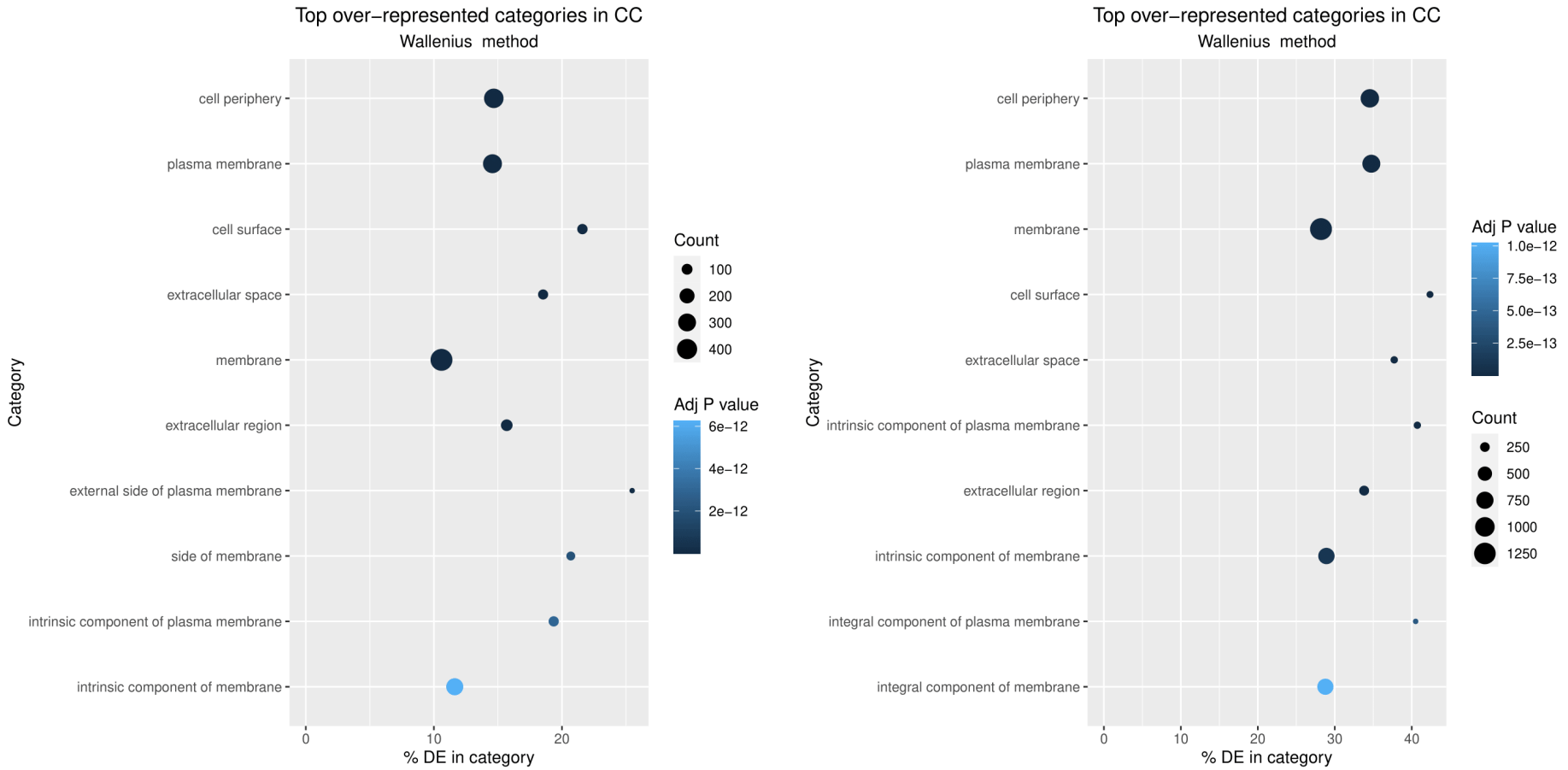

Appendix 6: gene ontology analysis of differentially expressed genes after dexamethasone treatment. *Normalised gene counts were compared between unstimulated BMDM and those treated with dexamethasone alone. Genes were annotated with their respective GO terms from mm10* mus musculus *genome assembly. 10 GO categories with the greatest number of significant differentially expressed genes were identified, organised by the categories of cellular component (CC), or molecular function (MF). Darkness of dot indicates greater statistical significance determined using FDR Benjamini-Hochberg method, whereas size indicates number of genes belonging to each GO annotation.*

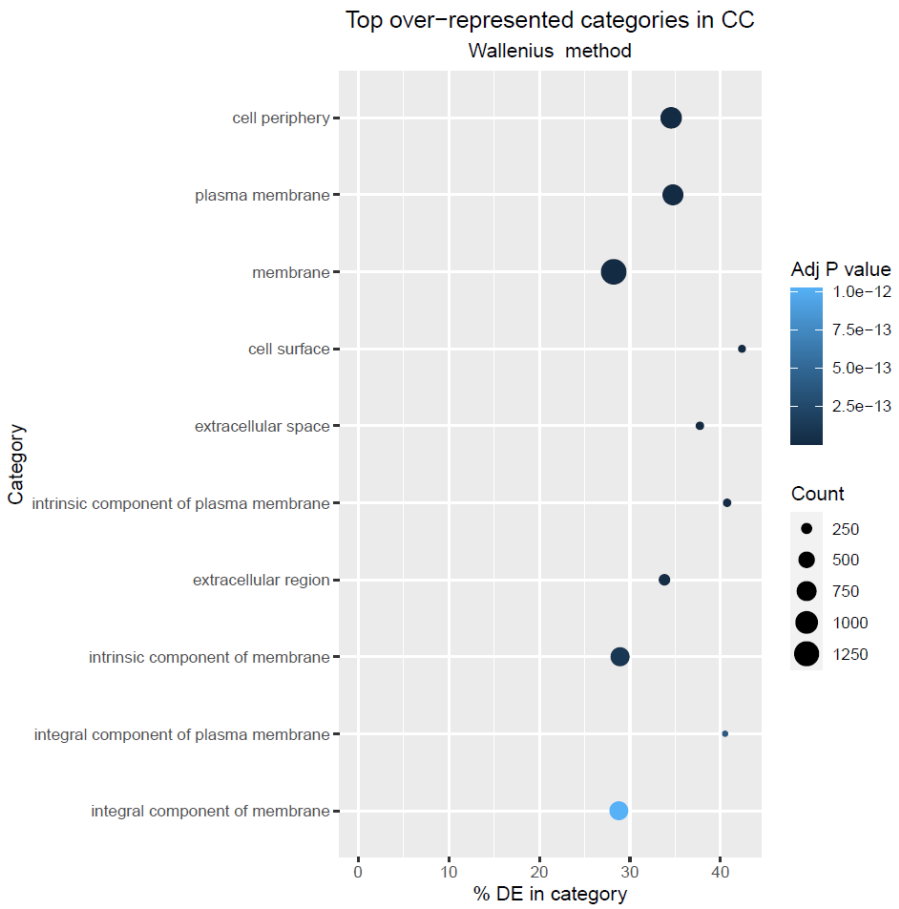

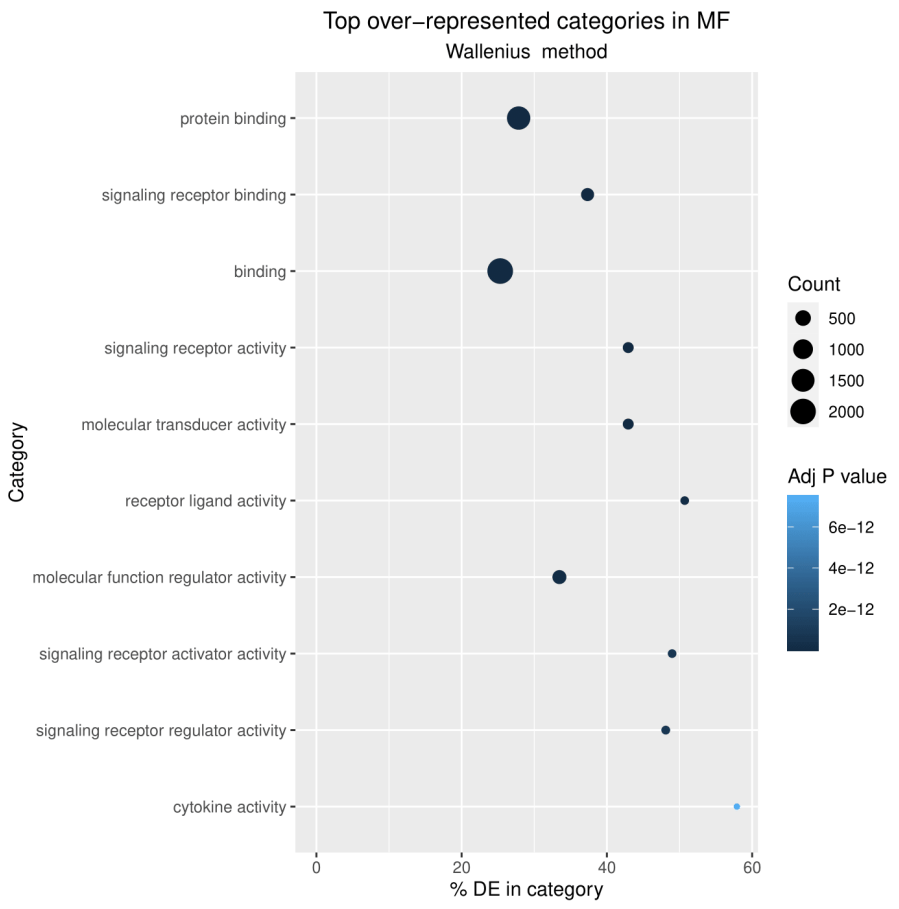

Appendix 7: gene ontology analysis of differentially expressed genes after TLR7 stimulation. *Normalised gene counts were compared between unstimulated BMDM and those stimulated with imiquimod (TLR7 ligand) alone. Genes were annotated with their respective GO terms from mm10* mus musculus *genome assembly. 10 GO categories with the greatest number of significant differentially expressed genes were identified, organised by the categories of cellular component (CC), or molecular function (MF). Darkness of dot indicates greater statistical significance determined using FDR Benjamini-Hochberg method, whereas size indicates number of genes belonging to each GO annotation.*

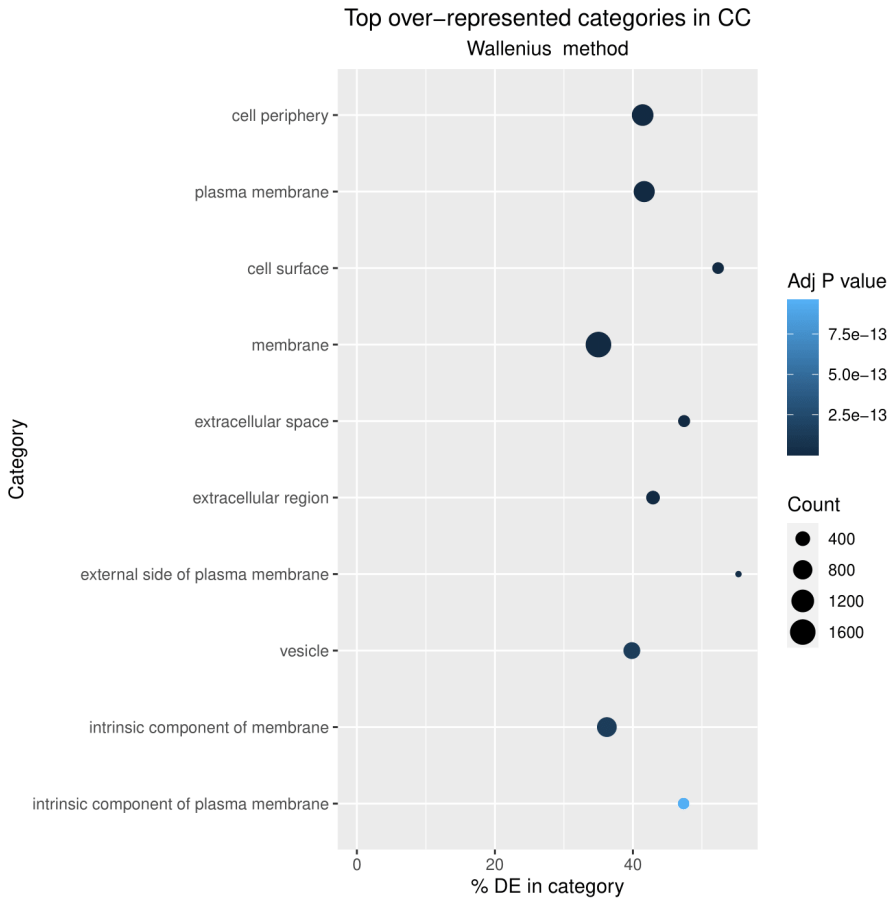

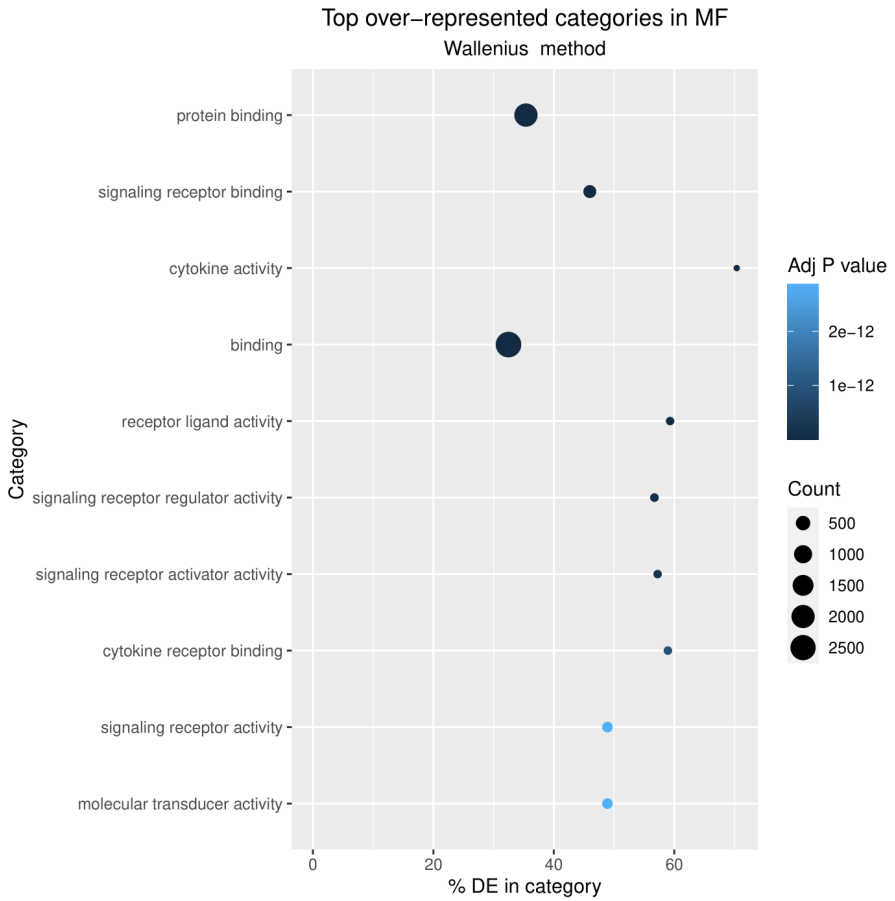

Appendix 8: gene ontology analysis of differentially expressed genes after TLR8 stimulation. *Normalised gene counts were compared between unstimulated BMDM and those stimulated with TL8-506 (TLR8 ligand) alone. Genes were annotated with their respective GO terms from mm10* mus musculus *genome assembly. 10 GO categories with the greatest number of significant differentially expressed genes were identified, organised by the categories of cellular component (CC), or molecular function (MF). Darkness of dot indicates greater statistical significance determined using FDR Benjamini-Hochberg method, whereas size indicates number of genes belonging to each GO annotation.*

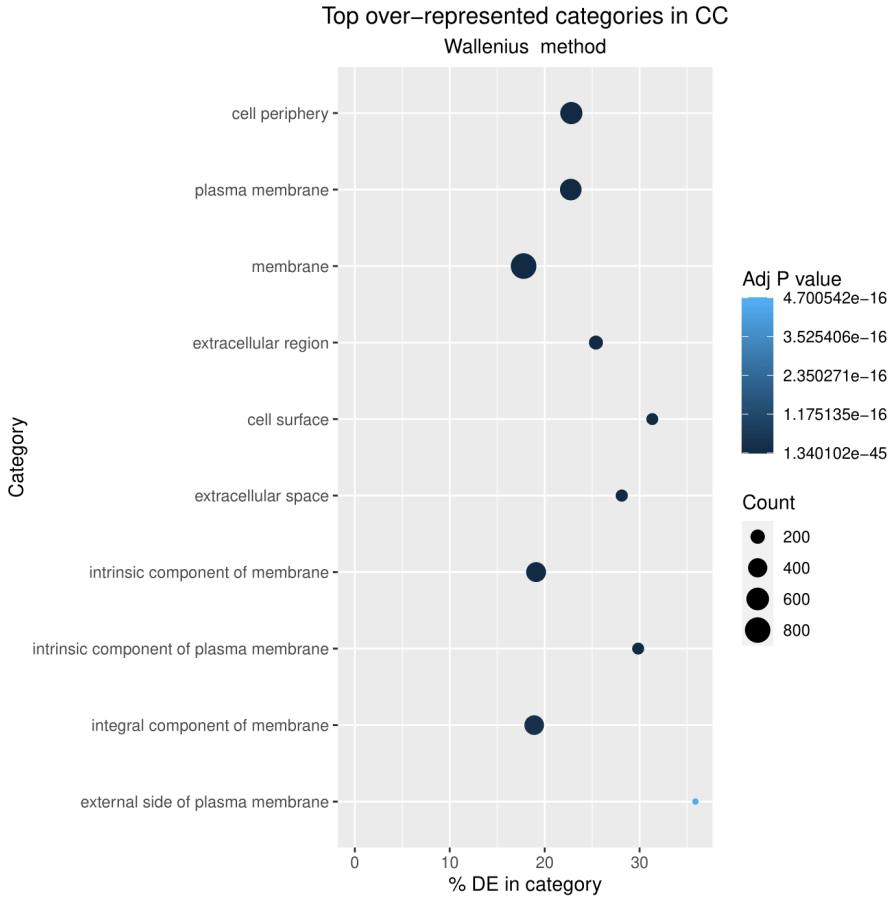

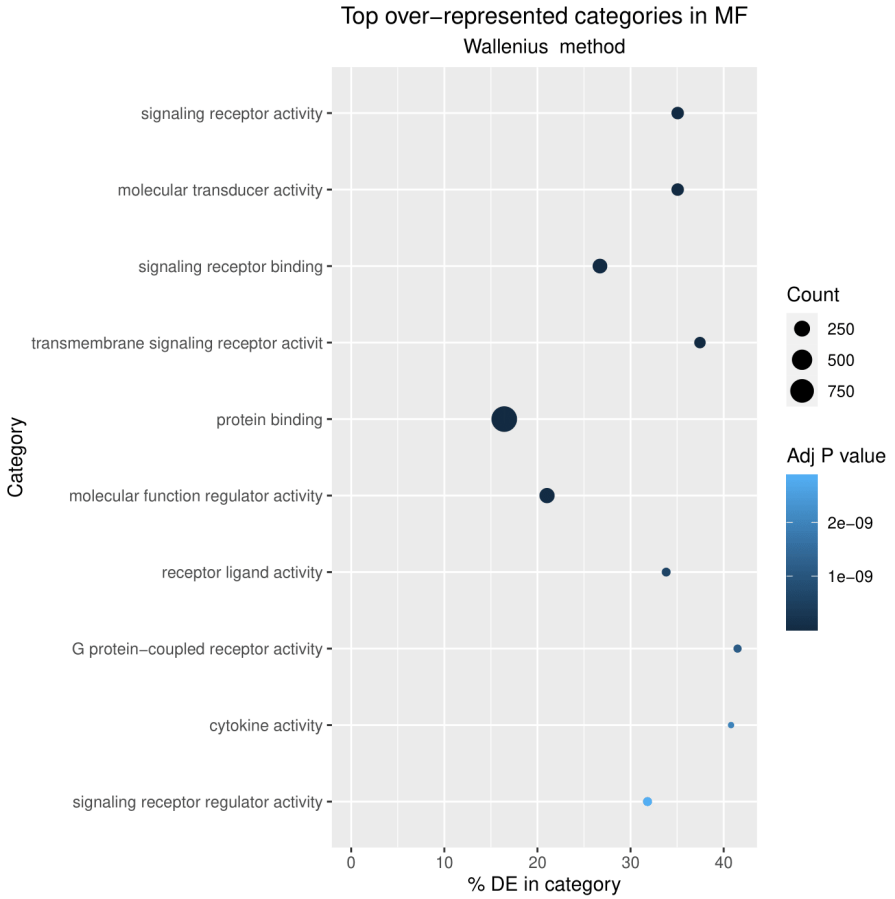

Appendix 9: gene ontology analysis of differentially expressed genes after NISV treatment of TLR7 stimulated cells. *Normalised gene counts were compared between BMDM stimulated with imiquimod (TLR7 ligand) and TLR7 stimulated cells treated with NISV. Genes were annotated with their respective GO terms from mm10* mus musculus *genome assembly. 10 GO categories with the greatest number of significant differentially expressed genes were identified, organised by the categories of cellular component (CC), or molecular function (MF). Darkness of dot indicates greater statistical significance determined using FDR Benjamini-Hochberg method, whereas size indicates number of genes belonging to each GO annotation.*

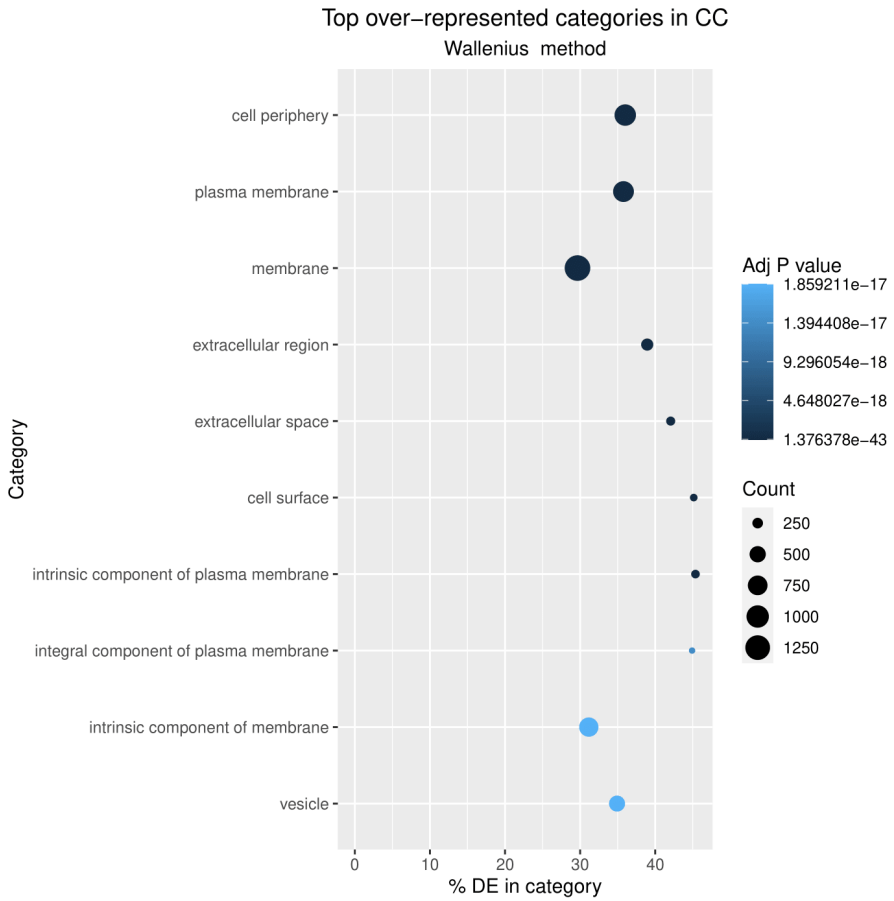

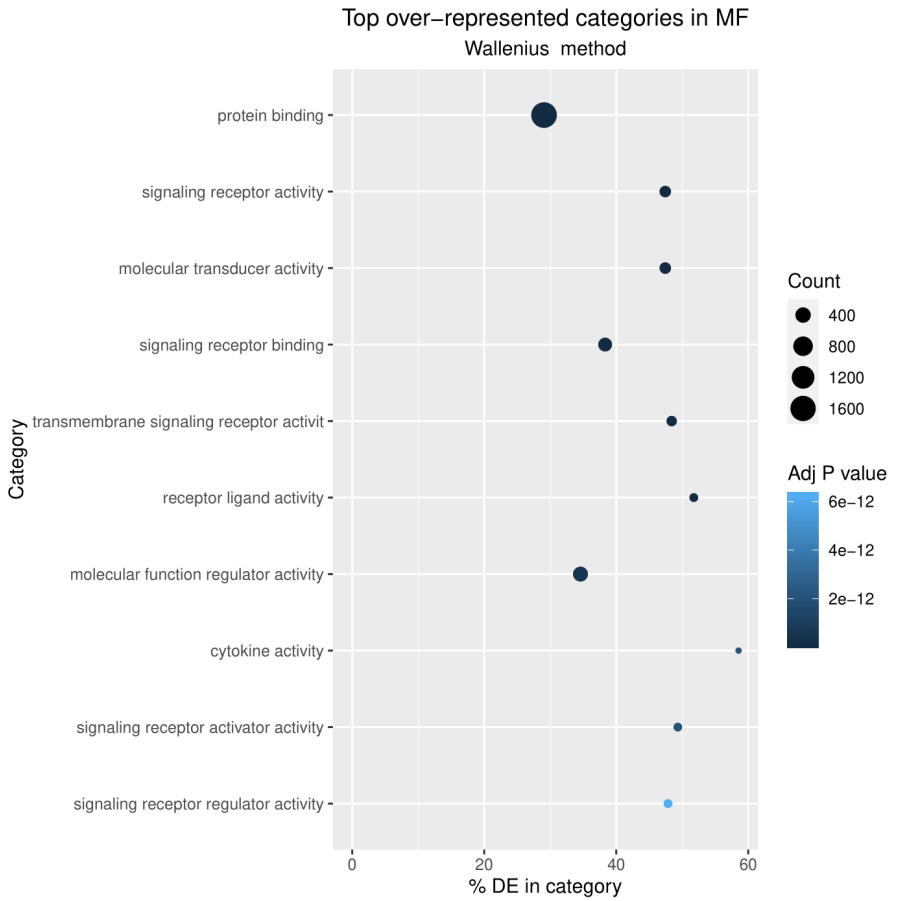

Appendix 10: gene ontology analysis of differentially expressed genes after NISV treatment of TLR8 stimulated cells. *Normalised gene counts were compared between BMDM stimulated with TL8-506 (TLR8 ligand) and TLR8 stimulated cells treated with NISV. Genes were annotated with their respective GO terms from mm10* mus musculus *genome assembly. 10 GO categories with the greatest number of significant differentially expressed genes were identified, organised by the categories of cellular component (CC), or molecular function (MF). Darkness of dot indicates greater statistical significance determined using FDR Benjamini-Hochberg method, whereas size indicates number of genes belonging to each GO annotation.*

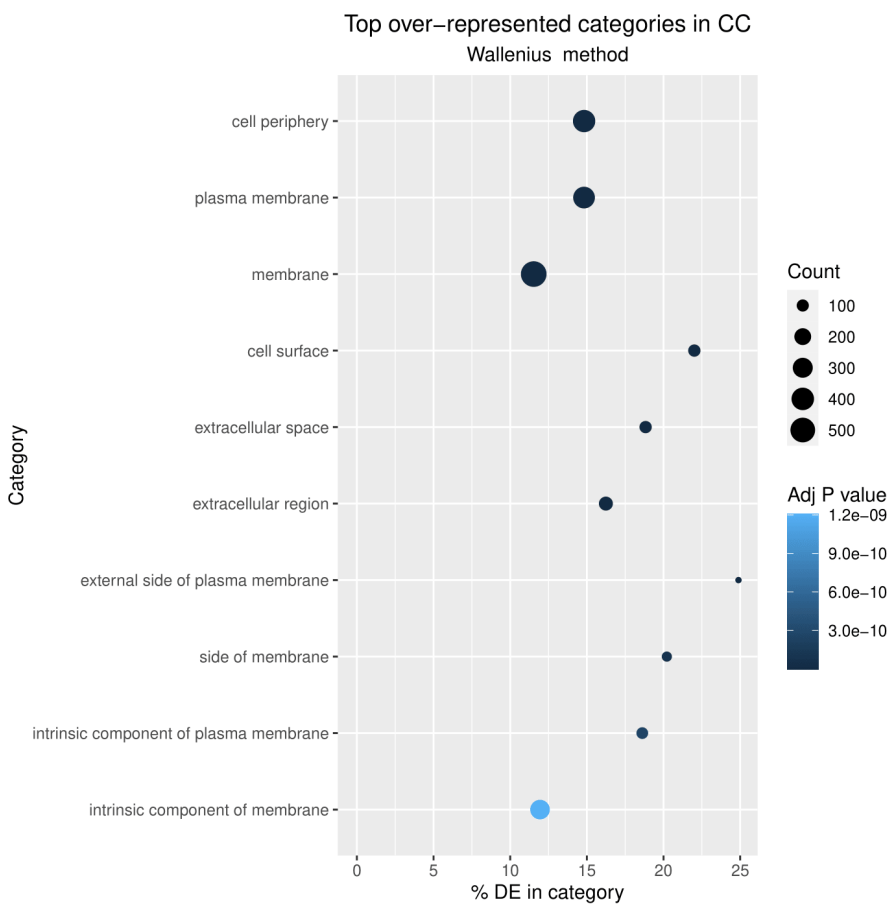

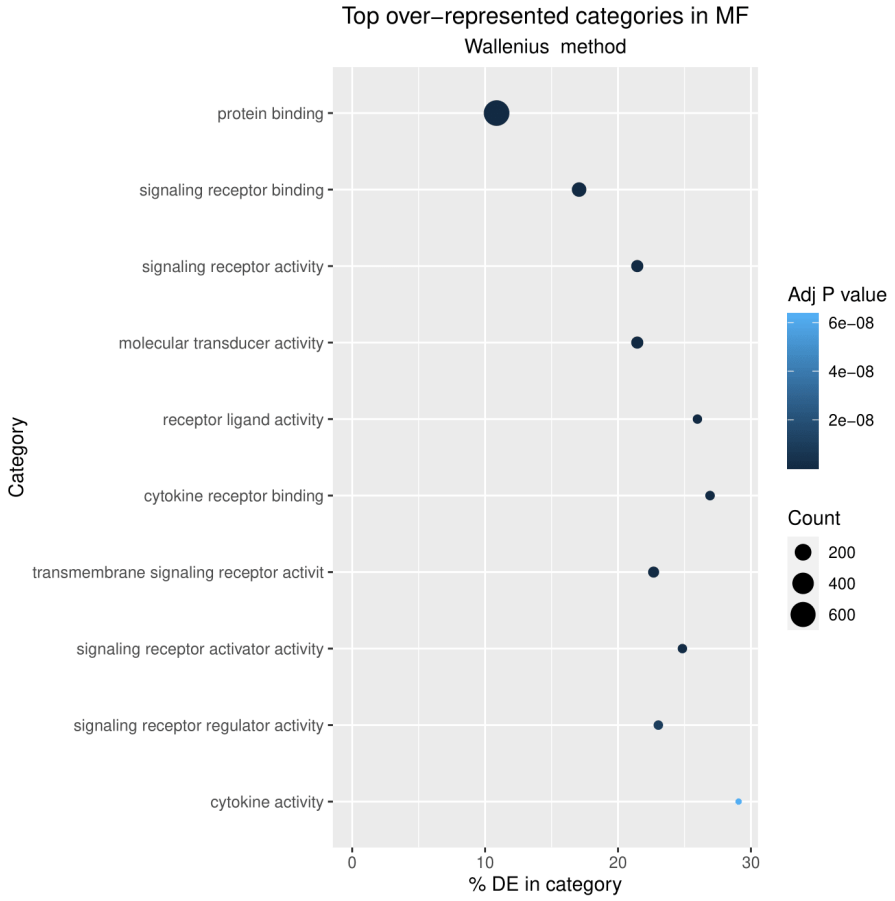

Appendix 11: gene ontology analysis of differentially expressed genes after dexamethasone treatment of TLR7 stimulated cells. *Normalised gene counts were compared between BMDM stimulated with imiquimod (TLR7 ligand) and TLR7 stimulated cells treated with NISV. Genes were annotated with their respective GO terms from mm10* mus musculus *genome assembly. 10 GO categories with the greatest number of significant differentially expressed genes were identified, organised by the categories of cellular component (CC), or molecular function (MF). Darkness of dot indicates greater statistical significance determined using FDR Benjamini-Hochberg method, whereas size indicates number of genes belonging to each GO annotation.*

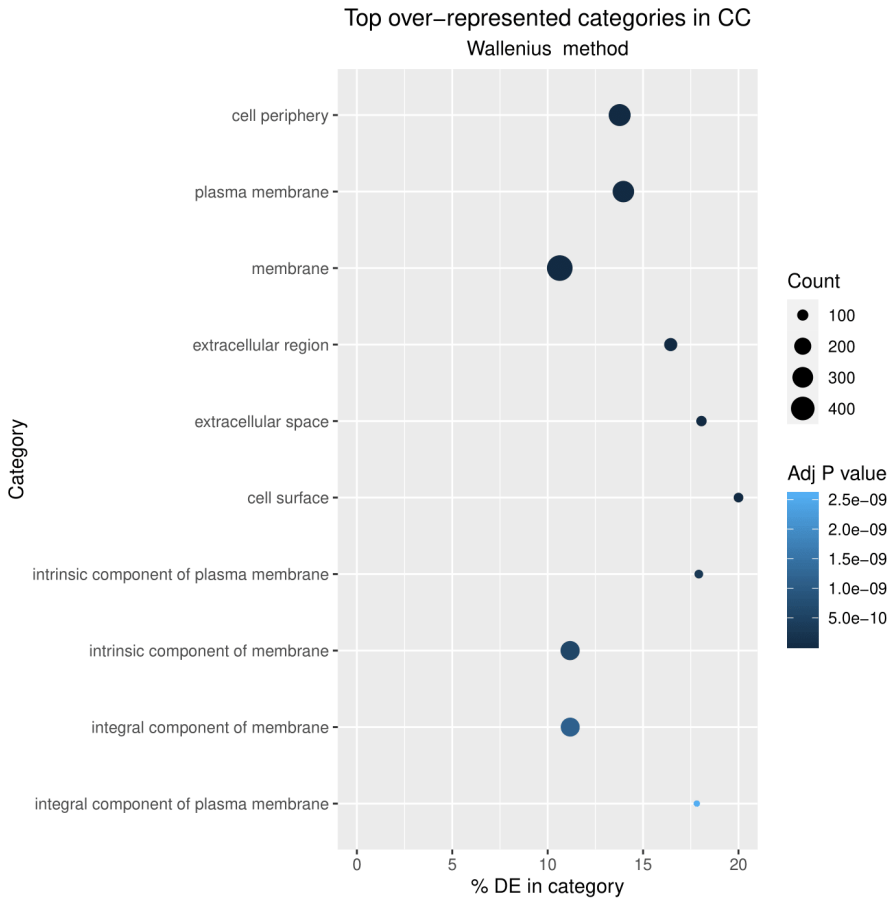

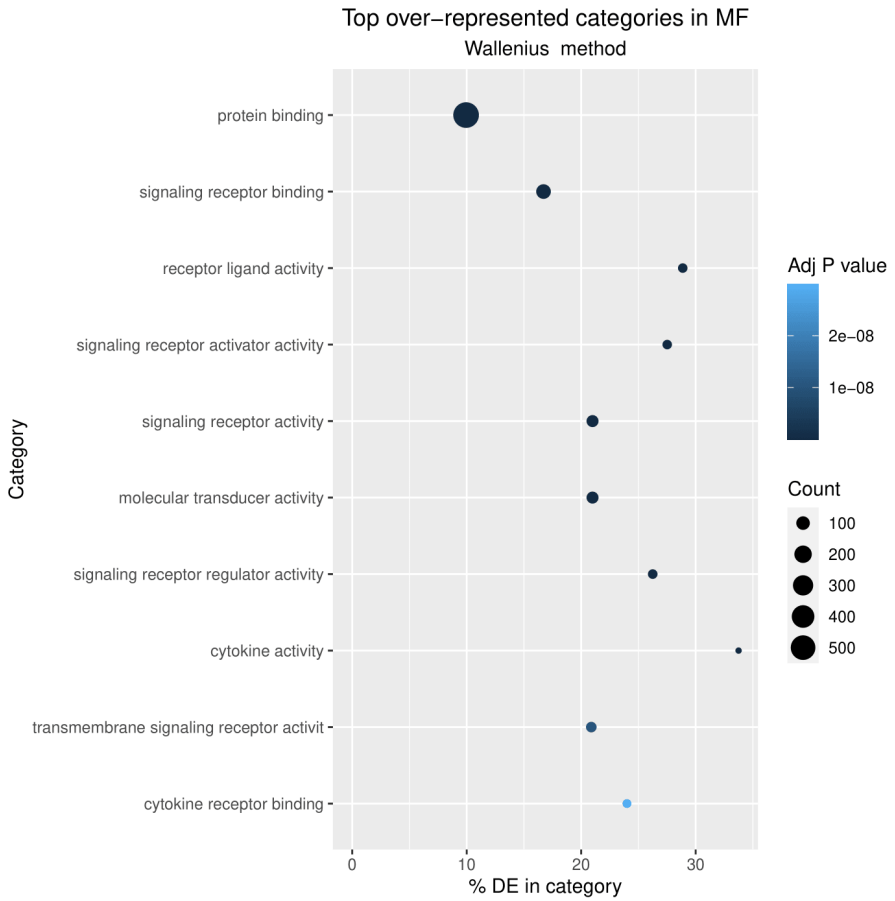

Appendix 12: gene ontology analysis of differentially expressed genes after dexamethasone treatment of TLR8 stimulated cells. *Normalised gene counts were compared between BMDM stimulated with TL8-506 (TLR8 ligand) and TLR8 stimulated cells treated with NISV. Genes were annotated with their respective GO terms from mm10* mus musculus *genome assembly. 10 GO categories with the greatest number of significant differentially expressed genes were identified, organised by the categories of cellular component (CC), or molecular function (MF). Darkness of dot indicates greater statistical significance determined using FDR Benjamini-Hochberg method, whereas size indicates number of genes belonging to each GO annotation.*

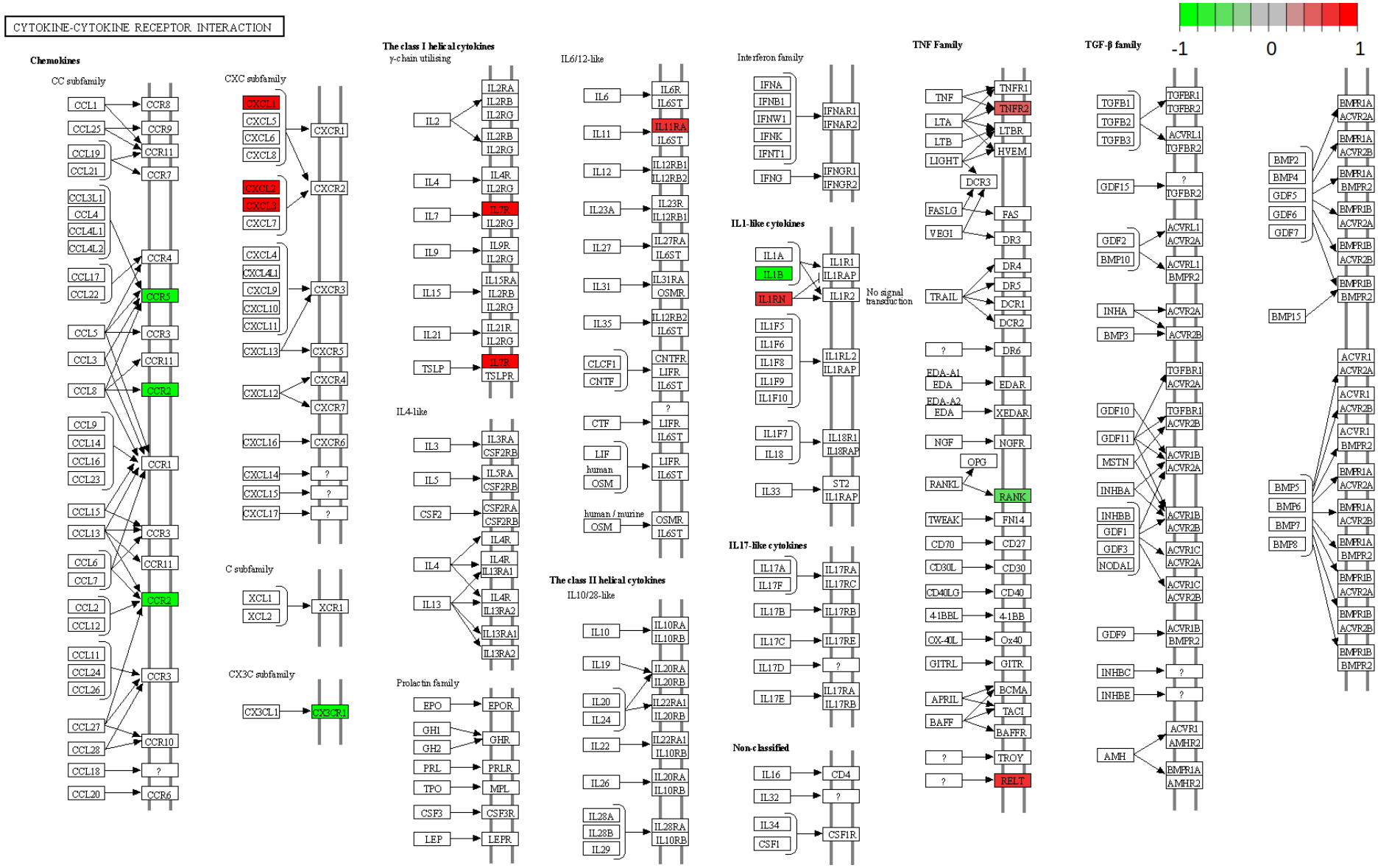

Appendix 13: Cytokine-cytokine receptor gene modulation by NISV. *Significant differential gene expression comparing unstimulated cells vs those treated with NISV alone represented as Log2FC. Green = decrease in gene expression, red = increase in gene expression.*

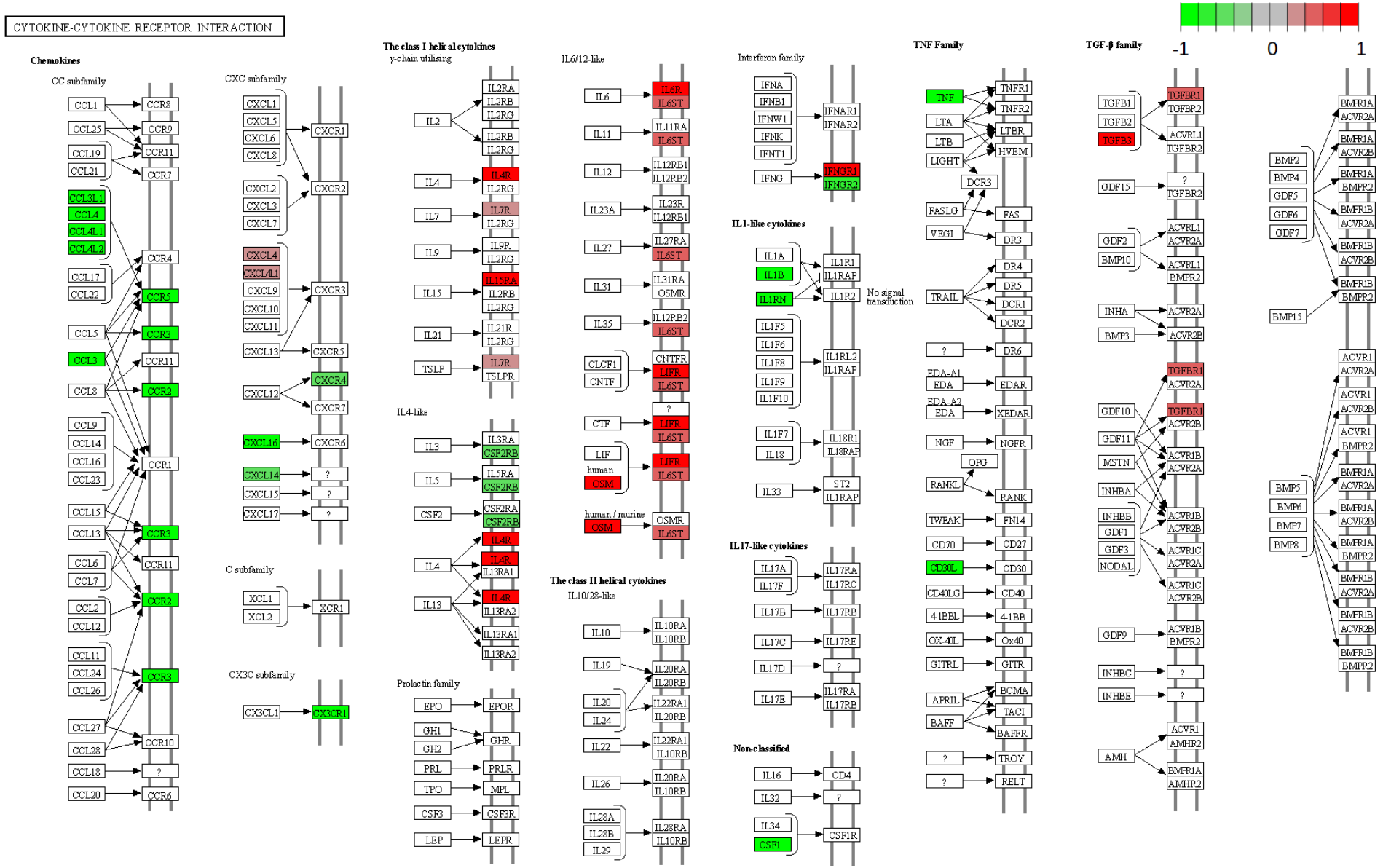

Appendix 14: Cytokine-cytokine receptor gene modulation by dexamethasone *Significant differential gene expression comparing unstimulated cells vs those treated with dexamethasone alone represented as Log2FC. Green = decrease in gene expression, red = increase in gene expression.*

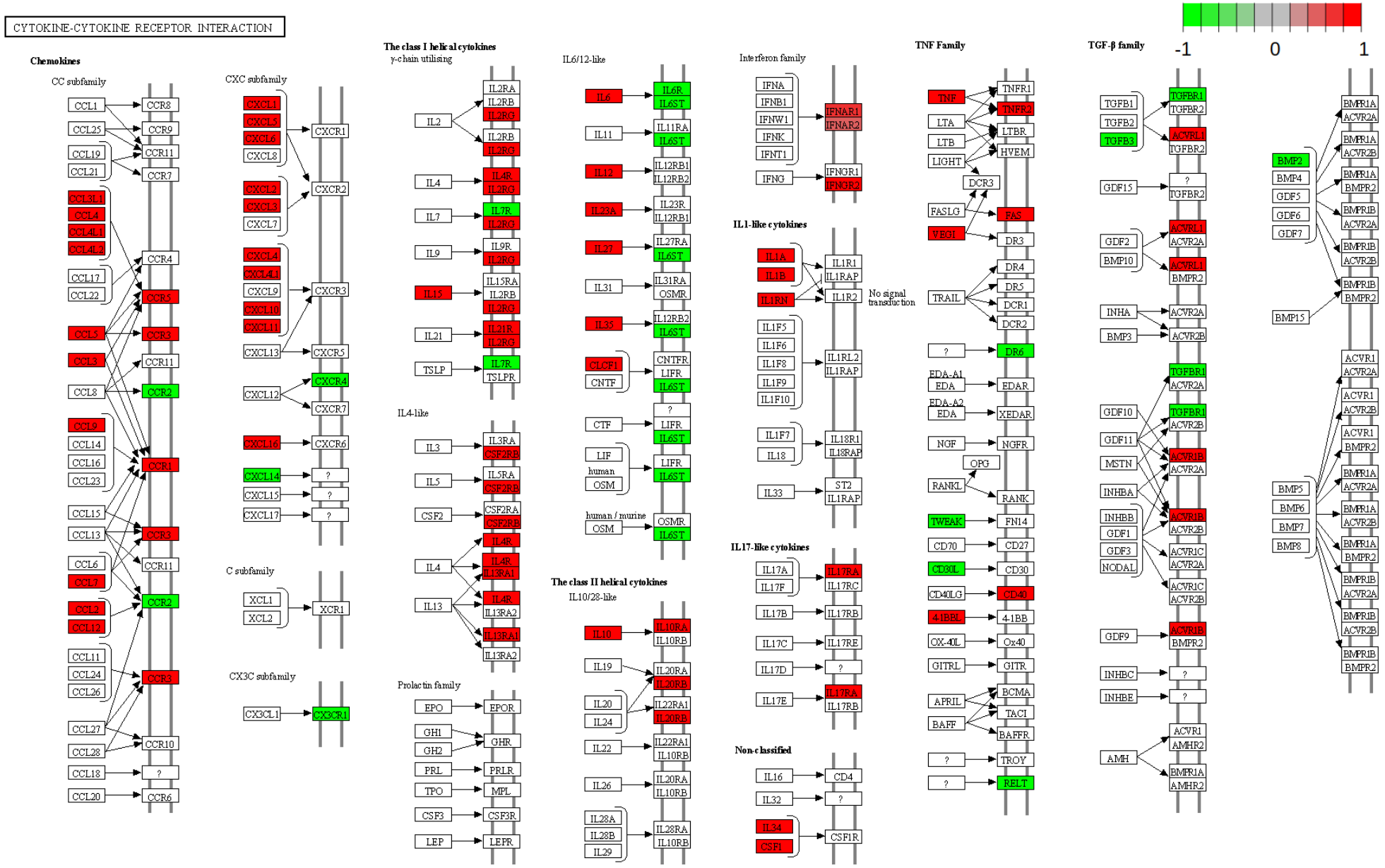

Appendix 15: Cytokine-cytokine receptor gene modulation by TLR7 Ligand imiquimod. *Significant differential gene expression comparing unstimulated cells vs those treated with imiquimod alone represented as Log2FC. Green = decrease in gene expression, red = increase in gene expression*

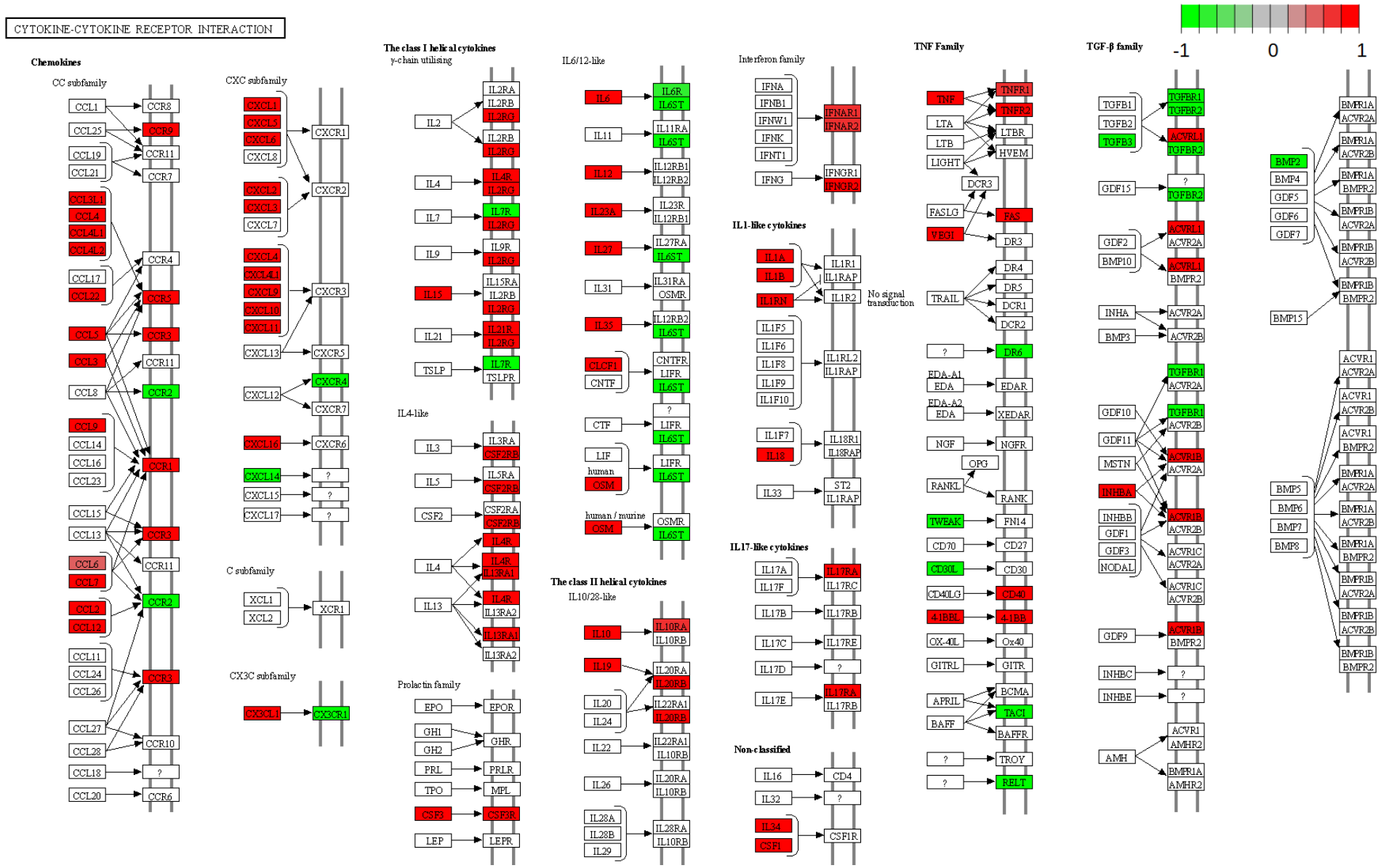

Appendix 16: Cytokine-cytokine receptor gene modulation by TLR8 Ligand TL8-506. *Significant differential gene expression comparing unstimulated cells vs those treated with TL8-506 alone represented as Log2FC. Green = decrease in gene expression, red = increase in gene expression.*

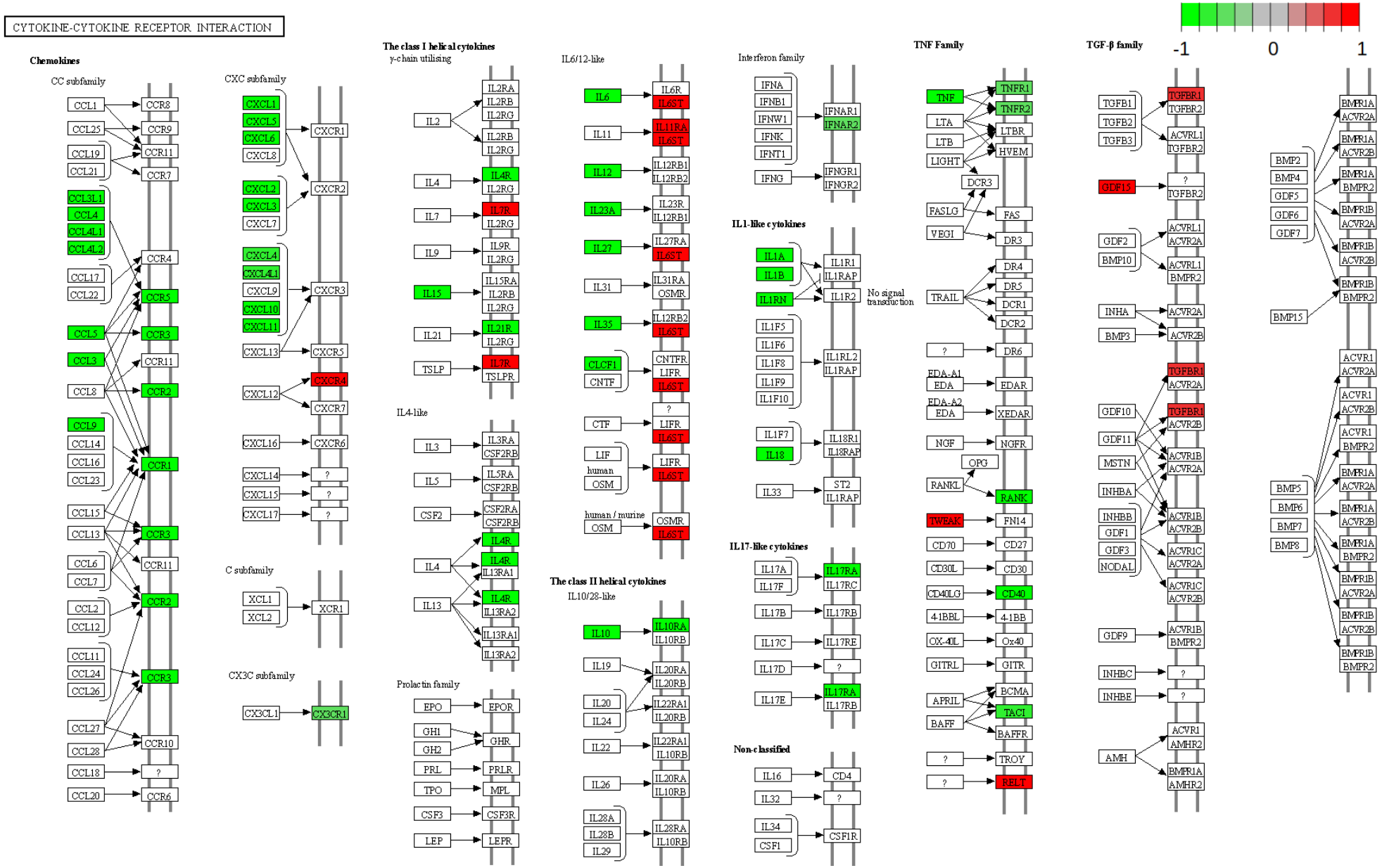

Appendix 17: Cytokine-cytokine receptor gene modulation by NISV in TLR7 stimulated cells. *Significant differential gene expression comparing TLR7 stimulated cells vs TLR7 stimulated cells treated with NISV represented as Log2FC. Green = decrease in gene expression, red = increase in gene expression.*

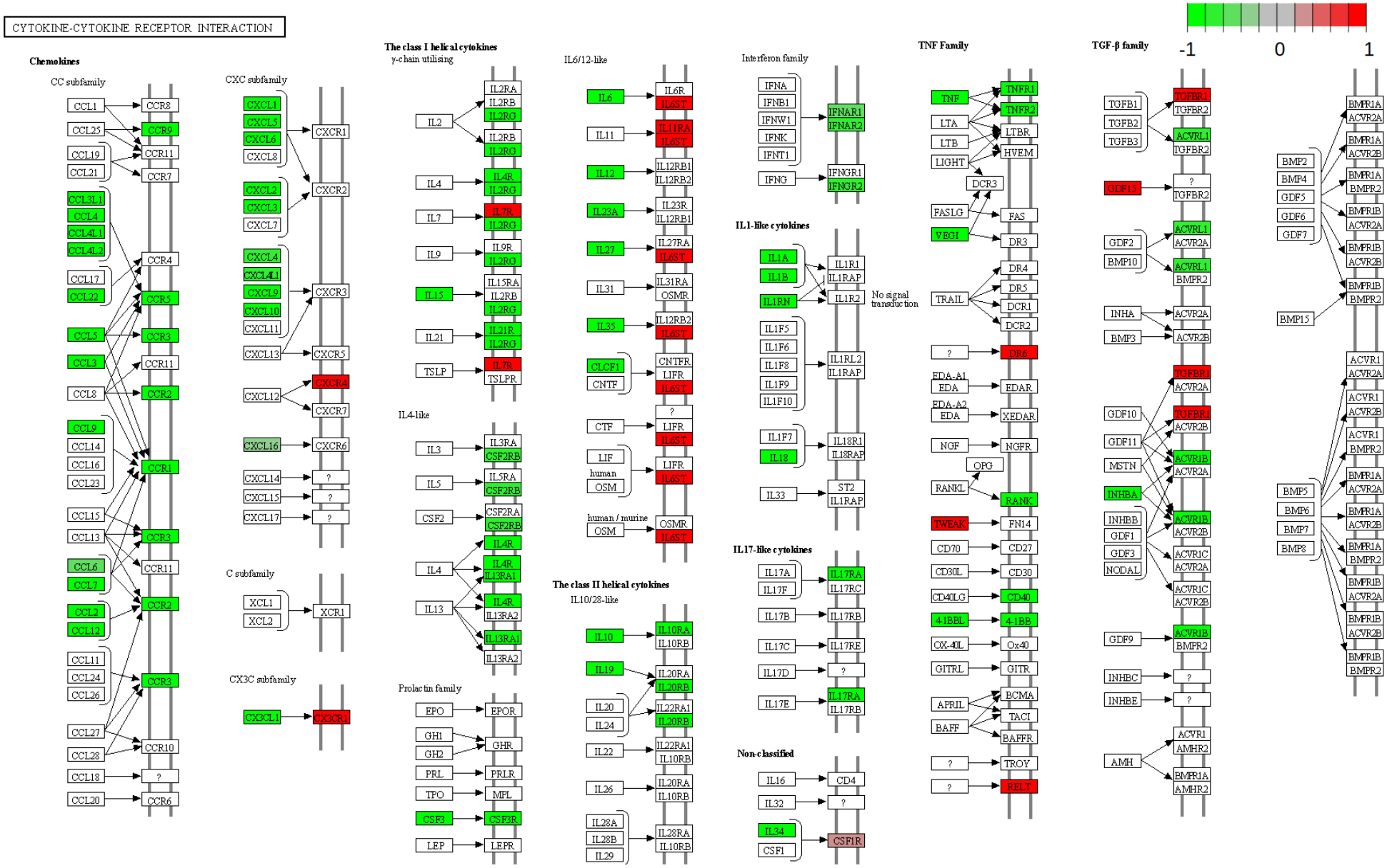

Appendix 18: Cytokine-cytokine receptor gene modulation by NISV in TLR8 stimulated cells. *Significant differential gene expression comparing TLR8 stimulated cells vs TLR8 stimulated cells treated with NISV represented as Log2FC. Green = decrease in gene expression, red = increase in gene expression.*

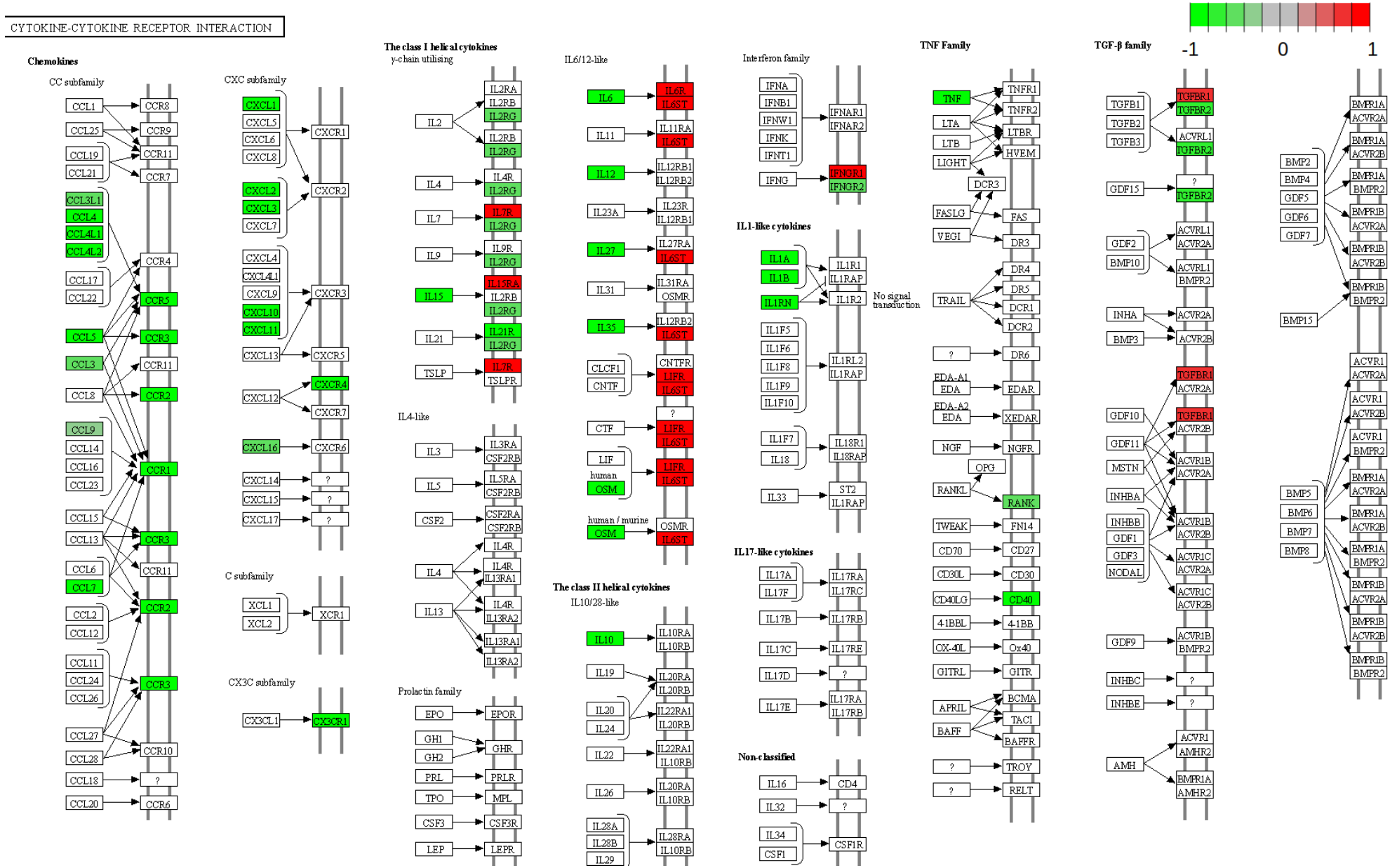

Appendix 19: Cytokine-cytokine receptor gene modulation by dexamethasone in TLR7 stimulated cells. *Significant differential gene expression comparing TLR7 stimulated cells vs TLR7 stimulated cells treated with dexamethasone represented as Log2FC. Green = decrease in gene expression, red = increase in gene expression.*

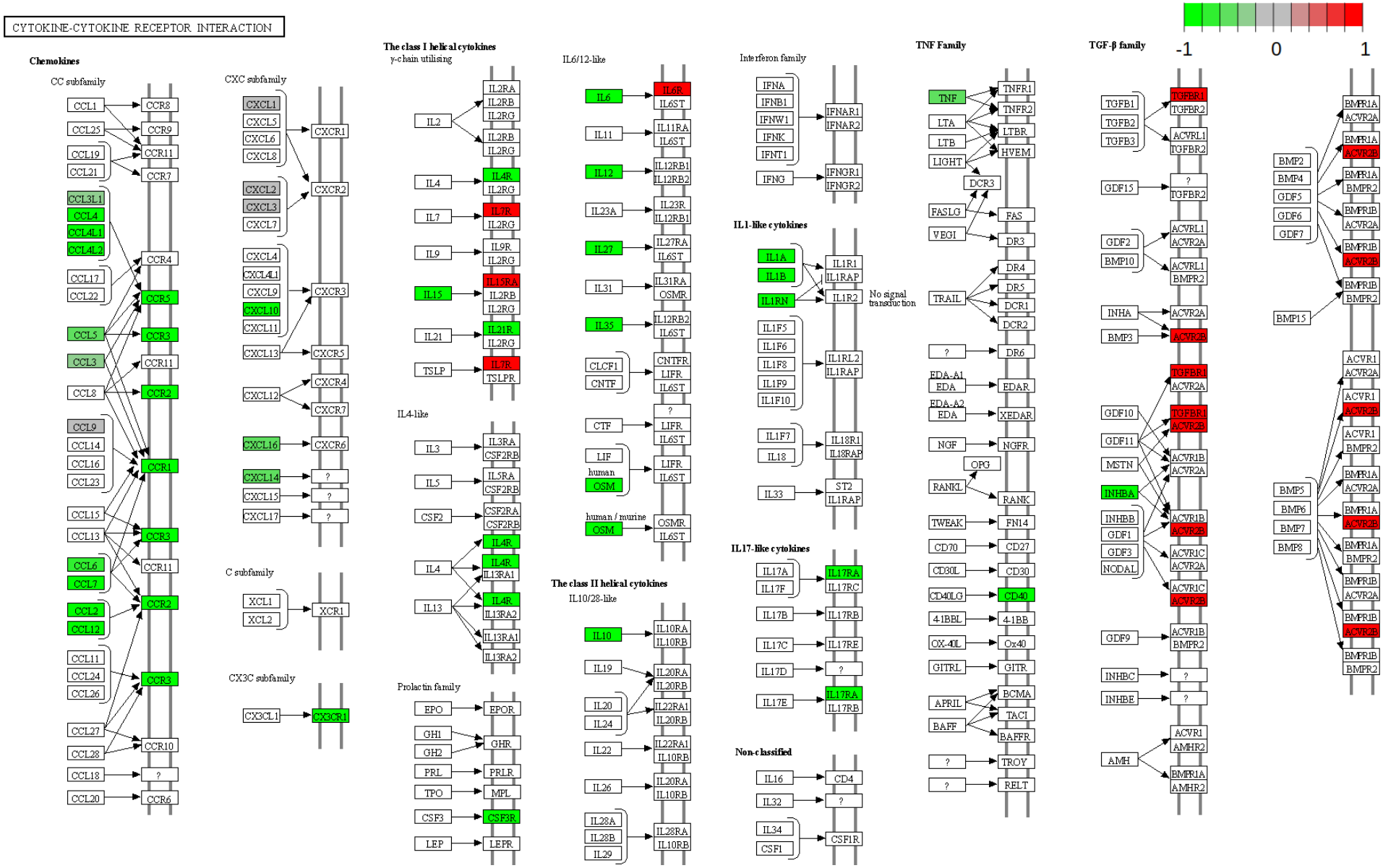

Appendix 20: Cytokine-cytokine receptor gene modulation by dexamethasone in TLR8 stimulated cells. *Significant differential gene expression comparing TLR8 stimulated cells vs TLR8 stimulated cells treated with dexamethasone represented as Log2FC. Green = decrease in gene expression, red = increase in gene expression.*

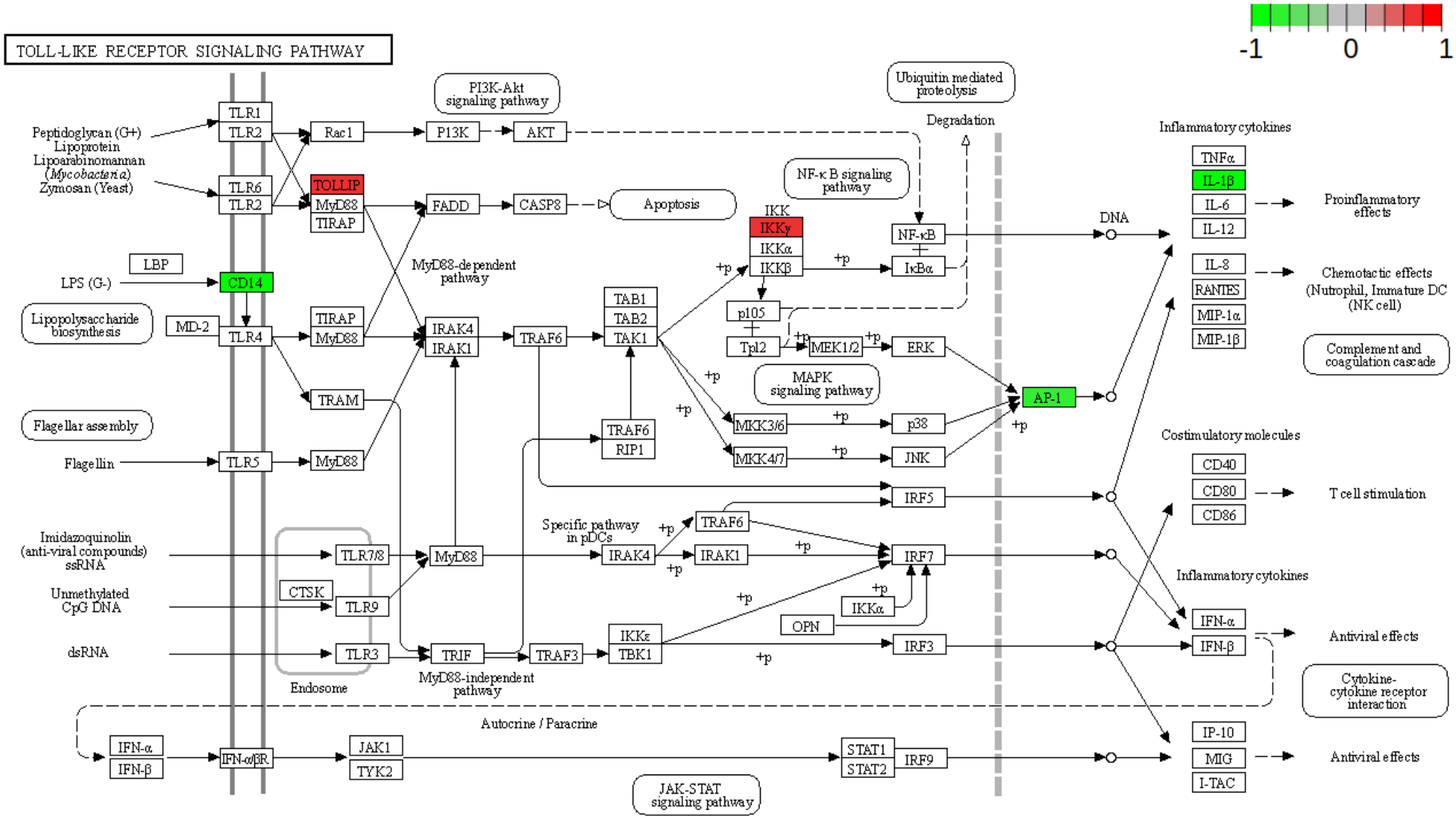

Appendix 21: Toll-like receptor signalling pathway gene modulation by NISV. *Significant differential gene expression comparing unstimulated cells to cells treated with NISV represented as Log2FC. Green = decrease in gene expression, red = increase in gene expression.*

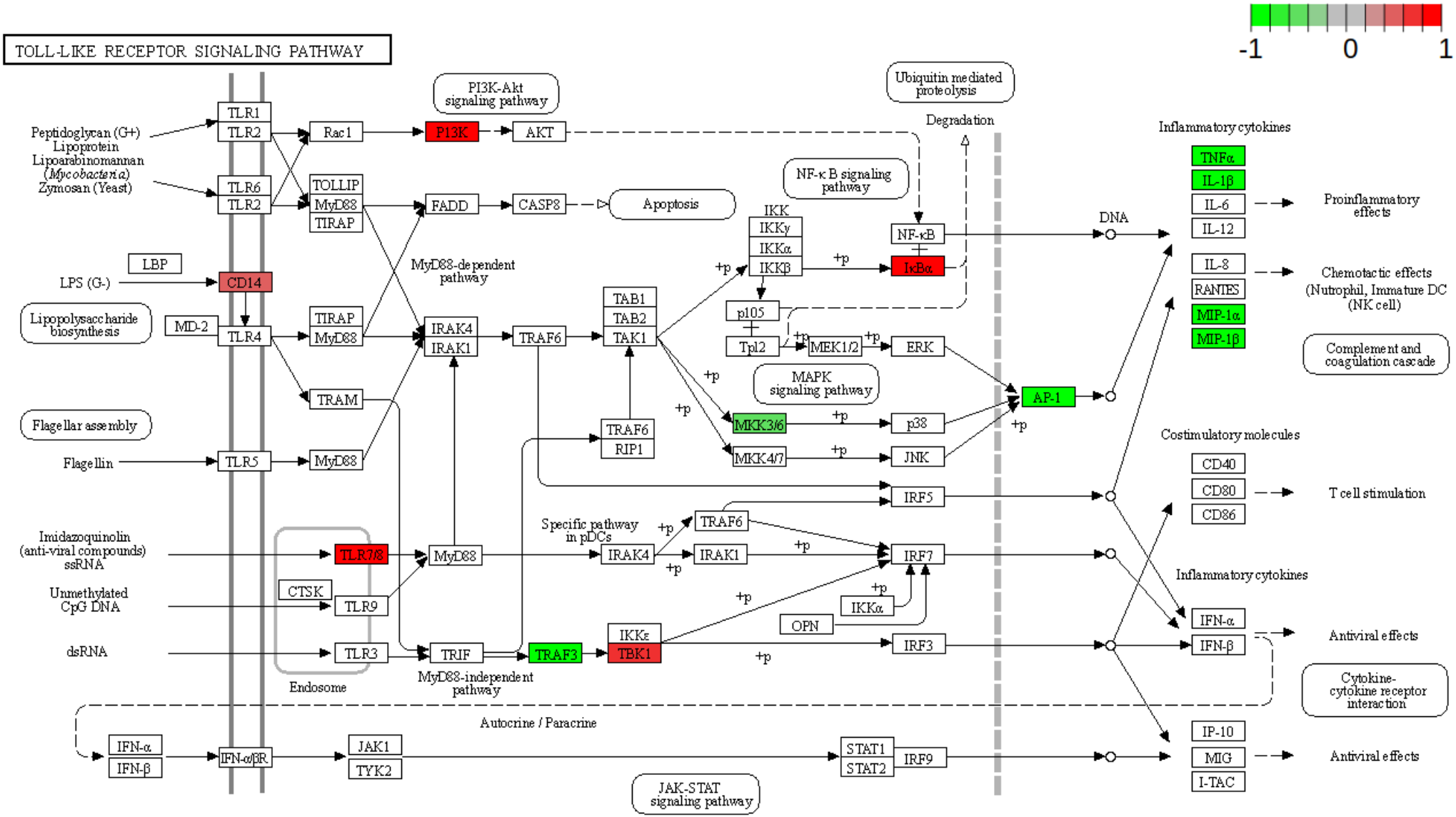

Appendix 22: Toll-like receptor signalling pathway gene modulation by dexamethasone. *Significant differential gene expression comparing unstimulated cells to cells treated with dexamethasone represented as Log2FC. Green = decrease in gene expression, red = increase in gene expression.*

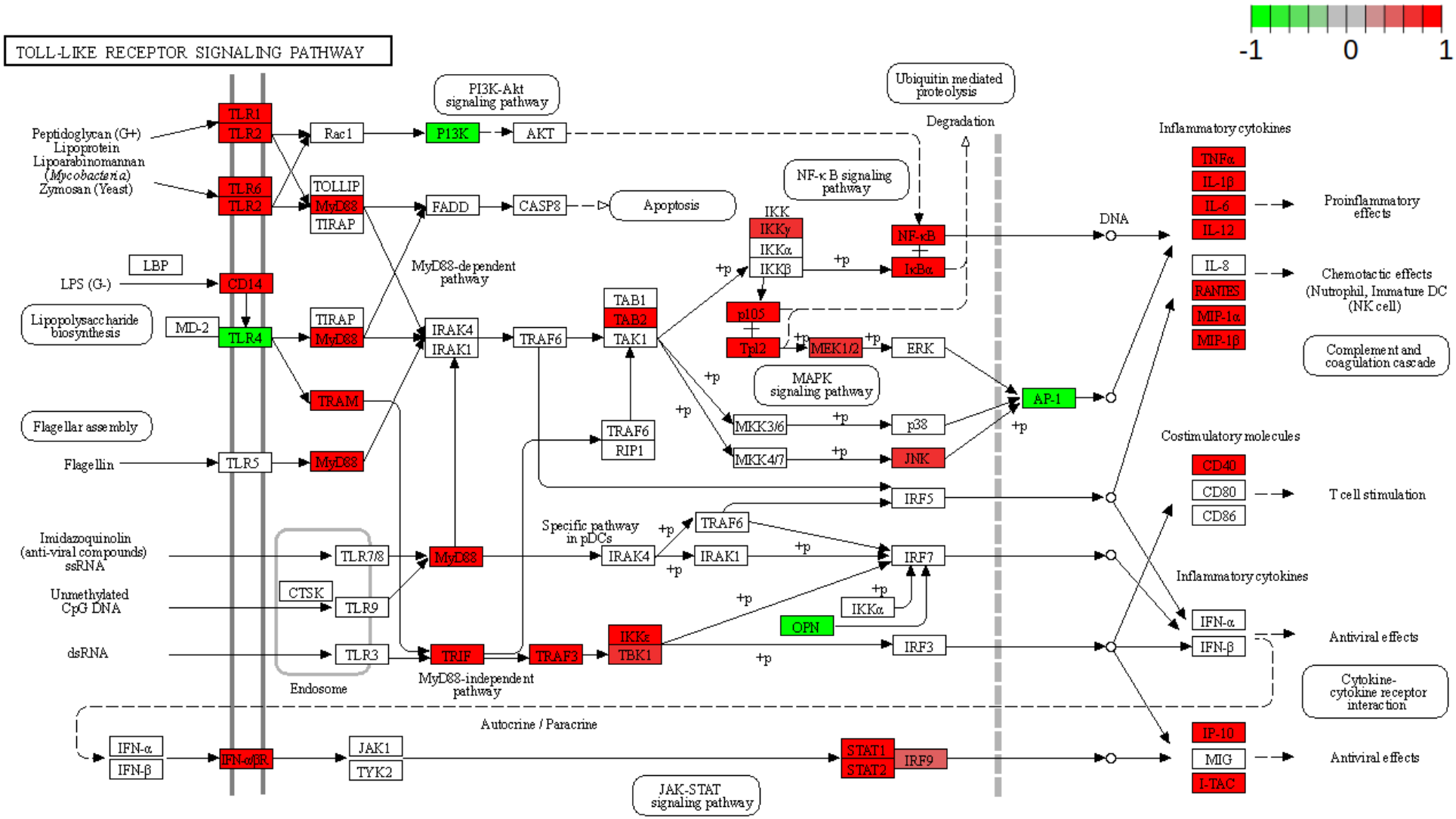

Appendix 23: Toll-like receptor signalling pathway gene modulation by TLR7 stimulation. *Significant differential gene expression comparing unstimulated cells to cells treated with the TLR7 ligand imiquimod represented as Log2FC. Green = decrease in gene expression, red = increase in gene expression.*

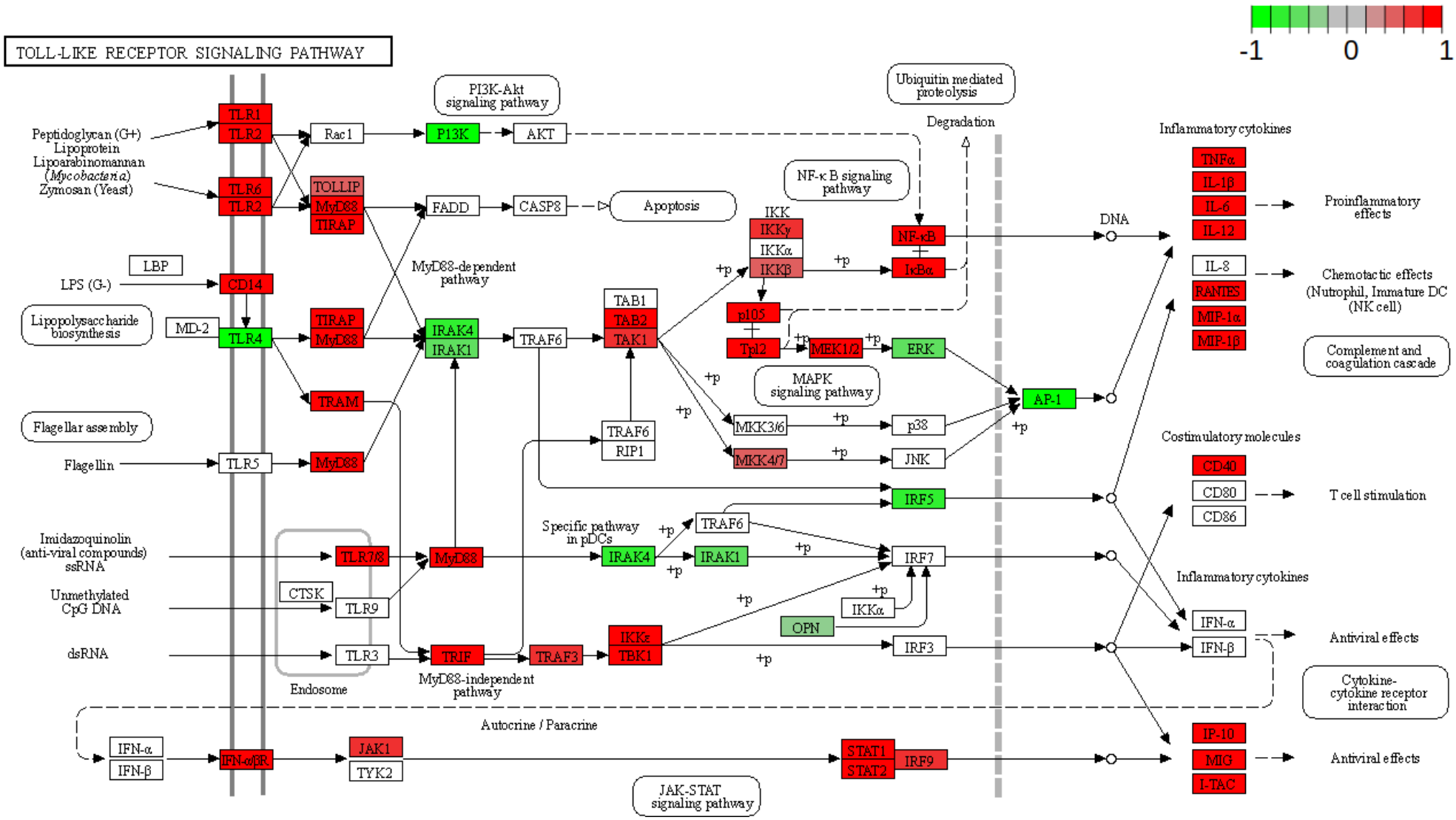

Appendix 24: Toll-like receptor signalling pathway gene modulation by TLR8 stimulation. *Significant differential gene expression comparing unstimulated cells to cells treated with the TLR8 ligand TL8-506 represented as Log2FC. Green = decrease in gene expression, red = increase in gene expression.*

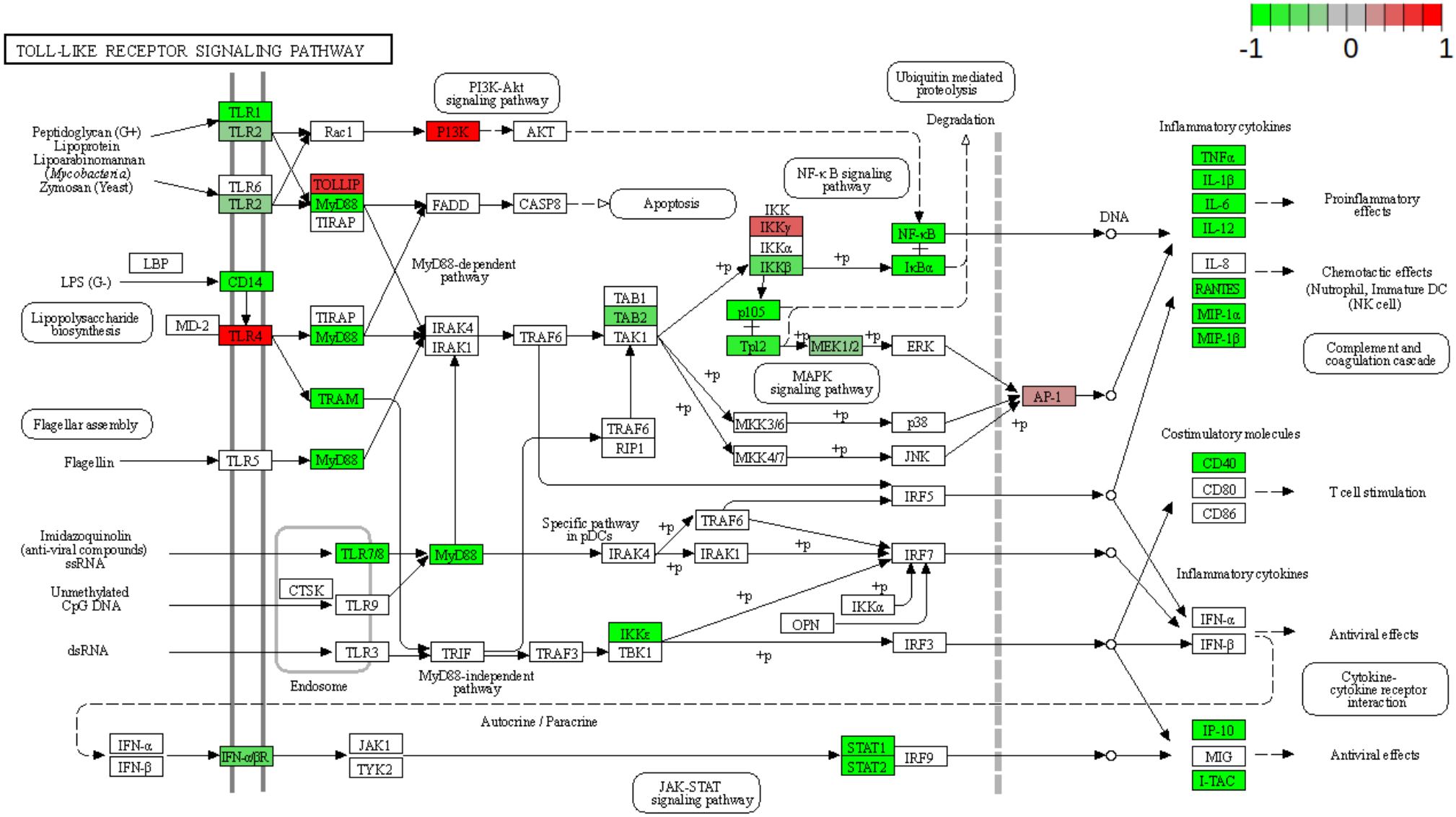

Appendix 25: Toll-like receptor signalling pathway gene modulation by NISV in TLR7 stimulated cells. *Significant differential gene expression comparing TLR7 stimulated cells to TLR7 stimulated cells treated with NISV represented as Log2FC. Green = decrease in gene expression, red = increase in gene expression.*

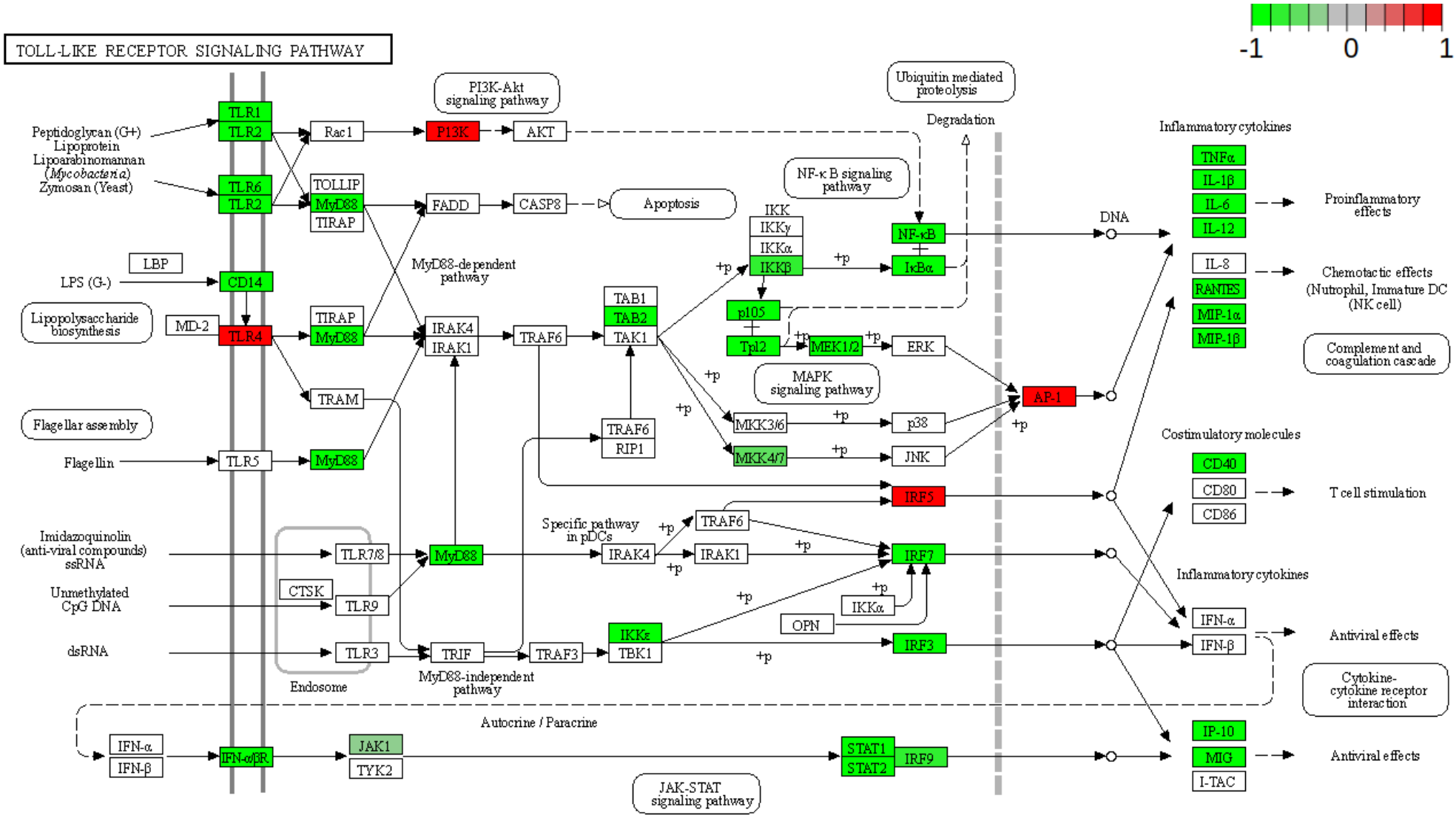

Appendix 26: Toll-like receptor signalling pathway gene modulation by NISV in TLR8 stimulated cells. *Significant differential gene expression comparing TLR8 stimulated cells to TLR8 stimulated cells treated with NISV represented as Log2FC. Green = decrease in gene expression, red = increase in gene expression.*

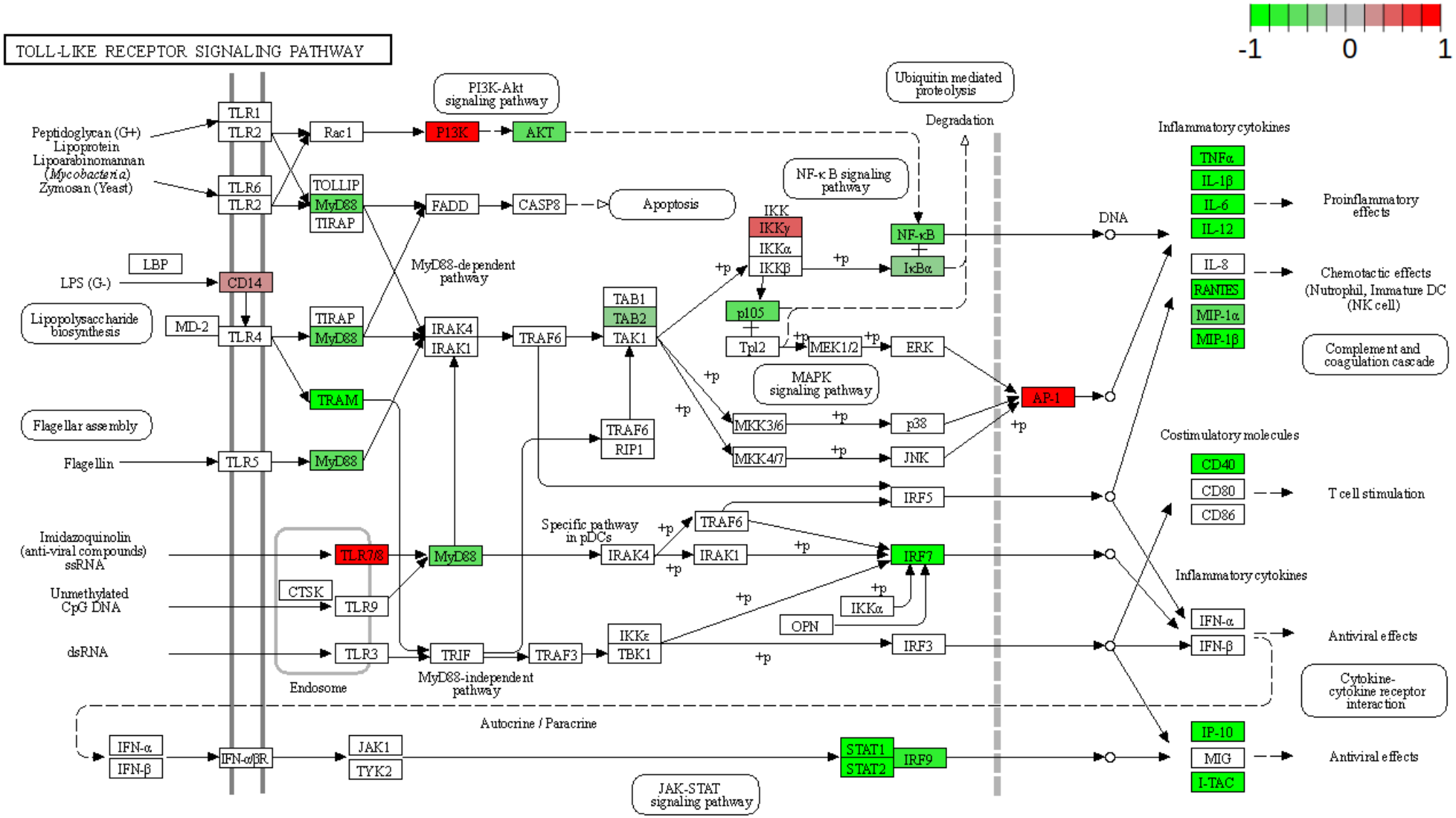

Appendix 27: Toll-like receptor signalling pathway gene modulation by dexamethasone in TLR7 stimulated cells. *Significant differential gene expression comparing TLR7 stimulated cells to TLR7 stimulated cells treated with dexamethasone represented as Log2FC. Green = decrease in gene expression, red = increase in gene expression.*

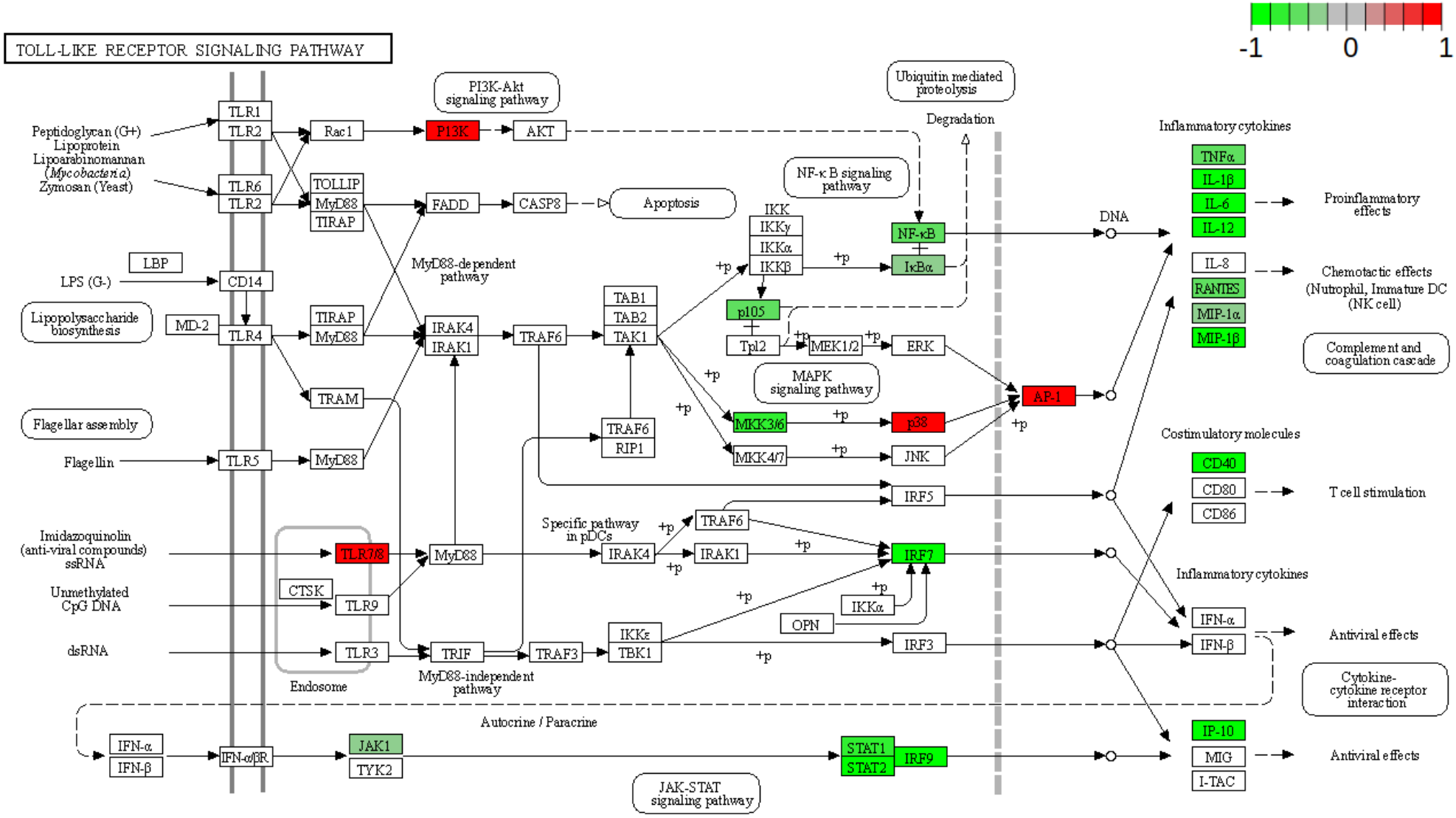

Appendix 28: Toll-like receptor signalling pathway gene modulation by dexamethasone in TLR8 stimulated cells. *Significant differential gene expression comparing TLR8 stimulated cells to TLR8 stimulated cells treated with dexamethasone represented as Log2FC. Green = decrease in gene expression, red = increase in gene expression.*